LIPID METABOLISM IN DEVELOPMENT AND ENVIRONMENTAL STRESS TOLERANCE FOR ENGINEERING AGRONOMIC TRAITS

EDITED BY: Zhi-Yan (Rock) Du, Susanne Hoffmann-Benning, Agnieszka Zienkiewicz, Krzysztof Zienkiewicz, Shiwen Wang and Lina Yin

PUBLISHED IN: Frontiers in Plant Science

frontiers Research Topics

ISSN 1664-8714
ISBN 978-2-88971-484-1
DOI 10.3389/978-2-88971-484-1

About Frontiers

Frontiers is more than just an open-access publisher of scholarly articles: it is a pioneering approach to the world of academia, radically improving the way scholarly research is managed. The grand vision of Frontiers is a world where all people have an equal opportunity to seek, share and generate knowledge. Frontiers provides immediate and permanent online open access to all its publications, but this alone is not enough to realize our grand goals.

Frontiers Journal Series

The Frontiers Journal Series is a multi-tier and interdisciplinary set of open-access, online journals, promising a paradigm shift from the current review, selection and dissemination processes in academic publishing. All Frontiers journals are driven by researchers for researchers; therefore, they constitute a service to the scholarly community. At the same time, the Frontiers Journal Series operates on a revolutionary invention, the tiered publishing system, initially addressing specific communities of scholars, and gradually climbing up to broader public understanding, thus serving the interests of the lay society, too.

Dedication to Quality

Each Frontiers article is a landmark of the highest quality, thanks to genuinely collaborative interactions between authors and review editors, who include some of the world's best academicians. Research must be certified by peers before entering a stream of knowledge that may eventually reach the public - and shape society; therefore, Frontiers only applies the most rigorous and unbiased reviews.
Frontiers revolutionizes research publishing by freely delivering the most outstanding research, evaluated with no bias from both the academic and social point of view. By applying the most advanced information technologies, Frontiers is catapulting scholarly publishing into a new generation.

What are Frontiers Research Topics?

Frontiers Research Topics are very popular trademarks of the Frontiers Journals Series: they are collections of at least ten articles, all centered on a particular subject. With their unique mix of varied contributions from Original Research to Review Articles, Frontiers Research Topics unify the most influential researchers, the latest key findings and historical advances in a hot research area! Find out more on how to host your own Frontiers Research Topic or contribute to one as an author by contacting the Frontiers Editorial Office: frontiersin.org/about/contact

LIPID METABOLISM IN DEVELOPMENT AND ENVIRONMENTAL STRESS TOLERANCE FOR ENGINEERING AGRONOMIC TRAITS

Topic Editors:
Zhi-Yan (Rock) Du, University of Hawaii at Manoa, United States
Susanne Hoffmann-Benning, Michigan State University, United States
Agnieszka Zienkiewicz, Nicolaus Copernicus University in Toruń, Poland
Krzysztof Zienkiewicz, Nicolaus Copernicus University in Toruń, Poland
Shiwen Wang, Northwest A and F University, China
Lina Yin, Northwest A and F University, China

Citation: Du, Z.-Y., Hoffmann-Benning, S., Zienkiewicz, A., Zienkiewicz, K., Wang, S., Yin, L., eds. (2021). Lipid Metabolism in Development and Environmental Stress Tolerance for Engineering Agronomic Traits. Lausanne: Frontiers Media SA. doi: 10.3389/978-2-88971-484-1

Table of Contents

frontiers in Plant Science

EDITORIAL
published: 24 August 2021
doi: 10.3389/fpls.2021.739786

Editorial: Lipid Metabolism in Development and Environmental Stress Tolerance for Engineering Agronomic Traits

Zhi-Yan Du[1], Susanne Hoffmann-Benning[2], Shiwen Wang[3], Lina Yin[3], Agnieszka Zienkiewicz[4] and Krzysztof Zienkiewicz[4]*

[1] Department of Molecular Biosciences and Bioengineering, University of Hawaii at Manoa, Honolulu, HI, United States, [2] Department of Biochemistry and Molecular Biology, Michigan State University, East Lansing, MI, United States, [3] Institute of Soil and Water Conservation, Northwest A&F University, Yangling, China, [4] Centre for Modern Interdisciplinary Technologies, Nicolaus Copernicus University in Toruń, Toruń, Poland

Keywords: lipid biosynthesis and turnover, membrane and storage lipids, development, biotic and abiotic stress, genetic engineering

Editorial on the Research Topic

Lipid Metabolism in Development and Environmental Stress Tolerance for Engineering Agronomic Traits

OPEN ACCESS

Edited and reviewed by:
Xue-Rong Zhou, Agriculture and Food, Commonwealth Scientific and Industrial Research Organisation (CSIRO), Australia

****Correspondence:***
Zhi-Yan Du
duz@hawaii.edu

Specialty section:
This article was submitted to Plant Metabolism and Chemodiversity, a section of the journal Frontiers in Plant Science

Received: *12 July 2021*
Accepted: *26 July 2021*
Published: *24 August 2021*

Citation:
Du Z-Y, Hoffmann-Benning S, Wang S, Yin L, Zienkiewicz A and Zienkiewicz K (2021) Editorial: Lipid Metabolism in Development and Environmental Stress Tolerance for Engineering Agronomic Traits. Front. Plant Sci. 12:739786. doi: 10.3389/fpls.2021.739786

Lipids are the essential building blocks of cellular membranes, and they play fundamental roles in numerous biological activities such as photosynthesis, protection, environmental and cellular communication, and storage of carbon and energy. Lipid metabolism is a dynamic and complicated process that includes lipid biosynthesis, transport, accumulation, turnover, and excretion, acting to regulate plant development and tolerance to various environmental stresses. Understanding how lipid metabolism regulates the development and growth in response to adverse conditions raises many interesting questions. Communication between membrane and storage lipids has been observed during the progress, for example, membrane degradation accompanied by lipid droplet (LD) accumulation. Recently, autophagy has been connected with lipid metabolism in plants and algae under stress conditions (Zienkiewicz and Zienkiewicz). Because of the vital role of lipid metabolism in photosynthetic organisms, exploring lipid processes is very important for engineering crops to obtain better agronomic traits including productivity, nutrition, stress tolerance and resilience.

This Research Topic includes 10 original review and research articles, with a special focus on lipid metabolism in crops. The review by Zienkiewicz and Zienkiewicz summarizes the most recent advances on LD degradation, which is a key process for the release of triacylglycerol (TAG). As the major reservoir of cellular carbon and energy, TAG is packed in LD, a dynamic organelle at the center of cellular metabolism. The review also compares the LD degradation in plants and algae (**Figure 1A**). Looking at lipid metabolism in the context of membrane composition and transport, Salvaing et al. report the function of the Arabidopsis ALA10, a phospholipid flippase of the P_4 type-ATPase family, in reducing the 18:2 desaturation of phosphatidylcholine in the endoplasmic reticulum (ER), while Liao et al. show the roles of two rice acyl-CoA-binding proteins, OsACBP4 (plasma membrane and ER) and OsACBP5 (apoplast), in the intra- and extracellular transport of acyl-CoA esters, respectively (**Figure 1B**). Other contributions directly address the role of lipid

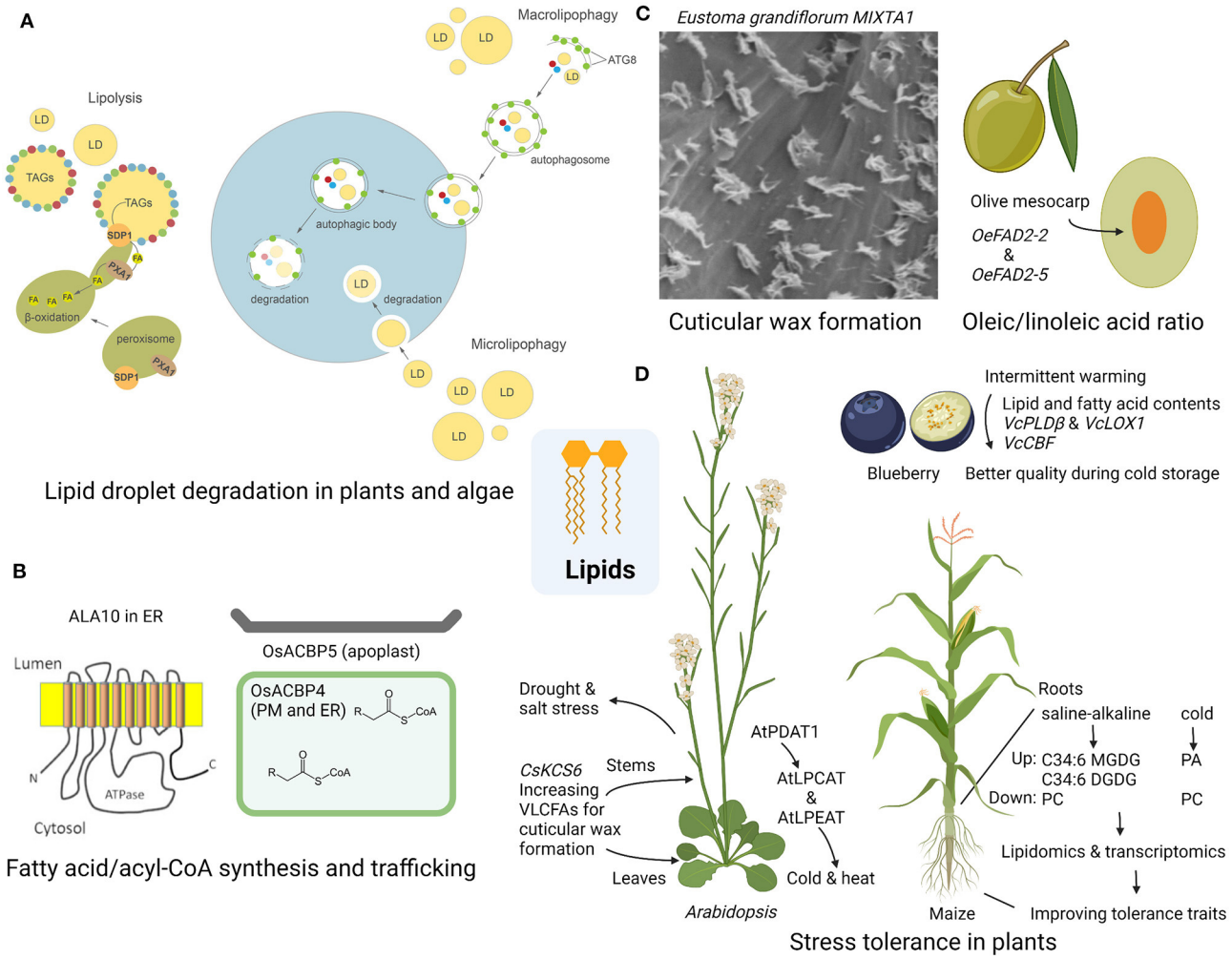

FIGURE 1 | Overview of the articles in this Research Topic. **(A)** Lipid droplet degradation in plants and algae (Zienkiewicz and Zienkiewicz). **(B)** Biosynthesis and trafficking of fatty acids (Salvaing et al.) and acyl-CoAs (Liao et al.). **(C)** Lipid metabolism in cuticular wax formation in *Eustoma grandiflorum* (Wang et al.) and fatty acid composition in olive mesocarps (Hernández et al.). **(D)** Understanding the lipid and fatty acid dynamics in different plants including *Arabidopsis* under drought-salt (Guo et al.) and cold stress (Demski et al.), blueberry fruit during cold storage (Dai et al.), and maize under saline-alkaline (Xu et al.) or cold stress (Zhao et al.).

metabolism during development, *EgMIXTA1*, an R2R3 MYB-type transcription factor, promotes the cuticular wax formation in *Eustoma grandiflorum* (lisianthus) leaves (Wang et al.); together with the specificities of extraplastidial acyltransferase enzymes, the olive *OeFAD2-2* and *OeFAD2-5* regulate the oleic/linoleic acid ratio in the mesocarp of olive cultivars (**Figure 1C**) (Hernández et al.). The Research Topic also highlights the significance of lipid metabolism in environmental stress response and tolerance (**Figure 1D**). In *Arabidopsis*, expression of *CsKCS6*, a gene coding the 3-Ketoacyl-CoA synthase (KCS) that catalyzes the biosynthesis of very-long-chain fatty acid (VLCFA) in *Citrus sinensis* (Newhall navel orange), reduces water loss and ion leakage and increases tolerance to drought and salt stress (Guo et al.); *Arabidopsis* phospholipid:diacylglycerol acyltransferase 1 (AtPDAT1) promotes the activities of acyl-CoA:lysophosphatidylcholine acyltransferase (LPCAT) and acylCoA:lysophosphatidylethanolamine acyltransferase (LPEAT) and improves resilience to heat and cold exposure (Demski et al.). In *Vaccinium corymbosum* L., cv. Duke (Duke blueberry), intermittent warming treatment of the fruit regulates its lipid metabolism such as increases in phosphatidylcholine, linoleic acid, and oleic acid, which enhances the low-temperature tolerance in the fruit (Dai et al.). In the roots of maize, integrated lipidomic and transcriptomic analyses reveal the membrane lipid remodeling and gene regulations under saline-alkaline (Xu et al.) or cold stress (Zhao et al.), which are applicable for engineering the crop for better performance under these stress conditions.

The collection of articles in this Research Topic demonstrates the significance of lipid metabolism in various biological processes and the findings will contribute to engineering agronomic traits of crops for the increasing demand for food and bioproducts.

AUTHOR CONTRIBUTIONS

All authors listed have made a substantial, direct and intellectual contribution to the work, and approved it for publication.

ACKNOWLEDGMENTS

The editors would like to thank all reviewers who evaluated manuscripts and contributors for this Research Topic. Research of the Topic Editors was supported by the funds from CTAHR (2303491) and OVCR, UHM (Z-YD), Natural Science Foundation of Shaanxi Province, China (2021JM-604) (LY), NSF (1841251) and USDA-NIMSS (NC-1203) (SH-B).

Conflict of Interest: The authors declare that the research was conducted in the absence of any commercial or financial relationships that could be construed as a potential conflict of interest.

Publisher's Note: All claims expressed in this article are solely those of the authors and do not necessarily represent those of their affiliated organizations, or those of the publisher, the editors and the reviewers. Any product that may be evaluated in this article, or claim that may be made by its manufacturer, is not guaranteed or endorsed by the publisher.

frontiers in Plant Science

ORIGINAL RESEARCH
published: 24 March 2020
doi: 10.3389/fpls.2020.00331

Subcellular Localization of Rice Acyl-CoA-Binding Proteins ACBP4 and ACBP5 Supports Their Non-redundant Roles in Lipid Metabolism

*Pan Liao[1,2], King Pong Leung[3], Shiu-Cheung Lung[1], Saritha Panthapulakkal Narayanan[1], Liwen Jiang[3] and Mee-Len Chye[1,2]**

[1] School of Biological Sciences, The University of Hong Kong, Pokfulam, China, [2] State Key Laboratory of Agrobiotechnology, CUHK, New Territories, China, [3] Centre for Cell and Development Biology and State Key Laboratory of Agrobiotechnology, School of Life Sciences, The Chinese University of Hong Kong, New Territories, China

OPEN ACCESS

Edited by:
Agnieszka Zienkiewicz, Nicolaus Copernicus University in Toruń, Poland

Reviewed by:
Enrique Martinez Force, Instituto de la Grasa (IG), Spain
Joaquín J. Salas, Instituto de la Grasa (IG), Spain

***Correspondence:**
Mee-Len Chye
mlchye@hku.hk

Specialty section:
This article was submitted to Plant Metabolism and Chemodiversity, a section of the journal Frontiers in Plant Science

Received: *03 January 2020*
Accepted: *05 March 2020*
Published: *24 March 2020*

Citation:
Liao P, Leung KP, Lung S-C, Panthapulakkal Narayanan S, Jiang L and Chye M-L (2020) Subcellular Localization of Rice Acyl-CoA-Binding Proteins ACBP4 and ACBP5 Supports Their Non-redundant Roles in Lipid Metabolism. Front. Plant Sci. 11:331. doi: 10.3389/fpls.2020.00331

Acyl-CoA-binding proteins (ACBPs), conserved at the acyl-CoA-binding domain, can bind acyl-CoA esters as well as transport them intracellularly. Six ACBPs co-exist in each model plant, dicot *Arabidopsis thaliana* (thale cress) and monocot *Oryza sativa* (rice). Although Arabidopsis ACBPs have been studied extensively, less is known about the rice ACBPs. *OsACBP4* is highly induced by salt treatment, but down-regulated following pathogen infection, while *OsACBP5* is up-regulated by both wounding and pathogen treatment. Their differential expression patterns under various stress treatments suggest that they may possess non-redundant functions. When expressed from the *CaMV35S* promoter, OsACBP4 and OsACBP5 were subcellularly localized to different endoplasmic reticulum (ER) domains in transgenic Arabidopsis. As these plants were not stress-treated, it remains to be determined if OsACBP subcellular localization would change following treatment. Given that the subcellular localization of proteins may not be reliable if not expressed in the native plant, this study addresses *OsACBP4:GFP* and *OsACBP5:DsRED* expression from their native promoters to verify their subcellular localization in transgenic rice. The results indicated that OsACBP4:GFP was targeted to the plasma membrane besides the ER, while OsACBP5:DsRED was localized at the apoplast, in contrast to their only localization at the ER in transgenic Arabidopsis. Differences in tagged-protein localization in transgenic Arabidopsis and rice imply that protein subcellular localization studies are best investigated in the native plant. Likely, initial targeting to the ER in a non-native plant could not be followed up properly to the final destination(s) unless it occurred in the native plant. Also, monocot (rice) protein targeting may not be optimally processed in a transgenic dicot (Arabidopsis), perhaps arising from the different processing systems for routing between them. Furthermore, changes in the subcellular localization of OsACBP4:GFP and OsACBP5:DsRED were not detectable following salt and pathogen treatment, respectively. These results

suggest that OsACBP4 is likely involved in the intracellular shuttling of acyl-CoA esters and/or other lipids between the plasma membrane and the ER, while OsACBP5 appears to participate in the extracellular transport of acyl-CoA esters and/or other lipids, suggesting that they are non-redundant proteins in lipid trafficking.

Keywords: acyl-CoA-binding protein, *Oryzae sativa*, pathogen treatment, salt treatment, subcellular localization

INTRODUCTION

During lipid biosynthesis and metabolism, lipids including acyl-CoA esters and their derivatives are transferred within and across subcellular compartments (Xiao and Chye, 2011a). The ATP-binding cassette (ABC) transporter proteins, lipid-transfer proteins (LTPs) and acyl-CoA-binding proteins (ACBPs) are candidates for facilitating lipid transfer in plants (Rea, 2007; Kang et al., 2011; Xiao and Chye, 2011a; Yurchenko et al., 2014). The ABC transporter proteins have been reported to participate in the transport of fatty acids, acyl-CoA esters, and wax/cutin components (Rea, 2007; Benning, 2009; Kang et al., 2011; Hurlock et al., 2014; Block and Jouhet, 2015; Fan et al., 2015; Hwang et al., 2016; Li-Beisson and Nakamura, 2016; Lefèvre and Boutry, 2018) while the LTPs have been reported to be involved in phospholipid and sulfolipid transfer between organelles (Kader et al., 1996; Kader, 1997; Jouhet et al., 2007; Liu et al., 2015). Previous reports on yeast and mammalian 10 kDa ACBPs have demonstrated their role in the trafficking of acyl-CoA esters within the cell, in maintaining an acyl-CoA pool and in glycerolipid biosynthesis (Schjerling et al., 1996; Knudsen et al., 2000; Faergeman and Knudsen, 2002). Our investigations on the six Arabidopsis ACBPs (AtACBPs) indicated their functions in maintaining an acyl-CoA pool and in glycerolipid biosynthesis, affecting plant development, stress responses, membrane biogenesis and signaling pathways (Xiao and Chye, 2011a; Du et al., 2016; Lung and Chye, 2016a, 2019; Lung et al., 2017, 2018; Chen et al., 2018; Hu et al., 2018). Furthermore, participation of AtACBPs in lipid trafficking based on their different subcellular localization has been proposed (Xiao and Chye, 2011a; Lung and Chye, 2016b). AtACBP2 and AtACBP3 were found to be non-redundant in Arabidopsis (Chye et al., 2000; Li and Chye, 2003; Chen et al., 2010; Gao et al., 2010) because AtACBP2 was localized at the plasma membrane (PM) and endoplasmic reticulum (ER) (Li and Chye, 2003) while AtACBP3 was targeted to the apoplast and is known to be a phloem-mobile protein (Zheng et al., 2012; Leung et al., 2006; Hu et al., 2018). Recombinant AtACBP2 has been observed to bind 18:1 phosphatidylcholine (PC) and 18:2 PC, lyso PC and several acyl-CoA esters (18:2 > 18:3 > 20:4∼16:0 > 18:1) *in vitro* (Chye et al., 2000; Chen et al., 2010; Gao et al., 2010). Together with AtACBP1, AtACBP2 was reported to play an important role in early embryogenesis, seed germination and seedling development (Chen et al., 2010; Du et al., 2013b). Furthermore, the overexpression of AtACBP2 protected transgenic Arabidopsis from drought stress (Du et al., 2013a). AtACBP2 is known to interact with its protein partners, LYSOPHOSPHOLIPASE2 (LYSOPL2) and a heavy-metal-binding farnesylated protein (FP6), via its ankyrin repeats and transgenic Arabidopsis overexpressing AtACBP2, AtLYSOPL2, or AtFP6 were more tolerant to oxidative (H_2O_2)- and cadmium-induced stress (Gao et al., 2009, 2010; Miao et al., 2019).

Recombinant AtACBP3 binds phospholipids PC and phosphatidylethanolamine (PE), polyunsaturated 20:4-CoA and unsaturated C18-CoA esters *in vitro* (Leung et al., 2006; Xiao et al., 2010; Hu et al., 2018). The overexpression of AtACBP3 accelerated starvation-induced and age-dependent leaf senescence (Xiao et al., 2010). Also, AtACBP3 was found to regulate autophagy-mediated leaf senescence by affecting the formation of ATG8-PE through interaction with PE (Xiao and Chye, 2010; Xiao et al., 2010). Transgenic Arabidopsis overexpressing AtACBP3 were upregulated in the expression of pathogenesis-related (PR) genes, displayed induced cell death that resulted in H_2O_2 and salicylic acid (SA) accumulation, and showed enhanced NON-EXPRESSOR OF PR GENES1 (NPR1)-dependent plant resistance to *Pseudomonas syringae* pv *tomato DC3000* (Xiao and Chye, 2011b), indicating a role of AtACBP3 in SA-dependent plant defense signaling. Microarray data on AtACBP3-overexpressors further confirmed AtACBP3 function in plant defense because many biotic and abiotic stress-related genes including *PR1*, *PR2,* and *PR5* were upregulated (Xiao and Chye, 2011b). More recently, AtACBP3 was reported to be involved in response to hypoxia by regulating very-long-chain fatty acid metabolism (Xie et al., 2015). The enhanced hypoxic tolerance in AtACBP3-overexpressors was dependent on NPR1 and CONSTITUTIVE TRIPLE RESPONSE1 (CTR1)-associated signaling pathways (Xie et al., 2015).

In the monocot *Oryza sativa* (rice), six ACBPs co-exist as in Arabidopsis (Meng et al., 2011). OsACBP1 and OsACBP2 were localized to the cytosol, while OsACBP3 was located in the cytosol and membranous structures (Meng et al., 2014). OsACBP4 and OsACBP5 were targeted to the ER (Meng et al., 2014; Meng and Chye, 2014), and OsACBP6 to the peroxisome (Meng et al., 2014). Although both GFP-tagged OsACBP4 and OsACBP5 were detected at ER-derived spherical structures and membranes of ER bodies in transgenic *OsACBP4:GFP* and *OsACBP5:GFP* Arabidopsis in which the reported fusions were driven by the *CaMV35S* promoter, only OsACBP4:GFP was observed in the central ER cisternae (Meng and Chye, 2014). Recombinant OsACBP4 was reported to bind PA (16:0, 18:0, 18:1), PC (18:0, 18:1, 18:2) and acyl-CoA esters (18:2 > 16:0 > 18:3) (Meng et al., 2011; Meng, 2012). Recombinant OsACBP5 was also shown to bind PA (18:0, 18:1), PC (18:0, 18:1, 18:2) and acyl-CoA esters (18:3 > 16:0) (Meng et al., 2011; Meng, 2012).

Upon abiotic stress treatment including salt and drought, the unfolded protein response (UPR) or NPR1 signaling pathway is triggered to protect cells (Wang et al., 2005; Srivastava et al., 2013, and references cited therein), and lipid compositional changes

occur rapidly and dynamically as a consequence (Wang, 2004; Chen et al., 2008; Du Z.-Y. et al., 2010; Xiao and Chye, 2011b; Liao et al., 2014a). While *OsACBP4* was highly induced by salt treatment, it was down-regulated following pathogen infection (Meng et al., 2011). In contrast, the expression of *OsACBP5* was up-regulated by both wounding and pathogen treatment (Meng et al., 2011). The differential subcellular expression patterns of *OsACBP4* and *OsACBP5* under these various stress treatments suggest that they may possess different functions. Although the subcellular localization of OsACBP4 and OsACBP5 had been previously investigated in transgenic *35S:OsACBP4:GFP* and *35S:OsACBP5:GFP* Arabidopsis, the plants were not subjected to any stress treatment (Meng et al., 2014; Meng and Chye, 2014). Interestingly OsACBP4 and OsACBP5 are classified into different ACBP classes consistent with their proposed variation in subcellular function (Meng et al., 2011). OsACBP4, the homolog of AtACBP2, is in class II, while OsACBP5, the homolog of AtACBP3, belongs to class III (Meng et al., 2011; Du et al., 2016). Given that the subcellular localization of proteins may not be reliable if they are not expressed in the native plant (Tian et al., 2004; Zhang et al., 2011; Bu et al., 2014), further investigations were carried out herein to study the subcellular localization of OsACBP4 and OsACBP5 using their native promoters in *OsACBP4promoter:OsACBP4:GFP* and *OsACBP5promoter:OsACBP5:DsRED* fusions expressed in stably-transformed rice. In this study, we demonstrated that OsACBP4:GFP was targeted to the PM besides the ER, while OsACBP5 was localized at the apoplast. Furthermore, changes in the subcellular localization of OsACBP4:GFP and OsACBP5:DsRED were not obvious under salt and pathogen treatment, respectively. These results suggest that OsACBP4 is involved in the intracellular transport of acyl-CoA esters and/or other lipids between the plasma membrane and the ER, while OsACBP5 appears to participate in the extracellular transport of acyl-CoA esters and/or other lipids. This study suggests that OsACBP4 and OsACBP5 are non-redundant proteins in lipid metabolism and provides clues on their functional localization in rice, a crop plant.

MATERIALS AND METHODS

Plant Material and Growth Conditions

Japonica rice (*Oryza sativa* cv Zhonghua11) was used in this study. Seeds of wild-type (WT) and transgenic rice were surface-sterilized with 75% ethanol for 1 min, soaked in 25% sodium hypochlorite for 20 min, rinsed four times in sterilized water, and germinated on half-strength Murashige and Skoog (1/2MS) medium, with and without 50 $\mu g\ ml^{-1}$ hygromycin. Rice seeds and seedlings were grown in magenta GA-7 plant tissue culture boxes at 25°C (16 h light)/22°C (8 h dark).

Stress Treatments

Four-, seven-, and fourteen-day-old seedlings were subjected to abiotic or biotic stress treatments. Salt treatment was performed as previously described (Meng et al., 2011) with a minor modification. Briefly, to test the expression of *OsACBP4* after salt treatment, the roots of 7- and 14-day-old WT seedlings were submerged in 200 mM sodium chloride (NaCl) solution, or distilled water as controls, and WT root samples were collected at 0, 6, 12, 24, and 48 h after treatment for RNA extraction (Islam et al., 2009). To test the subcellular localization of OsACBP4 after salt treatment, the roots of 4-day-old seedlings of three independent transgenic *OsACBP4promoter:OsACBP4:GFP*-DX2181 lines (876-5, 876-7, and 876-11) were similarly treated for 24 h before confocal laser-scanning microscopy.

For pathogen treatment, *Rhizoctonia solani* AG-1-1 (ATCC 66157), which causes sheath blight in rice, was used. *R. solani* was inoculated as previously reported (Panthapulakkal Narayanan et al., 2019). To test *OsACBP5* expression after pathogen treatment, 7- and 14-day-old WT seedlings were transferred to fresh Petri dishes containing filter paper wetted with 1 ml of sterilized water. Subsequently, infection was performed by inoculating *R. solani* agar plugs on roots. WT root samples were collected at 0, 6, 12, 18, 24, and 48 h after treatment for RNA extraction. To test the subcellular localization of OsACBP5 after pathogen treatment, 4-day-old rice seedlings of three independent transgenic *OsACBP5promoter:OsACBP5:DsRED* lines (927-9, 927-19, and 927-26) were transferred to fresh Petri dishes and infected for 18 h, using rice roots without infection as controls. Rice roots 18 h post-inoculation (hpi) were used in confocal laser-scanning microscopy. All these experiments were performed independently three times. For the plasmolysis experiments, the roots of 4-day-old seedlings were treated with 0.8 M mannitol for 2 h with shaking (Zhang et al., 2012).

Construction of Plasmids and Rice Transformation

The *OsACBP4promoter*-DX2181 construct was generated by inserting a 1.2 kb *Sal*I-*Hin*dIII 5′-flanking region of *OsACBP4* amplified by primers ML2465/ML2823 from rice Zhonghua11 (ZH11), into pGEM-T Easy vector (Promega) and cloning this 1.2 kb *OsACBP4pro* fragment into their corresponding sites in binary vector DX2181 (Du H. et al., 2010) to obtain plasmid pOS917. Then a 1.71 kb *Hin*dIII-*Bst*EII fragment of *OsACBP4* coding sequence (CDS) (without its stop codon) fused with GFP was amplified from pOS871 using ML2824/ML2825, inserted into pGEM-T Easy vector (Promega) and cloned into their corresponding sites in pOS917 to obtain plasmid pOS876 (*OsACBP4promoter:OsACBP4:GFP*-DX2181).

To obtain a construct of *OsACBP5promoter:OsACBP5:DsRED*-DX2181, a 2.2 kb *Hin*dIII-*Bam*HI fragment of the *OsACBP5* promoter was amplified by primers ML2470/ML2473 from rice ZH11, inserted into pGEM-T Easy vector (Promega), and cloned into the same sites of the DX2181 vector to form construct pOS820. The 1.71 kb *Bam*HI-*Xba*I fragment of the *OsACBP5 CDS* without its stop codon was amplified using ML2982/ML2983 from pOS581 (Meng et al., 2014) and cloned into pGEM-T Easy vector (Promega) to generate construct pOS924. The 0.69 kb *Xba*I-*Sac*I fragment of *DsRED* was amplified from pGDR plasmid using ML2984/ML2985 and cloned into pGEM-T Easy vector (Promega) and cloned into the same sites of

pOS924 to generate construct pOS926. Finally, the 2.4 kb *Bam*HI-*Sac*I fragment of the *OsACBP5* CDS without its stop codon fused with DsRED was excised from vector pOS926 and cloned into the same sites of vector pOS820 to form construct pOS927 (*OsACBP5promoter:OsACBP5:DsRED*-DX2181). DNA sequence analysis was performed to confirm the PCR fragments and inserts in all intermediate and final constructs.

Generation and Molecular Analyses of Transgenic Rice Lines

The final pOS876 and pOS927 constructs were sent to BioRun[1] (Wuhan, China) for rice ZH11 transformation as described previously (Guo et al., 2019). The transformed T_0 seeds were screened on MS medium containing 50 μg ml^{-1} hygromycin and the resistant transformants were further verified by polymerase chain reaction (PCR) (**Supplementary Figures S1A, S3A**), quantitative reverse transcription PCR (qRT-PCR) (**Supplementary Figures S1B, S3B**) and western blot analysis (**Supplementary Figures S1C, S3C**) using rabbit polyclonal anti-GFP or anti-Red fluorescent proteins (RFP) antibodies. Putative transgenic rice *OsACBP4promoter:OsACBP4:GFP*-DX2181 and *OsACBP5promoter:OsACBP5:DsRED*-DX2181 lines were designated as lines 876 and 927, respectively. Finally, three lines with relatively high expression of OsACBP4 (876-5, 876-7 and 876-11) or OsACBP5 (927-9, 927-19 and 927-26), respectively, in mRNA and protein levels, as well as enough seeds were selected from each construct for subsequent analyses.

Polymerase Chain Reaction (PCR)

To screen transgenic rice *OsACBP4promoter:OsACBP4:GFP*-DX2181 and *OsACBP5promoter:OsACBP5:DsRED*-DX2181 lines, PCR was conducted using a gene-specific forward primer in the *OsACBP4* CDS (ML1060) with a reverse primer in *GFP* (ML2825), or a gene-specific forward primer in *OsACBP5* CDS (ML1111) with a reverse primer in DsRED (ML2985), respectively. The conditions for PCR were as follows: 94°C held for 5 min, followed by 35 cycles of 94°C for 30 S, 57°C for 30 S, and 72°C for 1 min, and a final extension at 72°C for 10 min.

Quantitative Reverse Transcription PCR (qRT-PCR)

Total RNA from 1-, 2-, and 3-week-old old rice seedlings grown under normal condition, and after salt or pathogen treatments, were extracted with the RNeasy Plant Mini Kit (Qiagen, Hilden, Germany). The RNA (2 μg) was treated by DNase I (Qiagen) before reverse-transcription to first-strand cDNA using the EvoScript Universal cDNA Master Kit (Roche, Mannheim, Germany). Quantitative reverse transcription PCR (qRT-PCR) was performed with FastStart Universal SYBR Green Master Kit (Roche, Mannheim, Germany) on a StepOne Plus Real-time PCR System (Applied Biosystems, Foster City, CA, United States). The conditions for qRT-PCR were as follows: denaturation at 95°C for 10 min, followed by 40 cycles of 95°C for 15 s and 60°C for 30 s (Liao et al., 2019). Three experimental replicates for each reaction were carried out using *OsACBP4* or *OsACBP5* gene-specific primers (ML1109/ML1110 for *OsACBP4* and ML1111/ML1112 for *OsACBP5*), and the rice *ACTIN* (ML1115/ML1116) was used as an internal control. The qRT-PCR data were analyzed by the $2^{-\Delta\Delta Ct}$ method (Schmittgen and Livak, 2008). The relative expression was normalized to *OsACTIN*, and the relative mRNA levels in each transgenic rice line and the empty vector control were analyzed using data from three independent experiments. Significant differences between various samples were analyzed by the Student's *t*-test. Primers for qRT-PCR are shown in **Supplementary Table S1**.

Western Blot Analysis

Rice total protein was extracted (Chye et al., 1999; Liao et al., 2014b) from 1-week-old fresh rice leaves and protein concentration was measured by the Bradford assay (Bradford, 1976). Proteins (20 μg) were resolved on 10% SDS-PAGE and transferred to polyvinylidene difluoride membranes (Pall). Western blot analysis was performed as described previously (Lung et al., 2017; Liao et al., 2018). The blots were cross-reacted with rabbit polyclonal anti-GFP (1: 5000, A6455; Invitrogen) for *OsACBP4promoter:OsACBP4:GFP* transgenic lines or rabbit polyclonal anti-RFP (1:7000, R10367; Invitrogen) for *OsACBP5promoter:OsACBP5:DsRED* transgenic lines at 4°C overnight, followed by incubation with horseradish peroxidase-conjugated anti-rabbit secondary antibodies (1:50,000; Sigma-Aldrich) at room temperature for 1 h. Cross-reacting bands were detected by the Amersham ECL Prime Detection Reagent (GE Healthcare).

Confocal Laser-Scanning Microscopy

Four-day-old transgenic rice roots under different treatments were examined with a Zeiss LSM710 NLO confocal laser scanning microscope with a 63 × oil lens following Lung et al. (2017) or a Leica SP8 confocal microscope equipped with a 63 × water lens. Fluorescent signals were detected using the following excitation and emission wavelengths: GFP (488 nm/495–545 nm), DsRED (552 nm/560–660 nm), ER-Tracker (594 nm/615 nm), FM 4–64 (488 nm/560–660 nm), 4',6-diamidino-2-phenylindole (DAPI) (405 nm/410–480 nm). Images were processed using ZEN or LAS X software. For colocalization with an ER marker, 4-day-old seedlings were vacuum infiltrated with the ER-Tracker Red dye (1 μM, Invitrogen, E34250) for 30 min before two 5 min washes in distilled, deionized water (Lung et al., 2018). For colocalization with a PM marker, 4-day-old seedlings were incubated with the FM 4–64 dye (6 μM, Invitrogen, T13320) for 2 min. For colocalization with DAPI, 4-day-old seedlings were vacuum infiltrated with the DAPI dye (10 μg ml^{-1}, Roche, 10236276001) for 15 min (Schoor et al., 2015).

Statistical Analysis

Significant differences in gene expression of *OsACBP4* or *OsACBP5* between different samples were analyzed by the Student's *t*-test.

[1]http://www.biorun.net

RESULTS

OsACBP4 and *OsACBP5* Are Stress Responsive in Rice Roots

Results from qRT-PCR on 7- and 14-day-old rice roots indicated that *OsACBP4* was induced by salt treatment and *OsACBP5* activated by *R. solani* (**Figures 1A–D**). In 7-day-old roots, *OsACBP4* was induced at 12 h after salt treatment and its expression remained at relatively high levels from 24 h to 48 h (**Figure 1A**). In 14-day-old roots, *OsACBP4* peaked at 6 h and its expression maintained at relatively high levels from 12 to 48 h (**Figure 1B**). *OsACBP5* expression gradually increased from 6 to 18 h after *R. solani* treatment and then decreased, but was retained above their corresponding controls from 24 to 48 h in 7- and 14-day-old roots (**Figures 1C,D**). These results on salt and pathogen (*R. solani*) induction of expression led us to test the subcellular localization of OsACBP4 and OsACBP5 in young rice roots.

Localization of OsACBP4:GFP in the Plasma Membrane (PM) and ER in Rice Roots

The presence of the *OsACBP4:GFP* transgene in rice was verified by PCR (**Supplementary Figure S1A**), qRT-PCR (**Supplementary Figure S1B**), and western blot analyses (**Supplementary Figure S1C**). When the localization of OsACBP4:GFP was investigated in 4-day-old *OsACBP4promoter:OsACBP4:GFP* transgenic rice roots, the results indicated that OsACBP4:GFP signals were localized at the central cisternal ER (red arrows), the perinuclear ER (white arrows) and the PM or cell wall (**Figure 2A**). The ER localization of OsACBP4:GFP was further confirmed by its colocalization with the ER marker (**Figure 2B**). When OsACBP4 was further checked for its localization at the PM or cell wall by using 4-day-old *OsACBP4promoter:OsACBP4:GFP* transgenic rice seedlings subjected to cell plasmolysis under mannitol treatment, the results showed that the OsACBP4:GFP (green) signals colocalized with the membrane marker FM 4-64 (red) at the PM in rice root cells (**Figure 3**). These results demonstrated that OsACBP4 not only localized at the ER, but also at the PM. However, no changes in the localization of OsACBP4 were noted after salt treatment in rice roots (**Supplementary Figure S2**).

Localization of OsACBP5:DsRED in the Apoplast in Rice Roots

The presence of the *OsACBP5:DsRED* transgene in rice was verified by PCR (**Supplementary Figure S3A**), qRT-PCR (**Supplementary Figure S3B**), and western blot analyses (**Supplementary Figure S3C**). When the localization of OsACBP5:DsRED was investigated in 4-day-old *OsACBP5promoter:OsACBP5:DsRED* transgenic rice roots, the results showed that signals were localized in either the PM or the apoplast (**Figure 4A**). Given that DAPI cannot penetrate live cells effectively, it was used as cell wall/extracellular space stain, the results indicated that OsACBP5:DsRED signals colocalized with DAPI in rice roots, suggesting that OsACBP5 is localized at the cell wall or extracellular space (**Figure 4B**). When the localization of OsACBP5 was further addressed by using 4-day-old *OsACBP5promoter:OsACBP5:DsRED* transgenic rice seedlings under mannitol treatment to induce plasmolysis, the results showed that OsACBP5:DsRED signals were maintained at the apoplast in rice root cells (**Figure 4C**). However, no differences in localization of OsACBP5 were noted after pathogen treatment and plasmolysis in rice roots (**Figure 4D**).

DISCUSSION

OsACBP4- and OsACBP5-Tagged Proteins Are Localized Differentially in Transgenic Rice Roots

In contrast to previous observations in transgenic Arabidopsis root cells that OsACBP4 and OsACBP5, when regulated from the *CaMV35S* promoter, were localized to different ER domains (Meng and Chye, 2014), the results herein using transgenic rice indicated that OsACBP4 expressed from its native promoter was targeted to the ER and PM, while OsACBP5 was directed to the apoplast of root cells. Given the waxy structure in rice tissues such as leaves, it was difficult to observe the subcellular localization of proteins in rice leaves by a fluorescence microscope (Zhang et al., 2011), hence root cells were used instead. Although rice protoplasts have been more frequently used for subcellular localization assays of rice proteins (Zhang et al., 2011; Kim et al., 2012, 2015; Zhou et al., 2018), it is not suitable for proteins that are targeted to the extracellular space and would not be applicable for testing whether a protein is delivered to the PM or cell wall. Rice root cells, that have been successfully applied for subcellular localization assays of rice protein localization (Zhang et al., 2012; Chu et al., 2018), were successfully used in this study to overcome the limitations imposed by the use of rice protoplasts. The apoplastic localization of OsACBP5 is further supported by the predicted signal peptide of OsACBP5 by iPSORT and the secretory pathway predicted by TargetP1.1 (Meng et al., 2014). It is interesting to note that the localization of OsACBP4 at the PM and ER is consistent with the results reported for its homolog, AtACBP2 in Arabidopsis (Li and Chye, 2003).

When AtACBP2:GFP fusion protein was transiently expressed from the *CaMV35S* promoter in onion epidermal cells by particle gene bombardment, signals were observed at the PM and the ER (Li and Chye, 2003). The PM localization of AtACBP2 was further confirmed by examination of confocal images of bombarded onion epidermal cells subjected to plasmolysis (Li and Chye, 2003). Furthermore, the transmembrane domain of AtACBP2 was found essential in membrane targeting because the removal of this domain impaired membrane localization (Li and Chye, 2003). Conversely, the apoplast localization for OsACBP5 was consistent with the results on the localization for its homolog in Arabidopsis, AtACBP3 (Leung et al., 2006). When AtACBP3:DsRED fusion proteins were transiently expressed in onion epidermal cells and tobacco BY-2 cells from the

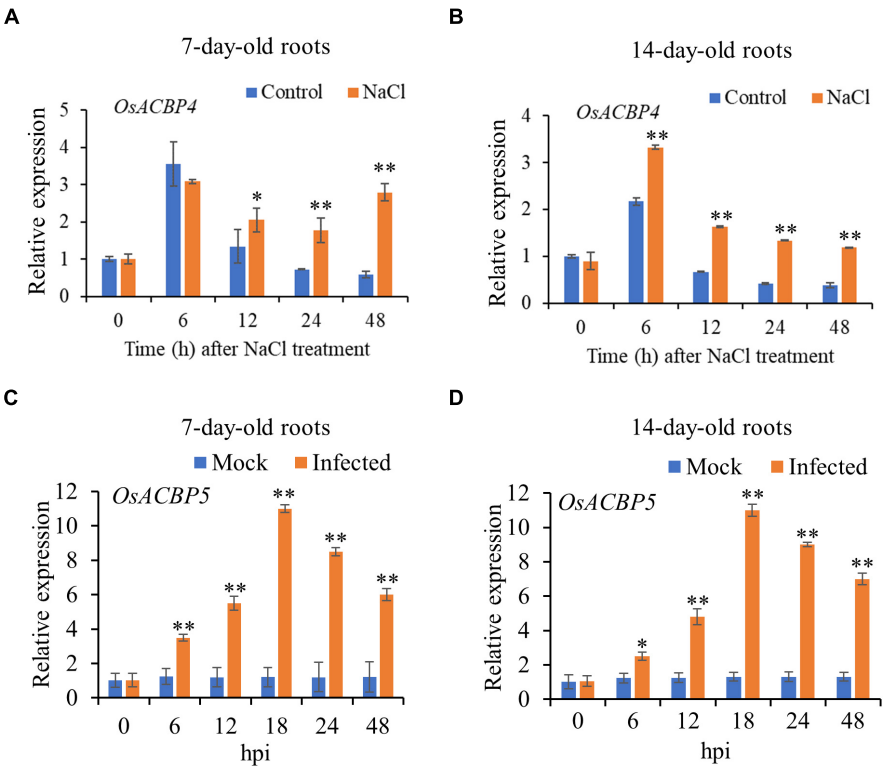

FIGURE 1 | Expression of *OsACBP4* and *OsACBP5* after stress treatment in wild-type (WT) rice roots. **(A)** *OsACBP4* expression in 7-day-old NaCl-treated roots; **(B)** *OsACBP4* expression in 14-day-old NaCl-treated roots; **(C)** *OsACBP5* expression in 7-day-old *Rhizoctonia solani*-treated roots; **(D)** *OsACBP5* expression in 14-day-old *R. solani*-treated roots. Total RNA was extracted from 7- and 14-day-old rice after NaCl treatment or after *R. solani* treatment at 0, 6, 12, 18, 24, and 48 h. Data are means ± SD of three independent replicates. Asterisks indicate a significant difference between the treatments and controls (*$P < 0.05$; **$P < 0.01$ by Student's *t*-test). hpi, hours post infection.

CaMV35S promoter following particle gene bombardment, signals were observed at the cell periphery (Leung et al., 2006). The extracellular localization of AtACBP3 was further verified by confocal microscopy of bombarded onion epidermal cells following plasmolysis (Leung et al., 2006). Differences in tagged-protein localization in transgenic Arabidopsis and rice imply that variation in protein subcellular localization may exist between host plants, particularly between dicots and monocots, and studies would be best investigated in the native plant. Monocot (rice) protein targeting may not be optimally processed in a transgenic dicot (Arabidopsis), perhaps arising from the different processing systems for routing between them. Likely, initial targeting to the ER in a non-native plant could not be followed up to the final destination, be it the PM or apoplast, unless it happened in the native plant.

Indeed, differences in targeting had previously been noted to occur between native and non-native plants (Leung et al., 2006; Xiao et al., 2010). For example, the homolog of OsACBP5, AtACBP3, was reported to be localized to the apoplast when a partial AtACBP3:DsRED fusion (consisting of the first 337 of 362 amino acids of AtACBP3 and lacking the acyl-CoA-binding domain) was transiently expressed in onion epidermal cells and tobacco BY-2 cells (Leung et al., 2006) in contrast to multiple signals during stable expression of AtACBP3:GFP in transgenic Arabidopsis (Xiao et al., 2010). The full-length AtACBP3:GFP when stably expressed in native Arabidopsis was targeted to the extracellular space, intracellular membranes and the ER/Golgi complex (Xiao et al., 2010). Although the results in transient expression suggested that the AtACBP3 signal sequence/transmembrane domain is deemed necessary in AtACBP3 targeting, the multiple localization of AtACBP3 in transgenic Arabidopsis indicates that other factors account for an accurate complete routing in the native plant. Some studies reported that fluorescent protein tags can affect localization results when they fused to different positions (N- or C-terminal) of a protein of interest (Snapp, 2005; Gao et al., 2012; Tanz et al., 2013). For example, GFP-ENDOMEMBRANE PROTEIN12 (EMP12) fusion was targeted to the Golgi apparatus in transgenic Arabidopsis, while EMP12-GFP fusion was localized to post-Golgi compartments and vacuoles (Tanz et al., 2013). It should be noted that GFP or DsRED was similarly fused to the C-terminal of OsACBP4 and OsACBP5 in transgenic Arabidopsis (Meng et al., 2014) and in transgenic rice in this study. Therefore, localization results obtained in this work should not be caused by the effect of differential positions of fluorescent protein tags. However, the subcellular localization of OsACBP4 and OsACBP5 when fluorescent protein tags are fused to their

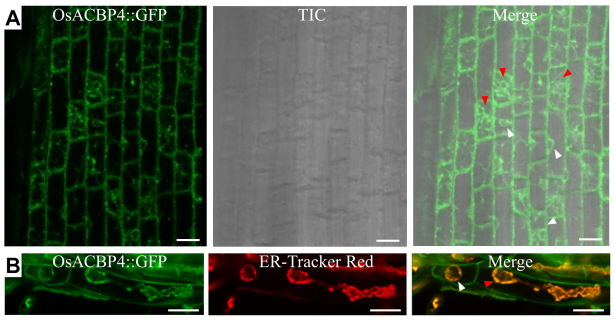

FIGURE 2 | Subcellular localization of OsACBP4:GFP in transgenic rice. **(A)** Root cells of 4-day-old transgenic rice seedlings were imaged by confocal laser scanning microscopy. Signals were detected at the central cisternal ER (red arrow), the perinuclear ER (white arrow) and plasma membrane or cell wall. **(B)** Colocalization of OsACBP4:GFP (green) with ER-Tracker Red (red) (E34250, Invitrogen) in root cells of 4-day-old transgenic rice seedlings. Signals were colocalized at the central cisternal ER (red arrows), the perinuclear ER (white arrows) and plasma membrane or cell wall. Bars = 20 μm. ACBP, acyl-CoA-binding protein; ER, endoplasmic reticulum; Os, *Oryza sativa*. Representative images were shown after observation with consistent results from at least 20 cells in **(A)** for central cisternal ER and perinuclear ER and in **(B)** for cisternal ER. Representative images were shown after observation with consistent results from at least 6 cells for perinuclear ER in **(B)**.

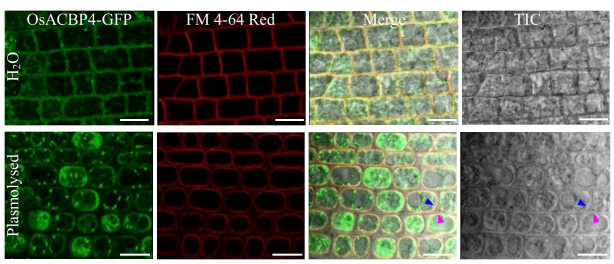

FIGURE 3 | Subcellular localization of OsACBP4:GFP in transgenic rice after plasmolysis. Root cells of 4-day-old transgenic rice seedlings were imaged by confocal laser scanning microscopy. Colocalization of OsACBP4:GFP (green) with FM 4–64 Red (red) (T13320, Invitrogen) in root cells of 4-day-old transgenic rice seedlings. Blue arrow indicates the plasma membrane and pink arrow shows the cell wall. Signals were colocalized at the plasma membrane but not the cell wall. Bars = 20 μm. ACBP, acyl-CoA-binding protein; Os, *Oryza sativa*. Representative images were shown after observation with consistent results from at least 20 cells.

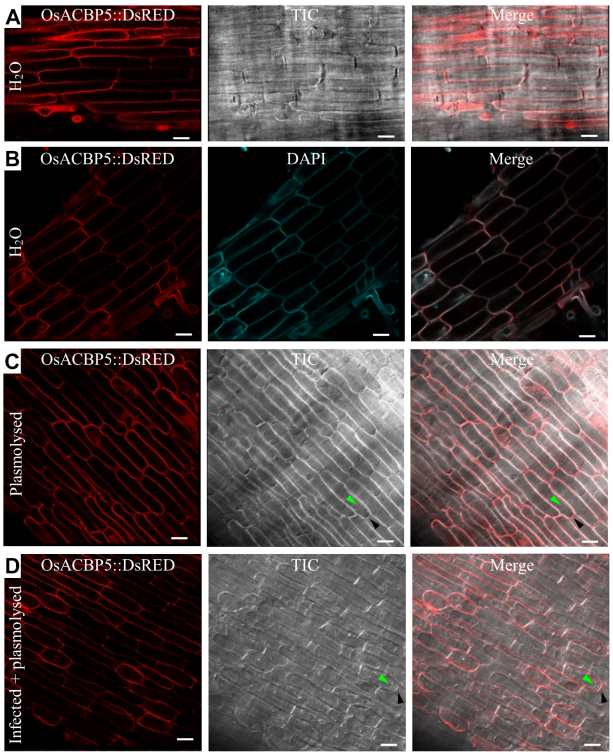

FIGURE 4 | Subcellular localization of OsACBP5:DsRED in transgenic rice after plasmolysis and *Rhizoctonia solani* infection. Root cells of 4-day-old transgenic rice seedlings were imaged by confocal laser scanning microscopy. **(A)** Signals of OsACBP5:DsRED were detected at plasma membrane or cell wall when incubated in water. **(B)** Colocalization of OsACBP5:DsRED (red) with 4′,6-diamidine-2′-phenylindole dihydrochloride (DAPI) (blue) (10236276001, Roche) at cell wall in root cells of 4-day-old transgenic rice seedlings when incubated in water. As DAPI cannot penetrate the live cell, it was used as a cell wall/extracellular space stain here. **(C)** Signals of OsACBP5:DsRED were detected at cell wall in root cells of 4-day-old transgenic rice seedlings after plasmolysis. **(D)** Signals of OsACBP5:DsRED were detected at cell wall in root cells of 4-day-old transgenic rice seedlings after infection and plasmolysis. Green arrow indicates plasma membrane and black arrow shows cell wall. Bars = 20 μm. ACBP, acyl-CoA-binding protein; Os, *Oryza sativa*. Representative images are presented following observation with consistent results from at least 20 cells.

N-terminal remains to be determined. Taken together, these results suggest that the subcellular localization of rice ACBPs and Arabidopsis ACBPs is conserved when investigated in the respective native plant, and reinforce a need for investigations on the subcellular localization of proteins in the original organism. This study also confirmed that OsACBP4 and OsACBP5 are non-redundant proteins in plant lipid metabolism. To better understand their functions in rice, it would be interesting to investigate the effects of OsACBP4 and OsACBP5 on the composition of acyl-CoA pools, fatty acids and membrane lipids in the near future.

OsACBP4 for Intracellular Transport of Acyl-CoA While OsACBP5 Is a Defense-Related Extracellular Protein

The subcellular localization results from this work together with the binding properties of recombinant OsACBP4 and OsACBP5 to lipids and acyl-CoA esters (Meng et al., 2011; Meng, 2012) suggest that OsACBP4 is likely involved in the intracellular transport of acyl-CoA esters and/or lipids between the PM and ER, while OsACBP5 participates in the extracellular transport of acyl-CoA esters and/or lipids. The dual localization intracellularly of an ACBP has been previously observed in mammalian cells (Hansen et al., 2008). The cellular localization of an ACBP using microinjection of fluorescently labeled bovine L-ACBP (FACI-50) in living HeLa and bovine mammary gland

epithelial cells revealed its co-localization to the ER and Golgi, and the depletion of fatty acids from cells significantly reduced FACI-50 association with the Golgi, while an overload of fatty acids enhanced Golgi-association (Hansen et al., 2008), suggesting that this ACBP, proposed to be involved in vesicular trafficking, localizes to the ER and the Golgi in a ligand-dependent manner. In comparison, the relationship between the subcellular distribution of OsACBP4 with the availability of ligands needs to be explored, but such studies involving intracellular lipids would be complex given their dynamics *in planta*.

The localization of AtACBP2, the homolog of OsACBP4, to the PM and ER further supports AtACBP2 function in protection against heavy metal and oxidative stresses, as demonstrated by the overexpression of AtACBP2 or its PM-localized protein interactors (AtFP6 and AtLYSOPL2), under the regulation of the *CaMV35S* promoter in transgenic Arabidopsis (Gao et al., 2009, 2010). AtACBP2-, AtFP6-, or AtLYSOPL2-overexpressors were more tolerant to cadmium (Cd) and hydrogen peroxide (H_2O_2) than the WT (Gao et al., 2009, 2010). Recombinant $(His)_6$-AtACBP2 was found to bind linoleoyl-CoA and linolenoyl-CoA esters which represent two precursors implicated in the repair of the phospholipid membrane and heavy metals, suggesting that AtACBP2 is involved in membrane biogenesis and protection of lipid membrane through binding to AtFP6, heavy metals and acyl-CoA esters (Gao et al., 2009, 2010). Recombinant AtACBP2 was also reported to bind lysoPC, implying that AtACBP2 also protects lipid membranes through interaction with AtLYSOPL2 and lysoPC (Gao et al., 2010; Miao et al., 2019). Furthermore, *AtACBP2pro:GUS* was expressed in embryos and guard cells in relation to *AtACBP2* function in abscisic acid (ABA) induction and drought response (Du et al., 2013a). AtACBP2-overexpressors showed enhanced drought tolerance and ABA-mediated reactive oxygen species production in the guard cells, thereby promoting stomatal closure, decreasing water loss and improving drought tolerance (Du et al., 2013a). Interestingly, *OsACBP4* has also been observed to be induced by drought treatment (Meng et al., 2014), and it remains to be tested as to whether *OsACBP4* overexpression in rice would confer drought tolerance.

The apoplast localization of OsACBP5 coincides well with its function against plant pathogens as demonstrated recently in transgenic Arabidopsis overexpressing *OsACBP5* from the *CaMV35S* promoter (Panthapulakkal Narayanan et al., 2019). OsACBP5-overexpressors showed broad-spectrum protection against plant pathogens and were more tolerant to the bacterial biotroph *P. syringae*, fungal necrotrophs (*R. solani*, *Botrytis cinereal*, *Alternaria brassicicola*) and a hemibiotroph (*Colletotrichum siamense*) than the WT and vector-transformed controls (Panthapulakkal Narayanan et al., 2019). Proteomics analysis of *R. solani*-infected Arabidopsis OsACBP5-overexpressors identified some biotic stress-related proteins including four cell wall-associated proteins, whose expression was induced after *R. solani* infection (Panthapulakkal Narayanan et al., 2019). It would be interesting to investigate if any interaction occurs between these cell wall-associated proteins and the apoplast-targeted OsACBP5 in protection of transgenic Arabidopsis. Consistently, transgenic Arabidopsis overexpressing the Arabidopsis homolog of OsACBP5, AtACBP3, had shown enhanced NPR1-dependent plant resistance against the bacterial pathogen *Pseudomonas syringae* pv *tomato* DC3000 (Xiao and Chye, 2011b). Furthermore, AtACBP3 was reported to be a phloem-mobile protein that was detected in WT Arabidopsis phloem exudates by western blot analysis and was targeted to the extracellular space as observed under immunoelectron microscopy (Hu et al., 2018). Similar to *OsACBP5* (Meng et al., 2011), *AtACBP3* expression was induced by wounding and the *atacbp3* mutant was less responsive to wounding in both local and distal leaves (Hu et al., 2018). Furthermore, GC-MS analysis showed that the levels of defense-related fatty acids such as C18:2-FA and C18:3-FA and methyl jasmonate were reduced in *atacbp3* and *AtACBP3*-RNAi in comparison to the WT (Hu et al., 2018). Subsequently, recombinant $(His)_6$-AtACBP3 was identified to bind defense-related acyl-CoA esters including C18:2-CoA and C18:3-CoA esters but not methyl jasmonate (Hu et al., 2018). Taken together, AtACBP3 was destined a role in defense; it was verified mobile from shoot to root, involved in the wounding response, and influenced fatty acid levels and jasmonate content in the phloem, possibly facilitated by its binding to acyl-CoA esters (Hu et al., 2018). In comparison, the apoplast localization of OsACBP5 observed herein coincides well with a biological function in defense as demonstrated in transgenic Arabidopsis overexpressing OsACBP5 followed by proteomic analysis (Panthapulakkal Narayanan et al., 2019). These results on OsACBP5 are consistent with those on its homolog, AtACBP3 (Leung et al., 2006; Xiao et al., 2010; Xiao and Chye, 2011b; Hu et al., 2018), indicating that the Class III (Meng et al., 2011) ACBPs function in plant defense.

OsACBP4 and OsACBP5 Do Not Appear to Translocate After Stress Treatments

No changes in the localization of OsACBP4 and OsACBP5 were noted after salt or pathogen treatments, respectively, although they were induced by salt or pathogen, respectively. These results imply that OsACBP4 and OsACBP5 do not need to translocate in the cell following stress. A plausible reason for the lack in movement may be due to a good liaison by OsACBP family members in performing their functions in lipid trafficking (e.g., apoplast localization for OsACBP5, ER, and PM localization for OsACBP4). OsACBP1 and OsACBP2 regulated from the *CaMV35S* promoter were localized to the cytosol in tobacco leaf epidermal cells and transgenic Arabidopsis cotyledon cells and plasmolyzed root cells, while OsACBP3 was targeted to the cytosol, irregular membranous, and punctate structures (Meng et al., 2014). Furthermore, OsACBP6 was detected at the peroxisomes in tobacco leaf epidermal cells, transgenic Arabidopsis cotyledon and root tip cells, as well as rice sheath cells (Meng et al., 2014). It appears that different members of the OsACBPs coordinate well to maintain acyl-CoA pools for intracellular and extracellular lipid trafficking during lipid metabolism. This possibility is feasible given the

similar binding abilities of recombinant OsACBP4 and OsACBP5 to acyl-CoA esters, PCs and PAs (Meng et al., 2011; Meng, 2012). It is noteworthy that OsACBP4 and AtACBP2, both belonging to the Class II ACBPs, were each reported to be localized to both PM and ER (**Figures 2**, **3**; Li and Chye, 2003). Indeed, TargetP1.1 predicted the transmembrane helix in OsACBP4 (amino acids 11–31) suggesting that it is associated with the ER while iPSORT predicted the presence of a putative N-terminal signal peptide in OsACBP4 (amino acids 1–30). Predotar v.1.03 further predicted OsACBP4 to be localized at the ER with a score of 0.6 (Meng et al., 2014). Furthermore, WoLF PSORT predicted OsACBP4 to be targeted at the ER, ER_PM and PM with scores of 5.5, 4.5, and 2.5, respectively[2]. Therefore, the presence of an N-terminal transmembrane helix in OsACBP4 likely directs OsACBP4 to the PM and ER to facilitate its movement between these two compartments. Similarly, Class III ACBPs (OsACBP5 and AtACBP3) are targeted to the apoplast. Given the multiple subcellular localization of AtACBP3 in transgenic AtACBP3:GFP Arabidopsis (Xiao et al., 2010), it was proposed that AtACBP3 could move from the ER to the PM before reaching the extracellular space (Xiao and Chye, 2011a). This is consistent with subcellular fractionation data that the native AtACBP3 protein and AtACBP3-GFP fusion protein were detected in the intercellular fluids, soluble and membrane fractions using anti-AtACBP3 and anti-GFP antibodies, respectively (Xiao et al., 2010). Therefore, some ACBPs do move between or amongst different subcellular compartments in the native plants. For example, OsACBP4 is likely involved in the intracellular shuttling of acyl-CoA esters and/or other lipids between the PM and ER.

Interestingly, ACBPs have been reported to influence the localization of other proteins following stress treatments. For example, under normoxia, AtACBP1 and AtACBP2 sequester the subgroup VII ethylene-responsive transcription factor RELATED TO AP2.12 (RAP2.12) at the PM through protein-protein interaction and protect it from degradation (Licausi et al., 2011). When oxygen levels were low (hypoxia), RAP2.12 dissociated from AtACBP1 and AtACBP2, was released from the PM and accumulated in the nucleus to activate hypoxia-responsive gene expression (Licausi et al., 2011). More recently, the release of RAP2.12 from the PM was found to be regulated by unsaturated long-chain acyl-CoAs such as oleoyl-CoA (18:1-CoA) and linolenoyl-CoA (18:3-CoA) (Schmidt et al., 2018; Zhou et al., 2020). These results together with the acyl-CoA binding capabilities of AtACBP1 and AtACBP2 (Li and Chye, 2004; Leung et al., 2006; Gao et al., 2009; Xue et al., 2014) imply that the accumulation of 18:3-CoA and/or 18:1-CoA esters induced by hypoxia, promotes the dissociation of RAP2.12 from AtACBP1 and AtACBP2 at the PM causing RAP2.12 entry to the nucleus to initiate downstream hypoxia signaling cascade in Arabidopsis (Licausi et al., 2011; Zhou et al., 2020). It remains to be tested whether OsACBP4 behaves like its Arabidopsis homologs, AtACBP1 and AtACBP2, in hypoxia-related stress responses and regulates the subcellular localization of other proteins.

This investigation has demonstrated the need in using a native promoter and the native plant in subcellular localization studies on a protein. Previously, AtACBP3:GFP expressed from the *CaMV35S* promoter in transgenic Arabidopsis (Xiao and Chye, 2011b) was deemed unsuitable for addressing changes in subcellular localization under different stress treatments because AtACBP3:GFP was degraded after *P. syringae* infection (Xiao and Chye, 2011b). Also, specific stress-responsive element(s) located in the native promoter may be necessary to activate gene expression after stress and may consequently affect protein localization (Duan et al., 2017). Furthermore, there have been reports that the subcellular localization of proteins may not be reliable if not expressed in the native plant (Zhang et al., 2011; Bu et al., 2014). To avoid any potential problems that may arise from use of a non-native promoter or a non-native plant, the studies reported herein employed native promoters to drive expression of the protein-tagged fusions in transgenic rice with satisfactory outcomes. Given that OsACBP5:GFP was localized to the ER in cotyledon, hypocotyl and root cells of transgenic Arabidopsis (Meng et al., 2014; Meng and Chye, 2014), we also tested whether OsACBP5:DsRed was targeted to the ER of the root cells in transgenic rice. However, no obvious ER localization was observed under normal conditions (**Figure 4**), indicating that OsACBP5 may not normally localize to the ER under normal conditions in rice root cells. An ER-Tracker (green) was further used to test the ER localization hypothesis for OsACBP5, signals of this ER marker appeared too strongly, and produced bleed-through artifacts in the red channel, making it difficult to conclude on whether OsACBP5 is localized to the ER membrane structures in rice, in spite of the precautions taken herein in using the native promoter in transgenic rice.

CONCLUSION

In conclusion, this study addressed *OsACBP4:GFP* and *OsACBP5:DsRED* expression from their native promoters and verified their subcellular localization in transgenic rice. The results revealed that OsACBP4:GFP is targeted to the PM besides the ER, while OsACBP5:DsRED is localized at the apoplast. Furthermore, changes in the subcellular localization of OsACBP4:GFP and OsACBP5:DsRED were not detectable following salt and pathogen treatment, respectively. These results imply that OsACBP4 is likely involved in the intracellular shuttling of acyl-CoA esters between PM and ER, while OsACBP5 appears to participate in the extracellular transport of acyl-CoA esters, suggesting that they are non-redundant proteins in lipid trafficking. Furthermore, differences in tagged-protein localization in transgenic Arabidopsis and rice imply that protein subcellular localization studies are best investigated in the native plant.

DATA AVAILABILITY STATEMENT

All datasets generated for this study are included in the article/**Supplementary Material**.

[2]https://wolfpsort.hgc.jp/

AUTHOR CONTRIBUTIONS

PL and M-LC designed the research. PL, KL, S-CL, and SP performed the experiments. PL, KL, S-CL, SP, M-LC, and LJ analyzed the data. PL and M-LC wrote the manuscript. S-CL revised the manuscript. All authors have read and approved the manuscript.

FUNDING

This work was supported by the Wilson and Amelia Wong Endowment Fund, Research Grants Council of Hong Kong (AoE/M-05/12) and Innovation Technology Fund of Innovation Technology Commission: Funding Support to State Key Laboratories in Hong Kong. PL was supported by a Postdoctoral Fellowship from the AoE/M-05/12 and the University of Hong Kong.

ACKNOWLEDGMENTS

We thank Prof. Yongjun Lin (Huazhong Agricultural University) for provision of the binary vector DX2181, Ms. Chi Kio Mak and Dr. Jian Liang for technical assistance.

SUPPLEMENTARY MATERIAL

The Supplementary Material for this article can be found online at: https://www.frontiersin.org/articles/10.3389/fpls.2020.00331/full#supplementary-material

REFERENCES

Benning, C. (2009). Mechanisms of lipid transport involved in organelle biogenesis in plant cells. *Annu. Rev. Cell Dev.* 25, 71–91. doi: 10.1146/annurev.cellbio.042308.113414

Block, M. A., and Jouhet, J. (2015). Lipid trafficking at endoplasmic reticulum–chloroplast membrane contact sites. *Curr. Opin. Cell Biol.* 35, 21–29. doi: 10.1016/j.ceb.2015.03.004

Bradford, M. M. (1976). A rapid and sensitive method for the quantitation of microgram quantities of protein utilizing the principle of protein-dye binding. *Anal. Biochem.* 72, 248–254. doi: 10.1006/abio.1976.9999

Bu, Y., Zhao, M., Sun, B., Zhang, X., Takano, T., and Liu, S. (2014). An efficient method for stable protein targeting in grasses (Poaceae): a case study in *Puccinellia tenuiflora*. *BMC Biotechnol.* 14:52. doi: 10.1186/1472-6750-14-52

Chen, M.-X., Hu, T.-H., Xue, Y., Zhu, F.-Y., Du, Z.-Y., Lo, C., et al. (2018). *Arabidopsis* acyl-coenzyme-A-binding protein ACBP1 interacts with AREB1 and mediates salt and osmotic signaling in seed germination and seedling growth. *Environ. Exp. Bot.* 156, 130–140. doi: 10.1016/j.envexpbot.2018.09.007

Chen, Q.-F., Xiao, S., and Chye, M.-L. (2008). Overexpression of the *Arabidopsis* 10-kilodalton acyl-coenzyme A-binding protein ACBP6 enhances freezing tolerance. *Plant Physiol.* 148, 304–315. doi: 10.1104/pp.108.123331

Chen, Q.-F., Xiao, S., Qi, W., Mishra, G., Ma, J., Wang, M., et al. (2010). The *Arabidopsis acbp1acbp2* double mutant lacking acyl-CoA-binding proteins ACBP1 and ACBP2 is embryo lethal. *New Phytol.* 186, 843–855. doi: 10.1111/j.1469-8137.2010.03231.x

Chu, T. T. H., Hoang, T. G., Trinh, D. C., Bureau, C., Meynard, D., and Vernet, A. (2018). Sub-cellular markers highlight intracellular dynamics of membrane proteins in response to abiotic treatments in rice. *Rice (N.Y.)* 11:23. doi: 10.1186/s12284-018-0209-2

Chye, M.-L., Huang, B.-Q., and Zee, S. Y. (1999). Isolation of a gene encoding *Arabidopsis* membrane-associated acyl-CoA binding protein and immunolocalization of its gene product. *Plant J.* 18, 205–214. doi: 10.1046/j.1365-313X.1999.00443.x

Chye, M.-L., Li, H.-Y., and Yung, M.-H. (2000). Single amino acid substitutions at the acyl-CoA-binding domain interrupt ^{14}[C] palmitoyl-CoA binding of ACBP2, an *Arabidopsis* acyl-CoA-binding protein with ankyrin repeats. *Plant Mol. Biol.* 44, 711–721. doi: 10.1023/A:1026524108095

Du, H., Wang, N., Cui, F., Li, X., Xiao, J., and Xiong, L. (2010). Characterization of the β-carotene hydroxylase gene *DSM2* conferring drought and oxidative stress resistance by increasing xanthophylls and abscisic acid synthesis in rice. *Plant Physiol.* 154, 1304–1318. doi: 10.1104/pp.110.163741

Du, Z.-Y., Arias, T., Meng, W., and Chye, M.-L. (2016). Plant acyl-CoA-binding proteins: an emerging family involved in plant development and stress responses. *Prog. Lipid Res.* 63, 165–181. doi: 10.1016/j.plipres.2016.06.002

Du, Z.-Y., Chen, M.-X., Chen, Q.-F., Xiao, S., and Chye, M.-L. (2013b). Overexpression of *Arabidopsis* acyl-CoA-binding protein ACBP2 enhances drought tolerance. *Plant Cell Environ.* 36, 300–314. doi: 10.1111/j.1365-3040.2012.02574.x

Du, Z.-Y., Chen, M.-X., Xiao, S., and Chye, M.-L. (2013a). *Arabidopsis* acyl-CoA-binding protein ACBP1 participates in the regulation of seed germination and seedling development. *Plant J.* 74, 294–309. doi: 10.1111/tpj.12121

Du, Z.-Y., Xiao, S., Chen, Q.-F., and Chye, M.-L. (2010). Depletion of the membrane-associated acyl-coenzyme A-binding protein ACBP1 enhances the ability of cold acclimation in *Arabidopsis*. *Plant Physiol.* 152, 1585–1597. doi: 10.1104/pp.109.147066

Duan, M., Zhang, R., Zhu, F., Zhang, Z., Gou, L., Wen, J., et al. (2017). A lipid-anchored NAC transcription factor is translocated into the nucleus and activates *glyoxalase I* expression during drought stress. *Plant Cell* 29, 1748–1772. doi: 10.1105/tpc.17.00044

Faergeman, N. J., and Knudsen, J. (2002). Acyl-CoA binding protein is an essential protein in mammalian cell lines. *Biochem. J.* 368, 679–682. doi: 10.1042/BJ20021413

Fan, J., Zhai, Z., Yan, C., and Xu, C. (2015). *Arabidopsis* TRIGALACTOSYLDIACYLGLYCEROL5 interacts with TGD1, TGD2, and TGD4 to facilitate lipid transfer from the endoplasmic reticulum to plastids. *Plant Cell* 27, 2941–2955. doi: 10.1105/tpc.15.00394

Gao, C., Yu, C. K. Y., Qu, S., San, M. W. Y., Li, K. Y., Lo, S. W., et al. (2012). The golgi-localized *Arabidopsis* endomembrane protein12 contains both endoplasmic reticulum export and golgi retention signals at its C terminus. *Plant Cell* 24, 2086–2104. doi: 10.1105/tpc.112.096057

Gao, W., Li, H.-Y., Xiao, S., and Chye, M.-L. (2010). Acyl-CoA-binding protein 2 binds lysophospholipase 2 and lysoPC to promote tolerance to cadmium-induced oxidative stress in transgenic *Arabidopsis*. *Plant J.* 62, 989–1003. doi: 10.1111/j.1365-313X.2010.04209.x

Gao, W., Xiao, S., Li, H.-Y., Tsao, S. W., and Chye, M.-L. (2009). *Arabidopsis thaliana* acyl-CoA-binding protein ACBP2 interacts with heavy-metal-binding farnesylated protein AtFP6. *New Phytol.* 181, 89–102. doi: 10.1111/j.1469-8137.2008.02631.x

Guo, Z.-H., Haslam, R. P., Michaelson, L. V., Yeung, E. C., Lung, S.-C., Napier, J. A., et al. (2019). The overexpression of rice ACYL-CoA-BINDING PROTEIN2 increases grain size and bran oil content in transgenic rice. *Plant J.* 100, 1132–1147. doi: 10.1111/tpj.14503

Hansen, J. S., Færgeman, N. J., Kragelund, B. B., and Knudsen, J. (2008). Acyl-CoA-binding protein (ACBP) localizes to the endoplasmic reticulum and Golgi in a ligand-dependent manner in mammalian cells. *Biochem. J.* 410, 463–472. doi: 10.1042/BJ20070559

Hu, T.-H., Lung, S.-C., Ye, Z.-W., and Chye, M.-L. (2018). Depletion of *Arabidopsis* ACYL-COA-BINDING PROTEIN3 affects fatty acid composition in the phloem. *Front. Plant Sci.* 9:2. doi: 10.3389/fpls.2018.00002

Hurlock, A. K., Roston, R. L., Wang, K., and Benning, C. (2014). Lipid trafficking in plant cells. *Traffic* 15, 915–932. doi: 10.1111/tra.12187

Hwang, J.-U., Song, W.-Y., Hong, D., Ko, D., Yamaoka, Y., Jang, S., et al. (2016). Plant ABC transporters enable many unique aspects of a

terrestrial plant's lifestyle. *Mol. Plant* 9, 338–355. doi: 10.1016/j.molp.2016.02.003

Islam, M. A., Du, H., Ning, J., Ye, H. Y., and Xiong, L. Z. (2009). Characterization of glossy1-homologous genes in rice involved in leaf wax accumulation and drought resistance. *Plant Mol. Biol.* 70, 443–456. doi: 10.1007/s11103-009-9483-0

Jouhet, J., Maréchal, E., and Block, M. A. (2007). Glycerolipid transfer for the building of membranes in plant cells. *Prog. Lipid Res.* 46, 37–55. doi: 10.1016/j.plipres.2006.06.002

Kader, J., De Physiologie, L., and Pierre, U. (1996). Lipid-transfer proteins in plants. *Annu. Rev. Plant Physiol. Plant Mol. Biol.* 47, 627–654. doi: 10.1146/annurev.arplant.47.1.627

Kader, J. C. (1997). Lipid-transfer proteins: a puzzling family of plant proteins. *Trends Plant Sci.* 2, 66–70. doi: 10.1016/S1360-1385(97)82565-4

Kang, J., Park, J., Choi, H., Burla, B., Kretzschmar, T., Lee, Y., et al. (2011). Plant ABC transporters. *Arabidopsis Book* 9:e0153. doi: 10.1199/tab.0153

Kim, H., Hwang, H., Hong, J. W., Lee, Y. N., Ahn, I. P., Yoon, I. S., et al. (2012). A rice orthologue of the ABA receptor, OsPYL/RCAR5, is a positive regulator of the ABA signal transduction pathway in seed germination and early seedling growth. *J. Exp. Bot.* 63, 1013–1024. doi: 10.1093/jxb/err338

Kim, N., Moon, S. J., Min, M. K., Choi, E. H., Kim, J. A., Koh, E. Y., et al. (2015). Functional characterization and reconstitution of ABA signaling components using transient gene expression in rice protoplasts. *Front. Plant Sci.* 6:614. doi: 10.3389/fpls.2015.00614

Knudsen, J., Neergaard, T. B. F., Gaigg, B., Jensen, M. V., and Hansen, J. K. (2000). Role of acyl-CoA binding protein in acyl-CoA metabolism and acyl-CoA –mediated cell signaling. *J. Nutr.* 130, 294S–298S. doi: 10.1093/jn/130.2.294S

Lefèvre, F., and Boutry, M. (2018). Towards identification of the substrates of ATP-binding cassette transporters. *Plant Physiol.* 178, 18–39. doi: 10.1104/pp.18.00325

Leung, K.-C., Li, H.-Y., Xiao, S., Tse, M.-H., and Chye, M. (2006). *Arabidopsis* ACBP3 is an extracellularly targeted acyl-CoA-binding protein. *Planta* 223, 871–881. doi: 10.1007/s00425-005-0139-2

Li, H., and Chye, M.-L. (2003). Membrane localization of *Arabidopsis* acyl-CoA binding protein ACBP2. *Plant Mol. Biol.* 51, 483–492. doi: 10.1023/A:1022330304402

Li, H., and Chye, M.-L. (2004). *Arabidopsis* acyl-CoA-binding protein ACBP2 interacts with an ethylene-responsive element binding protein AtEBP via its ankyrin repeats. *Plant Mol. Biol.* 54, 233–243. doi: 10.1023/B:PLAN.0000028790.75090.ab

Liao, P., Chen, Q.-F., and Chye, M.-L. (2014a). Transgenic *Arabidopsis* flowers overexpressing acyl-CoA-binding protein ACBP6 are freezing tolerant. *Plant Cell Physiol.* 55, 1055–1071. doi: 10.1093/pcp/pcu037

Liao, P., Chen, X., Wang, M., Bach, T. J., and Chye, M.-L. (2018). Improved fruit a-tocopherol, carotenoid, squalene and phytosterol contents through manipulation of *Brassica juncea* 3-HYDROXY-3-METHYLGLUTARYL-COA SYNTHASE1 in transgenic tomato. *Plant Biotechnol. J.* 16, 784–796. doi: 10.1111/pbi.12828

Liao, P., Lung, S.-C., Chan, W. L., Bach, T. J., Lo, C., and Chye, M.-L. (2019). Overexpression of HMG-CoA synthase promotes *Arabidopsis* root growth and adversely affects glucosinolate biosynthesis. *J. Exp. Bot.* 71, 272–289. doi: 10.1093/jxb/erz420

Liao, P., Wang, H., Wang, M., Hsiao, A.-S., Bach, T. J., and Chye, M.-L. (2014b). Transgenic tobacco overexpressing *Brassica juncea* HMG-CoA synthase 1 shows increased plant growth, pod size and seed yield. *PLoS One* 9:e98264. doi: 10.1371/journal.pone.0098264

Li-Beisson, Y., and Nakamura, Y. (2016). *Lipids in Plant and Algae Development*. Cham: Springer.

Licausi, F., Kosmacz, M., Weits, D. A., Giuntoli, B., Giorgi, F. M., Voesenek, L. A., et al. (2011). Oxygen sensing in plants is mediated by an N-end rule pathway for protein destabilization. *Nature* 479, 419–422. doi: 10.1038/nature10536

Liu, F., Zhang, X., Lu, C., Zeng, X., Li, Y., Fu, D., et al. (2015). Non-specific lipid transfer proteins in plants: presenting new advances and an integrated functional analysis. *J. Exp. Bot.* 66, 5663–5681. doi: 10.1093/jxb/erv313

Lung, S., and Chye, M.-L. (2016a). The binding versatility of plant acyl-CoA-binding proteins and their significance in lipid metabolism. *Biochim. Biophys. Acta Mol. Cell Biol. Lipids* 1861, 1409–1421. doi: 10.1016/j.bbalip.2015.12.018

Lung, S.-C., and Chye, M.-L. (2016b). Deciphering the roles of acyl-CoA-binding proteins in plant cells. *Protoplasma* 253, 1177–1195. doi: 10.1007/s00709-015-0882-6

Lung, S.-C., and Chye, M.-L. (2019). *Arabidopsis* acyl-CoA-binding proteins regulate the synthesis of lipid signals. *New Phytol.* 223, 113–117. doi: 10.1111/nph.15707

Lung, S.-C., Liao, P., Yeung, E. C., Hsiao, A., Xue, Y., and Chye, M.-L. (2018). *Arabidopsis* ACYL-COA-BINDING PROTEIN1 interacts with STEROL C4-METHYL OXIDASE1-2 to modulate gene expression of homeodomain-leucine zipper IV transcription factors. *New Phytol.* 218, 183–200. doi: 10.1111/nph.14965

Lung, S.-C., Liao, P., Yeung, E. C., Hsiao, A.-S., Xue, Y., and Chye, M.-L. (2017). Acyl-CoA-binding protein ACBP1 modulates sterol synthesis during embryogenesis. *Plant Physiol.* 174, 1420–1435. doi: 10.1104/pp.17.00412

Meng, W. (2012). *Characterization of Acyl-Coenzyme A-Binding Proteins from Rice*. Ph.D. thesis, The University of Hong Kong, Hong Kong. doi: 10.5353/th_b4961747

Meng, W., and Chye, M.-L. (2014). Rice acyl-CoA-binding proteins OsACBP4 and OsACBP5 are differentially localized in the endoplasmic reticulum of transgenic *Arabidopsis*. *Plant Signal. Behav.* 9:e29544. doi: 10.4161/psb.29544

Meng, W., Hsiao, A., Gao, C., Jiang, L., and Chye, M.-L. (2014). Subcellular localization of rice acyl-CoA-binding proteins (ACBPs) indicates that OsACBP6::GFP is targeted to the peroxisomes. *New Phytol.* 203, 469–482. doi: 10.1111/nph.12809

Meng, W., Su, Y. C. F., Saunders, R. M. K., and Chye, M.-L. (2011). The rice acyl-CoA-binding protein gene family: phylogeny, expression and functional analysis. *New Phytol.* 189, 1170–1184. doi: 10.1111/j.1469-8137.2010.03546.x

Miao, R., Lung, S.-C., Li, X., Li, X. D., and Chye, M.-L. (2019). Thermodynamic insights into an interaction between ACYL-COA-BINDING PROTEIN2 and LYSOPHOSPHOLIPASE2 in *Arabidopsis*. *J. Biol. Chem.* 294, 6214–6226. doi: 10.1074/jbc.RA118.006876

Panthapulakkal Narayanan, S., Liao, P., Taylor, P. W. J., Lo, C., and Chye, M.-L. (2019). Overexpression of a monocot acyl-CoA-binding protein confers broad-dpectrum pathogen protection in a dicot. *Proteomics* 19:1800368. doi: 10.1002/pmic.201800368

Rea, P. A. (2007). Plant ATP-binding cassette transporters. *Annu. Rev. Plant Biol.* 58, 347–375. doi: 10.1146/annurev.arplant.57.032905.105406

Schjerling, C. K., Hummel, R., Hansen, J. K., Børsting, C., Mikkelsen, J. M., Kristiansen, K., et al. (1996). Disruption of the gene encoding the acyl-CoA-binding protein (ACB1) perturbs acyl-CoA metabolism in *Saccharomyces cerevisiae*. *J. Biol. Chem.* 271, 22514–22521. doi: 10.1074/jbc.271.37.22514

Schmidt, R. R., Fulda, M., Paul, M. V., Anders, M., Plum, F., Weits, D. A., et al. (2018). Oxygen sensing in plants is mediated by an N-end rule pathway for protein destabilization. *Proc. Natl. Acad. Sci. U.S.A.* 115, E12101–E12110. doi: 10.1073/pnas.1809429115

Schmittgen, T. D., and Livak, K. J. (2008). Analyzing real-time PCR data by the comparative C_T method. *Nat. Protoc.* 3:1101. doi: 10.1038/nprot.2008.73

Schoor, S., Lung, S., Sigurdson, D., and Chuong, S. D. X. (2015). "Fluorescent staining of living plant cells," in *Plant Microtechniques and Protocols*, eds E. C. T. Yeung, C. Stasolla, M. J. Sumner, and B. Q. Huang (Cham: Springer), 153–165. doi: 10.1007/978-3-319-19944-3_9

Snapp, E. (2005). Design and use of fluorescent fusion proteins in cell biology. *Curr. Protoc. Cell Biol.* Chapter 21, 21.4.1–21.4.13. doi: 10.1002/0471143030.cb2104s27

Srivastava, R., Deng, Y., Shah, S., Rao, A. G., and Howella, S. H. (2013). BINDING PROTEIN is a master regulator of the endoplasmic reticulum stress sensor/transducer bZIP28 in *Arabidopsis*. *Plant Cell* 25, 1416–1429. doi: 10.1105/tpc.113.110684

Tanz, S. K., Castleden, I., Small, I. D., and Millar, A. H. (2013). Fluorescent protein tagging as a tool to define the subcellular distribution of proteins in plants. *Front. Plant Sci.* 4:214. doi: 10.3389/fpls.2013.00214

Tian, G. W., Mohanty, A., Chary, S. N., Li, S., Paap, B., Drakakaki, G., et al. (2004). High-throughput fluorescent tagging of full-length *Arabidopsis* gene products in planta. *Plant Physiol.* 135, 25–38. doi: 10.1104/pp.104.040139

Wang, D., Weaver, N. D., Kesarwani, M., and Dong, X. (2005). Induction of protein secretory pathway is required for systemic acquired resistance. *Science* 308, 1036–1040. doi: 10.1126/science.1108791

Wang, X. (2004). Lipid signaling. *Curr. Opin. Plant Biol. Biol.* 7, 329–336. doi: 10.1016/j.pbi.2004.03.012

Xiao, S., and Chye, M.-L. (2010). The *Arabidopsis thaliana* ACBP3 regulates leaf senescence by modulating phospholipid metabolism and ATG8 stability. *Autophagy* 6, 802–804. doi: 10.4161/auto.6.6.12576

Xiao, S., and Chye, M.-L. (2011a). New roles for acyl-CoA-binding proteins (ACBPs) in plant development, stress responses and lipid metabolism. *Prog. Lipid Res.* 50, 141–151. doi: 10.1016/j.plipres.2010.11.002

Xiao, S., and Chye, M.-L. (2011b). Overexpression of *Arabidopsis* ACBP3 enhances NPR1-dependent plant resistance to *Pseudomonas syringe* pv tomato DC3000. *Plant Physiol.* 156, 2069–2081. doi: 10.1104/pp.111.176933

Xiao, S., Gao, W., Chen, Q.-F., Chan, S.-W., Zheng, S.-X., Ma, J., et al. (2010). Overexpression of *Arabidopsis* acyl-CoA binding protein ACBP3 promotes starvation-induced and age-dependent leaf senescence. *Plant Cell* 22, 1463–1482. doi: 10.1105/tpc.110.075333

Xie, L., Yu, L., Chen, Q., Wang, F., Huang, L., Xia, F., et al. (2015). *Arabidopsis* acyl-CoA-binding protein ACBP3 participates in plant response to hypoxia by modulating very-long-chain fatty acid metabolism. *Plant J.* 81, 53–67. doi: 10.1111/tpj.12692

Xue, Y., Xiao, S., Kim, J., Lung, S. C., Chen, L., Tanner, J. A., et al. (2014). *Arabidopsis* membrane-associated acyl-CoA-binding protein AtACBP1 is involved in stem cuticle formation. *J. Exp. Bot.* 18, 5473–5483. doi: 10.1093/jxb/eru304

Yurchenko, O., Singer, S. D., Nykiforuk, C. L., Gidda, S., Mullen, R. T., Moloney, M. M., et al. (2014). Production of a Brassica napus low-molecular mass acyl-coenzyme A-binding protein in *Arabidopsis* alters the acyl-coenzyme A pool and acyl composition of oil in seeds. *Plant Physiol.* 165, 550–560. doi: 10.1104/pp.114.238071

Zhang, Q., Li, J., Zhang, W., Yan, S., Wang, R., Zhao, J., et al. (2012). The putative auxin efflux carrier *OsPIN3t* is involved in the drought stress response and drought tolerance. *Plant J.* 72, 805–816. doi: 10.1111/j.1365-313X.2012.05121.x

Zhang, Y., Su, J., Duan, S., Ao, Y., Dai, J., Liu, J., et al. (2011). A highly efficient rice green tissue protoplast system for transient gene expression and studying light/chloroplast-related processes. *Plant Methods* 7:30. doi: 10.1186/1746-4811-7-30

Zheng, S. X., Xiao, S., and Chye, M.-L. (2012). The gene encoding *Arabidopsis* acyl-coA-binding protein 3 is pathogen-inducible and subject to circadian regulation. *J. Exp. Bot.* 63, 2985–3000. doi: 10.1093/jxb/ers009

Zhou, X., Ni, L., Liu, Y., and Jiang, M. (2018). Phosphorylation of bip130 by OsMPK1 regulates abscisic acid-induced antioxidant defense in rice. *Biochem. Biophys. Res. Commun.* 514, 750–755. doi: 10.1016/j.bbrc.2019.04.183

Zhou, Y., Tan, W. J., Xie, L. J., Qi, H., Yang, Y. C., Huang, L. P., et al. (2020). Polyunsaturated linolenoyl-CoA modulates ERF-VII-mediated hypoxia signaling in *Arabidopsis*. *J. Integr. Plant Biol.* 62, 330–348. doi: 10.1111/jipb.12875

Conflict of Interest: The authors declare that the research was conducted in the absence of any commercial or financial relationships that could be construed as a potential conflict of interest.

frontiers in Plant Science

ORIGINAL RESEARCH
published: 15 July 2020
doi: 10.3389/fpls.2020.01070

PUB11-Dependent Ubiquitination of the Phospholipid Flippase ALA10 Modifies ALA10 Localization and Affects the Pool of Linolenic Phosphatidylcholine

Juliette Salvaing, César Botella, Catherine Albrieux, Valérie Gros, Maryse A. Block and Juliette Jouhet *

Univ. Grenoble Alpes, INRAE, CNRS, CEA, IRIG, LPCV, Grenoble, France

Biogenesis of photosynthetic membranes depends on galactolipid synthesis, which relies on several cell compartments, notably the endoplasmic reticulum (ER) and the chloroplast envelope. Galactolipid synthesis involves lipid trafficking between both membrane compartments. In *Arabidopsis*, ALA10, a phospholipid flippase of the P_4 type-ATPase family, counteracts the limitation of monogalactosyldiacylglycerol (MGDG) production and has a positive effect on leaf development. ALA10 locates in distinct domains of the ER depending on the ALIS (ALA interacting subunit) subunit it interacts with: close to the plasma membrane with ALIS1, or next to chloroplasts with ALIS5. It interacts with FAD2 (Fatty acid desaturase 2) and prevents accumulation of linolenic (18:3) containing phosphatidylcholine (PC) stimulating an increase of MGDG synthesis. Here we report that ALA10 interacts with PUB11 (plant U-box type 11), an E3 protein ubiquitin ligase, *in vitro* and *in vivo*. ALA10 is however ubiquitinated and degraded by the 26S proteasome in a PUB11-independent process. In *pub11* null mutant, the proteasome-dependent degradation of ALA10 is retained and ALA10 is still subject to ubiquitination although its ubiquitination profile appears different. In the absence of PUB11, ALA10 is constrained to the ER close to chloroplasts, which is the usual location when ALA10 is overexpressed. Additionally, in this condition, the decrease of 18:3 containing PC is no longer observed. Taken together these results suggest, that ALA10 contributes in chloroplast-distal ER interacting domains, to reduce the 18:3 desaturation of PC and that PUB11 is involved in reconditioning of ALA10 from chloroplast-proximal to chloroplast-distal ER interacting domains.

Keywords: glycerolipid, flippase, ubiquitination, membrane domain, lipid trafficking

OPEN ACCESS

Edited by:
Susanne Hoffmann-Benning, Michigan State University, United States

Reviewed by:
Rebecca L. Roston, University of Nebraska-Lincoln, United States
Anastasiya Lavell, Michigan State University, United States

***Correspondence:**
Juliette Jouhet
juliette.jouhet@cea.fr

Specialty section:
This article was submitted to Plant Metabolism and Chemodiversity, a section of the journal Frontiers in Plant Science

Received: *06 April 2020*
Accepted: *29 June 2020*
Published: *15 July 2020*

Citation:
Salvaing J, Botella C, Albrieux C, Gros V, Block MA and Jouhet J (2020) PUB11-Dependent Ubiquitination of the Phospholipid Flippase ALA10 Modifies ALA10 Localization and Affects the Pool of Linolenic Phosphatidylcholine. Front. Plant Sci. 11:1070. doi: 10.3389/fpls.2020.01070

INTRODUCTION

Each membrane of plant cells has a specific glycerolipid composition. Like in other eukaryotic organisms, a high proportion of phospholipids is present in the endomembrane network and in mitochondria with a prevalence of phosphatidylcholine (PC). For photosynthetic function, in chloroplasts, plant cells have also an important network of membranes and the chloroplast membranes show only a low proportion of phospholipids and a specific enrichment in non-phosphorylated galactolipids with up to 50% of monogalactosyldiacylglycerol (MGDG) (Block et al, 1983). The lipid composition of each membrane compartment is however sensitive to fluctuation of developmental and environmental stimuli (Sandelius and Liljenberg, 1982; Jouhet et al., 2007; Zheng et al., 2016). Moreover, the lipid composition is not homogenous laterally and transversally along membranes, displaying domain-specific dissimilarities with possible correlation between the organization of these domains and their role in response to distinct stimuli (Gronnier et al., 2018).

In plants, glycerolipids are primarily synthesized in the ER and in chloroplasts. Their synthesis is fed by the production of fatty acids (FA) in chloroplasts. Galactosylation of diacylglycerol (DAG) by the MGDG synthase MGD1 in the inner membrane of the chloroplast envelope gives rise to thylakoid MGDG (Boudiere et al., 2014). MGD1 is activated by phosphatidic acid (PA) from diverse origins, notably coming from phospholipase-mediated hydrolysis of extraplastidial PC (Dubots et al., 2010). In addition, MGD1 is supplied with its DAG substrates either generated from *de novo* synthesis in the chloroplast (the prokaryotic pathway), or derived from linoleic (18:2) containing PC of ER origin (the eukaryotic pathway). In PC, linoleate results from the desaturation of oleate (18:1) by Fatty acid desaturase 2 (FAD2) (Karki et al., 2019; Ohlrogge and Browse, 1995). Preservation of a pool of 18:2 containing PC suitable for MGDG synthesis is therefore dependent on the overall FA metabolism, i.e. FA synthesis in chloroplasts, FA export from chloroplasts and FA desaturation in the ER.

In leaves, diurnal oscillation of the overall FA composition was observed with an increase of oleic acid during the day and linolenic acid (18:3) during the dark period (Browse et al., 1981). Several steps of regulation are likely involved in diurnal oscillation of 18:1/18:3 lipids. The first one is the light/dark modulation of FA synthesis in chloroplasts due to light enhancement of acetyl-CoA carboxylase (ACCase) which altogether results in coordination of FA synthesis with photosynthesis (Sasaki et al., 1997). This however does not explain the increase of desaturated over saturated lipids during the dark period unless there is a limitation of desaturation during the day (Mei et al., 2015).

ALA10 has been previously identified as a modulator of the MGDG/PC ratio in leaves (Botella et al., 2016). Upon chemical inhibition of MGD enzymes by Galvestine-1, a strong enhancement in expression of ALA10 was observed suggesting a link between this protein and regulation of MGDG formation (Botte et al., 2011). Moreover, ALA10 is an ER phospholipid flippase of the P_4 type-ATPase family that interacts with FAD2. ALA10 expression affects PC fatty acyl desaturation by limiting FAD3 over FAD2 activity, thus enhancing the level of 18:2 containing PC and decreasing the level of 18:3 PC (Poulsen et al., 2015; Botella et al., 2016). ALA10 also interacts with a β-subunit, ALA-Interacting Subunit (ALIS), either ALIS1 or ALIS5, leading to a preferential endomembrane localization dependent on the interacting protein, close to the plasma membrane with ALIS1 or to chloroplasts with ALIS5 (Botella et al., 2016). In leaves, ALA10 improves MGDG level especially in response to treatment of plants with Galvestine-1 or to growth at low temperature (Botella et al., 2016; Nintemann et al., 2019). It has been proposed that this positive effect operates *via* the activation of MGD1 by PA since it was neither associated with overexpression of MGD nor with enhancement of feeding of DAG coming from PC.

Supporting a regulation role of ALA10 in response to environmental modification, *ALA10* expression is highly variable and the protein very sensitive to degradation (Botella et al., 2016). One peptide of ALA10 had been previously detected in the proteome of plantlets treated with the 26S proteasome inhibitor, MG132, (Maor et al., 2007; Manzano et al., 2008) and prepared by ubiquitin affinity purification (Manzano et al., 2008). Although the ubiquitination of this peptide was not detected, this suggests a possible regulation of ALA10 by ubiquitination.

Ubiquitination may have several functions extending from protein targeting to degradation by either 26S proteasome system or vesicular trafficking to lytic compartments, to modification of activity and modification of protein molecular surroundings (Guerra and Callis, 2012). In plants, roles in regulation of nutrient import, in dynamics of endosymbiotic organelles and in hormone-mediated signaling have been further analyzed (Barberon et al., 2011; Guerra and Callis, 2012; Ling et al., 2012; Jung et al., 2015). Several works are based on characterization of E3 protein-ubiquitin ligases [for reviews see (Ling and Jarvis, 2013; Sharma et al., 2016; Trujillo, 2018)]. Two closely related proteins of the Plant U-box protein family, PUB10 and PUB11, have been recently studied to investigate their role in plant signaling (Jung et al., 2015). Both proteins are able to auto-ubiquitinate *in vitro* and to ubiquitinate several MYC family transcription factors, most importantly MYC2, a key regulator of jasmonic acid (JA) signaling. In addition, only PUB10, but not PUB11, played a role in regulation of JA signaling.

Here, we investigated the role of PUB11 in ALA10 post-translational modification. We show the interaction of ALA10 with PUB11 and ubiquitination of ALA10. The function of ALA10 was investigated in relation with its impact on PC and MGDG metabolism in Arabidopsis leaves.

MATERIAL AND METHODS

Plant Materials and Growth Conditions

The *Arabidopsis thaliana ala10* and *pub11* lines, respectively SALK_024877 for insertion in At3g25610 and SALK_029828 for At1g23030, are in *Col-0* background and came from the SALK institute collection (Alonso et al., 2003). Characterization of the

ala10 mutant line was previously described in (Botella et al., 2016). The *pub11* line was previously reported in (Jung et al., 2015) and homozygous insertion was verified in this work by PCR analysis on genomic DNA using the T-DNA primer (LB, GGCAATCAGCTGTTGCCCGTCTCACTGGTG) and the gene-specific primer (PUB11Rv2, GAT TCT CTT CGC AGC ACC AT) for detection of the interrupted copy of the gene and two gene-specific primers (PUB11Rv2, GAT TCT CTT CGC AGC ACC AT and PUB11Fw3, AGA ACC AAT CCC AAA GCT CA) for control of WT copy.

Construction of L1 and L2 lines with ALA10-GFP expression in *Col-0* background is described in (Botella et al., 2016). For expression of ALA10-GFP expression in the *pub11* background, ALA10-GFP was obtained by PCR-amplification from an *Arabidopsis* cDNA library using ALA10 flanking primers (ALA10F2, ATGGCTGGTCCAAGTCGGAGAAGAAG and A L A 1 0 R 2 , TTAGACACCGACAAGATCCTTATAGATCTGATCGTG) and the cDNA fragment was cloned in pUC18 upstream of the GFP S65T cDNA and under the control of the cauliflower mosaic virus 35S promoter and the *nos* terminator. Construction was transferred into the pEL103 binary vector for *Agrobacterium tumefaciens* transformation. For expression of GFP-ALA10 expression in WT and *pub11* background, GFP-ALA10 construction in the pMDC45 binary plasmid was a gift from Rosa L. Lopez-Marques and described in Poulsen et al. (2015). *Arabidopsis* plants were transformed by floral dipping (Mittler and Lam, 1995; Clough and Bent, 1998). Transformants were selected by several rounds of selection on MS medium containing 50 µM kanamycin for ALA10-GFP and 25 mg/ml^{-1} hygromycin solution for GFP-ALA10 until the isolated line shows at least 85% of resistant plants.

In standard culture, plants were grown for 2 weeks on solid MS medium containing 0.5% sucrose, 0.8% agar, 0.5 g L^{-1} MES/KOH pH 5.7. In liquid culture, plants were grown for 10 days on the same medium without agar. Ten seeds were sawn in 1.5 ml medium in each well of a 6 well-plate. After 2 days of stratification at 4°C, plates were placed in a growth chamber at 20°C with white light 100 µmol m^{-2} s^{-1} under long-day (16-h light/8-h dark) conditions. Treatment of plants with MG132 was done on liquid culture by removing the medium and replacing with a new medium supplemented with 50 µM of MG132 prepared in DMSO or 0.1% DMSO for control. Medium replacement was done at 4:00 pm on day 9 and plant harvest at 1:00 pm on day 10. Plants were immediately frozen in liquid nitrogen and kept at −80°C before analysis.

Membrane Preparation

For protein purification, membranes were prepared as follows: frozen tissues were ground to powder in liquid nitrogen. Approximately 300 µl of thawed powder was homogenized in 1.5 ml of ice cold grinding medium (15 mM MOPS/NaOH pH 7.5, 2 mM EGTA, 0.6% w/v polyvinylpyrrolidone 25, 10 mM DTT, 1mM phenylmethylsulfonyl fluoride, 1mM benzamidine, 5 mM caproic acid, 5 mM iodoacetamide, 50 µM PR619, 10 µM MG132, 0.2% DMSO). Supernatant was then collected by microcentrifugation of the suspension at 400×*g* for 10 min at 4°C before microcentrifugation at 10,000×*g* for 10 min at 4°C. Membranes were collected in pellets.

Protein Immunopurification

Five membrane pellets corresponding to a total of 0.5 mg protein were homogenized in 0.75 ml of solubilization buffer (50 mM imidazole pH7.5, 500 mM 6-aminocaproic acid, 1 mM EDTA, 1% Triton X100). Mixture was incubated for 30 min on ice before centrifugation at 100,000×*g* for 20 min at 4°C (Hitashi microcentrifuge). Supernatant was collected and 45 µl withdrawn for control of column input. 50 µL of anti-GFP µMACS magnetic beads were added to approximately 700 µl supernatant and incubated for 1h on ice. Mixture was then loaded on prewashed µMACS column set on a magnetic support (Milteniy Biotech). The column was washed with 400 µl of solubilization buffer, 1.6 ml of solubilization buffer containing 0.1% Triton X100 instead of 1%, then 150 µl of 20 mM Tris–HCl pH 7.5. Proteins were then eluted with 95 µl of Miltenyi denaturing elution buffer at 95°C and kept at −80°C before analysis.

Protein Immunodetection

Protein was resolved by Laemmli SDS-PAGE on 4–15% polyacrylamide gel before electrotransfer to 0.2 µm nitrocellulose membrane in Laemmli buffer, 20% ethanol, 0.02% SDS. Protein transfer was controlled by Ponceau red staining of the membrane and positioned with Precision Plus Protein Dual Color standards (Eurogentec). The membranes were blocked in TBS, 0.1% Tween-20, 5% BSA. Immunostaining was done by incubation of the blot with specific antibodies in TBS, 0.1% Tween-20, 1% BSA, washing in TBS, 0.1% Tween-20 and detection by horseradish-peroxidase coupled reaction visualized on Chemidoc MP Imaging system (BioRad). Antibodies against ALA10 were obtained by rabbit immunization with the ALA10 C-terminus peptide RSARFHDQIYKDLVGV fused to the N-terminus of ovalbumin and affinity purification on the peptide. Antibodies were used at the following dilution: anti-ALA10 at 1/10,000, anti-GFP-HRP conjugated (Mitenyi Biotech) at 1/5,000, anti-ubiquitin (P4D1)-HRP conjugated (Cell signaling) at 1/1,000, anti-ubiquitin Lys48-specific (Millipore) at 1/1,000, anti-ubiquitin Lys63-specific (Millipore) at 1/1,000, anti SMT (Agrisera) at 1/5,000.

Proteomic Analysis by Mass Spectrometry

Protein Digestion

Proteins immunopurified from the L2 plant extract were run on a SDS-PAGE gel. The bands corresponding to the ALA10-GFP protein were manually excised for in-gel digestion with trypsin using a Freedom EVO150 robotic platform (Tecan Traging AG, Switzerland) as follows. Gel bands were washed six times by successive incubations in 25 mM NH_4HCO_3 and then in 50% (v/v) CH_3CN, 25 mM NH_4HCO_3. After dehydration in pure CH_3CN, reduction was carried out with 10 mM DTT in 25 mM NH_4HCO_3 (45 min at 53°C) and alkylation with 55 mM iodoacetamide in 25 mM NH_4HCO_3 (35 min in the dark). Alkylation was stopped by the addition of 10 mM DTT in

25 mm NH_4HCO_3 (10-min incubation). Gel pieces were then washed again in 25 mM NH_4HCO_3 and dehydrated with pure acetonitrile. Modified trypsin (sequencing grade, Promega) in 25 mM NH_4HCO_3 was added to the dehydrated gel pieces for incubation at 37°C overnight. Peptides were extracted from gel pieces in three sequential extraction steps (each 15 min) in 30 µl of 50% (v/v) CH_3CN, 30 µl of 5% (v/v) formic acid, and finally 30 µl of pure CH_3CN. The pooled supernatants were dried under vacuum.

Nano-LC–MS/MS Analyses

The dried extracted peptides were resuspended in 5% acetonitrile and 0.1% trifluoroacetic acid and analyzed *via* online nano-LC–MS/MS (Ultimate 3000 RSLCnano and Q-Exactive Plus, Thermo Fisher Scientific). Peptide mixtures were desalted on line using a reverse phase precolumn (Acclaim PepMap 100 C18, 5 µm bead size, 100 Å pore size, 5 mm × 300 µm, Thermo Fisher Scientific) and resolved on a C18 column (Reprosil-Pur 120 C18-AQ, 1.9 µm, 25 cm × 75 µm, Dr. Maisch HPLC GmbH). The nano-LC method consisted of a 60 min multi-linear gradient at a flow rate of 300 nl/min, ranging from 5 to 33% acetonitrile in 0.1% formic acid. Spray voltage was set at 1.5 kV and heated capillary was adjusted to 250°C. Survey full-scan MS spectra (m/z = 400–1600) were acquired with a resolution of 70,000, with AGC target set to 10^6 ions (maximum filling time 250 ms) and with lock mass option activated. The 10 most intense ions were fragmented by higher-energy collisional dissociation (nce = 30) with a resolution of 17,500, with AGC target set to 10^6 ions (maximum filling time 250 ms and minimum AGC target of 3×10^3), and dynamic exclusion set to 20 s. MS and MS/MS data were acquired using the Xcalibur software (Thermo Scientific).

Database Searches and Results Processing

Data were processed automatically using Mascot Distiller software (version 2.6, Matrix Science). Peptides and proteins were identified using Mascot (version 2.6, Matrix Science) through concomitant searches against TAIR (version 10.0), classical contaminants database (homemade), and their corresponding reversed databases. Trypsin/P was chosen as the enzyme and three missed cleavages were allowed. Precursor and fragment mass error tolerance were set, respectively, to 10 ppm and 25 mmu. Variable peptide modifications allowed during the search were: carbamidomethylation (C), acetyl (Protein N-ter), oxidation (M), and diGlycine (K). The Proline software (http://proline.profiproteomics.fr) was used to filter the results: conservation of rank 1 peptide-spectrum match (PSM) with a minimal length of 7 and a minimal score of 25. PSM score filtering was used to reach a False Discovery Rate (FDR) of PSM identification below 1% by employing the target-decoy approach. The mass spectrometry proteomics data have been deposited to the ProteomeXchange Consortium *via* the PRIDE (Perez-Riverol et al., 2019) partner repository with the dataset identifier PXD019412 and 10.6019/PXD019412".

Glycerolipid Analysis

Glycerolipids were extracted from approximately 150 mg of fresh material according to (Folch et al., 1951). Tissue were frozen in liquid nitrogen immediately after harvest, freeze-dried and ground in 4 ml of boiling ethanol for 5 min followed by addition of 2 ml of methanol and 8 ml of chloroform. After saturation with argon and filtration through glass wool, remains were rinsed with 3 ml of chloroform/methanol 2:1, v/v and lipids further extracted by addition of 5 ml of NaCl 1%. The chloroform phase was dried under argon before solubilization in pure chloroform and analysis of fatty acid content. For FA analysis, FAs were methylated using 3 ml of 2.5% H_2SO_4 in methanol during 1 h at 100°C (including standard amounts of 21:0). The reaction was stopped by the addition of 3 ml of water and 3 ml of hexane. The hexane phase was analyzed by gas liquid chromatography (Perkin Elmer) on a BPX70 (SGE) column and detected by flame ionization detector FID. Methylated fatty acids were identified by comparison of their retention times with those of standards and quantified by surface peak method using 21:0 for calibration. Lipids were analyzed by LC–MS/MS as described by (Jouhet et al., 2017). The lipid extracts corresponding to 25 nmol of total FA were dissolved in 100 µl of chloroform/methanol [2/1, (v/v)] containing 125 pmol of each of the three internal standards, DAG 18:0–22:6, PE 18:0–18:0, and SQDG 16:0–18:0. HPLC separation was performed on an Agilent 1200 HPLC system using a 150 mm × 3 mm (length × internal diameter) 5 µm diol column (Macherey-Nagel). Mass spectrometric analysis was done on a 6460 triple quadrupole mass spectrometer (Agilent) equipped with a Jet stream electrospray ion source. For adjustment of lipid quantification, each sample was run in tandem with a lipid extract from a qualified control (QC) of *A. thaliana* leaves. Analysis was done on five biological replicates or as specified. Statistical relevance was based on a Student's test or as indicated in the figure legend.

Confocal Microscopy of ALA10-GFP Lines

Confocal imaging: Slides were observed with an oil immersion 40× objective at room temperature by confocal laser scanning microscopy using a Zeiss LSM 800. GFP and chlorophyll were excited and signal collected sequentially (line by line, two to eight lines average) using the 488 nm laser diode for GFP and the 640 nm laser diode for chlorophyll. Fluorescence was collected between 505 and 514 nm, and 658 and 700 nm for GFP and chlorophyll respectively. All images were acquired using the same acquisition parameters.

BiFC Analysis

cDNAs encoding ALA10 and PUB11 were amplified by PCR and cloned in pENTR:D/TOPO (Invitrogen) using primers ALA10BiFCFw (CACCATGGCTGGTCCAAGTCGGAG) and ALA10BiFCRv (GACACCGACAAGATCCTTATAGATCT GATC) for ALA10, PUB11WTFw (CAACATGCCGG AATGTTCAAG) and PUB11WTRv (TGTCCTGCCGT TAATGTAACCTG) for PUB11. cDNAs were then transferred to pBiFP1 and pBiFP4 for fusion with YFP Nter and YFP Cter respectively. The constructs were coexpressed in *Arabidopsis* protoplasts as described in (Botella et al., 2016). 24 to 48 h after transfection, samples were observed by confocal microscopy with an immersion 40× objective at room temperature by confocal laser scanning microscopy using a

TCS-SP2 operating system (Leica). Fluorescence signals were visualized with an excitation line at 488 nm and a 10 nm collection window (average line by line of 2) for XY λ scan or excitation line at 488 nm with a 422 to 432 nm collection window (average line by line of 8) for YFP and excitation line at 633 nm line with a 658 to 700 nm collection window for chlorophyll (Sequential collection, 400 Hz, line by line).

RESULTS

ALA10 Interacts With PUB11

In order to better understand ALA10 function, we sought protein partners by using a SPLIT-ubiquitin Arabidopsis protein library developed by Hybrigenics Service using the full-length ALA10 protein as a bait (MBmate screen, Hybrigenics Service). Since no interacting protein was identified in this first experiment due to an autoactivating effect of ALA10 construct in yeast, we used the yeast 2-hybrid system for screening and restrained the sequence of the bait to the soluble C-terminal extension of ALA10, that does not share homology with the other ALAs and is reported as topologically located on the cytosolic side of the ER membrane (**Figures 1A, B**) (ULTImate Y2H screen, Hybrigenics Service). Since ALIS subunits are supposed to interact with ALA transmembrane domain (Andersen et al., 2016), they are not expected to be found by using this strategy. PUB11 was obtained as the single very high confidence candidate interacting protein, with 12 independent yeast clones, each covering at least 40% of the protein sequence, including the N-terminus region. The interaction between the C-terminal peptide of ALA10 and the full length PUB11 was confirmed by subsequent 2-hybrid tests (**Figure 1C**) (1-by-1 Y2H Interaction Assay, Hybrigenics Service). To verify the interaction *in planta*, we used the BiFC (Bimolecular Fluorescence Complementation) technique. *Arabidopsis* leaf protoplasts were transfected with expression vectors for expression of full length ALA10 and PUB11 fused in C-ter with each complementary half of YFP. With both associations of YFP halves, YFP fluorescence was observed surrounding chloroplasts. YFP reconstitution indicated the proximity of ALA10 and PUB11 *in vivo* and suggested an interaction between the expressed proteins in plant cells (**Figures 1D, E** and **Supplementary Figure 1**). Considering that the sequence of PUB11 is typical for E3 protein ligases with a U box motif (Andersen et al., 2004; Trujillo, 2018), we investigated ALA10 ubiquitination.

ALA10 Ubiquitination

Several putative sites of ubiquitination were predicted in the ALA10 sequence [**Figure 1A**, CKSAAP-Ubsite (Chen et al., 2011; Chen et al., 2013)]. To verify ALA10 ubiquitination, we purified the protein. For this, we started from ALA10-GFP overexpressing plant lines [called L1 and L2 (Botella et al., 2016)]. The ALA10-GFP fusion protein was purified from 10-day plantlets by GFP-affinity and analyzed by Western blot with

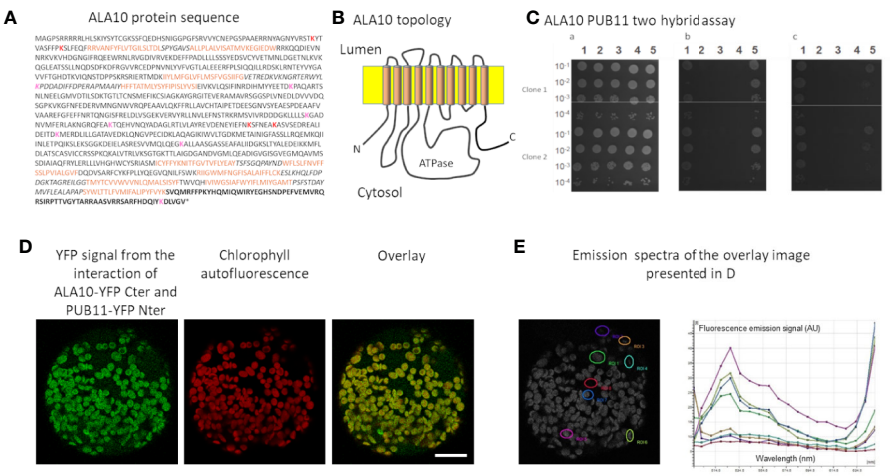

FIGURE 1 | Analysis of ALA10-PUB11 interaction. **(A)** ALA10 protein sequence. In bold characters the C-ter fragment used in yeast two-hybrid screening and assays. Brown characters indicate the transmembrane fragments according to http://aramemnon.uni-koeln.de (Schwacke et al., 2003). Italics characters show the lumen facing protein portions. Lysine predicted with high and low confidence as ubiquitination sites for yeast or human proteins by the CKSAAP-UbSite (Chen et al., 2013) are indicated in red and pink, respectively. **(B)** Schematic topology of ALA10 in the ER membrane. **(C)** GAL4 Y2H two-hybrid interaction assay of ALA10 C terminal fragment with PUB11. Serial dilutions of cells were plated on non-selective or selective media. In **a**—growth on medium without tryptophane and leucine. In **b**—growth without tryptophane, leucine and histidine. In **c**- same condition as in b- with 1 mM of 3-aminotriazole. In column **1**—Smad3/Smurf1 positive control (Colland and Daviet, 2004), **2**—binding and activation domain alone negative control, **3**—binding domain alone and PUB11-activation domain, **4**—ALA10 Cter-binding domain and activation domain alone, **5**—ALA10 Cter-binding domain and PUB11-activation domain. **(D)** BiFC observation of ALA10-YFP Cter domain with PUB11-YFP Nter domain. Representative image over 20 observations. Protoplasts of Arabidopsis leaves were transfected with ALA10 and PUB11 fused respectively with YFP C ter and YFP N ter cloned in pBIFP1 and pBiFP4 and observed as assayed with combinations of ALA10 alone and ALA10 with ALISs in Botella et al. (2016). YFP signal is in green and Chlorophyll signal in red. Bar: 20 nm. **(E)** Emission spectra of the signal recorded in the YFP window at several positions of the image. Each position is indicated by a specific color.

anti-ubiquitin antibodies (**Figures 2A, B**). A signal, though prone to quick degradation, was obtained after addition in the medium of iodoacetamide and of the desubiquitinase inhibitor PR619. The signal was diffuse, visible above the position of ALA10-GFP (164 kDa) with an optimum around 200 kDa suggesting addition of five or six ubiquitins (**Figure 2B**). The purified ALA10-GFP was more abundant in samples prepared from plants treated with MG132, a proteasome inhibitor, compared to MG132 free controls and a similar increase of the ubiquitin signal was observed (**Figures 2A, C**). However, the ubiquitin signal was stronger in L1 line than in L2 even though ALA10-GFP was detected in lower amount in L1. In support of ALA10 ubiquitination, the immunopurified band corresponding to the L2 ALA10-GFP was analyzed by mass spectrometry and contained ubiquitin peptides. We characterized in this fraction between 28 and 50 ALA10 peptides covering around 30% of the protein, as well as GFP peptides (from 6 to 11) and ubiquitin peptides (from 1 to 4) (**Supplementary Table 1**). A few other *Arabidopsis* proteins were detected but not in all repeated experiments. We tried to identify ubiquitinated ALA10 peptides by searching diGly mark as described in (van der Wal et al., 2018). However, we could not identify any ubiquitinated peptide of ALA10 or of any other proteins, possibly due to a partial ubiquitination of proteins or a lack of abundance and ionization of the ubiquitinated peptides. Altogether, although we could not determine its ubiquitination sites, these data suggested that ALA10 is ubiquitinated. In addition, since MG132 treatment lead to higher levels of ALA10GFP, ALA10 ubiquitination could lead to its degradation by 26S proteasome.

ALA10 Protein Level Is Sensitive to 26S Proteasome Degradation

In order to confirm this possibility and to understand the biological relevance of this degradation, we analyzed the expression profile of the ALA10 protein *in vivo*. We set up a western blot analysis of ALA10 at different times along the day in membrane extracts of 9- and 10-day old rosettes (**Figure 3A**), using the *ala10* mutant described in (Botella et al., 2016) as a control for detection of ALA10. ALA10 was detected as a weak signal above a major nonspecific signal at 130 kDa (**Figure 3B**),

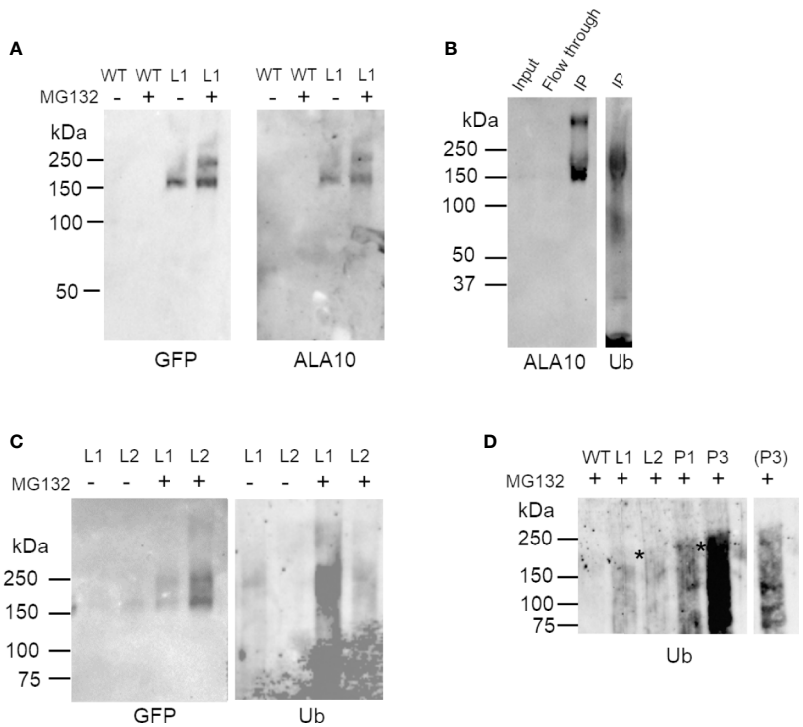

FIGURE 2 | Western blot analysis of ALA10 ubiquitination. **(A)** Immunopurification of ALA10-GFP from plants with stable expression of ALA10-GFP (L1). Comparison with WT. Proteins are prepared from membranes extracted from plants treated the day before harvest with 50 μM MG132, 0.1% DMSO (+) or with only DMSO (–). They are solubilized with 1% Triton X100 and loaded on μMACS microbeads conjugated to an anti-GFP monoclonal antibody (Miltenyi). Purified fraction is analyzed by western blot with antibodies against ALA10 or GFP. **(B)**- ALA10-GFP fusion protein stably expressed in L2 plants was immunopurified (IP) on μMACS microbeads conjugated to an anti-GFP monoclonal antibody (Miltenyi) and analyzed by Western blot with anti-ALA10 and anti-ubiquitin antibodies. Plants were treated the day before harvest with 50 μM MG132 in 0.1% DMSO. **(C)** Immunopurification of ALA10-GFP from plants pretreated or not with MG132, an inhibitor of the proteasome. Samples are two lines of plants with different level of expression of ALA10-GFP, L1 and L2. Plants were treated the day before harvest with 50 μM MG132, 0.1% DMSO (+) or with only DMSO for control (–). Samples are analyzed with anti-GFP and anti-ubiquitin antibodies. **(D)** Comparison of ALA10 ubiquitination in *pub11* relative to WT. ALA10-GFP was immunopurified in two lines of *pub11* with stable expression of ALA10-GFP, P1 and P3, and compared to WT, L1 and L2. Plants were treated the day before harvest with 50 μM MG132, 0.1% DMSO. A shorter exposure of P3 lane is shown on the side. Stars indicate position of the highest ubiquitin signals that were detected in the L or P lanes.

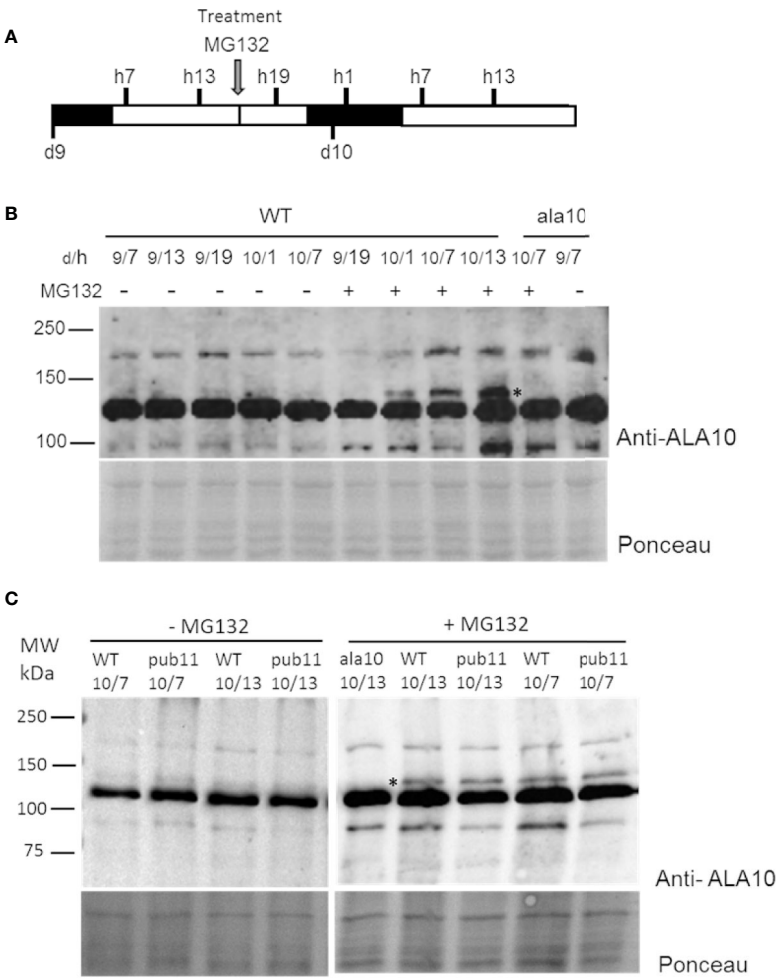

FIGURE 3 | Analysis of ALA10 protein level at different times along days 9 and 10 of culture treated with MG132. **(A)** Time schedule of plantlet collection. Plantlets were grown hydroponically with a 16 h light/8 h dark photoperiod. They were treated at day 9, hour 16 by transfer to a medium containing 50 μM MG132, 0.1% DMSO (+). As a control (–), plantlets were transferred into the same medium containing only 0.1% DMSO. Plantlets were collected at hour 7, 13 and 19 of day 9 (9/h) and at hour 1, 7 and 13 of day 10 (10/h) and immediately frozen in liquid nitrogen. **(B)** Western blot analysis with ALA10 antibodies of WT and *ala10* membrane proteins of plantlets treated or not with MG132. **(C)** Western blot comparison of WT and *pub11* with ALA10 antibodies. A star indicates ALA10 position identified by comparison of WT and *ala10*. Ponceau staining is used for loading control.

but we could not observe any difference of expression along the day in normal conditions. We observed that pretreatment of plants with MG132 increased ALA10 levels, supporting a degradation of ALA10 by 26S proteasome. We then checked whether ALA10 levels were modified in plants deprived of PUB11. An insertion mutant of the SALK collection was selected for a deletion of the pub11 gene (**Supplementary Figures 2A, B**) (Jung et al., 2015). In this mutant ALA10 levels looked relatively similar to those in the WT, with a similar increase after MG132 treatment (**Figure 3C**). Consequently, PUB11 did not appear critical for the degradation of ALA10 by 26S proteasome or for other process affecting protein content in presence of MG132.

In order to determine whether suppression of PUB11 coordinated or not with suppression of ALA10 ubiquitination, we transformed the *pub11* mutant to obtain stable expression of the ALA10-GFP fusion protein as previously done for L1 and L2 in the WT background. We wanted to analyze the ubiquitination of the ALA10-GFP fusion protein immunopurified from the transformed plants but the immunopurification of ALA10-GFP was not successful from the two independent lines. We then treated the plants with MG132 in order to increase ALA10-GFP content and prevent protein degradation. In this condition, in the two *pub11* ALA10-GFP lines (P1 and P3) we analyzed, we observed by western blot an ubiquitin signal in the immunopurified ALA10-GFP fraction that appeared stronger and different from those observed in the PUB11 ALA10-GFP lines, i.e. L1 and L2 (**Figure 2D**). In the P1 and P3 lines, the ubiquitin signal was diffuse with an optimum rather close to 240 kDa, consistent with the addition of eight or nine ubiquitins but with also some signals below 150 kDa, suggesting some degradation of ALA10. This indicated that ALA10 was still

ubiquitinated in the absence of PUB11, but with a different pattern. Thus, PUB11 did not appear to catalyze the ubiquitination of ALA10 necessary for its degradation by 26S proteasome but nevertheless played a role in its ubiquitination pattern, its absence enhancing a distinct type of ALA10 ubiquitination.

ALA10 Accumulates in Chloroplast-Associated Membranes in the Absence of PUB11

Another major effect of protein ubiquitination is modification of the protein localization, which can affect both fate and activity of the protein (Barberon et al., 2011; Guerra and Callis, 2012). It was previously reported that ALA10 can display different localizations in the ER of mesophyll cells, with accumulation either next to the plasma membrane or next to the chloroplasts (Botella et al., 2016). In order to localize the protein in plants missing PUB11, we analyzed by confocal imaging the *pub11* mutants with stable expression of the ALA10-GFP fusion protein. In guard cells of both *pub11* lines exhibiting ALA10-GFP expression, we observed the GFP signal mainly around the chloroplasts, whereas in the WT background control, GFP was stronger at the periphery of the cell and at typical position for ER imaging such as around the nucleus (**Figure 4A**). The same observation was done in mesophyll cells (**Figure 4B**). Moreover, a similar difference was observed between WT and *pub11* lines with the GFP-ALA10 fusion protein holding GFP at the Cter of ALA10 instead at the Nter (**Supplementary Figure 3**). Based on these observations, PUB11 was necessary for the localization of ALA10 in a portion of the ER membrane non-associated with chloroplasts.

Suppression of PUB11 Influences the Positive Effect of ALA10 on 18:3 Containing PC and MGDG Synthesis

Previous report showed that ALA10had a positive effect on leaf development, by counteracting MGDG synthesis limitation (Botella et al., 2016). We previously showed that ALA10 modulates the MGDG/PC ratio possibly through MGD1 activation by PA. At the molecular level, ALA10 interacts with FAD2 in the ER, limiting PC desaturation to 18:2; therefore, chloroplastic PC is enriched in 18:2, resulting in an enhancement of MGDG synthesis. This effect on PC pools occurs in quantitatively minor membrane domains; it is therefore challenging to analyze it at the level of the whole cell lipid extract, and requires the analysis of large sets of plantlets. We here compared the lipid composition of leaves in plant lines, which express or not exogenous ALA10-GFP either in a WT or a *pub11* background. Aerial parts of 15 days old seedlings were analyzed. The dry weight of rosettes showed a slight increase in the *pub11*/ALA10-GFP lines (P1 and P3) and a slight decrease in one of the ALA10-GFP overexpressor lines (L1) (**Supplementary Figure 4A**). We did not detect a significant variation of fresh weigh relative to dry weight (**Supplementary Figure 4A**). Per dry weight, the fatty acid content variations between each lines were not statistically significant (**Figure 5A**). Similarly, no difference was observed for the lipid content, except in the L1 line, where

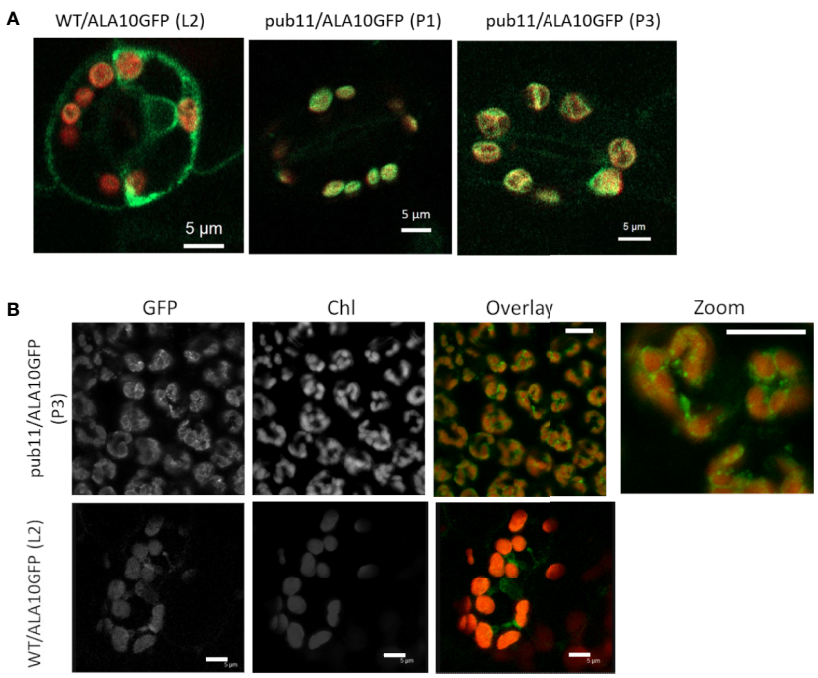

FIGURE 4 | Localization of ALA10 in the *pub11* mutant by confocal microscopy. **(A)** and **(B)** Confocal imaging in WT or in *pub11* background with stable expression of ALA10-GFP in guard cells **(A)** and in mesophyll cells **(B)**. In **(A)** overlay of the signals in the GFP (green) and chlorophyll (red) windows. Observation in two different lines compared with WT. In **(B)**, observation in mesophyll cells of a line of *pub11* with stable expression of ALA10-GFP. Scale 5 µm.

we observe an increase of MGDG, consistent with the increase of MGDG/PC ratio in this line (**Figure 5B** and **Supplementary Figures 5A, C**) already noticed in (Botella et al., 2016). However, this increase was not statistically significant when expressing the lipid contents in mol% (**Supplementary Figure 5B**). We also noticed a very low level of PA in the *pub11* lines whereas this amount is highly variable in the WT and L1 and L2 lines.

In this context, whereas in proportion the profiles of lipid classes appear rather similar in all lines, the overall fatty acid proportion was slightly altered with an increase of 18:3 in *pub11*/ALA10-GFP (P1 and P3) and a decrease of 18:3 in WT/ALA10-GFP (L1 and L2) lines compared to non overexpressor lines (WT and *pub11*). This implies a dual role of ALA10 depending on PUB11 (**Figure 5A** and **Supplementary Figure 4B**). This difference of fatty acid was detectable only in two classes of lipids: PC and MGDG (**Figure 5C** and **Supplementary Figure 5C**). The 36:5 and 36:6 molecular species of PC, corresponding respectively to 18:2/18:3 and 18:3/18:3 molecules, were decreased in the L1 and L2 lines (**Figure 5C**). This effect was lost when ALA10 was overexpressed in the *pub11* mutant context. The MGDG composition was also modified with a decrease of 34:6 compensated by an increase of 36:6 in the L1 and L2 lines (**Supplementary Figure 5C**), indicating an increase of the eukaryotic pathway relative to the prokaryotic pathway. Because in the L1 lines, MGDG quantity was significantly higher than in the other lines, there was no decrease of the 34:X MGDG species (prokaryotic pathway) but rather an increase of the 36:X MGDG species (eukaryotic pathway) (**Supplementary Figure 5C**). Altogether, although these analyses are difficult to perform and interpret, results are consistent with the fact that in the ALA10 overexpressing lines there is less 18:3 PC and more eukaryotic MGDG but that this effect is lost when PUB11 is absent.

DISCUSSION

Our data show that ALA10 is a P_4-type ATPase prone to degradation by 26S proteasome. The protein was previously found in two proteomes of young seedlings treated by MG132 (Maor et al., 2007; Manzano et al., 2008). We here observed a strong increase of ALA10 amounts when the plants were treated by MG132 notably the day after treatment. Since we detected ubiquitin associated with purified ALA10 and an increase of this ubiquitin association after MG132 treatment, our data suggest that ALA10 is ubiquitinated and that its ubiquitination can lead to its degradation by the 26S proteasome. Considering that PUB11 is an E3 ubiquitin ligase (Jung et al., 2015), the interaction of ALA10 with PUB11 which we showed by yeast 2H and *in vivo* BiFC also supports ALA10 ubiquitination. Yet, we could not verify that ALA10 is directly ubiquitinated by PUB11. Deletion of PUB11 did not suppress the increase of ALA10 concentration when plants were treated with MG132 therefore suggesting that ALA10 degradation by 26S proteasome is not

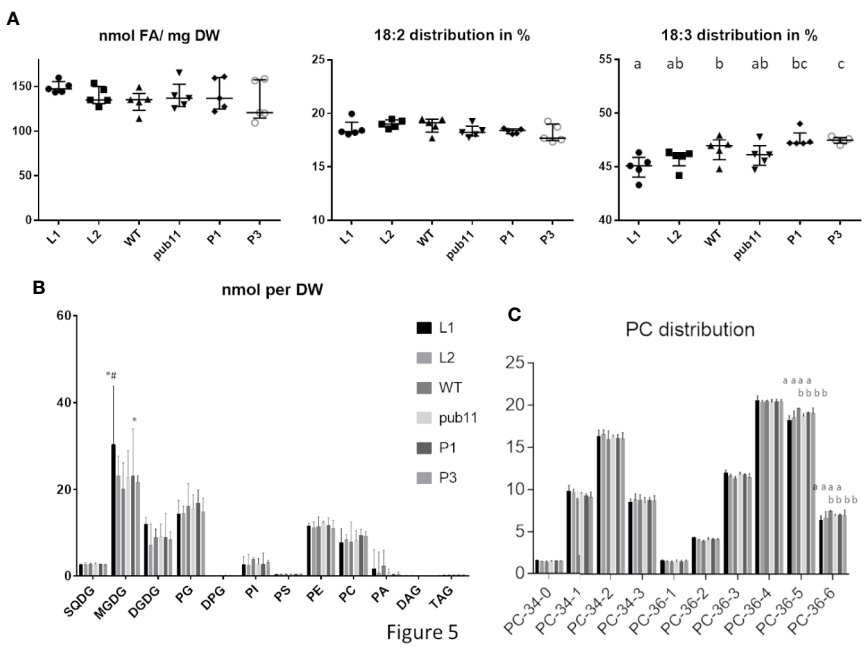

FIGURE 5 | Lipid composition of aerial part of 15 d old plantlets of *pub11* lines overexpressing ALA10-GFP. **(A)** Fatty acid content and distribution of 18:2 and 18:3 fatty acids. (n = 5, Unpaired t test with Welch's correction, P <0.05, differences between means that share a letter are not statistically significant). **(B)** Glycerolipid content. Glycerolipids were analyzed by MS and all glycerolipid data are expressed in nmol as adjusted to a standard reference of *Arabidopsis* leaf lipid extract run in parallel. All contents are expressed per dry weight. Lines which are compared are WT, *pub11* and overexpressors of ALA10-GFP in WT (L1 and L2) and in *pub11* (P1 and P3). Lipid are analyzed by MS (Jouhet et al., 2017). N = 5. * and # indicate statistically significant differences (Student's t test with Welch's correction, P <0.05) with WT (*) and *pub11* (#). **(C)** Relative distribution of the main molecular species of PC. (n = 5, two way ANOVA corrected for multiple comparison for C, P <0.05, differences between means that share a letter are not statistically significant).

directly related to the interaction of ALA10 with PUB11. Moreover, ALA10 ubiquitination was not suppressed in the *pub11* mutant and the pattern of ALA10 ubiquitination looked different in this mutant. Thus, our results rather support that there are several types of ubiquitination of ALA10 and that PUB11 plays a role in ubiquitination of ALA10 independently of its 26S proteasome degradation.

What is then the function of the PUB11-dependent ubiquitination of ALA10? Several possible functions of ubiquitin modification have already been reported in plants, from alteration of abundance to modification of localization and shift in interaction properties (Guerra and Callis, 2012; Xie et al., 2015). Here we show that PUB11 does not seem to have an impact on ALA10 abundance but rather influences ALA10 localization. In the absence of PUB11, ALA10 is mainly present in the vicinity of chloroplasts and reduced or absent in the ER not associated with chloroplasts. This indicates a role of PUB11 in ALA10 localization. We previously showed that ALA10 localizes in different domains of the ER depending on the β subunit it interacts with, near chloroplasts with ALIS5 and close to the plasma membrane with ALIS1 (Botella et al., 2016). Our interpretation is that PUB11-dependent ubiquitination of ALA10 is detrimental to the interaction of ALA10 with specifically ALIS5, and favorable to both its interaction with ALIS1 and its localization close to the plasma membrane. In the absence of PUB11, improved molecular accessibility of ALA10 to ALIS5 would therefore favor its localization next to chloroplasts.

In plants, several cases where ubiquitination modifies protein localization have been described, for instance ubiquitination of iron and boron translocators in the plasma membrane. These ubiquitinations have a role in reducing the translocator abundance at the cell surface, and consequently inhibiting the ion uptake that prevents its toxicity in the cell (Barberon et al., 2011; Kasai et al., 2011; Zelazny et al., 2011). By endocytosis of the ubiquitinated protein, the translocator is sorted from the plasma membrane to the lytic vacuole where it is degraded. Our results suggest a role somewhat different for PUB11-dependent ubiquitination of ALA10 since we observed that the main degradation of ALA10 is related to 26S proteasome activity and independent of PUB11. Since PUB11 primarily affected the amount of ALA10 next to chloroplasts, this suggests a role of PUB11 in the turnover of chloroplast-associated ALA10.

ALA10 is a phospholipid flippase acting mainly on PC (Poulsen et al., 2015; Jensen et al., 2017). In *Arabidopsis* leaves, ALA10 interacts with FAD2 in the ER leading to an imbalance of PC desaturation towards an increase of 18:2-containing PC (Botella et al., 2016). FA desaturations in the ER are limiting steps during cell growth (Mei et al., 2015). Because of the light-dependence of FA synthesis, the increase in desaturated FAs during the dark period suggests also a daylight limitation of FA desaturation mainly in the ER on PC (Browse et al., 1981; Sasaki et al., 1997). Considering that ALA10 interacts with FAD2 and prevents production of 18:3-containing PC, it is likely that ALA10 contributes to preservation of an 18:2 pool of PC to the detriment of further desaturation into 18:3-containing PC. The preserved pool of 18:2-containing PC could feed the eukaryotic pathway for synthesis of galactolipids since an overexpression of FAD3 was reported to increase 18:3-enriched PC and PE and decrease MGDG (Shah et al., 1997). Consistently, we observed that PC 36:6 was slightly affected in the WT/ALA10-GFP lines compared to the WT and that this effect was lost in the *pub11*/ALA10-GFP lines. Since PC 36:6 contains two 18:3 FA, this suggests that PUB11 could play a role in ALA10-dependent limitation of 18:3-containing PC, possibly through ubiquitination of ALA10 and subsequent localization change.

Furthermore, because PA production seems altered in all *pub11* mutant backgrounds, this might explain why the increase of MGDG synthesis is not conserved when ALA10-GFP is overexpressed in *pub11* background. The decrease of the eukaryotic pathway proportion in MGDG production as well as a potential decrease of PA in *pub11* mutants support what was described in (Botella et al., 2017) and recently found by (Karki et al., 2019) where the authors showed that different pools of PC, probably localized in different membrane domains, are involved upstream MGDG production.

This work unravels a new partner of plant flippases, an ubiquitin ligase. To better understand these new functions in the context of the plant membrane homeostasis, it is crucial to understand plant flippase regulations to provide insights into the cellular processes driven by these proteins. The elucidation of ER membrane domain composition at different location of the cell might be a key element to apprehend these lipid homeostasis regulation and adaptation.

DATA AVAILABILITY STATEMENT

The mass spectrometry proteomics data have been deposited to the ProteomeXchange Consortium *via* the PRIDE [1] partner repository with the dataset identifier PXD019412 and 10.6019/PXD019412.

AUTHOR CONTRIBUTIONS

JJ conceived the original screening, supervised and complemented the writing. CB performed part of the experiments. CA provided technical assistance to MB. JS performed part of the experiments. VG provided technical assistance to JJ. MB and JJ conceived the project, supervised the experiments, and wrote the article with contributions of all the authors.

FUNDING

Authors were supported by LabEX GRAL, ANR-10-LABX-49-01 financed within the University Grenoble Alpes graduate school (Ecoles Universitaires de Recherche) CBH-EUR-GS (ANR-17-EURE-0003), by the French ANR through Glyco@Alps (ANR-

15-IDEX-02) and Young Scientist grant ChloroMitoLipid (ANR–12–JSV2–0001).

ACKNOWLEDGMENTS

Authors wish to thank Gloria Gateva and Chloé Gonthier for technical assistance, Morgane Michaud, Denis Falconet, Eric Maréchal and Fabrice Rebeillé for helpful discussion of the results, Sabine Brugière and Yohann Coute from the platform EDyP-Service for their proteomic analysis.

SUPPLEMENTARY MATERIAL

The Supplementary Material for this article can be found online at: https://www.frontiersin.org/articles/10.3389/fpls.2020.01070/full#supplementary-material

SUPPLEMENTAL TABLE 1 | Result of mass spectrometry analysis of the immunopurified ALA10-GFP fraction purified on a SDS-PAGE gel between 150 and 200 kDa. Results are from 3 independent biological and immunopurification experiments. In purple is emphasized the peptides corresponding to ALA10 protein, in green to GFP and in yellow to the ubiquitin.

REFERENCES

Alonso, J. M., Stepanova, A. N., Leisse, T. J., Kim, C. J., Chen, H., Shinn, P., et al. (2003). Genome-wide insertional mutagenesis of Arabidopsis thaliana. *Science* 301, 653–657. doi: 10.1126/science.1086391

Andersen, P., Kragelund, B. B., Olsen, A. N., Larsen, F. H., Chua, N. H., Poulsen, F. M., et al. (2004). Structure and biochemical function of a prototypical Arabidopsis U-box domain. *J. Biol. Chem.* 279, 40053–40061. doi: 10.1074/jbc.M405057200

Andersen, J. P., Vestergaard, A. L., Mikkelsen, S. A., Mogensen, L. S., Chalat, M., and Molday, R. S. (2016). P4-ATPases as Phospholipid Flippases-Structure, Function, and Enigmas. *Front. Physiol.* 7, 275. doi: 10.3389/fphys.2016.00275

Barberon, M., Zelazny, E., Robert, S., Conejero, G., Curie, C., Friml, J., et al. (2011). Monoubiquitin-dependent endocytosis of the iron-regulated transporter 1 (IRT1) transporter controls iron uptake in plants. *Proc. Natl. Acad. Sci. U.S.A.* 108, E450–E458. doi: 10.1073/pnas.1100659108

Block, M. A., Dorne, A. J., Joyard, J., and Douce, R. (1983). Preparation and characterization of membrane fractions enriched in outer and inner envelope membranes from spinach chloroplasts. I. Electrophoretic and immunochemical analyses. *J. Biol. Chem.* 258, 13273–13280.

Botella, C., Sautron, E., Boudiere, L., Michaud, M., Dubots, E., Yamaryo-Botte, Y., et al. (2016). ALA10, a Phospholipid Flippase, Controls FAD2/FAD3 Desaturation of Phosphatidylcholine in the ER and Affects Chloroplast Lipid Composition in Arabidopsis thaliana. *Plant Physiol.* 170, 1300–1314. doi: 10.1104/pp.15.01557

Botella, C., Jouhet, J., and Block, M. A. (2017). Importance of phosphatidylcholine on the chloroplast surface. *Prog. Lipid Res.* 65, 12–23. doi: 10.1016/j.plipres.2016.11.001

Botte, C. Y., Deligny, M., Roccia, A., Bonneau, A. L., Saidani, N., Hadre, H., et al. (2011). Chemical inhibitors of monogalactosyldiacylglycerol synthases in *Arabidopsis thaliana*. *Nat. Chem. Biol.* 7, 834–842.

Boudiere, L., Michaud, M., Petroutsos, D., Rebeille, F., Falconet, D., Bastien, O., et al. (2014). Glycerolipids in photosynthesis: Composition, synthesis and trafficking. *Biochim. Biophys. Acta.* 1837, 470–480.

Browse, J., Roughan, P. G., and Slack, C. R. (1981). Light control of fatty acid synthesis and diurnal fluctuations of fatty acid composition in leaves. *Biochem. J.* 196, 347–354. doi: 10.1042/bj1960347

Chen, Z., Chen, Y. Z., Wang, X. F., Wang, C., Yan, R. X., and Zhang, Z. (2011). Prediction of ubiquitination sites by using the composition of k-spaced amino acid pairs. *PloS One* 6, e22930.

Chen, Z., Zhou, Y., Song, J., and Zhang, Z. (2013). hCKSAAP_UbSite: improved prediction of human ubiquitination sites by exploiting amino acid pattern and properties. *Biochim. Biophys. Acta* 1834, 1461–1467. doi: 10.1371/journal.pone.0022930

Clough, S. J., and Bent, A. F. (1998). Floral dip: a simplified method for Agrobacterium-mediated transformation of Arabidopsis thaliana. *Plant J.* 16, 735–743. doi: 10.1046/j.1365-313x.1998.00343.x

Colland, F., and Daviet, L. (2004). Integrating a functional proteomic approach into the target discovery process. *Biochimie* 86, 625–632. doi: 10.1016/j.biochi.2004.09.014

Dubots, E., Audry, M., Yamaryo, Y., Bastien, O., Ohta, H., Breton, C., et al. (2010). Activation of the chloroplast monogalactosyldiacylglycerol synthase MGD1 by phosphatidic acid and phosphatidylglycerol. *J. Biol. Chem.* 285, 6003–6011.

Folch, J., Ascoli, I., Lees, M., Meath, J. A., and Le, B. N. (1951). Preparation of lipide extracts from brain tissue. *J. Biol. Chem.* 191, 833–841.

Gronnier, J., Gerbeau-Pissot, P., Germain, V., Mongrand, S., and Simon-Plas, F. (2018). Divide and Rule: Plant Plasma Membrane Organization. *Trends Plant Sci.* 23, 899–917.

Guerra, D. D., and Callis, J. (2012). Ubiquitin on the move: the ubiquitin modification system plays diverse roles in the regulation of endoplasmic reticulum- and plasma membrane-localized proteins. *Plant Physiol.* 160, 56–64. doi: 10.1104/pp.112.199869

Jensen, M. S., Costa, S. R., Duelli, A. S., Andersen, P. A., Poulsen, L. R., Stanchev, L. D., et al. (2017). Phospholipid flipping involves a central cavity in P4 ATPases. *Sci. Rep.* 7, 17621. doi: 10.1038/s41598-017-17742-y

Jouhet, J., Marechal, E., and Block, M. A. (2007). Glycerolipid transfer for the building of membranes in plant cells. *Prog. Lipid. Res.* 46, 37–55.

Jouhet, J., Lupette, J., Clerc, O., Magneschi, L., Bedhomme, M., Collin, S., et al. (2017). LC-MS/MS versus TLC plus GC methods: Consistency of glycerolipid and fatty acid profiles in microalgae and higher plant cells and effect of a nitrogen starvation. *PloS One* 12, e0182423. doi: 10.1371/journal.pone.0182423

Jung, C., Zhao, P., Seo, J. S., Mitsuda, N., Deng, S., and Chua, N. H. (2015). PLANT U-BOX PROTEIN10 Regulates MYC2 Stability in Arabidopsis. *Plant Cell* 27, 2016–2031. doi: 10.1105/tpc.15.00385

Karki, N., Johnson, B. S., and Bates, P. D. (2019). Metabolically Distinct Pools of Phosphatidylcholine Are Involved in Trafficking of Fatty Acids out of and into the Chloroplast for Membrane Production. *Plant Cell* 31, 2768–2788. doi: 10.1105/tpc.19.00121

Kasai, K., Takano, J., Miwa, K., Toyoda, A., and Fujiwara, T. (2011). High boron-induced ubiquitination regulates vacuolar sorting of the BOR1 borate transporter in Arabidopsis thaliana. *J. Biol. Chem.* 286, 6175–6183. doi: 10.1074/jbc.M110.184929

Ling, Q., Huang, W., Baldwin, A., and Jarvis, P. (2012). Chloroplast biogenesis is regulated by direct action of ubiquitin-prosteasome system. *Science* 338, 655–659.

Ling, Q., and Jarvis, P. (2013). Dynamic regulation of endosymbiotic organelles by ubiquitination. *Trends Cell Biol.* 23, 399–408.

Manzano, C., Abraham, Z., Lopez-Torrejon, G., and Del Pozo, J. C. (2008). Identification of ubiquitinated proteins in Arabidopsis. *Plant Mol. Biol.* 68, 145–158. doi: 10.1007/s11103-008-9358-9

Maor, R., Jones, A., Nuhse, T. S., Studholme, D. J., Peck, S. C., and Shirasu, K. (2007). Multidimensional protein identification technology (MudPIT) analysis of ubiquitinated proteins in plants. *Mol. Cell Proteomics* 6, 601–610. doi: 10.1074/mcp.M600408-MCP200

Mei, C., Michaud, M., Cussac, M., Albrieux, C., Gros, V., Marechal, E., et al. (2015). Levels of polyunsaturated fatty acids correlate with growth rate in plant cell cultures. *Sci. Rep.* 5, 15207. doi: 10.1038/srep15207

Mittler, R., and Lam, E. (1995). In Situ Detection of nDNA Fragmentation during the Differentiation of Tracheary Elements in Higher Plants. *Plant Physiol.* 108, 489–493. doi: 10.1104/pp.108.2.489

Nintemann, S. J., Palmgrem, M., and Lopez-Marques, R. L. (2019). Catch You on the Flip Side: A Critical Review of Flippase Mutant Phenotypes. *Trends Plant Sci.* 24, 468–478.

Ohlrogge, J., and Browe, J. (1995). Lipid biosynthesis. *Plant Cell.* 7, 957–970.

Perez-Riverol, Y., Csordas, A., Bai, J., Bernal-Llinares, M., Hewapathirana, S., Kundu, D. J., et al. (2019). The PRIDE database and related tools and resources

in 2019: improving support for quantification data. *Nucleic Acids Res.* 47, D442–D450. doi: 10.1093/nar/gky1106

Poulsen, L. R., Lopez-Marques, R. L., Pedas, P. R., McDowell, S. C., Brown, E., Kunze, R., et al. (2015). A phospholipid uptake system in the model plant Arabidopsis thaliana. *Nat. Commun.* 6, 7649. doi: 10.1038/ncomms8649

Sandelius, A. S., and Liljenberg, C. (1982). Light-Induced-Changes in the Lipid-Composition and Ultrastructure of Plastids from Potato-Tubers. *Physiol. Plantarum* 56, 266–272.

Sasaki, Y., Kozaki, A., and Hatano, M. (1997). Link between light and fatty acid synthesis: thioredoxin-linked reductive activation of plastidic acetyl-CoA carboxylase. *Proc. Natl. Acad. Sci. U.S.A.* 94, 11096–11101. doi: 10.1073/pnas.94.20.11096

Schwacke, R., Schneider, A., van der Graaff, E., Fischer, K., Catoni, E., Desimone, M., et al. (2003). ARAMEMNON, a novel database for Arabidopsis integral membrane proteins. *Plant Physiol.* 131, 16–26. doi: 10.1104/pp.011577

Shah, S., Xin, Z., and Browse, J. (1997). Overexpression of the FAD3 desaturase gene in a mutant of Arabidopsis. *Plant Physiol.* 114, 1533–1539. doi: 10.1104/pp.114.4.1533

Sharma, B., Joshi, D., Yadav, P. K., Gupta, A. K., and Bhatt, T. K. (2016). Role of Ubiquitin-Mediated Degradation System in Plant Biology. *Front. Plant Sci.* 7, 806.

Trujillo, M. (2018). News from the PUB: plant U-box type E3 ubiquitin ligases. *J. Exp. Bot.* 69, 371–384. doi: 10.1093/jxb/erx411

van der Wal, L., Bezstarosti, K., Sap, K. A., Dekkers, D. H. W., Rijkers, E., Mientjes, E., et al. (2018). Improvement of ubiquitylation site detection by Orbitrap mass spectrometry. *J. Proteomics* 172, 49–56. doi: 10.1016/j.jprot.2017.10.014

Xie, L., Lang-Mladek, C., Richter, J., Nigam, N., and Hauser, M. T. (2015). UV-B induction of the E3 ligase ARIADNE12 depends on CONSTITUTIVELY PHOTOMORPHOGENIC 1. *Plant. Physiol. Biochem.* 93, 18–28. doi: 10.1016/j.plaphy.2015.03.006

Zelazny, E., Barberon, M., Curie, C., and Vert, G. (2011). Ubiquitination of transporters at the forefront of plant nutrition. *Plant Signal Behav.* 6, 1597–1599. doi: 10.4161/psb.6.10.17134

Zheng, G. W., Li, L. X., and Li, W. Q. (2016). Glycerolipidome responses to freezing- and chilling-induced injuries: examples in Arabidopsis and rice. *BMC Plant. Biol.* 16.

Conflict of Interest: The authors declare that the research was conducted in the absence of any commercial or financial relationships that could be construed as a potential conflict of interest.

frontiers in Plant Science

REVIEW
published: 09 September 2020
doi: 10.3389/fpls.2020.579019

Degradation of Lipid Droplets in Plants and Algae—Right Time, Many Paths, One Goal

*Krzysztof Zienkiewicz and Agnieszka Zienkiewicz**

Centre for Modern Interdisciplinary Technologies, Nicolaus Copernicus University in Toruń, Toruń, Poland

In eukaryotic cells, lipids in the form of triacylglycerols (TAGs) are the major reservoir of cellular carbon and energy. These TAGs are packed into specialized organelles called lipid droplets (LDs). They can be found in most, if not all, types of cells, from bacteria to human. Recent data suggest that rather than being simple storage organelles, LDs are very dynamic structures at the center of cellular metabolism. This is also true in plants and algae, where LDs have been implicated in many processes including energy supply; membrane structure, function, trafficking; and signal transduction. Plant and algal LDs also play a vital role in human life, providing multiple sources of food and fuel. Thus, a lot of attention has been paid to metabolism and function of these organelles in recent years. This review summarizes the most recent advances on LDs degradation as a key process for TAGs release. While the initial knowledge on this process came from studies in oilseeds, the findings of the last decade revealed high complexity and specific mechanisms of LDs degradation in plants and algae. This includes identification of numerous novel proteins associated with LDs as well as a prominent role for autophagy in this process. This review outlines, systemizes, and discusses the most current data on LDs catabolism in plants and algae.

Keywords: lipid droplets (LDs), triacylglycerols (TAGs), lipid droplet degradation, lipolysis, lipase, autophagy, lipophagy

OPEN ACCESS

Edited by:
Kazufumi Yazaki,
Kyoto University, Japan

Reviewed by:
Takashi L. Shimada,
Chiba University, Japan
Yonghua Li-Beisson,
Commissariat à l'Energie Atomique et aux Energies Alternatives (CEA), France

***Correspondence:**
Agnieszka Zienkiewicz
agazet@umk.pl

Specialty section:
This article was submitted to Plant Metabolism and Chemodiversity, a section of the journal Frontiers in Plant Science

Received: *01 July 2020*
Accepted: *24 August 2020*
Published: *09 September 2020*

Citation:
Zienkiewicz K and Zienkiewicz A (2020) Degradation of Lipid Droplets in Plants and Algae—Right Time, Many Paths, One Goal. Front. Plant Sci. 11:579019. doi: 10.3389/fpls.2020.579019

INTRODUCTION

Lipids in plants and algae can be generally divided into two major groups, storage lipids and membrane lipids. The former serve as energy and carbon reservoirs, and the latter are building blocks for photosynthetic and non-photosynthetic membranes (Li-Beisson et al., 2013). Additionally, land plants deposit a lipidic layer composed of waxes and cutin on their surface, which serves as an impermeable barrier protecting them from excessive water loss, pathogens, and toxins (Nawrath et al., 2013; Serrano et al., 2014). The storage lipids are represented mainly by triacylglycerols (TAGs) and to a much lesser degree by sterol esters, whereas lipid composition of membranes is more complex and differs between cell compartments, cell types, and organisms (Bouvier-Navé et al., 2010; Horn et al., 2011; Goold et al., 2015; Shimada et al., 2019). Broadly, galactolipids are much more abundant in plastidial membranes, whereas non-plastidial membranes are composed mostly of phospholipids (Li-Beisson et al., 2013). Synthesis of lipids in plant and algal cells starts in plastids, where fatty acids (FAs) are generated. These molecules are further used as substrates in the key cellular pathways of membrane lipid and TAGs

synthesis. Before entering complex metabolic pathways FAs often undergo modifications, like desaturation or elongation. Regardless of their modification level, FAs can reside in the chloroplast, where they function as substrates for synthesis of plastidial membrane lipids, like monogalactosyldiacylglycerol (MGDG) or digalactosyldiacylglycerol (DGDG) (Wang and Benning, 2012; Lavell and Benning, 2019). When exported to the cytosol, free FAs are first exported by FATTY ACID EXPORT1 (FAX1) across the chloroplast inner envelope and then undergo vectorial acylation by the chloroplast outer envelope-localized long-chain acyl-CoA synthetase 9 (LACS9) (Schnurr et al., 2002; Li et al., 2015; Li et al., 2016; Li et al., 2019). The resulting conjugates of FAs with coenzyme A (CoA)—acyl-CoAs are transported into endoplasmic reticulum (ER) and incorporated into the cellular pool of carbon and energy in the form of TAGs (Li et al., 2016). The major pathway of TAGs synthesis is the glycerol-3-phosphate (G-3-P) (or Kennedy) pathway (**Figure 1**) (Ohlrogge and Browse, 1995; Chapman and Ohlrogge, 2012). In this pathway, G-3-P is successively esterified with acyl chains from acyl-CoAs. These reactions occur in a precise manner and are catalyzed by specific acyltransferases located in the endoplasmic reticulum (ER) membrane. In the first reaction, catalyzed by glycerol-3-phosphate acyltransferase (GPAT), G-3-P is linked to acyl-CoA and lysphosphatidic acid (LPA) is generated. LPA is then converted into phosphatidic acid (PA) by esterification with another acyl-CoA. This reaction is catalyzed by lysophosphatidate acyltransferase (LPAT). PA can serve as a substrate for synthesis of phospholipids or TAGs. In the latter case, dephosphorylation of PA by phosphatidic acid phosphatase (PAP) leads to formation of diacylglycerol (DAG) (Li-Beisson et al., 2013). The synthesized DAG is further converted into TAG by acyl-CoA:diacylglycerol acyltransferases (DGATs), and this reaction is considered a committed step of TAG formation (Zhang et al., 2009; Turchetto-Zolet et al., 2011; Sanjaya et al., 2013; Zienkiewicz et al., 2016; Zienkiewicz et al., 2017; Zienkiewicz et al., 2018). In addition to DGAT-mediated pathway DAG can also be acylated into TAG by the phospholipid:diacylglycerol acyltransferase (PDAT) (**Figure 1**). This enzyme has been shown to synthesize TAG *via* acyl-CoA-independent transacylation of DAG using phosphatidylcholine (PC) as acyl donor (**Figure 1**) (Dahlqvist et al., 2000; Zhang et al., 2009; Yoon et al., 2012).

TAGs synthesized in the ER membrane are continuously deposited between leaflets of the membrane bilayer, finally forming spherical organelles referred to in the literature by many terms, such as lipid droplets (thereafter LDs), oil bodies (OBs), oleosomes, or spherosomes (**Figure 1**). A prominent role for LDs formation at ER membrane in plants has been shown for SEIPIN proteins (Cai et al., 2015; Taurino et al., 2018; Greer et al., 2020). Indeed, loss of function *Arabidopsis thaliana* SEIPIN isoforms as well as their overexpression results in altered size of

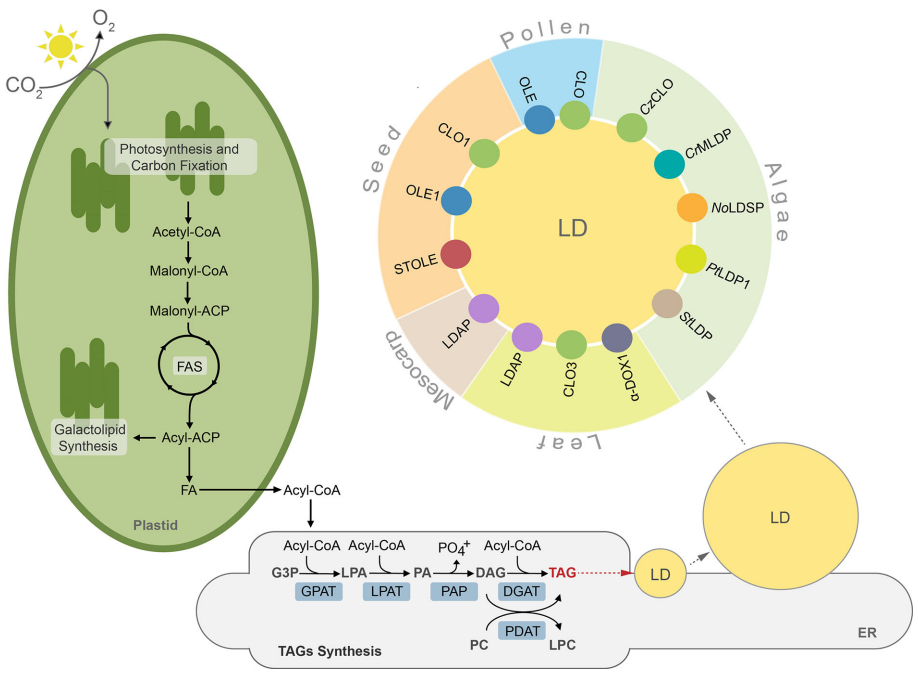

FIGURE 1 | TAGs synthesis, lipid droplet formation and their protein equipment in plant and algal cells. ACP, acyl carrier protein; CoA, coenzyme A; CLO, caleosin; *Cr*MLDP *Chlamydomonas reinhardtii* major lipid droplet protein; *Cz*CLO, *Chromochloris zofingiensis* caleosin; DAG, diacylglycerol; DGAT, acylCoA:diacylglycerol acyltransferase, α-DOX1, dioxygenase 1; FA, fatty acid; FAS, fatty acid synthase, G3P, glycerol-3-phosphate; GPAT, acyl-CoA:glycerol-3-phosphate-acyltransferase; LD, lipid droplet; LDAP, lipid droplet associated protein; LPA, lysophosphatidic acid; LPAT, acyl-CoA:lysophosphatidic acid acyltransferase; LPC, lysophosphatidylcholine, *No*LDSP, *Nannochloropsis oceanica* lipid droplet surface protein; OLE, oleosin; PA, phosphatidic acid; PAP, phosphatidic acid phosphatase, PDAT, phospholipid:diacylglycerol acyltransferase; PC, phosphatidylcholine; *Pt*LDP1, *Phaeodactylum tricornutum* lipid droplet protein 1; StLDP, Stramenopile-type lipid droplet protein; STOLE, steroleosin; TAG, triacylglycerol.

LDs, however, the exact role of these proteins in LDs formation remains to be clarified (Cai et al., 2015; Taurino et al., 2018). Recent studies showed also that mutation in the gene encoding *At*VAP27-1 (Vesicle-Associated Membrane Protein (VAMP)–Associated Proteins (VAPs)) resulted in formation of aberrant and enlarged LDs. Moreover, a direct interaction between Arabidopsis SEIPIN isoforms (2 and 3) and *At*VAP27-1 indicates that these two proteins most probably cooperate during formation of LDs (Greer et al., 2020). A putative SEIPIN ortholog has also been identified in diatom *Phaeodactylum tricornutum*. Overexpression of this SEIPIN in *P. tricornutum* resulted in biogenesis of larger LDs, suggesting similarities in the functional nature of SEIPINs between plants and algae (Lu et al., 2017).

After their complete formation, LDs separate from the ER membrane and localize to the cytosol (Chapman and Ohlrogge, 2012; Murphy, 2012; Olzmann and Carvalho, 2019). LDs have been identified in cells of diverse organisms, including bacteria (Zhang et al., 2017), yeast (Grillitsch et al., 2011), algae (Zienkiewicz et al., 2020), plants (Tzen et al., 1993), nematodes (O'Rourke et al., 2009), and mammals (Birsoy et al., 2013). This indicates their highly conserved role in cellular lipid metabolism. Until recently LDs were considered as a simple TAG storage compartment, however, intense studies in the last decade revealed that LDs represent highly dynamic structures, involved in a plethora of diverse cellular processes, like regulation of energy homeostasis, remodeling of membranes, and signaling (Chitraju et al., 2017; Welte and Gould, 2017; Yang and Benning, 2018; Fernandez-Santos et al., 2020). According to the common structural model, LDs are composed of a hydrophobic core filled mostly with TAGs surrounded by a phospholipid monolayer, and are decorated with a set of specific proteins (**Figure 1**). These proteins are considered essential for biogenesis, stabilization, and mobilization of LDs, and are cell-, tissue-, and organism-specific (**Figure 1**, **Table S1**) (Tzen et al., 1993; Huang, 2018).

LIPID DROPLETS—MULTIPLE VARIANTS OF THE SAME ORGANELLE?

In plants, structural proteins of LDs were first and best characterized in seeds (Tzen et al., 1990; Tzen et al., 1993; Jolivet et al., 2004; Huang, 2018; Du et al., 2019). The set of major LD structural proteins found in seeds includes oleosin, caleosin, and steroleosin, however their individual isoforms are also present in non-seed tissues (**Table S1**) (Chapman et al., 2012; Huang, 2018). Oleosins are the most abundant integral membrane proteins of oilseed LDs. They are anchored in the phospholipid monolayer by a hydrophobic α-helical hairpin domain with a proline knot, and their C- and N- termini face the cytosol (Abell et al., 1997; Napier et al., 2001; Alexander et al., 2002). As *Arabidopsis thaliana* mutant of one of the seed-specific oleosins *ole1* accumulates larger LDs when compared to wild type plants, it has been proposed that oleosins control the structure and size of LDs by preventing their uncontrolled fusion (Siloto et al., 2006; Shimada et al., 2008). Caleosins are much less abundant compared to oleosins in the LDs fraction from oilseeds. Their name derives from the ability to bind calcium ions (by a single EF-hand binding motif) and structural similarity to oleosins (Chen et al., 1999). Phylogenetic studies so far suggest that caleosin proteins were likely the ancestors of oleosins, as the putative genes encoding for caleosin-, but not oleosin-like proteins, are present in algae, non-vascular plants, and fungi (Jiang and Tzen, 2010; Rahman et al., 2018a; Rahman et al., 2018b). The ability to bind calcium ions, together with the presence of several phosphorylation sites and possession of peroxygenase activity suggest that caleosins mediate signaling between diverse developmental and stress signals and LDs (Hanano et al., 2006; Purkrtova et al., 2008). Unlike caleosins and oleosins, steroleosins possess only two structural motifs: an N-terminal hydrophobic region responsible for association with LD membranes through conserved proline residues, and a C-terminal domain with hydroxysteroid dehydrogenase (HSD) activity (d'Andrea et al., 2007). Steroleosins are thought to play a role in brassinosteroid-mediated cellular signaling during plant growth and development (Lin et al., 2002). Recent advances in LDs proteomics identified many new LD-associated proteins in seeds and seedlings, however their functions remain to be deciphered (Zhi et al., 2017; Kretzschmar et al., 2020).

After the seed, pollen grains are one of the most active sites in TAGs biosynthesis (Piffanelli et al., 1998; Zienkiewicz et al., 2014a). Mature pollen grains of many plants, especially oleaginous species, accumulate a high number of LDs in the cytoplasm of the vegetative cell (Zienkiewicz et al., 2014a). Similar to seeds, pollen LDs are coated with oleosin and caleosin, but no pollen steroleosin has yet been identified (Kim et al., 2002; Jiang et al., 2008; Zienkiewicz et al., 2010; Zienkiewicz K. et al., 2011). Interestingly, oleosin-like and caleosin proteins are also present in the pollen coat (Mayfield et al., 2001; Rejon et al., 2016), anther loculus, as well as in tapetal cells (Zienkiewicz K. et al., 2011; Levesque-Lemay et al., 2016). The latter tissue is directly involved in pollen development and is extremely rich in lipidic structures known as tapetosomes. They are released from degrading tapetum during anther development and targeted to the surface of developing pollen grains, eventually forming the pollen coat (Parish and Li, 2010; Levesque-Lemay et al., 2016). Interestingly, each tapetosome consists of multiple LDs clustered together and coated by oleosins (Hsieh and Huang, 2005) and/or caleosin (Zienkiewicz K. et al., 2011). This could explain the presence of both these proteins in the pollen coat (**Table S1**) and suggests that mature pollen grains are equipped with LD-associated proteins of both gametophytic and sporophytic origin.

Depending on developmental stage and/or physiological state of the plant, LDs can also be present in non-seed organs such as fruits, leaves, stems, and roots (Lersten et al., 2006; Shimada et al., 2015; Pyc et al., 2017a; Huang, 2018). Leaf LDs seem to be equipped with a different set of integral proteins than seeds (**Table S1**) (Pyc et al., 2017a; Fernandez-Santos et al., 2020). A leaf-specific isoform of caleosin, CLO3, has been shown to decorate leaf LDs and to be directly involved in triggering the

oxylipin-mediated response to pathogen attack in *A. thaliana* (Hanano et al., 2015; Shimada et al., 2015). Infection of Arabidopsis by the pathogenic fungus *Colletotrichum higginisianum* leads to localization of α-dioxygenase 1 (α-DOX1) on the surface of leaf LDs and the formation of 2-hydroperoxy-octadecatrienoic acid (2-HPOT) from α-linolenic acid released from TAGs stored in LDs. 2-HPOT is then converted by CLO3 into 2-hydroxy-octadecatrienoic acid (2-HOT), which possesses anti-fungal activity (Shimada et al., 2014). Additionally, accumulation of phytoalexin deficient 3 (PAD3) protein involved in camalexin synthesis was observed on the surface of leaf LDs after *Pseudomonas syringae* pv *tomato* (*Pst*) DC3000 *avrRpm1* infection, supporting the role of leaf LDs in the plant defense response (Fernandez-Santos et al., 2020). Besides caleosin, three isoforms of Lipid Droplet Associated Proteins (LDAPs) have been identified in the leaves of Arabidopsis. LDAPs have been shown to be essential for the maintenance and regulation of LD metabolism and to play nonredundant functions in the stress response and post-germinative growth (Gidda et al., 2016). In addition to the above mentioned LD-associated proteins, a few proteins with diverse functions were also identified in the proteome of leaf LDs, including LDAP-interacting protein (LDIP) (Pyc et al., 2017b), glycerol-3-phosphate-acyltransferase 4 (GPAT4) and 8 (GPAT8) (Fernandez-Santos et al., 2020), strictosidine synthase (STR), 2-oxoglutarate (2OG) and farnesylcysteine lyase (FCLY) (Brocard et al., 2017). These observations suggest the multifunctional nature of LDs and support the direct involvement of non-seed LDs in stress-response and defense-related pathways in plants. Among non-seed tissues, few but extremely large LDs (over 10 μm of diameter) have also been found in mesocarp cells of some oleaginous fruits, like olive and avocado (Horn et al., 2013; Bartolini et al., 2014). Similar to seed LDs, mesocarp LDs are filled with TAGs, but they mostly lack oleosin and are equipped with LDAP protein instead (Horn et al., 2013; Zhi et al., 2017).

Under favorable growth conditions, algae usually accumulate small amounts of TAGs, whereas upon stresses such as nutrient limitation (e.g. nitrogen (N) deprivation), elevated temperatures, or high light intensities they synthesize massive amounts (Goold et al., 2015; Li-Beisson et al., 2015; Zienkiewicz et al., 2016). Algal LDs are equipped with specific LD-associated proteins, different from their plant counterparts (Moellering and Benning, 2010; Vieler et al., 2012a; Zienkiewicz et al., 2016; Leyland et al., 2020). The major LD protein MLDP was first identified in green algae, *Chlamydomonas reinhardtii* (Moellering and Benning, 2010; Nguyen et al., 2011) and then in *Dunaiella salina* (Davidi et al., 2012), *Scenedesmus quadricauda* (Javee et al., 2016), *Chromochloris zofingiensis* (Wang et al., 2019), and *Lobosphaera incisa* (Siegler et al., 2017). MLDPs are different from oleosin in lacking the central hydrophobic region, and appear to be specific to the lineage of green algae. Similar to structural proteins covering LDs in land plants, *Cr*MLDP also seems to be involved in the control of LD size and stabilization (Tsai et al., 2015). In turn, LDs of the oleaginous alga *Nannochloropsis oceanica* are decorated with Lipid Droplet Surface Protein (LDSP), which has been shown to localize on the LD surface during N deprivation (Vieler et al., 2012a; Vieler et al., 2012b; Zienkiewicz et al., 2020). *No*LDSP protein, similar to plant oleosin, possesses a proline-rich hydrophobic domain in its central region, however the proline knot motif found in oleosin is absent in *No*LDSP (Vieler et al., 2012a). Major LD structural proteins were also identified in the diatom *P. tricornutum*, including LD-associated protein (*Pt*LDP1) (Wang et al., 2017), a homolog of oleosome-associated-protein 1 (DOAP1) from *Fistulifera solaris* (Maeda et al., 2014), and Stramenopile-type lipid droplet protein (StLDP) (Yoneda et al., 2016). Overexpression of both these proteins in *P. tricornutum* was correlated with increased TAGs content and enlarged LDs during N deprivation (Yoneda et al., 2016; Wang et al., 2017), suggesting their analogous role to plant oleosin. Recently, three caleosin-related proteins were identified by proteomic analyses of LDs from *C. zofingiensis*, and co-localization for two of them on LDs was confirmed in *Saccharomyces cerevisiae* (Wang et al., 2019). Besides the major structural proteins detected in algal LDs, multiple proteomic studies have been performed to identify new LD proteins in diverse algal strains (Siegler et al., 2017; Lupette et al., 2019; Wang et al., 2019), however their specific localization and potential role in LD homeostasis have yet to be investigated.

Regardless of LD protein and TAG composition, their mobilization is crucial for providing energy and carbon during periods of active metabolism. This process is highly coordinated with development (e.g. seed germination) as well as responses to specific environmental conditions (e.g. nutrient deprivation). The release of TAGs from LDs requires the coordinated action of molecular machineries governing protein and lipid breakdown. Below we characterize the current state of knowledge regarding these pathways and interactions.

LDS LIPOLYSIS—TAG LIPASES AND CO-WORKERS

TAG lipases play one of the most essential roles in LDs degradation in plants and algae. These enzymes hydrolyze TAGs stored in LDs leading to the release of FAs, DAGs, MAGs, and glycerol (Graham, 2008; Kelly and Feussner, 2016). Glycerol is subsequently phosphorylated, oxygenated, and enters into glycolysis, whereas FAs undergo β-oxidation into acetyl-CoAs (Eastmond and Graham, 2001). In plants (Graham, 2008; Pracharoenwattana et al., 2010; Rinaldi et al., 2016) and green algae (Kong et al., 2018a; Kong et al., 2018b) the latter process takes place in peroxisomes (glyoxysomes), meanwhile in diatoms both mitochondrial and peroxisomal FAs β-oxidation is tough to occur (Chauton et al., 2013; Jallet et al., 2020).

So far, the TAG lipases directly involved in LD mobilization are best characterized in plants, mainly in germinating seeds and growing seedlings of *A. thaliana* (Eastmond, 2006; Quettier and Eastmond, 2009; Kelly et al., 2011). LDs accumulation during seed development is critical for germination and seedling growth later on (Huang, 1996; Graham, 2008; Zienkiewicz A. et al., 2011; Zienkiewicz et al., 2014b). Based on the analysis of TAGs

breakdown in Arabidopsis *sdp1*, *sdp1L*, and *sdp1 sdp1L* mutants it was demonstrated that among these two TAG lipases only *At*SDP1 (SUGAR DEPENDENT 1) plays a key role in mobilization of TAGs from LDs during seed germination (Eastmond, 2006; Kelly et al., 2011). In addition, the loss of *SDP1* function caused increased TAG content in the seeds of Arabidopsis (van Erp et al., 2014), rapeseed (*Brassica napus* L.) (Kelly et al., 2013a), Jatropha (*Jatropha curcas*) (Kim et al., 2014), and soybean (*Glycine max* L.) (Kanai et al., 2019), suggesting that SDP1 might be involved in TAGs turnover in developing seeds as well. Indeed, a decrease in oil content has often been observed during desiccation phase of seed development in some species (Baud et al., 2002; Chia et al., 2005; Kelly et al., 2013a). It has been proposed that at early stages of post-germinative growth, the inactive form of *At*SDP1 first localizes to the surface of peroxisomes and is then delivered to LDs *via* peroxules, initiating TAGs hydrolysis (**Figure 2**) (Thazar-Poulot et al., 2015; Cui et al., 2016; Esnay et al., 2020). The released FAs are then transported into peroxisomes by *At*PXA1 (an ATP-binding cassette (ABC) transporter) and enter the β-oxidation process (Zolman et al., 2001). Interestingly, Arabidopsis *sdp1* and *sdp1 sdp1L* mutants exhibit residual TAG hydrolysis on sugar-deficient medium, suggesting that additional lipases could also be involved in this process (Kelly et al., 2011). Therefore, the mobilization of TAGs was also analyzed in an Arabidopsis mutant with a lesion in *ADIPOSE TRIGLYCERIDE LIPASE-LIKE* (*ATGL*). *ATGL* encodes a lipase similar to human ATGL and COMPARATIVE GENE IDENTIFIER-58 (CGI-58), which possess TAG lipase, phospholipase A (PLA), and lysophosphatidic acid acyltransferase (LPAAT) activities (Eastmond, 2006; Ghosh et al., 2009; Kelly et al., 2011). However, no significant difference in the rate of TAGs breakdown was observed between wild type plants and these single mutants (Kelly et al., 2011). It was reported recently that *At*OBL1, a homolog of acid lipase from *Ricinus communis* (*Rc*OBL1, oil body lipase 1, Eastmond, 2004) possesses activity towards TAGs in Arabidopsis seeds (Müller and Ischebeck, 2018). Although *At*OBL1 is able to cleave TAGs and is associated with LDs, seed germination and TAGs breakdown rates in the *obl1* mutant were similar to those observed in wild type plants (Müller and Ischebeck, 2018). A specific LD lipoxygenase (LOX) and phospholipase A (PLA) seem to be involved in an alternative pathway of seed LDs degradation (Rudolph et al., 2011). LOX activity leads to formation of (9Z,11E,13S)-13-hydroperoxy octadeca-9,11-dienoic acid (13-HPOD) by oxygenation of linoleate moieties (18:2) of TAGs mobilized from LDs. The 13-HPOD liberated from TAGs can be later reduced to 13-HOD by the peroxygenase activity of caleosin (Rudolph et al., 2011). The LOX and PLA activities were detected *in vitro* on isolated LDs of cucumber (*Cucumis sativus*) (Rudolph et al., 2011) and olive (*Olea europaea* L.) (Zienkiewicz et al., 2014b) during seed germination. Thus, it was proposed that PLA might be responsible for LD membrane degradation and thereby facilitate access of LOX and lipase to TAG.

Pollen development, germination, and pollen tube growth are essential for sexual reproduction in flowering plants. During pollen hydration LDs polarize near the germinative aperture, and as the pollen grain starts to germinate, they enter the emerging pollen tube where their progressive degradation takes place (Zienkiewicz et al., 2013; Taurino et al., 2018). *At*SDP1L,

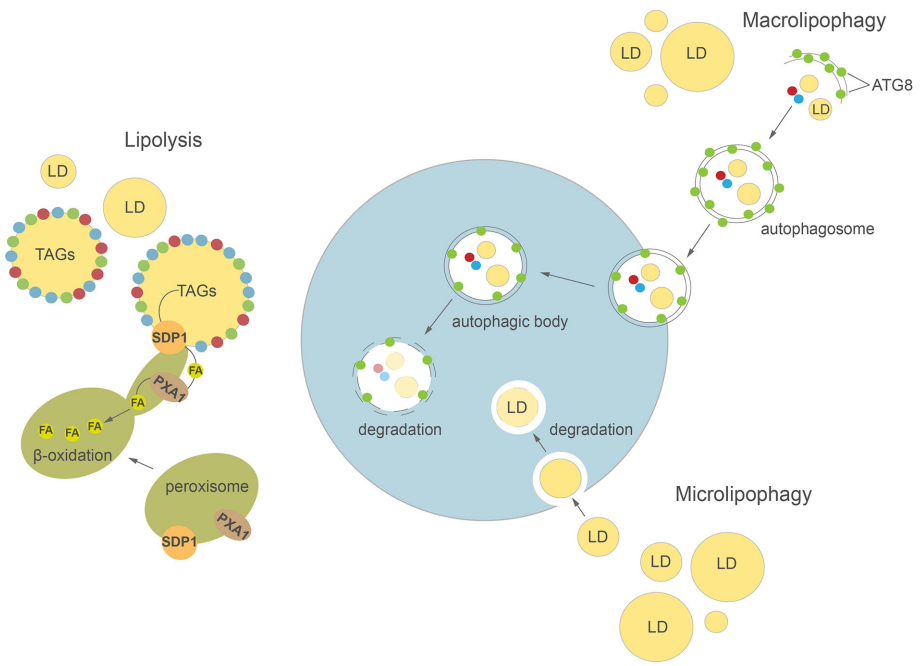

FIGURE 2 | Cellular pathways of lipid droplets degradation in plants and algae. Detailed description in the text. ATG8, AUTOPHAGY-RELATED PROTEIN 8; FA, fatty acid; LD, lipid droplet; SDP1, SUGAR DEPENDENT 1; TAGs, triacylglycerols.

unlike other putative TAG lipases identified in Arabidopsis, showed exceptionally high expression in mature pollen grains (Kelly et al., 2011). This suggests that *At*SDP1L may be involved in LDs breakdown during pollen germination. Two homologs of *Rc*OBL1, TAG lipase from tobacco (*Nt*OBL1) and *At*OBL1 from Arabidopsis mentioned above, have been characterized in pollen tubes (Müller and Ischebeck, 2018). Interestingly, similar to *Rc*OBL1 and unlike *At*SDP1 in seeds, both proteins localized to LDs when ectopically expressed in growing tobacco pollen tubes. Moreover, Arabidopsis *obl1* mutants showed slower pollen tube growth *in vivo*. The authors suggested that acyl groups released from TAGs by OBL1 might be directly channeled into the ER, where they serve as substrates for rapid membrane synthesis (Müller and Ischebeck, 2018).

LD-associated lipase activities were also found *in vitro* and *in situ* in germinating pollen and growing pollen tubes of olive (*Olea europaea* L.) (Rejon et al., 2012; Zienkiewicz et al., 2013). Their direct role in proper pollen tube growth has been confirmed by *in vitro* olive pollen germination in medium with and without sucrose, with higher lipase activity resulting in the latter case (Zienkiewicz et al., 2013). In these studies, TAG lipase activity was found only on LDs isolated from germinating pollen tubes, and not from the mature pollen grain. Similar localization pattern was also found for LOX protein (Zienkiewicz et al., 2013). In turn, PLA activity co-localized with LDs in both mature and germinating olive pollen (Zienkiewicz et al., 2013). This indicates that there are substantial differences in the temporal and spatial localization pattern of machinery governing LDs breakdown in pollen grains compared to seeds, where all the lipid degrading enzymes seem to be recruited to the LDs surface during or just after seed imbibition (Rudolph et al., 2011; Thazar-Poulot et al., 2015). Most probably, this reflects the distinct energy demands of pollen grains and seeds, which are tightly connected with their biological functions. The initiation of pollen germination and pollen tube growth occur much faster than seed imbibition and germination. This could explain the presence of some LDs degrading enzymes "on-site," available to act as soon as pollen germination starts.

Previous studies have shown that disruption of *At*SDP1 also leads to TAG accumulation in other vegetative tissues, such us leaves, stems, and roots (Kelly et al., 2013b; Fan et al., 2014). Moreover, the expression level of *AtSDP1* increases during natural leaf senescence, thus it is possible that this lipase is involved in regulation of TAG homeostasis during leaf development (Troncoso-Ponce et al., 2013). The transcript levels corresponding to *AtCGI-58* were up-regulated during leaf senescence as well (Troncoso-Ponce et al., 2013), and loss of function of *At*CGI-58 resulted in a significant increase in TAG content of leaf mesophyll cells (James et al., 2010). While in mammals CGI-58 has been shown to act as an activator of adipose triglyceride lipase ATGL, and thus to directly regulate TAG breakdown (Lass et al., 2006), such a role has not been confirmed for plants, where CGI-58 likely regulates the activity of PXA1 but not of TAG lipase (Park et al., 2013). Consequently, the plant CGI-58 does not seem to be a bona fide TAG lipase, but rather an element of regulatory circuit of TAG homeostasis. Importantly, many putative lipases are expressed during leaf senescence (Troncoso-Ponce et al., 2013), suggesting more lipases could be involved in LD turnover in leaves.

LDs mobilization is an essential step during the transition of algal cells from quiescence to autotrophy in response to restored favorable growth conditions (Siaut et al., 2011; Tsai et al., 2018; Zienkiewicz et al., 2020). Thus, comparative transcriptomics between stress (N deprivation) and optimal (N resupply) growth conditions led to the identification of many putative TAG lipases highly expressed after triggering of the massive TAG degradation (Jaeger et al., 2017; Zienkiewicz et al., 2020). However, only a few of them have been functionally characterized to date (**Table 1**). Among 49 putative lipases encoded by the genome of the oleaginous marine diatom *P. tricornutum*, only one patatin-SDP1-like lipase, named tgl1, has been functionally characterized to date (Barka et al., 2016). The TAG lipase activity of tgl1 has been confirmed *in vitro* and *in vivo*. In the latter case, the *tgl1* knockdown mutants of *P. tricornutum* accumulated much higher amounts of TAGs when compared to the wild type (Barka et al., 2016). In *C. reinhardtii*, among over 130 putative lipases encoded by its genome, only one TAG lipase has been identified and characterized recently. This TAG lipase, LIP4, shares 44% amino acid identity with *At*SDP1 (**Table 1**) (Warakanont et al., 2019). The expression of *LIP4* is downregulated in response to N deprivation and up-regulated after N resupply, whereas its mutation resulted in delay of TAG degradation, which consequently led to TAG over-accumulation in *Crlip4* mutant (Warakanont et al., 2019). Two homologs of *At*SDP1, named *No*TGL1 and *No*TGL2, have also been recently reported in *N. oceanica* (Nobusawa et al., 2019). Over-accumulation of TAGs was observed only in the *N. oceanica* knockout of *NoTGL1*, but not of *NoTGL2*, after N resupply. Moreover, *No*TGL1 was found to be a specific resident of ER, thus the authors proposed its involvement in degradation of TAG *de novo* synthesized in the ER (Nobusawa et al., 2019). Proteomic analysis of another oleaginous green alga, *L. incisa*, revealed the presence of the putative TAG lipase *Li*SDP1. *Li*SDP1

TABLE 1 | Functionally characterized TAG lipases involved in LDs degradation identified in plants and algae.

Organism	TAG Lipase	Reference
Plants		
Arabidopsis thaliana *Brassica napus* L. *Glycine max* L. *Jatropha curcas*	SDP1—Sugar Dependent 1	Eastmond, 2006; Kelly et al., 2011; Kelly et al., 2013a; Kim et al., 2014; Kanai et al., 2019
Arabidopsis thaliana	OBL1—Oil Body Lipase 1	Müller and Ischebeck, 2018
Algae		
Chlamydomonas reinhardtii	LIP4	Warakanont et al., 2019
Lobosphaera incisa	SDP1—Sugar Dependent 1	Siegler et al., 2017
Nannochloropsis oceanica	TGL1 and TGL2	Nobusawa et al., 2019
Phaeodactylum tricornutum	Tgl1	Barka et al., 2016

shares 44% identity with *At*SDP1 (Siegler et al., 2017). Ectopic expression of *LiSDP1* in *A. thaliana sdp1 sdp1-L* mutants resulted in only partial complementation of the TAG lipase-deficient plants. *Li*SDP1 from *L. incisa* was absent in LD isolates from N-deprived cultures and did not localize to LDs when ectopically expressed in tobacco pollen tube. The authors did not exclude that *Li*SDP1 might be specifically recruited to the surface of LDs when needed (Siegler et al., 2017). By searching for human lipase homologs in the genome of *Thalassiosira pseudonana*, Trentacoste et al. (2013) identified a homolog of CGI-58, encoded by *Thaps3_264297*. The resulting protein has been shown to possess TAG lipase, PLA, and LPAAT activities *in vitro*, and a knockdown of *Thaps3_264297* resulted in increased TAG content and accumulation of LDs compared to the wild type strain (Trentacoste et al., 2013). However, taking into account the proposed role of plant CGI-58 the exact role of algal CGI-58 still needs to be elucidated.

LIPOPHAGY—A NEW PLAYER IN THE FIELD

Autophagy is a highly conserved process involved in regulation of intracellular degradation and recycling of individual molecules as well as whole organelles, *via* lysosomes in animals or vacuoles in yeast and plants (Avin-Wittenberg et al., 2012; Bento et al., 2016; Marshall and Vierstra, 2018; Couso et al., 2018). In plants, autophagy plays an important role in many developmental processes, such as seed development (Di Berardino et al., 2018; Sera et al., 2019) and leaf senescence (Avila-Ospina et al., 2014; Li et al., 2014). Autophagy is highly induced by various abiotic stresses, including nutrient deprivation (Sun et al., 2018; Janse van Rensburg et al., 2019), drought (Bao et al., 2020), and biotic stresses e.g. pathogen infection (Dagdas et al., 2016). Two major types of autophagy have been described in plants: macroautophagy and microautophagy (**Figure 2**). During macroautophagy, numerous autophagy-related (ATG) proteins participate in the induction of autophagy and formation of a double-membrane structure called an autophagosome (Yoshimoto and Ohsumi, 2018). Autophagosomes containing different cargo (macromolecules or damaged organelles) fuse with the tonoplast and subsequently enter the vacuolar lumen as autophagic bodies. The content of autophagic bodies then undergoes progressive degradation (Soto-Burgos et al., 2018). In microautophagy, cytoplasmic contents are directly captured into the vacuolar lumen by invagination of the tonoplast. Previous studies in yeast and mammalian cells demonstrated a close relationship between LD homeostasis and autophagy (van Zutphen et al., 2014; Petan et al., 2018). Indeed, autophagy may either provide FAs for LDs biogenesis (Rambold et al., 2015) or participate in their degradation in the process of lipophagy (Singh et al., 2009; van Zutphen et al., 2014). In animals, depending on the size of LDs, their degradation can be achieved either by macrolipophagy, where small, entire LDs are enclosed together with other cytoplasmic contents in an autophagosome, or by piecemeal microlipophagy, where only a small portion of a large LD is trapped in an autophagosome and then pinches off as a double membrane autolipophagosome (Singh et al., 2009; Khaldoun et al., 2014; Garcia et al., 2018). In yeast, distinct forms of microlipophagy contribute to LD degradation depending on growth conditions (van Zutphen et al., 2014; Vevea et al., 2015; Seo et al., 2017). For example, under acute glucose starvation, the molecular machinery of macroautophagy participates in the induction of microlipophagy. ATG14 is recruited to liquid-ordered membrane (Lo) domains at the surface of vacuole, where together with ATG6 it forms recruitment sites for LDs and initiates their microlipophagy (Seo et al., 2017). In contrast, under lipid and ER stress, microlipophagy depends on ESCRT (endosomal sorting complexes required for transport) machinery rather than ATG proteins (Vevea et al., 2015). Similarly, microlipophagy induced after diauxic shifts has been shown to be independent of the core ATGs but dependent on ESCRT proteins (Oku et al., 2017). Our knowledge on LDs TAG degradation inside the vacuole/lysosome is rather scarce and fragmentary. Nevertheless, one of the few reports showed that vacuolar lipase ATG15 acts in degradation of neutral lipids of LDs after their incorporation into the vacuole in yeast (Maeda et al., 2015).

Over the last decade research has also produced increasing evidence of an important role for autophagy in LDs degradation in plants (Kurusu et al., 2014; Fan et al., 2019) and algae (Zhao et al., 2014; Schwarz et al., 2017; Tsai et al., 2018). In plants, lipophagy seems to be involved among others in male reproductive development, pollen germination, and pollen tube growth (Kurusu et al., 2014; Hanamata et al., 2019; Hanamata et al., 2020; Zhao et al., 2020). The potential role of lipophagy in pollen grain maturation was demonstrated in a study on the *Oryza sativa atg7* mutant (Kurusu et al., 2014). Mutation in *OsATG7* was associated with a lower number of LDs in mature pollen and a higher accumulation of LDs in tapetal cells compared to wild type plants. These results, together with the observation that in wild type plants LDs were enclosed in the vacuoles of rice tapetal cells, suggest that ATG7-dependent tapetal autophagy may be responsible for LDs degradation and lipid metabolism in the tapetum (Kurusu et al., 2014). Recently, a detailed analysis of the germinating pollen lipidome in tobacco was performed using ATG-suppressed RNAi lines (Zhao et al., 2020). This study showed that silencing of *ATG2* and *ATG5* leads to a decrease in the number of autophagosomes at the germinative pollen aperture and is accompanied by inhibition of pollen germination and significant accumulation of TAGs and DAGs in pollen grains. Lipophagy may also contribute to the degradation of LDs during seed germination and seedling growth. The potential implication of autophagy in LDs degradation during seed germination was suggested by earlier studies of the Arabidopsis *clo1* mutant (Poxleitner et al., 2006). During seed germination, LDs were commonly observed in the vacuolar lumen of wild type cotyledon cells, while loss of function of *AtCLO1* resulted in the absence of LDs inside the vacuoles and slower degradation of eicosenoic acid (20:1) (Poxleitner et al., 2006). It is therefore possible that turnover of some pools of LDs is regulated by caleosin-dependent microlipophagy during seed germination.

Other data showed that during *in vitro* germination of olive seeds, the neutral lipids stained by Sudan Black B co-localize in the area of protein bodies (known also as protein storage vacuoles), together with lipase activity, suggesting that LDs degradation takes place inside protein bodies (Zienkiewicz et al., 2014b). A significant accumulation of TAGs was observed in etiolated carbon-starved seedlings of the Arabidopsis *atg5* mutant (Avin-Wittenberg et al., 2015), indicating the potential role of autophagic machinery in LDs degradation. It was demonstrated recently that LDs breakdown in senescent watermelon (*Cirullus lanatus*) leaves occurs *via* different pathways: small vacuole-associated and central vacuole-associated (Zhang et al., 2020). In leaf cells without a central vacuole, LDs interact with autophagosome-like structures before they enter small vacuoles. Meanwhile, in the cells of senescent leaves containing the central vacuole, LDs are delivered into the vacuolar lumen *via* a process morphologically resembling microlipophagy (Zhang et al., 2020). Lipophagy has also been implicated in LD turnover in Arabidopsis leaves during dark-induced starvation (Fan et al., 2019). Under extended darkness, DsRed-Atg8e-labeled autophagic structures were observed to be associated with LDs in the leaves of *tgd1* (*trigalactosyldiacylglycerol1*) mutant. Moreover, ultrastructural analysis of leaf cells from dark-treated *Atsdp1-4* plants, deficient in cytosolic lipolysis, demonstrated the entrance and appearance of LDs in the central vacuole. The authors suggested that this process is likely mediated by the microlipophagy pathway (Fan et al., 2019). Interestingly, disruption of molecular macroautophagy machinery in Arabidopsis double mutants *atg2-1 sdp1-4* and *atg5-1 sdp1-4* leads to inhibition of dark-induced lipophagy in the leaves. Taken together, the findings described by Fan et al. (2019) showed that microlipophagy observed in Arabidopsis leaves depends on core components of macroautophagy pathway, as has been described previously in yeast (van Zutphen et al., 2014).

A large number of studies on autophagy-mediated LDs degradation in algae have been performed using *C. reinhardtii* as a reference. Ultrastructural analysis of *C. reinhardtii* cells under N resupply (NR) conditions showed the appearance of small LDs in the vacuolar lumen is controlled by a process morphologically resembling microlipophagy (Tsai et al., 2018). A mutation in *CrATG8*, encoding one of the core ATG proteins required for the formation of the autophagosome, results in delayed degradation of TAGs after NR compared to wild type lines (Kajikawa et al., 2019). In addition, by using mCherry-ATG8 as a tool to monitor the intracellular movements of autophagosomes (Yoshimoto et al., 2004; Klionsky et al., 2007), the fusion between autophagosomes and LDs was observed at later stages of N deprivation (Tran et al., 2019). Similar to *C. reinhardtii*, small LDs were observed to be sequestered by the vacuole *via* a pathway resembling microautophagy in another green alga, *Auxenochlorella protothecoides*, during its heterotrophy to autotrophy transition (Zhao et al., 2014). Interestingly, the authors suggested that small portions of large LDs might also be degraded in the vacuolar lumen through a process reminiscent of the piecemeal microautophagy commonly observed in mammalian cells. Microlipophagy-like degradation of LDs was observed as well in *N. oceanica* under NR conditions (Zienkiewicz et al., 2020). Moreover, by using a biomolecular fluorescence complementation (BiFC) assay it was demonstrated that *No*ATG8 protein interacts *in vivo* with *No*LDSP —a major LD surface protein in *N. oceanica* (Zienkiewicz et al., 2020). It has been proposed that this interaction might be involved in the targeting and/or fusion of LDs into the vacuole. The ATG8-interacting motif (AIM) was also identified in Stramenopile-type lipid droplet protein (StLDP), suggesting a possible link between autophagy and LD degradation in *P. tricornutum* (Leyland et al., 2020). The latest analyses revealed that salt stress is also associated with appearance of LDs in the vacuolar lumen in *Parachlorella kessleri* (You et al., 2019). Interestingly, in the unicellular alga *Micrasterias denticulate*, LDs degradation occurring under carbon starvation seems to be mediated by macrolipophagy, as LDs were trapped in autophagosomes and then delivered into small vacuoles (Schwarz et al., 2017).

LD PROTEIN TURNOVER—THE MISSING PUZZLE IN THE CROSSTALK BETWEEN LIPOLYSIS AND LIPOPHAGY?

Previous studies in animals revealed that association of ATGL with the surface of LDs depends on the degradation of the LDs structural proteins perilipin 2 (PLIN2) and perilipin 3 (PLIN3) *via* chaperone-mediated autophagy (CMA) (Kaushik and Cuervo, 2015). Sathyanarayan et al. (2017) proposed a model where the removal of PLINs facilitates access of ATGL to TAGs, and ATGL acts as a signal for LDs recognition by autophagosomes and thus an inducer of bulk LDs degradation *via* lipophagy (Sathyanarayan et al., 2017). In plants, oleosins and LDAPs have been proposed to protect LDs from the action of TAG lipases (Siloto et al., 2006; Gidda et al., 2016). Recently, two independent groups reported that ubiquitinated oleosins interact with the PUX10 protein through its UBA domain. *Via* its UBX domain, PUX10 in turn recruits CDC48, enabling further degradation of oleosins by the proteasome (Deruyffelaere et al., 2018; Kretzschmar et al., 2018). On the other hand, it has been found that *At*OLE1 can interact with *At*ATG8e protein through the AIM motif (ATG8 interacting motif) (Marshall et al., 2019). This implies that autophagy can also participate in oleosin turnover during seed germination. Interestingly, ATGL and hormone-sensitive lipase (HSL) contain several putative LIR (LC3-interacting region) motifs responsible for direct interaction with microtubule associated protein 1 LC3 (ATG8 family protein) (Martinez-Lopez et al., 2016). Mutating the ATGL LIR motif blocked ATGL associations with the LD surface and lipolysis, suggesting the direct crosstalk between lipolysis and autophagy in animal cells. It remains unknown if the degradation of plant and algal TAG lipases is also controlled by autophagy machinery.

CONCLUDING REMARKS

The past decade has seen considerable progress in the identification and characterization of mechanisms governing LDs degradation in plant and algal cells. The studies reviewed here revealed the

complexity of intracellular molecular networks related to LDs metabolism, and highlighted the fundamental meaning of these organelles for developmental programs and physiological responses in plants and algae. This includes essential functions of LDs structural proteins (oleosins, celeosins, and their counterparts in algal cells) as well as lipolysis and lipophagy pathways of TAGs breakdown. However, there are still many unanswered questions. For example, what is the nature of cross-talk between lipolysis and lipophagy in plant and algal cells? And what specific lipophagy receptors on the surface of LDs could be involved in activation of the autophagic machinery and lipophagy initiation? Moreover, it is still unclear whether, similar to animal cells, plant and algal TAG lipases are implicated in the induction of lipophagy, and if autophagy is responsible for their degradation. Answering these questions will help us gain a better comprehensive understanding of induction and regulation of LDs mobilization in plants and algae. Future research is needed to uncover the fascinating and multifaceted mechanisms that govern LDs turnover in plant and algal cells, as this knowledge is crucial for the development of more applied research and engineering of lipid-rich biomass production from algae and oil crops.

AUTHOR CONTRIBUTIONS

KZ and AZ conceived, wrote the manuscript and designed the figures. All authors contributed to the article and approved the submitted version.

ACKNOWLEDGMENTS

The authors thank Dr. Tegan Haslam for the critical reading of the manuscript, valuable comments and English corrections.

SUPPLEMENTARY MATERIAL

The Supplementary Material for this article can be found online at: https://www.frontiersin.org/articles/10.3389/fpls.2020.579019/full#supplementary-material

SUPPLEMENTARY TABLE 1 | LD-associated proteins identified in plants and algae. The corresponding references are given next to the table.

REFERENCES

Abell, B. M., Holbrook, L. A., Abenes, M., Murphy, D. J., Hills, M. J., and Moloney, M. M. (1997). Role of the proline knot motif in oleosin endoplasmic reticulum topology and oil body targeting. *Plant Cell* 9, 1481–1493. doi: 10.1105/tpc.9.8.1481

Alexander, L. G., Sessions, R. B., Clarke, A. R., Tatham, A. S., Shewry, P. R., and Napier, J. A. (2002). Characterization and modelling of the hydrophobic domain of a sunflower oleosin. *Planta* 214, 546–551. doi: 10.1007/s004250100655

Avila-Ospina, L., Moison, M., Yoshimoto, K., and Masclaux-Daubresse, C. (2014). Autophagy, plant senescence, and nutrient recycling. *J. Exp. Bot.* 65, 3799–3811. doi: 10.1093/jxb/eru039

Avin-Wittenberg, T., Honig, A., and Galili, G. (2012). Variations on a theme: plant autophagy in comparison to yeast and mammals. *Protoplasma* 249, 285–299. doi: 10.1007/s00709-011-0296-z

Avin-Wittenberg, T., Bajdzienko, K., Wittenberg, G., Alseekh, S., Tohge, T., Bock, R., et al. (2015). Global analysis of the role of autophagy in cellular metabolism and energy homeostasis in Arabidopsis seedlings under carbon starvation. *Plant Cell* 27, 306–322. doi: 10.1105/tpc.114.134205

Bao, Y., Song, W.-M., Wang, P., Yu, X., Li, B., Jiang, C., et al. (2020). COST1 regulates autophagy to control plant drought tolerance. *Proc. Natl. Acad. Sci. U. S. A.* 117, 7482–7493. doi: 10.1073/pnas.1918539117

Barka, F., Angstenberger, M., Ahrendt, T., Lorenzen, W., Bode, H. B., and Buchel, C. (2016). Identification of a triacylglycerol lipase in the diatom *Phaeodactylum tricornutum*. *Biochim. Biophys. Acta* 1861, 239–248. doi: 10.1016/j.bbalip.2015.12.023

Bartolini, S., Leccese, A., and Andreini, L. (2014). Influence of canopy fruit location on morphological, histochemical and biochemical changes in two oil olive cultivars. *Plant Biosyst. - Int. J. Deal. all Asp. Plant Biol.* 148, 1221–1230. doi: 10.1080/11263504.2014.980360

Baud, S., Boutin, J. P., Miquel, M., Lepiniec, L., and Rochat, C. (2002). An integrated overview of seed development in *Arabidopsis thaliana* ecotype WS. *Plant Physiol. Biochem.* 40, 151–160. doi: 10.1016/S0981-9428(01)01350-X

Bento, C. F., Renna, M., Ghislat, G., Puri, C., Ashkenazi, A., Vicinanza, M., et al. (2016). Mammalian autophagy: How does it work? *Annu. Rev. Biochem.* 85, 685–713. doi: 10.1146/annurev-biochem-060815-014556

Birsoy, K., Festuccia, W. T., and Laplante, M. (2013). A comparative perspective on lipid storage in animals. *J. Cell Sci.* 126, 1541–1552. doi: 10.1242/jcs.104992

Bouvier-Navé, P., Berna, A., Noiriel, A., Compagnon, V., Carlsson, A. S., Banas, A., et al. (2010). Involvement of the phospholipid sterol acyltransferase1 in plant sterol homeostasis and leaf senescence. *Plant Physiol.* 152, 107–119. doi: 10.1104/pp.109.145672

Brocard, L., Immel, F., Coulon, D., Esnay, N., Tuphile, K., Pascal, S., et al. (2017). Proteomic analysis of lipid droplets from Arabidopsis aging leaves brings new insight into their biogenesis and functions. *Front. Plant Sci.* 8:894:894. doi: 10.3389/fpls.2017.00894

Cai, Y., Goodman, J. M., Pyc, M., Mullen, R. T., Dyer, J. M., and Chapman, K. D. (2015). Arabidopsis SEIPIN proteins modulate triacylglycerol accumulation and influence lipid droplet proliferation. *Plant Cell.* 27, 2616–2636. doi: 10.1105/tpc.15.00588

Chapman, K. D., and Ohlrogge, J. B. (2012). Compartmentation of triacylglycerol accumulation in plants. *J. Biol. Chem.* 287, 2288–2294. doi: 10.1074/jbc.R111.290072

Chapman, K. D., Dyer, J. M., and Mullen, R. T. (2012). Biogenesis and functions of lipid droplets in plants: Thematic Review Series: Lipid Droplet Synthesis and Metabolism: from Yeast to Man. *J. Lipid Res.* 53, 215–226. doi: 10.1194/jlr.R021436

Chauton, M. S., Winge, P., Brembu, T., Vadstein, O., and Bones, A. M. (2013). Gene regulation of carbon fixation, storage, and utilization in the diatom *Phaeodactylum tricornutum* acclimated to light/dark cycles. *Plant Physiol.* 161, 1034–1048. doi: 10.1104/pp.112.206177

Chen, J. C., Tsai, C. C., and Tzen, J. T. (1999). Cloning and secondary structure analysis of caleosin, a unique calcium-binding protein in oil bodies of plant seeds. *Plant Cell Physiol.* 40, 1079–1086. doi: 10.1093/oxfordjournals.pcp.a029490

Chia, T. Y., Pike, M. J., and Rawsthorne, S. (2005). Storage oil breakdown during embryo development of *Brassica napus* (L.). *J. Exp. Bot.* 5, 1285–1296. doi: 10.1093/jxb/eri129

Chitraju, C., Mejhert, N., Haas, J. T., Diaz-Ramirez, L. G., Grueter, C. A., Imbriglio, J. E., et al. (2017). Triglyceride synthesis by DGAT1 protects adipocytes from lipid-induced ER stress during lipolysis. *Cell Metab.* 26, 407–418.e3. doi: 10.1016/j.cmet.2017.07.012

Couso, I., Pérez-Pérez, M. E., Martínez-Force, E., Kim, H. S., He, Y., Umen, J. G., et al. (2018). Autophagic flux is required for the synthesis of triacylglycerols and ribosomal protein turnover in Chlamydomonas. *J. Exp. Bot.* 69, 1355–1367. doi: 10.1093/jxb/erx372

Cui, S., Hayashi, Y., Otomo, M., Mano, S., Oikawa, K., Hayashi, M., et al. (2016). Sucrose production mediated by lipid metabolism suppresses the physical interaction of peroxisomes and oil bodies during germination of. *Arabidopsis thaliana J. Biol. Chem.* 291, 19734–19745. doi: 10.1074/jbc.M116.748814

Dagdas, Y. F., Belhaj, K., Maqbool, A., Chaparro-Garcia, A., Pandey, P., Petre, B., et al. (2016). An effector of the Irish potato famine pathogen antagonizes a host autophagy cargo receptor. *Elife* 5, e10856. doi: 10.7554/eLife.10856

Dahlqvist, A., Stahl, U., Lenman, M., Banas, A., Lee, M., Sandager, L., et al. (2000). Phospholipid:diacylglycerol acyltransferase: an enzyme that catalyzes the acyl-CoA-independent formation of triacylglycerol in yeast and plants. *Proc. Natl. Acad. Sci. U. S. A.* 97, 6487–6492. doi: 10.1073/pnas.120067297

Davidi, L., Katz, A., and Pick, U. (2012). Characterization of major lipid droplet proteins from Dunaliella. *Planta* 236, 19–33. doi: 10.1007/s00425-011-1585-7

Deruyffelaere, C., Purkrtova, Z., Bouchez, I., Collet, B., Cacas, J.-L., Chardot, T., et al. (2018). PUX10 is a CDC48A adaptor protein that regulates the extraction of ubiquitinated oleosins from seed lipid droplets in Arabidopsis. *Plant Cell* 30, 2116–2136. doi: 10.1105/tpc.18.00275

Di Berardino, J., Marmagne, A., Berger, A., Yoshimoto, K., Cueff, G., Chardon, F., et al. (2018). Autophagy controls resource allocation and protein storage accumulation in Arabidopsis seeds. *J. Exp. Bot.* 69, 1403–1414. doi: 10.1093/jxb/ery012

d'Andrea, S., Canonge, M., Beopoulos, A., Jolivet, P., Hartmann, M. A., Miquel, M., et al. (2007). At5g50600 encodes a member of the short-chain dehydrogenase reductase superfamily with 11beta- and 17beta-hydroxysteroid dehydrogenase activities associated with *Arabidopsis thaliana* seed oil bodies. *Biochimie* 89, 222–229. doi: 10.1016/j.biochi.2006.09.013

Du, C., Liu, A., Niu, L., Cao, D., Liu, H., Wu, X., et al. (2019). Proteomic identification of lipid-bodies-associated proteins in maize seeds. *Acta Physiol. Plant* 41, 70. doi: 10.1007/s11738-019-2854-5

Eastmond, P. J., and Graham, I. A. (2001). Re-examining the role of the glyoxylate cycle in oilseeds. *Trends Plant Sci.* 6, 72–78. doi: 10.1016/s1360-1385(00)01835-5

Eastmond, P. J. (2004). Cloning and characterization of the acid lipase from castor beans. *J. Biol. Chem.* 279, 45540–45545. doi: 10.1074/jbc.M408686200

Eastmond, P. J. (2006). SUGAR-DEPENDENT1 encodes a patatin domain triacylglycerol lipase that initiates storage oil breakdown in germinating Arabidopsis seeds. *Plant Cell* 18, 665–675. doi: 10.1105/tpc.105.040543

Esnay, N., Dyer, J. M., Mullen, R. T., and Chapman, K. D. (2020). Lipid droplet–peroxisome connections in plants. *Contact* 3:2515256420908765. doi: 10.1177/2515256420908765

Fan, J., Yan, C., Roston, R., Shanklin, J., and Xu, C. (2014). Arabidopsis lipins, PDAT1 acyltransferase, and SDP1 triacylglycerol lipase synergistically direct fatty acids toward β-oxidation, thereby maintaining membrane lipid homeostasis. *Plant Cell* 26, 4119–4134. doi: 10.1105/tpc.114.130377

Fan, J., Yu, L., and Xu, C. (2019). Dual role for autophagy in lipid metabolism in Arabidopsis. *Plant Cell* 31, 1598–1613. doi: 10.1105/tpc.19.00170

Fernandez-Santos, R., Izquierdo, Y., Lopez, A., Muniz, L., Martinez, M., Cascon, T., et al. (2020). Protein profiles of lipid droplets during the hypersensitive defense response of Arabidopsis against Pseudomonas infection. *Plant Cell Physiol.* 61, 1144–1157. doi: 10.1093/pcp/pcaa041

Garcia, E. J., Vevea, J. D., and Pon, L. A. (2018). Lipid droplet autophagy during energy mobilization, lipid homeostasis and protein quality control. *Front. Biosci. (Landmark Ed.* 23, 1552–1563. doi: 10.2741/4660

Ghosh, A. K., Chauhan, N., Rajakumari, S., Daum, G., and Rajasekharan, R. (2009). At4g24160, a soluble acyl-coenzyme A-dependent lysophosphatidic acid acyltransferase. *Plant Physiol.* 151, 869–881. doi: 10.1104/pp.109.144261

Gidda, S. K., Park, S., Pyc, M., Yurchenko, O., Cai, Y., Wu, P., et al. (2016). Lipid droplet-associated proteins (LDAPs) are required for the dynamic regulation of neutral lipid compartmentation in plant cells. *Plant Physiol.* 170, 2052–2071. doi: 10.1104/pp.15.01977

Goold, H., Beisson, F., Peltier, G., and Li-Beisson, Y. (2015). Microalgal lipid droplets: composition, diversity, biogenesis and functions. *Plant Cell Rep.* 34, 545–555. doi: 10.1007/s00299-014-1711-7

Graham, I. A. (2008). Seed storage oil mobilization. *Annu. Rev. Plant Biol.* 59, 115–142. doi: 10.1146/annurev.arplant.59.032607.092938

Greer, M. S., Cai1, Y., Gidda, S. K., Esnay, N., Kretzschmar, F. K., Seay, D., et al. (2020). SEIPIN isoforms interact with the membrane-tethering protein VAP27-1 for lipid droplet formation. *Plant Cell*. doi: 10.1105/tpc.19.00771

Grillitsch, K., Connerth, M., Kofeler, H., Arrey, T. N., Rietschel, B., Wagner, B., et al. (2011). Lipid particles/droplets of the yeast *Saccharomyces cerevisiae* revisited: lipidome meets proteome. *Biochim. Biophys. Acta* 1811, 1165–1176. doi: 10.1016/j.bbalip.2011.07.015

Hanamata, S., Sawada, J., Toh, B., Ono, S., Ogawa, K., Fukunaga, T., et al. (2019). Monitoring autophagy in rice tapetal cells during pollen maturation. *Plant Biotechnol. (Tokyo Jpn.)* 36, 99–105. doi: 10.5511/plantbiotechnology.19.0417a

Hanamata, S., Sawada, J., Ono, S., Ogawa, K., Fukunaga, T., Nonomura, K.-I., et al. (2020). Impact of autophagy on gene expression and tapetal programmed cell death during pollen development in rice. *Front. Plant Sci.* 11:172:172. doi: 10.3389/fpls.2020.00172

Hanano, A., Burcklen, M., Flenet, M., Ivancich, A., Louwagie, M., Garin, J., et al. (2006). Plant seed peroxygenase is an original heme-oxygenase with an EF-hand calcium binding motif. *J. Biol. Chem.* 281, 33140–33151. doi: 10.1074/jbc.M605395200

Hanano, A., Bessoule, J.-J., Heitz, T., and Blee, E. (2015). Involvement of the caleosin/peroxygenase RD20 in the control of cell death during Arabidopsis responses to pathogens. *Plant Signal. Behav.* 10, e991574. doi: 10.4161/15592324.2014.991574

Horn, P. J., Ledbetter, N. R., James, C. N., Hoffman, W. D., Case, C. R., Verbeck, G. F., et al. (2011). Visualization of lipid droplet composition by direct organelle mass spectrometry. *J. Biol. Chem.* 286, 3298–3306. doi: 10.1074/jbc.M110.186353

Horn, P. J., James, C. N., Gidda, S. K., Kilaru, A., Dyer, J. M., Mullen, R. T., et al. (2013). Identification of a new class of lipid droplet-associated proteins in plants. *Plant Physiol.* 162, 1926–1936. doi: 10.1104/pp.113.222455

Hsieh, K., and Huang, A. H. C. (2005). Lipid-rich tapetosomes in Brassica tapetum are composed of oleosin-coated oil droplets and vesicles, both assembled in and then detached from the endoplasmic reticulum. *Plant J.* 43, 889–899. doi: 10.1111/j.1365-313X.2005.02502.x

Huang, A. H. (1996). Oleosins and oil bodies in seeds and other organs. *Plant Physiol.* 110, 1055–1061. doi: 10.1104/pp.110.4.1055

Huang, A. H. C. (2018). Plant lipid droplets and their associated proteins: potential for rapid advances. *Plant Physiol.* 176, 1894–1918. doi: 10.1104/pp.17.01677

Jaeger, D., Winkler, A., Mussgnug, J. H., Kalinowski, J., Goesmann, A., and Kruse, O. (2017). Time-resolved transcriptome analysis and lipid pathway reconstruction of the oleaginous green microalga *Monoraphidium neglectum* reveal a model for triacylglycerol and lipid hyperaccumulation. *Biotechnol. Biofuels* 10, 197. doi: 10.1186/s13068-017-0882-1

Jallet, D., Xing, D., Hughes, A., Moosburner, M., Simmons, M. P., Allen, A. E., et al. (2020). Mitochondrial fatty acid β-oxidation is required for storage-lipid catabolism in a marine diatom. *New Phytol.* doi: 10.1111/nph.16744

James, C. N., Horn, P. J., Case, C. R., Gidda, S. K., Zhang, D., Mullen, R. T., et al. (2010). Disruption of the Arabidopsis CGI-58 homologue produces Chanarin-Dorfman-like lipid droplet accumulation in plants. *Proc. Natl. Acad. Sci. U. S. A.* 107, 17833–17838. doi: 10.1073/pnas.0911359107

Janse van Rensburg, H. C., Van den Ende, W., and Signorelli, S. (2019). Autophagy in plants: both a puppet and a puppet master of sugars. *Front. Plant Sci.* 10:14:14. doi: 10.3389/fpls.2019.00014

Javee, A., Sulochana, S. B., Pallissery, S. J., and Arumugam, M. (2016). Major lipid body protein: a conserved structural component of lipid body accumulated during abiotic stress in *S. quadricauda* CASA-CC202. *Front. Energy Res.* 4:2016.00037:37. doi: 10.3389/fenrg.2016.00037

Jiang, P.-L., and Tzen, J. T. C. (2010). Caleosin serves as the major structural protein as efficient as oleosin on the surface of seed oil bodies. *Plant Signal. Behav.* 5, 447–449. doi: 10.4161/psb.5.4.10874

Jiang, P.-L., Jauh, G.-Y., Wang, C.-S., and Tzen, J. T. C. (2008). A unique caleosin in oil bodies of lily pollen. *Plant Cell Physiol.* 49, 1390–1395. doi: 10.1093/pcp/pcn103

Jolivet, P., Roux, E., D'Andrea, S., Davanture, M., Negroni, L., Zivy, M., et al. (2004). Protein composition of oil bodies in *Arabidopsis thaliana* ecotype WS. *Plant Physiol. Biochem. PPB* 42, 501–509. doi: 10.1016/j.plaphy.2004.04.006

Kajikawa, M., Yamauchi, M., Shinkawa, H., Tanaka, M., Hatano, K., Nishimura, Y., et al. (2019). Isolation and characterization of Chlamydomonas autophagy-related mutants in nutrient-deficient conditions. *Plant Cell Physiol.* 60, 126–138. doi: 10.1093/pcp/pcy193

Kanai, M., Yamada, T., Hayashi, M., Mano, S., and Nishimura, M. (2019). Soybean (Glycine max L.) triacylglycerol lipase GmSDP1 regulates the quality and quantity of seed oil. *Sci. Rep.* 9, 8924. doi: 10.1038/s41598-019-45331-8

Kaushik, S., and Cuervo, A. M. (2015). Degradation of lipid droplet-associated proteins by chaperone-mediated autophagy facilitates lipolysis. *Nat. Cell Biol.* 17, 759–770. doi: 10.1038/ncb3166

Kelly, A. A., and Feussner, I. (2016). Oil is on the agenda: Lipid turnover in higher plants. *Biochim. Biophys. Acta* 1861, 1253–1268. doi: 10.1016/j.bbalip.2016.04.021

Kelly, A. A., Quettier, A. L., Shaw, E., and Eastmond, P. J. (2011). Seed storage oil mobilization is important but not essential for germination or seedling establishment in Arabidopsis. *Plant Physiol.* 157, 866–875. doi: 10.1104/pp.111.181784

Kelly, A. A., Shaw, E., Powers, S. J., Kurup, S., and Eastmond, P. J. (2013a). Suppression of the SUGAR-DEPENDENT1 triacylglycerol lipase family during seed development enhances oil yield in oilseed rape (*Brassica napus* L.). *Plant Biotechnol. J.* 11, 355–361. doi: 10.1111/pbi.12021

Kelly, A. A., van Erp, H., Quettier, A.-L., Shaw, E., Menard, G., Kurup, S., et al. (2013b). The sugar-dependent1 lipase limits triacylglycerol accumulation in vegetative tissues of Arabidopsis. *Plant Physiol.* 162, 1282–1289. doi: 10.1104/pp.113.219840

Khaldoun, S. A., Emond-Boisjoly, M.-A., Chateau, D., Carriere, V., Lacasa, M., Rousset, M., et al. (2014). Autophagosomes contribute to intracellular lipid distribution in enterocytes. *Mol. Biol. Cell* 25, 118–132. doi: 10.1091/mbc.E13-06-0324

Kim, H. U., Hsieh, K., Ratnayake, C., and Huang, A. H. C. (2002). A novel group of oleosins is present inside the pollen of Arabidopsis. *J. Biol. Chem.* 277, 22677–22684. doi: 10.1074/jbc.M109298200

Kim, M. J., Yang, S. W., Mao, H.-Z., Veena, S. P., Yin, J.-L., and Chua, N.-H. (2014). Gene silencing of Sugar-dependent 1 (JcSDP1), encoding a patatin-domain triacylglycerol lipase, enhances seed oil accumulation in *Jatropha curcas*. *Biotechnol. Biofuels* 7:36. doi: 10.1186/1754-6834-7-36

Klionsky, D. J., Cuervo, A. M., and Seglen, P. O. (2007). Methods for monitoring autophagy from yeast to human. *Autophagy* 3, 181–206. doi: 10.4161/auto.3678

Kong, F., Burlacot, A., Liang, Y., Légeret, B., Alseekh, S., Brotman, Y., et al. (2018a). Interorganelle communication: peroxisomal MALATE DEHYDROGENASE2 connects lipid catabolism to photosynthesis through redox coupling in Chlamydomonas. *Plant Cell.* 30, 1824–1847. doi: 10.1105/tpc.18.00361

Kong, F., Romero, I. T., Warakanont, J., and Li-Beisson, Y. (2018b). Lipid catabolism in microalgae. *New Phytol.* 218, 1340–1348. doi: 10.1111/nph.15047

Kretzschmar, F. K., Mengel, L. A., Müller, A. O., Schmitt, K., Blersch, K. F., Valerius, O., et al. (2018). PUX10 is a lipid droplet-localized scaffold protein that interacts with CELL DIVISION CYCLE48 and is involved in the degradation of lipid droplet proteins. *Plant Cell* 30, 2137–2160. doi: 10.1105/tpc.18.00276

Kretzschmar, F. K., Doner, N. M., Krawczyk, H. E., Scholz, P., Schmitt, K., Valerius, O., et al. (2020). Identification of low-abundance lipid droplet proteins in seeds and seedlings. *Plant Physiol.* 182, 1326–1345. doi: 10.1104/pp.19.01255

Kurusu, T., Koyano, T., Hanamata, S., Kubo, T., Noguchi, Y., Yagi, C., et al. (2014). OsATG7 is required for autophagy-dependent lipid metabolism in rice postmeiotic anther development. *Autophagy* 10, 878–888. doi: 10.4161/auto.28279

Lass, A., Zimmermann, R., Haemmerle, G., Riederer, M., Schoiswohl, G., Schweiger, M., et al. (2006). Adipose triglyceride lipase-mediated lipolysis of cellular fat stores is activated by CGI-58 and defective in Chanarin-Dorfman Syndrome. *Cell Metab.* 3, 309–319. doi: 10.1016/j.cmet.2006.03.005

Lavell, A. A., and Benning, C. (2019). Cellular organization and regulation of plant glycerolipid metabolism. *Plant Cell Physiol.* 60, 1176–1183. doi: 10.1093/pcp/pcz016

Lersten, N. R., Czlapinski, A. R., Curtis, J. D., Freckmann, R., and Horner, H. T. (2006). Oil bodies in leaf mesophyll cells of angiosperms: overview and a selected survey. *Am. J. Bot.* 93, 1731–1739. doi: 10.3732/ajb.93.12.1731

Levesque-Lemay, M., Chabot, D., Hubbard, K., Chan, J. K., Miller, S., and Robert, L. S. (2016). Tapetal oleosins play an essential role in tapetosome formation and protein relocation to the pollen coat. *New Phytol.* 209, 691–704. doi: 10.1111/nph.13611

Leyland, B., Boussiba, S., and Khozin-Goldberg, I. (2020). A review of diatom lipid droplets. *Biol. (Basel)* 9, 38. doi: 10.3390/biology9020038

Li, F., Chung, T., and Vierstra, R. D. (2014). AUTOPHAGY-RELATED11 plays a critical role in general autophagy- and senescence-induced mitophagy in Arabidopsis. *Plant Cell* 26, 788–807. doi: 10.1105/tpc.113.120014

Li, N., Gügel, I. L., Giavalisco, P., Zeisler, V., Schreiber, L., Soll, J., et al. (2015). FAX1, a novel membrane protein mediating plastid fatty acid export. *PloS Biol.* 3, e1002053. doi: 10.1371/journal.pbio.1002053

Li, N., Xu, C., Li-Beisson, Y., and Philippar, K. (2016). Fatty acid and lipid transport in plant cells. *Trends Plant Sci.* 21, 145–158. doi: 10.1016/j.tplants.2015.10.011

Li, N., Zhang, Y., Meng, H., Li, S., Wang, S., Xiao, Z., et al. (2019). Characterization of *Fatty Acid Exporters* involved in fatty acid transport for oil accumulation in the green alga *Chlamydomonas reinhardtii*. *Biotechnol. Biofuels* 12, 14. doi: 10.1186/s13068-018-1332-4

Li-Beisson, Y., Shorrosh, B., Beisson, F., Andersson, M. X., Arondel, V., Bates, P. D., et al. (2013). Acyl-lipid metabolism. *Arab. B.* 11, e0161. doi: 10.1199/tab.0161

Li-Beisson, Y., Beisson, F., and Riekhof, W. (2015). Metabolism of acyl-lipids in *Chlamydomonas reinhardtii*. *Plant J.* 82, 504–522. doi: 10.1111/tpj.12787

Lin, L.-J., Tai, S. S. K., Peng, C.-C., and Tzen, J. T. C. (2002). Steroleosin, a sterol-binding dehydrogenase in seed oil bodies. *Plant Physiol.* 128, 1200–1211. doi: 10.1104/pp.010928

Lu, Y., Wang, X., Balamurugan, S., Yang, W.-D., Liu, J.-S., Dong, H.-P., et al. (2017). Identification of a putative seipin ortholog involved in lipid accumulation in marine microalga *Phaedactylum tricornutum*. *J. App. Phycol.* 29, 2821–2829. doi: 10.1007/s10811-017-1173-8

Lupette, J., Jaussaud, A., Seddiki, K., Morabito, C., Brugière, S., Schaller, H., et al. (2019). The architecture of lipid droplets in the diatom *Phaeodactylum tricornutum*. *Algal. Res.* 38:101415. doi: 10.1016/J.ALGAL.2019.101415

Maeda, Y., Sunaga, Y., Yoshino, T., and Tanaka, T. (2014). Oleosome-associated protein of the oleaginous diatom *Fistulifera solaris* contains an endoplasmic reticulum-targeting signal sequence. *Mar. Drugs* 12, 3892–3903. doi: 10.3390/md12073892

Maeda, Y., Oku, M., and Sakai, Y. (2015). A defect of the vacuolar putative lipase Atg15 accelerates degradation of lipid droplets through lipolysis. *Autophagy* 11, 1247–1258. doi: 10.1080/15548627.2015.1056969

Marshall, R. S., and Vierstra, R. D. (2018). Autophagy: the master of bulk and selective recycling. *Annu. Rev. Plant Biol.* 69, 173–208. doi: 10.1146/annurev-arplant-042817-040606

Marshall, R. S., Hua, Z., Mali, S., McLoughlin, F., and Vierstra, R. D. (2019). ATG8-binding UIM proteins define a new class of autophagy adaptors and receptors. *Cell* 177, 766–781.e24. doi: 10.1016/j.cell.2019.02.009

Martinez-Lopez, N., Garcia-Macia, M., Sahu, S., Athonvarangkul, D., Liebling, E., Merlo, P., et al. (2016). Autophagy in the CNS and periphery coordinate lipophagy and lipolysis in the brown adipose tissue and liver. *Cell Metab.* 23, 113–127. doi: 10.1016/j.cmet.2015.10.008

Mayfield, J. A., Fiebig, A., Johnstone, S. E., and Preuss, D. (2001). Gene families from the *Arabidopsis thaliana* pollen coat proteome. *Science* 292, 2482–2485. doi: 10.1126/science.1060972

Moellering, E. R., and Benning, C. (2010). RNA interference silencing of a major lipid droplet protein affects lipid droplet size in *Chlamydomonas reinhardtii*. *Eukaryot Cell* 9, 97–106. doi: 10.1128/ec.00203-09

Müller, A. O., and Ischebeck, T. (2018). Characterization of the enzymatic activity and physiological function of the lipid droplet-associated triacylglycerol lipase AtOBL1. *New Phytol.* 217, 1062–1076. doi: 10.1111/nph.14902

Murphy, D. J. (2012). The dynamic roles of intracellular lipid droplets: from archaea to mammals. *Protoplasma* 249, 541–585. doi: 10.1007/s00709-011-0329-7

Napier, J. A., Beaudoin, F., Tatham, A. S., Alexander, L. G., and Shewry, P. R. (2001). The seed oleosins: structure, properties and biological role. *Adv. Bot. Res.* 35, 111–138. doi: 10.1016/S0065-2296(01)35005-X

Nawrath, C., Schreiber, L., Franke, R. B., Geldner, N., Reina-Pinto, J. J., and Kunst, L. (2013). Apoplastic diffusion barriers in Arabidopsis. *Arab. B.* 11, e0167. doi: 10.1199/tab.0167

Nguyen, H. M. ,., Baudet, M., Cuiné, S., Adriano, J., Barthe, D., Billon, E., et al. (2011). Proteomic profiling of oil bodies isolated from the unicellular green microalga *Chlamydomonas reinhardtii*: with focus on proteins involved in lipid metabolism. *Proteomics* 11, 4266–4273. doi: 10.1002/pmic.201100114

Nobusawa, T., Yamakawa-Ayukawa, K., Saito, F., Nomura, S., Takami, A., and Ohta, H. (2019). A homolog of Arabidopsis SDP1 lipase in Nannochloropsis is involved in degradation of de novo-synthesized triacylglycerols in the endoplasmic reticulum. *Biochim. Biophys. Acta Mol. Cell Biol. Lipids* 1864, 1185–1193. doi: 10.1016/j.bbalip.2019.05.013

Ohlrogge, J., and Browse, J. (1995). Lipid biosynthesis. *Plant Cell* 7, 957–970. doi: 10.1105/tpc.7.7.957

Oku, M., Maeda, Y., Kagohashi, Y., Kondo, T., Yamada, M., Fujimoto, T., et al. (2017). Evidence for ESCRT- and clathrin-dependent microautophagy. *J. Cell Biol.* 216, 3263–3274. doi: 10.1083/jcb.201611029

Olzmann, J. A., and Carvalho, P. (2019). Dynamics and functions of lipid droplets. *Nat. Rev. Mol. Cell Biol.* 20, 137–155. doi: 10.1038/s41580-018-0085-z

O'Rourke, E. J., Soukas, A. A., Carr, C. E., and Ruvkun, G. (2009). *C. elegans* major fats are stored in vesicles distinct from lysosome-related organelles. *Cell Metab.* 10, 430–435. doi: 10.1016/j.cmet.2009.10.002

Parish, R. W., and Li, S. F. (2010). Death of a tapetum: A programme of developmental altruism. *Plant Sci.* 178, 73–89. doi: 10.1016/j.plantsci.2009.11.001

Park, S., Gidda, S. K., James, C. N., Horn, P. J., Khuu, N., Seay, D. C., et al. (2013). The α/β hydrolase CGI-58 and peroxisomal transport protein PXA1 coregulate lipid homeostasis and signaling in Arabidopsis. *Plant Cell.* 25, 1726–1739. doi: 10.1105/tpc.113.111898

Petan, T., Jarc, E., and Jusovic, M. (2018). Lipid droplets in cancer: guardians of fat in a stressful world. *Molecules* 23, 1941. doi: 10.3390/molecules23081941

Piffanelli, P., Ross, J. H. E., and Murphy, D. J. (1998). Biogenesis and function of the lipidic structures of pollen grains. *Sex Plant Reprod.* 11, 65–80. doi: 10.1007/s004970050122

Poxleitner, M., Rogers, S. W., Lacey Samuels, A., Browse, J., and Rogers, J. C. (2006). A role for caleosin in degradation of oil-body storage lipid during seed germination. *Plant J.* 47, 917–933. doi: 10.1111/j.1365-313X.2006.02845.x

Pracharoenwattana, I., Zhou, W., and Smith, S. M. (2010). Fatty acid beta-oxidation in germinating Arabidopsis seeds is supported by peroxisomal hydroxypyruvate reductase when malate dehydrogenase is absent. *Plant Mol. Biol.* 72, 101–109. doi: 10.1007/s11103-009-9554-2

Purkrtova, Z., Le Bon, C., Kralova, B., Ropers, M.-H., Anton, M., and Chardot, T. (2008). Caleosin of *Arabidopsis thaliana* : effect of calcium on functional and structural properties. *J. Agric. Food Chem.* 56, 11217–11224. doi: 10.1021/jf802305b

Pyc, M., Cai, Y., Greer, M. S., Yurchenko, O., Chapman, K. D., Dyer, J. M., et al. (2017a). Turning over a new leaf in lipid droplet biology. *Trends Plant Sci.* 22, 596–609. doi: 10.1016/j.tplants.2017.03.012

Pyc, M., Cai, Y., Gidda, S. K., Yurchenko, O., Park, S., Kretzschmar, F. K., et al. (2017b). Arabidopsis lipid droplet-associated protein (LDAP) - interacting protein (LDIP) influences lipid droplet size and neutral lipid homeostasis in both leaves and seeds. *Plant J.* 92, 1182–1201. doi: 10.1111/tpj.13754

Quettier, A.-L., and Eastmond, P. J. (2009). Storage oil hydrolysis during early seedling growth. *Plant Physiol. Biochem. PPB* 47, 485–490. doi: 10.1016/j.plaphy.2008.12.005

Rahman, F., Hassan, M., Hanano, A., Fitzpatrick, D. A., McCarthy, C. G. P., and Murphy, D. J. (2018a). Evolutionary, structural and functional analysis of the caleosin/peroxygenase gene family in the Fungi. *BMC Genomics* 19, 976. doi: 10.1186/s12864-018-5334-1

Rahman, F., Hassan, M., Rosli, R., Almousally, I., Hanano, A., and Murphy, D. J. (2018b). Evolutionary and genomic analysis of the caleosin/peroxygenase (CLO/PXG) gene/protein families in the Viridiplantae. *PloS One* 13, e0196669. doi: 10.1371/journal.pone.0196669

Rambold, A. S., Cohen, S., and Lippincott-Schwartz, J. (2015). Fatty acid trafficking in starved cells: regulation by lipid droplet lipolysis, autophagy, and mitochondrial fusion dynamics. *Dev. Cell* 32, 678–692. doi: 10.1016/j.devcel.2015.01.029

Rejon, J. D., Zienkiewicz, A., Rodriguez-Garcia, M.II, and Castro, A. J. (2012). Profiling and functional classification of esterases in olive (*Olea europaea*) pollen during germination. *Ann. Bot.* 110, 1035–1045. doi: 10.1093/aob/mcs174

Rejon, J. D., Delalande, F., Schaeffer-Reiss, C., Alche, J., de, D., Rodriguez-Garcia, M.II, et al. (2016). The pollen coat proteome: at the cutting edge of plant reproduction. *Proteomes* 4, 5. doi: 10.3390/proteomes4010005

Rinaldi, M. A., Patel, A. B., Park, J., Lee, K., Strader, L. C., and Bartel, B. (2016). The Roles of β-oxidation and cofactor homeostasis in peroxisome distribution and function in *Arabidopsis thaliana*. *Genetics* 204, 1089–1115. doi: 10.1534/genetics.116.193169

Rudolph, M., Schlereth, A., Korner, M., Feussner, K., Berndt, E., Melzer, M., et al. (2011). The lipoxygenase-dependent oxygenation of lipid body membranes is promoted by a patatin-type phospholipase in cucumber cotyledons. *J. Exp. Bot.* 62, 749–760. doi: 10.1093/jxb/erq310

Sanjaya, M. R., Durrett, T. P., Kosma, D. K., Lydic, T. A., Muthan, B., Bagyalakshmi, M., et al. (2013). Altered lipid composition and enhanced nutritional value of Arabidopsis leaves following introduction of an algal diacylglycerol acyltransferase 2. *Plant Cell.* 25, 677–693. doi: 10.1105/tpc.112.104752

Sathyanarayan, A., Mashek, M. T., and Mashek, D. G. (2017). ATGL promotes autophagy/lipophagy via SIRT1 to control hepatic lipid droplet catabolism. *Cell Rep.* 19, 1–9. doi: 10.1016/j.celrep.2017.03.026

Schnurr, J. A., Shockey, J. M., de Boer, G. J., and Browse, J. A. (2002). Fatty acid export from the chloroplast. Molecular characterization of a major plastidial acyl-coenzyme A synthetase from Arabidopsis. *Plant Physiol.* 129, 1700–1709. doi: 10.1104/pp.003251

Schwarz, V., Andosch, A., Geretschlager, A., Affenzeller, M., and Lutz-Meindl, U. (2017). Carbon starvation induces lipid degradation via autophagy in the model alga Micrasterias. *J. Plant Physiol.* 208, 115–127. doi: 10.1016/j.jplph.2016.11.008

Seo, A. Y., Lau, P.-W., Feliciano, D., Sengupta, P., Gros, M. A., Cinquin, B., et al. (2017). AMPK and vacuole-associated Atg14p orchestrate mu-lipophagy for energy production and long-term survival under glucose starvation. *Elife* 6, e21690. doi: 10.7554/eLife.21690

Sera, Y., Hanamata, S., Sakamoto, S., Ono, S., Kaneko, K., Mitsui, Y., et al. (2019). Essential roles of autophagy in metabolic regulation in endosperm development during rice seed maturation. *Sci. Rep.* 9, 18544. doi: 10.1038/s41598-019-54361-1

Serrano, M., Coluccia, F., Torres, M., L'Haridon, F., and Metraux, J.-P. (2014). The cuticle and plant defense to pathogens. *Front. Plant Sci.* 5:274:274. doi: 10.3389/fpls.2014.00274

Shimada, T. L., Shimada, T., Takahashi, H., Fukao, Y., and Hara-Nishimura, I. (2008). A novel role for oleosins in freezing tolerance of oilseeds in *Arabidopsis thaliana*. *Plant J.* 55, 798–809. doi: 10.1111/j.1365-313X.2008.03553.x

Shimada, T. L., Takano, Y., Shimada, T., Fujiwara, M., Fukao, Y., Mori, M., et al. (2014). Leaf oil body functions as a subcellular factory for the production of a phytoalexin in Arabidopsis. *Plant Physiol.* 164, 105–118. doi: 10.1104/pp.113.230185

Shimada, T. L., Takano, Y., and Hara-Nishimura, I. (2015). Oil body-mediated defense against fungi: From tissues to ecology. *Plant Signal. Behav.* 10, e989036. doi: 10.4161/15592324.2014.989036

Shimada, T. L., Shimada, T., Okazaki, Y., Higashi, Y., Saito, K., Kuwata, K., et al. (2019). HIGH STEROL ESTER 1 is a key factor in plant sterol homeostasis. *Nat. Plants* 5, 1154–1166. doi: 10.1038/s41477-019-0537-2

Siaut, M., Cuiné, S., Cagnon, C., Fessler, B., Nguyen, M., Carrier, P., et al. (2011). Oil accumulation in the model green alga *Chlamydomonas reinhardtii*: characterization, variability between common laboratory strains and relationship with starch reserves. *BMC Biotechnol.* 2011 11:7. doi: 10.1186/1472-6750-11-7

Siegler, H., Valerius, O., Ischebeck, T., Popko, J., Tourasse, N. J., Vallon, O., et al. (2017). Analysis of the lipid body proteome of the oleaginous alga *Lobosphaera incisa*. *BMC Plant Biol.* 17, 98. doi: 10.1186/s12870-017-1042-2

Siloto, R. M. P., Findlay, K., Lopez-Villalobos, A., Yeung, E. C., Nykiforuk, C. L., and Moloney, M. M. (2006). The accumulation of oleosins determines the size of seed oil bodies in Arabidopsis. *Plant Cell* 18, 1961–1974. doi: 10.1105/tpc.106.041269

Singh, R., Kaushik, S., Wang, Y., Xiang, Y., Novak, I., Komatsu, M., et al. (2009). Autophagy regulates lipid metabolism. *Nature* 458, 1131–1135. doi: 10.1038/nature07976

Soto-Burgos, J., Zhuang, X., Jiang, L., and Bassham, D. C. (2018). Dynamics of autophagosome formation. *Plant Physiol.* 176, 219–229. doi: 10.1104/pp.17.01236

Sun, X., Jia, X., Huo, L., Che, R., Gong, X., Wang, P., et al. (2018). MdATG18a overexpression improves tolerance to nitrogen deficiency and regulates anthocyanin accumulation through increased autophagy in transgenic apple. *Plant Cell Environ.* 41, 469–480. doi: 10.1111/pce.13110

Taurino, M., Costantini, S., De Domenico, S., Stefanelli, F., Ruano, G., Delgadillo, M. O., et al. (2018). SEIPIN proteins mediate lipid droplet biogenesis to promote pollen transmission and reduce seed dormancy. *Plant Physiol.* 176, 1531–1546. doi: 10.1104/pp.17.01430

Thazar-Poulot, N., Miquel, M., Fobis-Loisy, I., and Gaude, T. (2015). Peroxisome extensions deliver the Arabidopsis SDP1 lipase to oil bodies. *Proc. Natl. Acad. Sci. U. S. A.* 112, 4158–4163. doi: 10.1073/pnas.1403322112

Tran, Q.-G., Yoon, H. R., Cho, K., Lee, S.-J., Crespo, J. L., Ramanan, R., et al. (2019). Dynamic interactions between autophagosomes and lipid droplets in *Chlamydomonas reinhardtii*. *Cells* 8, 992. doi: 10.3390/cells8090992

Trentacoste, E. M., Shrestha, R. P., Smith, S. R., Gle, C., Hartmann, A. C., Hildebrand, M., et al. (2013). Metabolic engineering of lipid catabolism increases microalgal lipid accumulation without compromising growth. *Proc. Natl. Acad. Sci. U. S. A.* 110, 19748–19753. doi: 10.1073/pnas.1309299110

Troncoso-Ponce, M. A., Cao, X., Yang, Z., and Ohlrogge, J. B. (2013). Lipid turnover during senescence. *Plant Sci.* 205–206, 13–19. doi: 10.1016/J.PLANTSCI.2013.01.004

Tsai, C.-H., Zienkiewicz, K., Amstutz, C. L., Brink, B. G., Warakanont, J., Roston, R., et al. (2015). Dynamics of protein and polar lipid recruitment during lipid droplet assembly in *Chlamydomonas reinhardtii*. *Plant J.* 83, 650–660. doi: 10.1111/tpj.12917

Tsai, C. H., Uygun, S., Roston, R., Shiu, S. H., and Benning, C. (2018). Recovery from N deprivation is a transcriptionally and functionally distinct state in Chlamydomonas. *Plant Physiol.* 176, 2007–2023. doi: 10.1104/pp.17.01546

Turchetto-Zolet, A., Maraschin, F. S., de Morais, G. L., Cagliari, A., Andrade, C. M., Margis-Pinheiro, M., et al. (2011). Evolutionary view of acyl-CoA diacylglycerol acyltransferase (DGAT), a key enzyme in neutral lipid biosynthesis. *BMC Evol. Biol.* 11:263. doi: 10.1186/1471-2148-11-263

Tzen, J. T., Lai, Y. K., Chan, K. L., and Huang, A. H. (1990). Oleosin isoforms of high and low molecular weights are present in the oil bodies of diverse seed species. *Plant Physiol.* 94, 1282–1289. doi: 10.1104/pp.94.3.1282

Tzen, J. T. C., Cao, Y., Laurent, P., Ratnayake, C., and Huang, A. H. C. (1993). Lipids, proteins, and structure of seed oil bodies from diverse species. *Plant Physiol.* 101, 267–276. doi: 10.1104/pp.101.1.267

van Erp, H., Kelly, A. A., Menard, G., and Eastmond, P. J. (2014). Multigene engineering of triacylglycerol metabolism boosts seed oil content in Arabidopsis. *Plant Physiol.* 165, 30–36. doi: 10.1104/pp.114.236430

van Zutphen, T., Todde, V., de Boer, R., Kreim, M., Hofbauer, H. F., Wolinski, H., et al. (2014). Lipid droplet autophagy in the yeast *Saccharomyces cerevisiae*. *Mol. Biol. Cell* 25, 290–301. doi: 10.1091/mbc.E13-08-0448

Vevea, J. D., Garcia, E. J., Chan, R. B., Zhou, B., Schultz, M., Di Paolo, G., et al. (2015). Role for lipid droplet biogenesis and microlipophagy in adaptation to lipid imbalance in yeast. *Dev. Cell* 35, 584–599. doi: 10.1016/j.devcel.2015.11.010

Vieler, A., Brubaker, S. B., Vick, B., and Benning, C. (2012a). A lipid droplet protein of Nannochloropsis with functions partially analogous to plant oleosins. *Plant Physiol.* 158, 1562–1569. doi: 10.1104/pp.111.193029

Vieler, A., Wu, G., Tsai, C. H., Bullard, B., Cornish, A. J., Harvey, C., et al. (2012b). Genome, functional gene annotation, and nuclear transformation of the heterokont oleaginous alga *Nannochloropsis oceanica* CCMP1779. *PloS Genet.* 8, e1003064. doi: 10.1371/journal.pgen.1003064

Wang, Z., and Benning, C. (2012). Chloroplast lipid synthesis and lipid trafficking through ER-plastid membrane contact sites. *Biochem. Soc Trans.* 40, 457–463. doi: 10.1042/BST20110752

Wang, X., Hao, T.-B., Balamurugan, S., Yang, W.-D., Liu, J.-S., Dong, H.-P., et al. (2017). A lipid droplet-associated protein involved in lipid droplet biogenesis and triacylglycerol accumulation in the oleaginous microalga *Phaeodactylum tricornutum*. *Algal. Res.* 26, 215–224. doi: 10.1016/J.ALGAL.2017.07.028

Wang, X., Wei, H., Mao, X., and Liu, J. (2019). Proteomics analysis of lipid droplets from the oleaginous alga *Chromochloris zofingiensis* reveals novel proteins for lipid metabolism. *Genomics Proteomics Bioinf.* 17, 260–272. doi: 10.1016/J.GPB.2019.01.003

Warakanont, J., Li-Beisson, Y., and Benning, C. (2019). LIP4 is involved in triacylglycerol degradation in *Chlamydomonas reinhardtii*. *Plant Cell Physiol.* 60, 1250–1259. doi: 10.1093/pcp/pcz037

Welte, M. A., and Gould, A. P. (2017). Lipid droplet functions beyond energy storage. *Biochim. Biophys. Acta Mol. Cell Biol. Lipids* 1862, 1260–1272. doi: 10.1016/j.bbalip.2017.07.006

Yang, Y., and Benning, C. (2018). Functions of triacylglycerols during plant development and stress. *Curr. Opin. Biotechnol.* 49, 191–198. doi: 10.1016/j.copbio.2017.09.003

Yoneda, K., Yoshida, M., Suzuki, I., and Watanabe, M. M. (2016). Identification of a major lipid droplet protein in a marine diatom *Phaeodactylum tricornutum*. *Plant Cell Physiol.* 57, 397–406. doi: 10.1093/pcp/pcv204

Yoon, K., Han, D., Li, Y., Sommerfeld, M., and Hu, Q. (2012). Phospholipid: diacylglycerol acyltransferase is a multifunctional enzyme involved in membrane lipid turnover and degradation while synthesizing triacylglycerol in the unicellular green microalga *Chlamydomonas reinhardtii*. *Plant Cell.* 24, 3708–3724. doi: 10.1105/tpc.112.100701

Yoshimoto, K., and Ohsumi, Y. (2018). Unveiling the molecular mechanisms of plant autophagy-from autophagosomes to vacuoles in plants. *Plant Cell Physiol.* 59, 1337–1344. doi: 10.1093/pcp/pcy112

Yoshimoto, K., Hanaoka, H., Sato, S., Kato, T., Tabata, S., Noda, T., et al. (2004). Processing of ATG8s, ubiquitin-like proteins, and their deconjugation by ATG4s are essential for plant autophagy. *Plant Cell* 16, 2967–2983. doi: 10.1105/tpc.104.025395

You, Z., Zhang, Q., Peng, Z., and Miao, X. (2019). Lipid droplets mediate salt stress tolerance in *Parachlorella kessleri*. *Plant Physiol.* 181, 510–526. doi: 10.1104/pp.19.00666

Zhang, M., Fan, J., Taylor, D. C., and Ohlrogge, J. B. (2009). DGAT1 and PDAT1 acyltransferases have overlapping functions in Arabidopsis triacylglycerol biosynthesis and are essential for normal pollen and seed development. *Plant Cell.* 21, 3885–3901. doi: 10.1105/tpc.109.071795

Zhang, C., Yang, L., Ding, Y., Wang, Y., Lan, L., Ma, Q., et al. (2017). Bacterial lipid droplets bind to DNA via an intermediary protein that enhances survival under stress. *Nat. Commun.* 8:15979. doi: 10.1038/ncomms15979

Zhang, C., Qu, Y., Lian, Y., Chapman, M., Chapman, N., Xin, J., et al. (2020). A new insight into the mechanism for cytosolic lipid droplet degradation in senescent leaves. *Physiol. Plant* 168, 835–844. doi: 10.1111/ppl.13039

Zhao, L., Dai, J., and Wu, Q. (2014). Autophagy-like processes are involved in lipid droplet degradation in *Auxenochlorella protothecoides* during the heterotrophy-autotrophy transition. *Front. Plant Sci.* 5:400:400. doi: 10.3389/fpls.2014.00400

Zhao, P., Zhou, X.-M., Zhao, L.-L., Cheung, A. Y., and Sun, M.-X. (2020). Autophagy-mediated compartmental cytoplasmic deletion is essential for tobacco pollen germination and male fertility. *Autophagy* 1–13. doi: 10.1080/15548627.2020.1719722

Zhi, Y., Taylor, M. C., Campbell, P. M., Warden, A. C., Shrestha, P., El Tahchy, A., et al. (2017). Comparative lipidomics and proteomics of lipid droplets in the mesocarp and seed tissues of Chinese Tallow (*Triadica sebifera*). *Front. Plant Sci.* 8:1339:1339. doi: 10.3389/fpls.2017.01339

Zienkiewicz, K., Castro, A. J., Alche, J., de, D., Zienkiewicz, A., Suarez, C., et al. (2010). Identification and localization of a caleosin in olive (*Olea europaea* L.) pollen during in vitro germination. *J. Exp. Bot.* 61, 1537–1546. doi: 10.1093/jxb/erq022

Zienkiewicz, A., Jimenez-Lopez, J. C., Zienkiewicz, K., de Dios Alche, J., and Rodriguez-Garcia, M.II (2011). Development of the cotyledon cells during olive (Olea europaea L.) in vitro seed germination and seedling growth. *Protoplasma* 248, 751–765. doi: 10.1007/s00709-010-0242-5

Zienkiewicz, K., Zienkiewicz, A., Rodriguez-Garcia, M.II, and Castro, A. J. (2011). Characterization of a caleosin expressed during olive (*Olea europaea* L.) pollen ontogeny. *BMC Plant Biol.* 11:122. doi: 10.1186/1471-2229-11-122

Zienkiewicz, A., Zienkiewicz, K., Rejon, J. D., Rodriguez-Garcia, M.II, and Castro, A. J. (2013). New insights into the early steps of oil body mobilization during pollen germination. *J. Exp. Bot.* 64, 293–302. doi: 10.1093/jxb/ers332

Zienkiewicz, A., Krzysztof, Z., and Rodriguez-Garcia, M.II (2014a). "Storage lipids in developing and germinating pollen grain of flowering plants", in *Reproductive Biology of Plants*. Eds. Ramawat, K., Merillon, J. M., and Shivanna, K. (Boca Raton: CRC Press), 133–146. doi: 10.1201/b16535

Zienkiewicz, A., Zienkiewicz, K., Rejon, J. D., Alche, J., de, D., Castro, A. J., et al. (2014b). Olive seed protein bodies store degrading enzymes involved in mobilization of oil bodies. *J. Exp. Bot.* 65, 103–115. doi: 10.1093/jxb/ert355

Zienkiewicz, K., Du, Z. Y., Ma, W., Vollheyde, K., and Benning, C. (2016). Stress-induced neutral lipid biosynthesis in microalgae - Molecular, cellular and physiological insights. *Biochim. Biophys. Acta*. 1861, 1269–1281. doi: 10.1016/j.bbalip.2016.02.008

Zienkiewicz, K., Zienkiewicz, A., Poliner, E., Du, Z. Y., Vollheyde, K., Herrfurth, C., et al. (2017). Nannochloropsis, a rich source of diacylglycerol acyltransferases for engineering of triacylglycerol content in different hosts. *Biotechnol. Biofuels* 10:8. doi: 10.1186/s13068-016-0686-8

Zienkiewicz, K., Benning, U., Siegler, H., and Feussner, I. (2018). The type 2 acyl CoA:diacylglycerol acyltransferase family of the oleaginous microalga *Lobosphaera incisa*. *BMC Plant Biol.* 18, 98. doi: 10.1186/s12870-018-1510-3

Zienkiewicz, A., Zienkiewicz, K., Poliner, E., Pulman, J. A., Du, Z.-Y., Stefano, G., et al. (2020). The microalga Nannochloropsis during transition from quiescence to autotrophy in response to nitrogen availability. *Plant Physiol.* 182, 819–839. doi: 10.1104/pp.19.00854

Zolman, B. K., Silva, I. D., and Bartel, B. (2001). The Arabidopsis *pxa1* mutant is defective in an ATP-binding cassette transporter-like protein required for peroxisomal fatty acid β-oxidation. *Plant Physiol.* 127, 1266–1278. doi: 10.1104/pp.010550

Conflict of Interest: The authors declare that the research was conducted in the absence of any commercial or financial relationships that could be construed as a potential conflict of interest.

frontiers in Plant Science

ORIGINAL RESEARCH
published: 06 October 2020
doi: 10.3389/fpls.2020.564656

Ectopic Expression of *CsKCS6* From Navel Orange Promotes the Production of Very-Long-Chain Fatty Acids (VLCFAs) and Increases the Abiotic Stress Tolerance of *Arabidopsis thaliana*

Wenfang Guo, Qi Wu, Li Yang, Wei Hu, Dechun Liu and Yong Liu**

Department of Pomology, College of Agronomy, Jiangxi Agricultural University, Nanchang, China

OPEN ACCESS

Edited by:
Agnieszka Zienkiewicz, Nicolaus Copernicus University in Toruñ, Poland

Reviewed by:
Tegan Haslam, The University of British Columbia, Canada
Joaquín J. Salas, Instituto de la Grasa (IG), Spain

***Correspondence:**
Dechun Liu
ldc873380800@163.com
Yong Liu
liuyongjxau@163.com

Specialty section:
This article was submitted to Plant Metabolism and Chemodiversity, a section of the journal Frontiers in Plant Science

Received: *22 June 2020*
Accepted: *14 September 2020*
Published: *06 October 2020*

Citation:
Guo W, Wu Q, Yang L, Hu W, Liu D and Liu Y (2020) Ectopic Expression of CsKCS6 From Navel Orange Promotes the Production of Very-Long-Chain Fatty Acids (VLCFAs) and Increases the Abiotic Stress Tolerance of Arabidopsis thaliana. Front. Plant Sci. 11:564656. doi: 10.3389/fpls.2020.564656

Cuticular wax is closely related to plant resistance to abiotic stress. 3-Ketoacyl-CoA synthase (KCS) catalyzes the biosynthesis of very-long-chain fatty acid (VLCFA) wax precursors. In this study, a novel *KCS* family gene was isolated from Newhall navel orange and subsequently named *CsKCS6*. The CsKCS6 protein has two main domains that belong to the thiolase-like superfamily, the FAE1-CUT1-RppA and ACP_syn_III_C domains, which exist at amino acid positions 80–368 and 384–466, respectively. *CsKCS6* was expressed in all tissues, with the highest expression detected in the stigma; in addition, the transcription of *CsKCS6* was changed in response to drought stress, salt stress and abscisic acid (ABA) treatment. Heterologous expression of *CsKCS6* in *Arabidopsis* significantly increased the amount of VLCFAs in the cuticular wax on the stems and leaves, but there were no significant changes in total wax content. Compared with that of the wild-type (WT) plants, the leaf permeability of the transgenic plants was lower. Further research showed that, compared with the WT plants, the transgenic lines experienced less water loss and ion leakage after dehydration stress, displayed increased survival under drought stress treatment and presented significantly longer root lengths and survival under salt stress treatment. Our results indicate that *CsKCS6* not only plays an important role in the synthesis of fatty acid precursors involved in wax synthesis but also enhances the tolerance of transgenic *Arabidopsis* plants to abiotic stress. Thus, the identification of *CsKSC6* could help to increase the abiotic stress tolerance of *Citrus* in future breeding programs.

Keywords: Newhall navel orange, cuticular wax, *KCS6*, abiotic stresses, transgenic *Arabidopsis*

INTRODUCTION

Very-long-chain fatty acids (VLCFAs), which refer mainly to a class of fatty acids with more than 18 carbon atoms, are precursor materials for the synthesis of plant cuticular waxes (Kunst and Samuels, 2003). The biosynthesis of VLCFAs involves catalysis by the multienzyme fatty acid elongase (FAE) complex. The catalytic process involves four main steps: condensation, reduction,

dehydration and re-reduction (Haslam and Kunst, 2013). 3-Ketoacyl-CoA synthase (KCS) is the rate-limiting enzyme of the condensation reaction and is a key enzyme in the fatty acid extension pathway (Rossak et al., 2001).

There are many genes that encode KCS enzymes. *FAE1*, which is expressed only in seeds, was the first KCS family gene cloned from *Arabidopsis*, and its encoded protein catalyzes the synthesis of C_{20} and C_{22} fatty acids and storage lipids (James et al., 1995). To date, 21 *KCS* genes have been annotated in the Arabidopsis genome, and they are divided into four subfamilies, *FAE1*-like, *KCS1*-like, *FDH*-like, and *CER6*, based on their amino acid sequence homology (Costaglioli et al., 2005). Subsequently, Joubès et al. (2008) divided the existing 21 Arabidopsis KCS proteins into eight subclasses based on phylogeny. Guo et al. (2015) collected KCS genes from 26 sequenced plant genomes and reconstructed the phylogenetic tree of the *KCS* family genes to reveal the molecular basis of the functional divergence of different *KCS* genes. Furthermore, three *KCS* genes, including *KCS1* (Todd et al., 1999; Lee and Suh, 2013), *FDH* (Yephremov et al., 1999; Pruitt et al., 2000) and *CER6* (Millar et al., 1999; Fiebig et al., 2000; Hooker et al., 2002), have been shown to be involved in the formation of the cuticle in Arabidopsis: it has been reported that *KCS1* is expressed in all tissues of Arabidopsis plants, and complete loss of function of *KCS1* leads to a decrease in C_{26} and C_{30} alcohol and aldehyde compounds, respectively (Lee and Suh, 2013). *FDH* is expressed mainly in the flowers and young leaves of Arabidopsis; the *FDH* gene participates in the synthesis of VLCFAs in epidermal cells and is involved in both the regulation of plant morphological structure and the response to biotic stress (Yephremov et al., 1999; Pruitt et al., 2000; Joubès et al., 2008). *KCS6*/*CER6*/*CUT1* is expressed in the aboveground tissues of Arabidopsis, especially the flowers and siliques. Overexpression of *KCS6*/*CER6* caused an increase in the wax content of the stem epidermis of Arabidopsis. Moreover, its functional defect mutant *cer6* accumulated a large quantity of C_{24} VLCFA derivatives, indicating that this gene is involved in the biosynthesis of C_{24} (or longer) VLCFAs (Millar et al., 1999; Fiebig et al., 2000; Hooker et al., 2002).

Cuticular wax is the first protective barrier that covers the surface of terrestrial plants and is in contact with the outside environment (Riederer and Schneider, 1990; Jenks et al., 1994). Therefore, cuticular wax plays an important role in plant resistance to various stresses (Krauss et al., 1997; Sieber et al., 2000). In recent years, many wax synthesis genes have been used to improve plant resistance to abiotic stresses. *ECERIFERUM* (*CER1*) genes are involved in the wax biosynthesis pathway. *cer1* mutants present glossy green stems and altered wax alkane biosynthesis (Bourdenx et al., 2011; Bernard et al., 2012). Overexpression of *OsGL1-2* increases the number of wax crystals of rice leaves, thereby improving the drought resistance of the plant (Islam et al., 2009). Transformation of *Arabidopsis* with *WXP1* and *WXP2* also increased the wax content of the transformants and their resistance to water stress and drought stress (Zhang et al., 2005, 2007). The apple AP2/EREBP transcription factor *MdSHINE2* provides drought resistance by regulating wax biosynthesis (Zhang et al., 2019a). Similarly, the R2R3 MYB transcription factor *MdMYB30* modulates plant resistance against pathogens by regulating cuticular wax biosynthesis (Zhang et al., 2019b). Overexpression of *BnKCS1-1*, *BnKCS1-2*, and *BnCER1-2* in *Brassica napus* increased the wax crystal density on the leaf surface, and the water loss rate decreased together with increased drought tolerance, which was enhanced in transgenic plants (Wang et al., 2020).

Citrus is a perennial woody plant species with a high degree of heterozygosity. The relationship between wax genes and citrus resistance to abiotic stress may be more complex than that of model plant species such as *Arabidopsis*. In our previous studies, we analyzed the wax structure, chemical composition, and transcript levels of wax genes in Newhall navel orange (Liu et al., 2012, 2015). No wax-related genes have been identified in citrus so far; thus, the molecular mechanism underlying wax synthesis and its effect on citrus abiotic stress resistance is still unknown. In this study, a *KCS6* homologous gene, which was named *CsKCS6*, was cloned from Newhall navel orange. The expression patterns of *CsKCS6* in different tissues and in response to different abiotic stress conditions were analyzed by quantitative real-time PCR (qRT-PCR). The important role of *CsKCS6* in citrus wax synthesis and its effects on abiotic tolerance were identified by overexpressing the gene in *Arabidopsis*. The results broadened our knowledge concerning the molecular mechanism underlying cuticular wax synthesis in citrus.

MATERIALS AND METHODS

Plant Materials and Growth Conditions

Tissue samples of from adult trees of Newhall navel orange (*Citrus sinensis*) were collected in an orchard in Xinfeng County, Jiangxi Province, China. Young leaves of Newhall navel orange trees were collected for gene cloning, and leaves, flowers, receptacles, petals, pistils, stigmas, ovaries, flavedos, albedos, and flesh were collected from five trees per biological replicate for organ-specific expression analysis. Flavedo, albedo and flesh samples were collected from five trees per biological replicate at 60, 120, and 210 days after flowering, respectively, for analysis of expression during fruit development. Three biological replicates were used for these expression analyses.

Prior to the stress treatments, 1-year-old grafted seedlings of Newhall navel orange whose height was 30 ± 2 cm were transferred to pots that contained Hoagland's solution in a growth chamber for 7 days to acclimate to the new conditions. The plants were then subjected to 4°C for 0, 1, 3, 6, 9, 12, and 24 h for the cold treatment. For the drought stress, salt stress and abscisic acid (ABA) treatments, we transferred the plants to Hoagland's solution that contained 20% PEG6000, 250 mM NaCl, or 100 μM ABA, respectively, for 0, 1, 3, 6, 9, 12, and 24 h. The seedlings for each treatment were grown under a light/dark cycle of 16/8 h at 25°C. For each treatment, the leaves were sampled from 18 randomly selected seedlings at each time point, and each treatment was repeated three times for each time point.

Cloning and Sequence Analysis of *CsKCS6*

The *KCS6* homologous cDNA sequence (Cs7g13310) from sweet orange was retrieved from the sweet orange genomic database[1]. A pair of gene-specific primers (P1) (**Supplementary Table S1**) based on the *KCS6* homologous cDNA sequence were designed for CDS sequence cloning. The leaves of 1-year-old grafted seedlings of Newhall navel orange were sampled to extract the total RNA. RNA extraction method refers to TaKaRa MiniBEST Plant RNA Extraction Kit (TaKaRa, Japan) instructions. The integrity of RNA was detected by 1% agarose gel electrophoresis. The total RNA yield and quality were further determined using a NanoDrop 2000 spectrophotometer (Thermo Fisher Scientific, Waltham, United States). Using the total RNA extracted above as a template, TaKaRa PrimeScript^{TM} RT reagent Kit with gDNA Eraser reverse transcription kit (TaKaRa, Japan) was used for cDNA synthesis. Bioinformatic analysis, which included a plant KCS6 homology analysis, multiple sequence alignment and a KCS6 phylogenetic analysis, was conducted using the methods of a previous report (Liu et al., 2017).

Expression Analysis of *CsKCS6* in Navel Orange

Real-time quantitative PCR (qRT-PCR) was used for *CsKCS6* transcript analysis with the specific primer P2 (**Supplementary Table S1**). The citrus *ACTIN* gene was amplified with the specific primer P3 (**Supplementary Table S1**) to serve as a control gene for normalizing the expression between different samples. The real-time quantitative detection is done using SYBR§ Premix Ex Taq^{TM} kit (TaKaRa, Japan). The reactions were performed by an initial incubation at 95°C pre-denaturation for 30 s, then 95°C denaturation for 5 s, 60°C annealing for 30 s and 40 cycles. The $2^{-\Delta\Delta CT}$ method was used to calculate the relative changes in gene expression. qPCR was performed in four replicates for each sample, and data are indicated as the mean ± SD ($n = 3$).

Construction of the *CsKCS6* Expression Vector and Its Genetic Transformation Into *Arabidopsis*

The full-length CDS of the Newhall navel orange *CsKCS6* gene was cloned into a pCAMBIA1301 with CaMV35S promoter plant expression vector using the amplification-specific primer P4 (**Supplementary Table S1**) with *Bam*HI and *BstpI* restriction sites. A vector-containing plasmid was introduced into *Agrobacterium tumefaciens* strain LBA4404, which was subsequently transformed into *Arabidopsis* by the *Agrobacterium*-mediated floral-dip method, as described by Zhou et al. (2019). Seeds of T_0 transgenic plants were sown in Murashige and Skoog (MS) media to which hygromycin (10 mg L^{-1}) was added to screen for positive T_1 transgenic plants based on their resistance to hygromycin, and using the leaves of resistant seedlings as templates, PCR detection was carried out using gene specific primers of P4 and P7 (**Supplementary Table S1**). The expression level of positive transgenic plants was further tested by qPCR amplification of *CsKCS6* and *AtACTIN* using two different primers: P5 and P6 (**Supplementary Table S1**). Seeds of the T_1-positive *Arabidopsis* plants were grown on MS solid media that contained hygromycin (10 mg L^{-1}) to produce T_2 transgenic plants, which were used in subsequent experiments.

[1]http://citrus.hzau.edu.cn/orange/

Extraction of Cuticular Waxes and Gas Chromatography-Mass Spectrometry (GC–MS) Analysis

Approximately 100 mg of leaves and stems of 6-week-old wild-type (WT) and transgenic Arabidopsis plants were removed. The sample is gently moistened with distilled water and then the tissue surface is tenderly drained with filter paper, after which they were placed in a reaction flask. Cuticular waxes were extracted described by immersing tissues for 1 min in 2 mL of chloroform containing 10 μg of tetracosane as an internal standard. The extracts were dried under a gentle stream of nitrogen gas. The dried wax residues were derivatized by adding 20 μL of silylation reagent (BSTFA) and 20 μL of pyridine and incubated for 40 min at 70°C. The chromatographic column used in the experiment adopts a universal (30 m × 0.25 mm × 0.25 μm) hp-5MS capillary column with polydimethylsiloxane as the stationary phase. The chromatographic conditions were the inlet temperature of 280°C, the column flow rate of 2 mL/min and a constant flow rate; the Aux-2 temperature of 280°C, helium as the carrier gas, sample injection without splitting and the injection volume of 1 μL. The mass spectrometry program is set to electron impact ionization mode, energy 70 eV, mass scanning range 50 ∼ 600 amu and full scanning mode. The temperature rise process is to hold at 50°C for 1 min, raise the temperature to 170°C at 20°C/min, and hold for 2 min; then raise the temperature to 300°C at 5°C/min and hold for 8 min. The ion peaks of various wax components are detected by GC–MS (GCMS-QP2010, Shimadzu, Agilent). According to the mass spectrum library to search and determine and compare the FID peak area data, the single wax compound was quantified relative to the internal standard. Three biological replicates were used for each sample. The specific methods used were described by Chen et al. (2011) and Liu et al. (2012).

Scanning Electron Microscopy (SEM)

Scanning electron microscopy (SEM) was used to observe the ultrastructure of the wax crystals of the stems and rosette leaves of 6-week-old *Arabidopsis*. The samples were fixed in 4% glutaraldehyde for 12 h and then rinsed with 0.1 mM phosphate buffer at a pH of 7.2, three times for 10 min each. Ethanol at concentrations of 30, 50, 70, 80, and 90% was dehydrated once for 15 min using a JFC-1100-type ion sputtering instrument for gold plating. The samples were ultimately observed with a JSM-T300 scanning electron microscope (JEOL, Tokyo, Japan) after they were freeze-dried and adhered to the sample table (Liu et al., 2012).

Toluidine Blue (TB) Staining and Chlorophyll Content Assays

Six-week-old healthy *Arabidopsis* leaves were stained in a 0.05% TB staining solution at 25°C for 10 min. The samples were then rinsed with deionized water at least three times before being images.

Healthy leaves of transgenic plants and WT plants at 6 weeks of age were taken in equal amounts, and their chlorophyll leaching content was measured according to the method of Zhang et al. (2019a).

Physiological Measurements of *Arabidopsis* Plants Under Drought and Salt Treatments

The water loss rate and ion leakage rate of the leaves after dehydration treatment were measured according to previously described methods (Dai et al., 2018; Xie et al., 2018).

Seeds of WT and *CsKCS6*-overexpressing *Arabidopsis* were selected and sown on MS media that were supplemented with 100 mM NaCl. Thirty seeds were sown per treatment, and the germination percentage was determined daily (Seo et al., 2009). WT and transgenic *Arabidopsis* seedlings that had grown on MS media for 7 days were transferred to fresh MS media supplemented with 100 and 200 mM NaCl and allowed to grow for 2 weeks, at which time they were imaged and their root length ($\geq$5 mm) was measured.

WT and transgenic *Arabidopsis* that had grown on MS media for 4 weeks were transplanted into soil. After 10 days, the plants were then subjected to drought (water replenishment for 3 days after 10 days of natural drought) and salt (100/200 mM NaCl solutions were poured into the pots every 3 days, at 50 ml pot^{-1}) treatments. Twenty plants were included per treatment, each of which included three biological replicates (Dai et al., 2018).

Data Presentation and Statistical Analysis

All quantitative data are given as the means and standard errors. Statistical analyses were conducted using Student's *t*-test and Duncan's multiple range tests in SPSS version 22. Statistical significance was considered at the $P < 0.01$ and $P < 0.05$ level for *t*-test and at $P < 0.05$ for Duncan's multiple range tests.

RESULTS

Cloning and Sequence Analysis of *CsKCS6*

In the past, a novel navel orange variety, named 'Ganqi 3,' was bred from a bud mutation of 'Newhall' navel orange. Further study revealed that the expression level of *CsKCS6* in 'Ganqi 3' fruit peels were significant lower than that in 'Newhall' fruit peels, indicating the *CsKCS6* might be involved in cuticular wax biosynthesis (Liu et al., 2016). Using the cDNA of the 'Newhall Navel Orange' leaf as a template, PCR amplification was performed using *CsKCS6* specific primers (**Supplementary Table S1**). Sequence analysis showed that The full-length cDNA sequence of *CsKCS6* (GenBank accession number MT259183) was 1750 bp, with an open reading frame (ORF) of 1491 bp. The CsKCS6 protein comprised 496 amino acids, with a putative molecular weight of 56.22 kDa and an isoelectric point of 9.18. Sequence analysis revealed that CsKCS6 is highly homologous to other KCS6 proteins in plants, including *Citrus clementina* CcKCS6 (98%), *Hevea brasiliensis* HbKCS6 (67%), *Jatropha curcas* JcKCS6 (68%), *Glycine max* GmKCS6 (67%), *Malus domestica* MdKCS6 (69%), *Populus euphratica* PeKCS6 (68%), *Theobroma cacao* TcKCS6 (70%), and *Sesamum indicum* SiKCS6 (67%). Structural analysis revealed that the FAE1-CUT1-RppA conserved domain was found at amino acid positions of 80–368 in CsKCS6 and that the ACP_syn_III_C conserved domain was found at 384–466. Both major domains belong to the thiolase-like superfamily. Among them, the Cys residue at amino acid position of 225 is the catalytic active site of the condensing enzyme and is highly conserved among different species (**Figure 1**). In this study, we used the maximum likelihood method of MEGA 6 software to construct a phylogenetic tree of plant KCS6 proteins. The results showed that the CsKCS6 protein formed a large branch with the KCS6 proteins of dicotyledonous plant species such as *Citrus clementina*, *Malus domestica*, *Gossypium raimondii,* and *Glycine max*. The CsKCS6 protein was most closely related to the clementine CcKCS6 and clustered onto the same small branch. In addition, the KCS6 protein of the monocotyledonous plant species *Musa acuminata*, *Zea mays*, *Oryza brachyantha*, and *Phoenix dactylifera* was classified as another large branch, and this protein was the most related to CsKCS6. The evolution of these protein sequences is essentially consistent with the process of plant evolution in nature (**Figure 2**).

Analysis of the *CsKCS6* Expression Pattern in Navel Orange

The spatiotemporal expression of *CsKCS6* in Newhall navel orange was determined via qPCR. The results showed that *CsKCS6* Significantly high expression in the stigmas, followed by the petals and pistils. But substantially lower expression in tissues such as flavedo, albedo, flesh, leaf, receptacle, and ovary (**Figure 3A**). The expression level of *CsKCS6* in the flavedo and flesh of Newhall navel orange increased with fruit development. However, no significant changes were observed in the albedo of Newhall navel orange during fruit development (**Figures 3B–D**).

In this study, the expression patterns of *CsKCS6* gene in leaves of 'Newhall' navel orange under abiotic stress were investigated by qPCR. After 4°C treatment, the expression level of *CsKCS6* declined significantly at 1 h (about threefold lower than 0 h), remained this level from 1 to 12 h, and then decreased again at 24 h (**Figure 4A**). Under the 250 mM NaCl stress, the expression level of *CsKCS6* decreased significantly at 6 h, increased at 3 h, declined again at 6 h, increased to the maximum value (about 1.5-fold higher than 0 h) at 12 h, and then decreased significantly at 24 h (**Figure 4B**). After simulated drought treatment with 20% PEG6000, the *CsKCS6* transcript decreased significantly at 1 h,

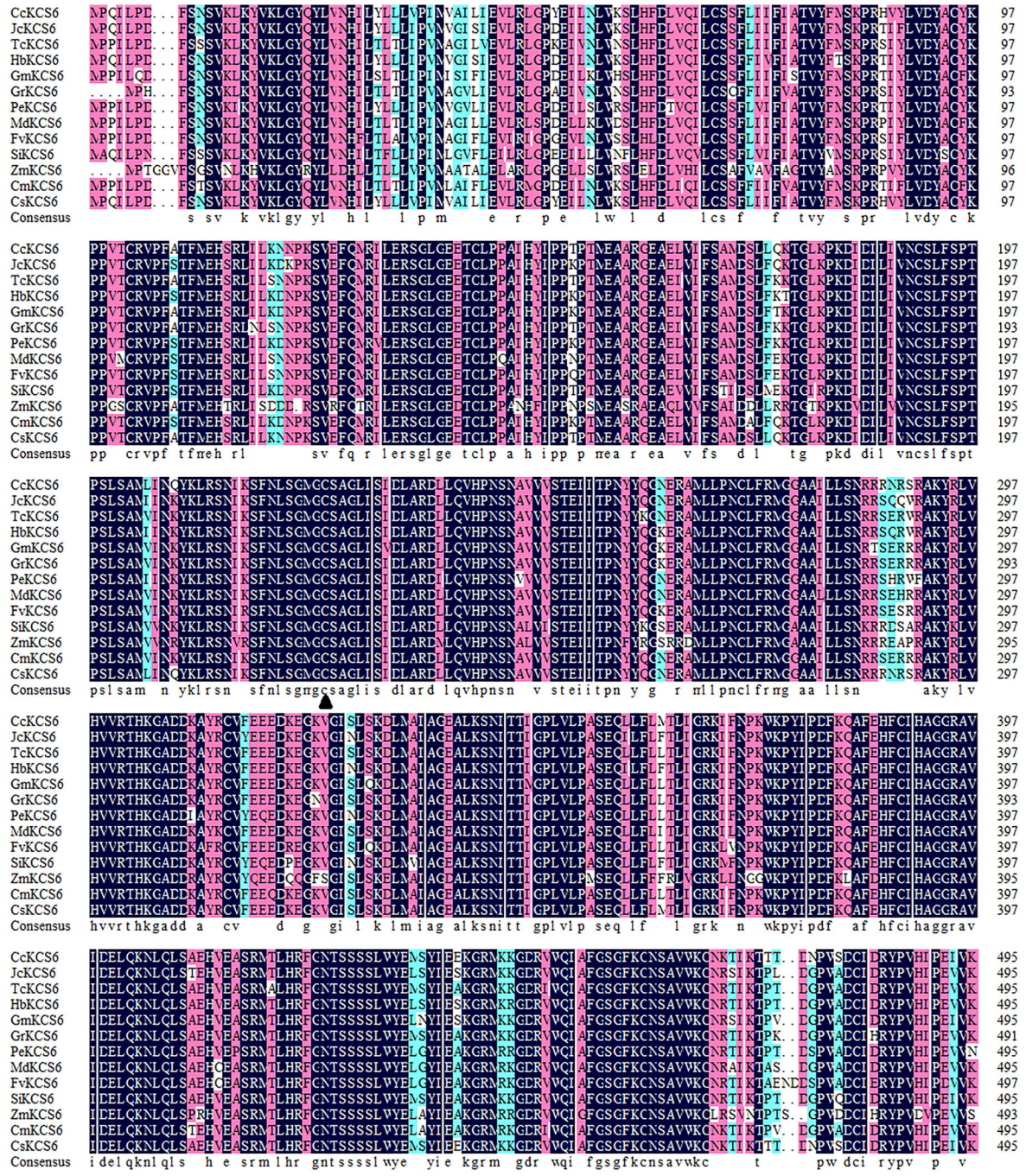

FIGURE 1 | Multiple amino acid sequence alignment of CsKCs6 with its homologous proteins from different plant species, including *Citrus clementina* CcKCS6 (XP_006437664.1), *Jatropha curcas* JcKCS6 (XP_012082087.1), *Theobroma cacao* TcKCS6 (XP_007044356.2), *Hevea brasiliensis* HbKCS6 (XP_021637941.1), *Glycine max* GmKCS6 (XP_003555901.1), *Gossypium raimondii* GrKCS6 (XP_012467884.1), *Populus euphratica* PeKCS6 (XP_011007926.1), *Malus domestica* MdKCS6 (XP_008339680.2), *Fragaria vesca* subsp. *Vesca* FvKCS6 (XP_004299082.1), *Sesamum indicum* SiKCS6 (XP_011099559.1), *Zea mays* ZmKCS6 (NP_001310469.1), *Cucumis melo* CmKCS6 (XP_008446598.1), *Arabidopsis thaliana* AtKCS6 (AAM65060.1), *Ginkgo biloba* GbKCS6 (AAY52458.1), and *Citrus sinensis* CsKCS6. The Cys amino acid (c) site is marked with solid triangle (▲).

increased to the maximum value (about twofold higher than 0 h) at 3 h and then decreased gradually from 3 to 24 h (**Figure 4C**). After 100 μM ABA treatment, the expression level of *CsKCS6* decreased significantly at 1 h, peaked at 3 h (about 2.8-fold higher than 0 h), decreased again from 3 to 9 h. Surprisingly, the *CsKCS6* expression increased again to a high level (about 1.5-fold higher than 0 h) at 12 h after ABA treatment, but finally declined at 24 h (**Figure 4D**).

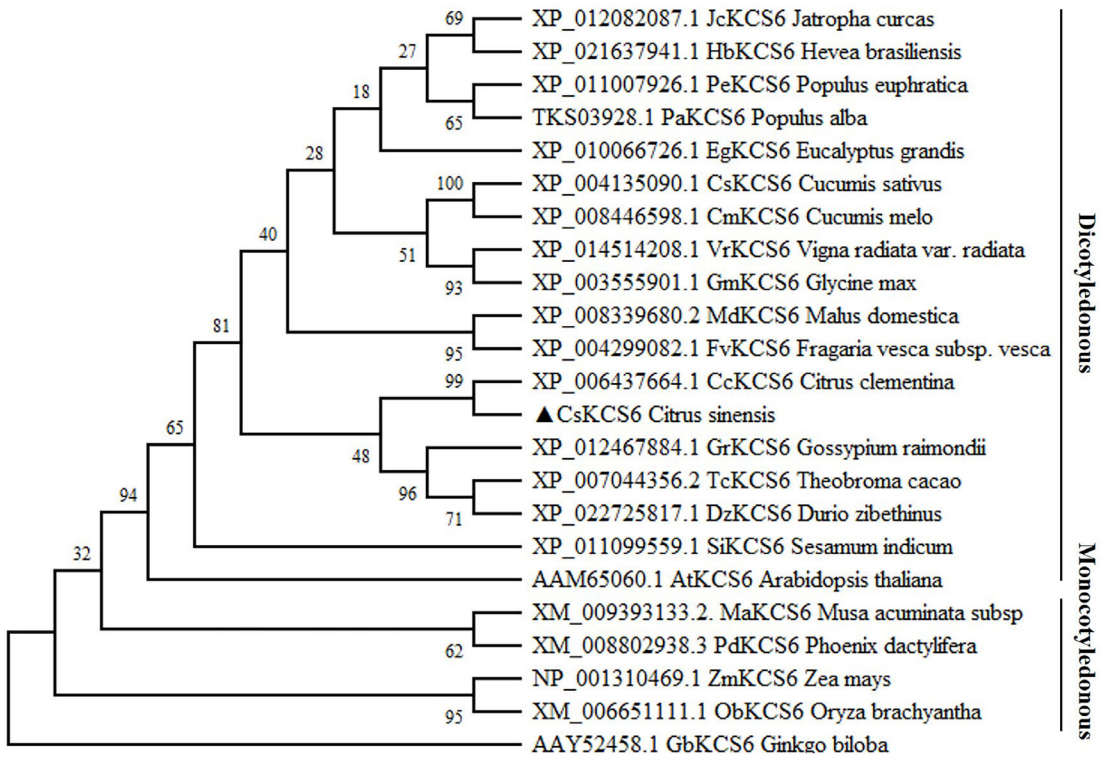

FIGURE 2 | Phylogenetic tree of the homologs of CsKCS6 and other KCS proteins. The solid lines represent monocotyledonous and dicotyledonous plants.

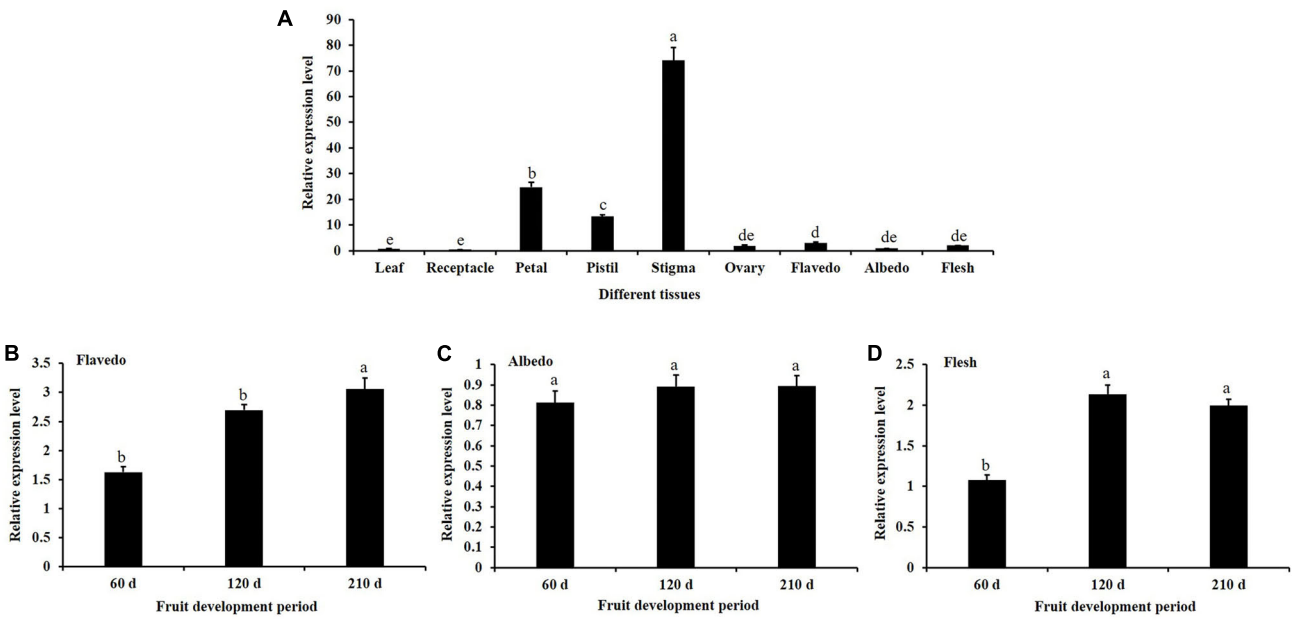

FIGURE 3 | Expression analysis of *CsKCS6* in Newhall navel orange. **(A)** Spatial-specific expression of *CsKCS6* in different organs. **(B–D)** Expression pattern of *CsKCS6* in flavedo, albedo and flesh tissues during the fruit development period. The y-axis shows the relative gene expression levels, as calculated by the $2^{-\Delta\Delta CT}$ method, in which *CsACTIN* served as the endogenous reference. Data are shown as the means ± SE calculated from three biological replicates. Different small letters represent significant differences at $P < 0.05$ according to Duncan's multiple range tests.

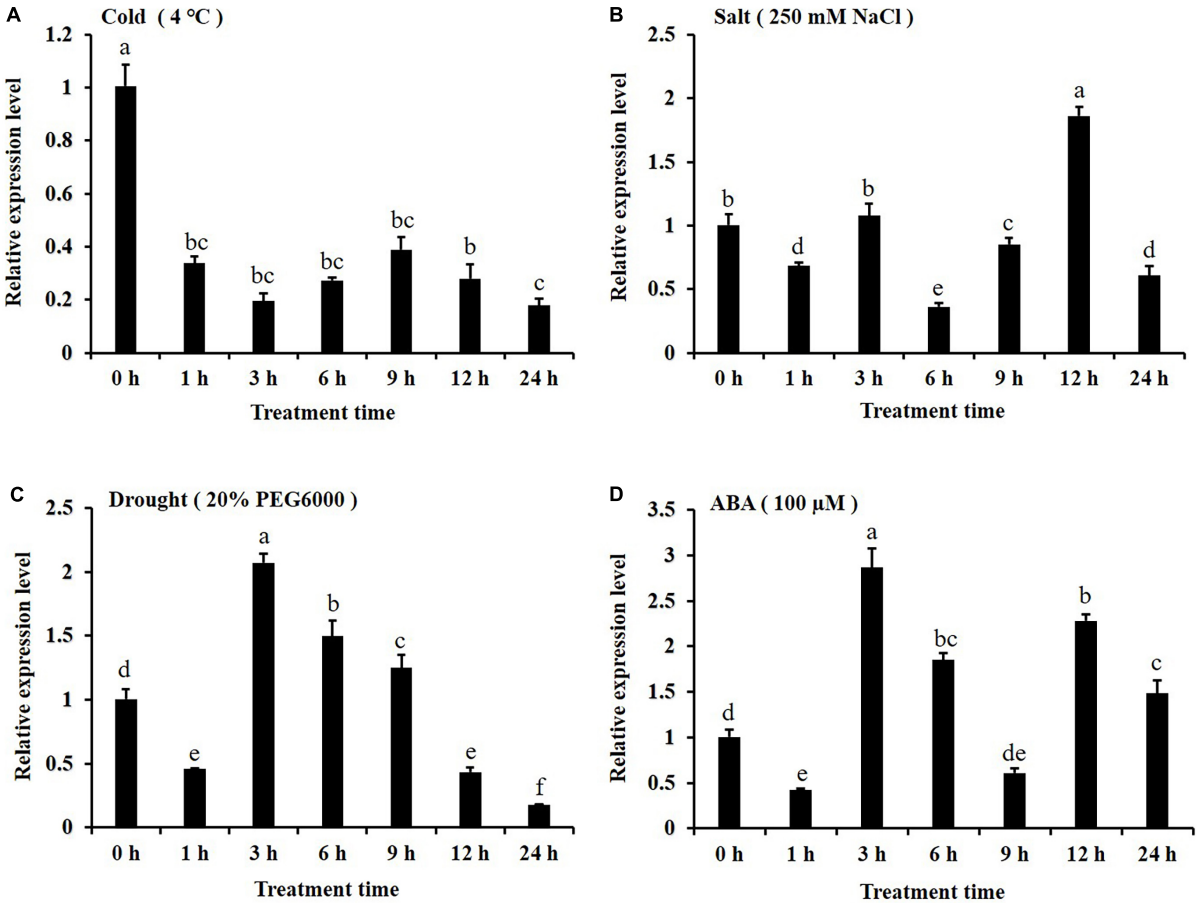

FIGURE 4 | Expression of *CsKCS6* in the leaves of Newhall navel orange plants under abiotic stress according to qRT-PCR **(A–D)** after cold (4°C), salt, drought and ABA treatments. The y-axis shows the relative gene expression levels, as calculated by the $2^{-\Delta\Delta CT}$ method, in which *CsACTIN* served as the endogenous reference. Data are shown as the means ± SE calculated from three biological replicates. Different small letters represent significant differences at $P < 0.05$ according to Duncan's multiple range tests.

Phenotypic Analysis of Transgenic *Arabidopsis* Overexpressing *CsKCS6*

To investigate the function of *CsKCS6* in plants, we introduced a 35S:*CsKCS6*-pCAMBIA1301 vector into *Agrobacterium tumefaciens* strain LBA4404, which were then transformed into *Arabidopsis* plants. The T_0 generation seeds were screened on MS medium containing 10 mg/L hygromycin to obtain nine resistant seedlings. PCR detection was performed using specific primers of *CsKCS6* and *Hyg* (**Supplementary Table S1-P4, P7**) after transplanting, and five positive plants were identified (**Supplementary Figure S1**). The cDNA was derived from the leaves of T_2 generation *Arabidopsis* plants. Semi-quantitative PCR detection showed that *CsKCS6* was strongly expressed in the leaves of five transgenic lines, while *CsKCS6* was not detected in WT. Therefore, OE-CsKCS6-1 and OE-CsKCS6-2 were used for further research (**Figure 5A**).

Observing the performance of transgenic Arabidopsis seedlings and wild-type seedlings of the same age, it is found that the trichome density on the surface of the leaves and stems of the transgenic plants is higher than that of the wild-type plants, and the transgenic leaves and stems of the plants are rougher than the wild-type plants (**Figures 5B,C,E,F**). Subsequently, we obtained photos of transgenic and wild-type *Arabidopsis thaliana* through stereomicroscopes, and then statistical analysis based on the pictures showed that the number of trichomes per square millimeter on the transgenic *Arabidopsis* leaves was more than twofold that of the WT, forming a very significant difference (**Figure 5D**). The number of trichomes on the stems of transgenic *Arabidopsis* was also significantly higher than that of the WT, with a difference of about threefold (**Figure 5G**).

Cuticular Wax Morphology and Composition of Wax Present on Leaves of the WT and Transgenic *Arabidopsis* Plants

Scanning electron microscopy was used to observe the morphology of the cuticular wax present on the leaf surfaces of the WT and transgenic *Arabidopsis*. The results showed that the trichomes on the leaf surfaces of the transgenic lines

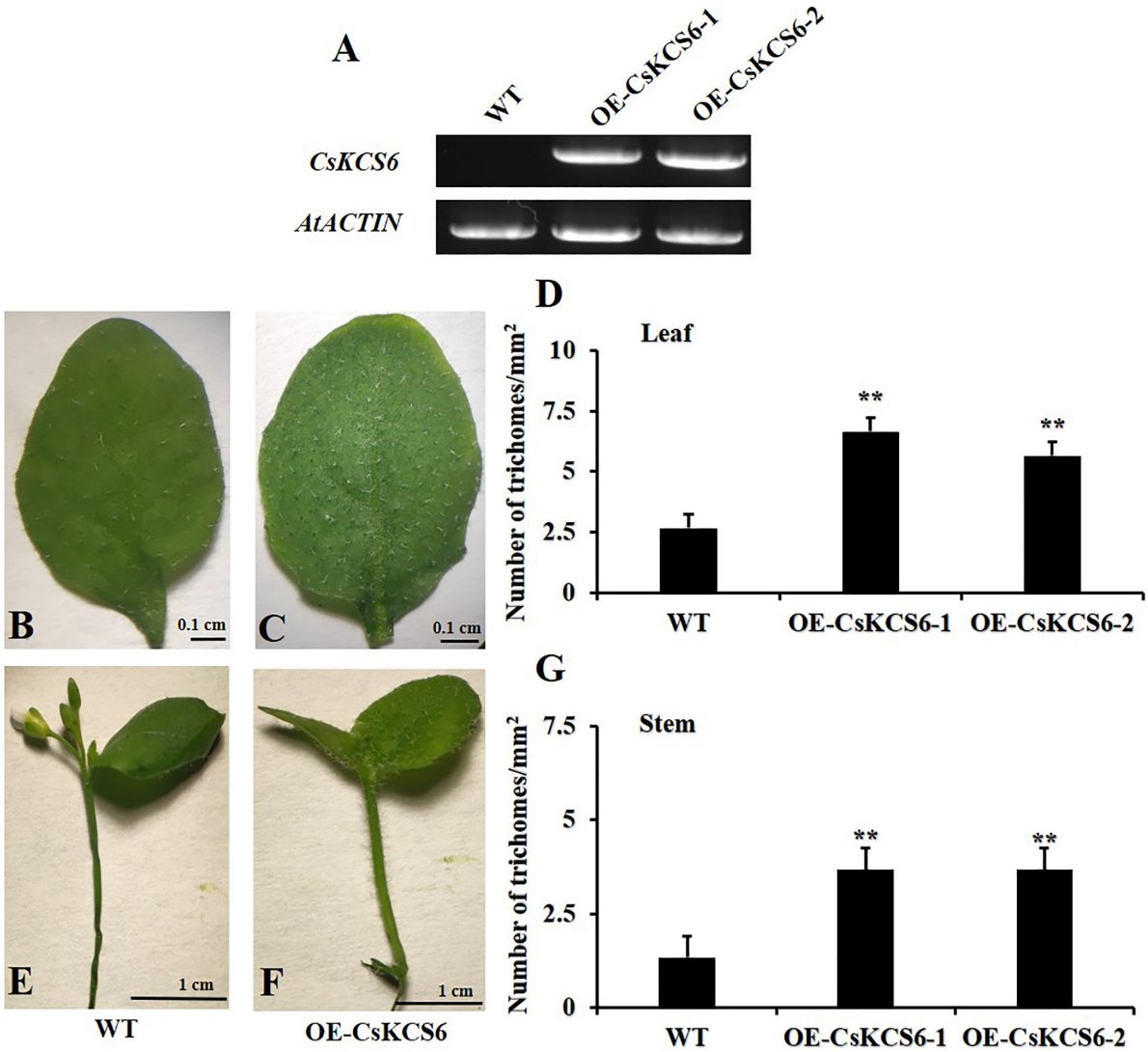

FIGURE 5 | Phenotypes of the WT and two transgenic *Arabidopsis* lines (OE-KCS6-1, OE-KCS6-2). **(A)** Expression of *CsKCS6* in different leaves of the WT and transgenic *Arabidopsis* lines. *AtACTIN* was used as a reference gene. **(B)** Leaves of the WT and **(C)** transgenic lines of 6-week-old. **(D)** The trichome densities in leaves of two *Arabidopsis* genotypes show in **(B,C)**. **(E)** Stems of the WT and **(F)** transgenic lines. **(G)** The trichome densities in stems of two *Arabidopsis* genotypes show in **(E,F)**. The data are shown as the means ± SE of three biological replicates. The asterisks indicate that the values of the transgenic *Arabidopsis* line are significantly different from the values of the WT (*$P < 0.05$; **$P < 0.01$).

were more abundant than those of the WT (**Figures 6A,B**), this phenotypic difference is consistent with the statistics of trichomes in **Figure 5D**. However, no significant difference was detected in the morphology of the cuticular wax between the adaxial and abaxial sides of the leaves of the WT and transgenic *Arabidopsis* plants (**Figures 6C–F**).

GC–MS analysis revealed that the total wax content of the two transgenic lines was similar to that of the WT (**Figure 7A**). The amount of fatty acids in the transgenic lines was about twofold higher than that in the WT plants. However, the contents of primary alcohols and sterols in the transgenic strain lines were reduced about 2- and 1.5-fold respectively in compare with the WT. There was no significant difference in the contents of alkanes and secondary alcohols (**Figure 7B**). Meanwhile, the two transgenic lines had much greater amounts (increased by about 40%) of fatty acids with even chain length $\geq C_{24}$ compared to the WT plants. But the amounts of C_{32} and C_{34} primary alcohol reduced by 35% in the transgenic lines (**Figure 7C**).

Morphology and Composition of Cuticular Wax on the Stems of WT and Transgenic *Arabidopsis* Plants

Scanning electron microscopy was used to observe the morphology of the cuticular wax on the surface of the stems of WT and transgenic *Arabidopsis* plants. The results showed

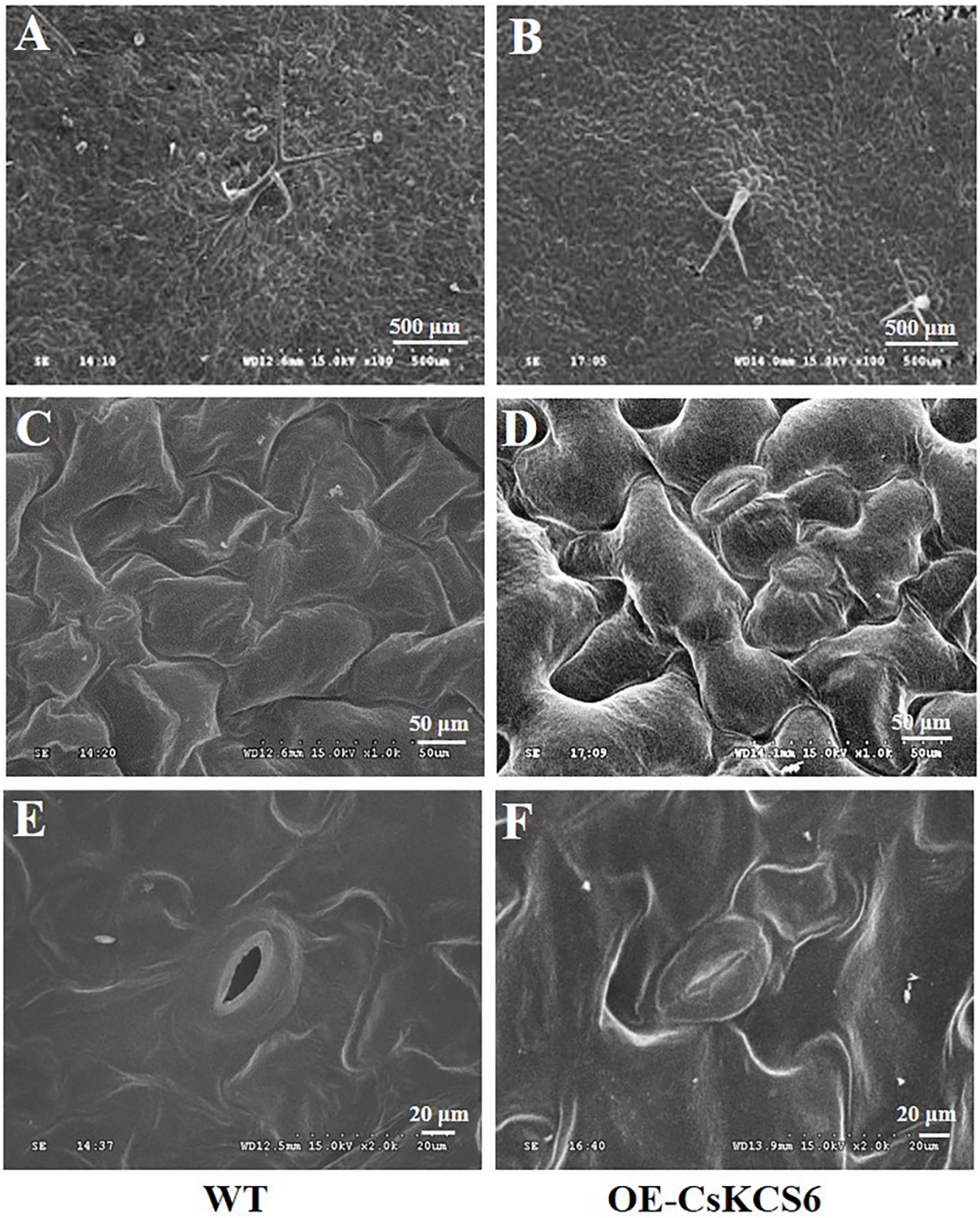

FIGURE 6 | Morphology of the wax of the leaf surfaces of WT and transgenic plants. **(A)** Wax on the trichomes of WT and **(B)** transgenic plants (100×, Bar = 500 μm). **(C)** Wax on the adaxial side of the leaves of the WT and **(D)** transgenic plants (1000×, Bar = 50 μm). **(E)** Wax on the abaxial side of the leaves of WT and **(F)** transgenic plants (2000×, Bar = 20 μm).

that obviously more trichomes were present on the surfaces of the stems of the transgenic *Arabidopsis* plants than on those of the WT plants (**Figures 8A,B**), this phenotypic difference is consistent with the statistics of trichomes in **Figure 5G**. There were many granular wax crystals deposited on the surface of the stems of both genotypes (**Figures 8C,D**). In addition, many shallow ridges were detected on the stem surfaces of the transgenic *Arabidopsis* plants, which were not observed on the leaf surfaces of the WT plants.

GC–MS analysis revealed that the total wax content on the stem surfaces of the two transgenic lines was similar to that of the WT (**Figure 9A**). The total amount of fatty acids was increased by more than twofold compared with the WT plants. The alkanes amount in the transgenic lines increased by only about 18%

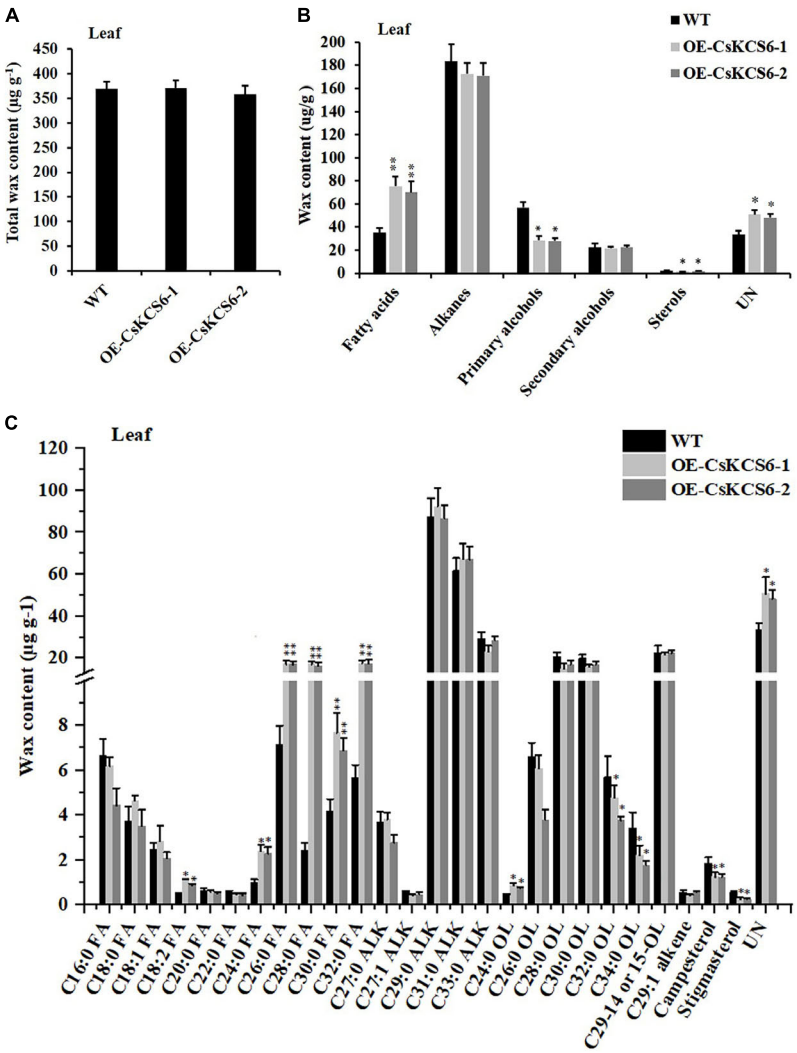

FIGURE 7 | Cuticular wax content and composition of leaves of WT and transgenic *Arabidopsis* plants. **(A)** Total wax content, **(B)** wax composition, and **(C)** identified waxes in the leaves of the WT and two transgenic plants. FA, fatty acids; ALK, alkanes; OL, alcohols; UN, unknown component. The values are means ± SE of three biological replicates, and the asterisks indicate significant differences between WT plants and transgenic lines (*$P < 0.05$; **$P < 0.01$).

in comparison to the WT plants. In contrast, the amounts of primary alcohols, aldehydes, and ketones decreased significantly in the transgenic lines. The most drastic decline was observed in aldehydes, which reduced by more than 30% in the transgenic lines (**Figure 9B**). Notably, the increase in fatty acids content was mainly observed in even chain length chains of C_{16} and C_{26-30}. And the decrease of aldehydes was mainly attribute to the reduction of C_{26}, C_{28}, and C_{30} aldehyde (**Figure 9C**).

Analysis of Cuticular Permeability of the Leaves

To explore whether the epidermal permeability was altered in *CsKCS6* transgenic lines, the epidermis of leaves collected from the CsKCS6 transgenic lines and WT was stained with TB, and the chlorophyll leaching contents was measured under alcohol treatment. The results showed that both sides of the leaves of the WT were stained much deeply than were the transgenic lines (**Figure 10A**). Furthermore, the chlorophyll leaching contents of the WT and transgenic lines continuously increased after the alcohol treatment; however, the chlorophyll leaching contents of the transgenic lines was lower than that of the WT at all the time points of the alcohol treatment, and the difference was significant after 60 min, and the chlorophyll leaching content extracted was only about half of that of the WT at 180 min (**Figure 10B**).

Ectopic Expression of *CsKCS6* in *Arabidopsis* Enhanced Drought Tolerance

To study whether *CsKCS6* is involved in the response to osmotic stress, the plant phenotype, survival, water loss rate and ion leakage of the WT and two transgenic lines were analyzed. After drought treatment for 10 days and rewatering

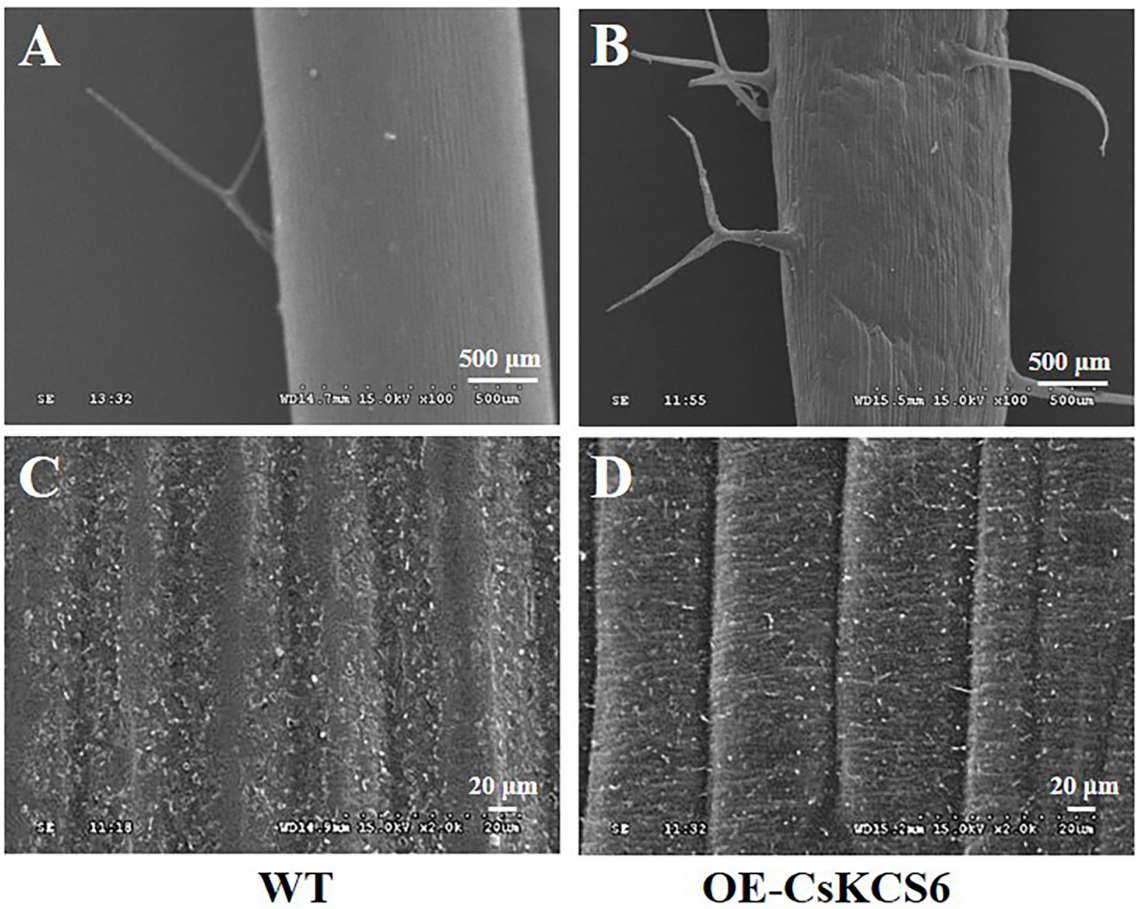

FIGURE 8 | Morphology of the cuticular wax on the stem surfaces of WT and transgenic *Arabidopsis*. **(A)** Trichomes of WT stems and **(B)** trichomes of transgenic *Arabidopsis* stems (100×, Bar = 500 μm). **(C)** Wax on the surfaces of the stems of WT and **(D)** transgenic *Arabidopsis* stems (2000×, Bar = 20 μm).

for 3 days, the leaf wilting of the WT plants was more severe than that of the two transgenic lines (**Figures 11A,B**). Moreover, the survival percentages of OE-KCS6-1 and OE-KCS6-2 were 21.66 and 23.33%, respectively, which were significantly higher than the survival rate of the WT plants (6.66%) after drought treatment (**Figure 11C**).

In addition, the transpiration rates of the leaves of the transgenic *Arabidopsis* plants were significantly lower than those of WT plants from 80 to 150 min after dehydration (**Figure 11D**). Compared with that of the WT plants, the ion leakage in the leaves of the transgenic *Arabidopsis* plants was also obviously reduced after the dehydration treatment. These results indicate that ectopic expression of *CsKCS6* can reduce the cell membrane permeability of *Arabidopsis* leaves (**Figure 11E**). Taken together, these results suggest that ectopic expression of *CsKCS6* can improve the drought tolerance of transgenic *Arabidopsis*.

Ectopic Expression of CsKCS6 in *Arabidopsis* Enhanced Salt Tolerance

To analyze the role of *CsKCS6* in the plant response to salt stress, we investigated the effects of salt stress on the seed germination and root length of the WT and two transgenic lines. The seed germination rate of the two transgenic *Arabidopsis* lines was significantly lower than that of the WT within the first 5 days of 100 mM NaCl treatment. Interestingly, the germination rate of the two transgenic lines was similar to that of the WT plants after 8 days of 100 mM NaCl treatment (**Figures 12A,B**).

Statistical analysis showed that there was no significant difference in root length between the 2-week-old transgenic and wild-type Arabidopsis, and both could reach about 2.4 cm. However, after 100 and 200 mM NaCl treatment, the root length of the transgenic lines was about 2.2 and 1.8 cm respectively, which was significantly higher than that of the WT plants (about 1.7 and1.4 cm) (**Figures 12C,D**).

In addition, we compared the phenotypic differences between the WT and two transgenic lines after salt stress treatment, and more severe damage was observed in the WT plants than in the two transgenic lines after the 100 and 200 mM NaCl treatments (**Figures 12E,F**). Furthermore, after 100 mM NaCl treatment, the survival rate of wild-type Arabidopsis is only 60%, while the survival rate of transgenic lines reaches about 80%. When the concentration of NaCl treatment reaches 200 mM, the survival rate of the transgenic lines

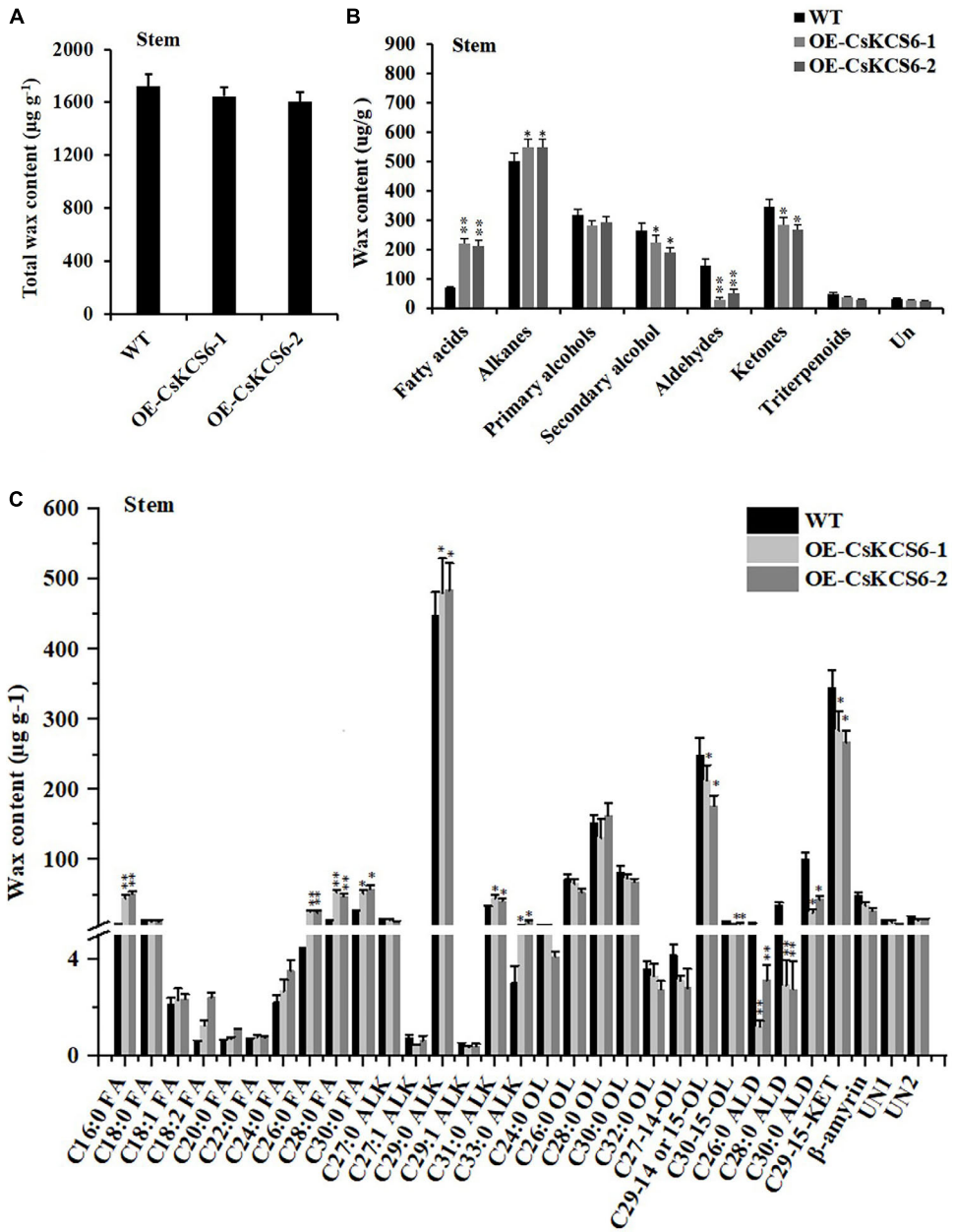

FIGURE 9 | Content and composition of the cuticular wax of the stems of WT and transgenic *Arabidopsis* plants. **(A)** Wax content, **(B)** wax composition, and **(C)** identified waxes in the stems of the WT and two transgenic plants. FA, fatty acids; ALK, alkanes; OL, alcohols; ALD, aldehydes; KET, ketones; UN, unknown component. The values are the means ± SE of three biological replicates, and the asterisks indicate significant differences between the WT and transgenic lines (*$P < 0.05$; **$P < 0.05$).

(40%) was about twofold higher than that of the WT (20%) (**Figure 12G**).

DISCUSSION

Very-long-chain fatty acids are biosynthesized from the extension of C_{16} or C_{18} fatty acids, and the extension is catalyzed by the multienzyme complex FAE; thus, FAE components are direct precursors of cuticular wax biosynthesis. The first step of VLCFA biosynthesis is to produce β-ketoacyl-CoA, which is catalyzed by KCS (Kunst and Samuels, 2003; Yeats and Rose, 2013).

Members of the KCS family are often described as 3-ketoacyl-CoA synthases, type III polyketide synthases and FAEs, while the characteristic regions of the KCS6 protein usually contain active site residues and motifs involved in substrate binding (Funa et al., 2002). In this study, multiple sequence alignment revealed that

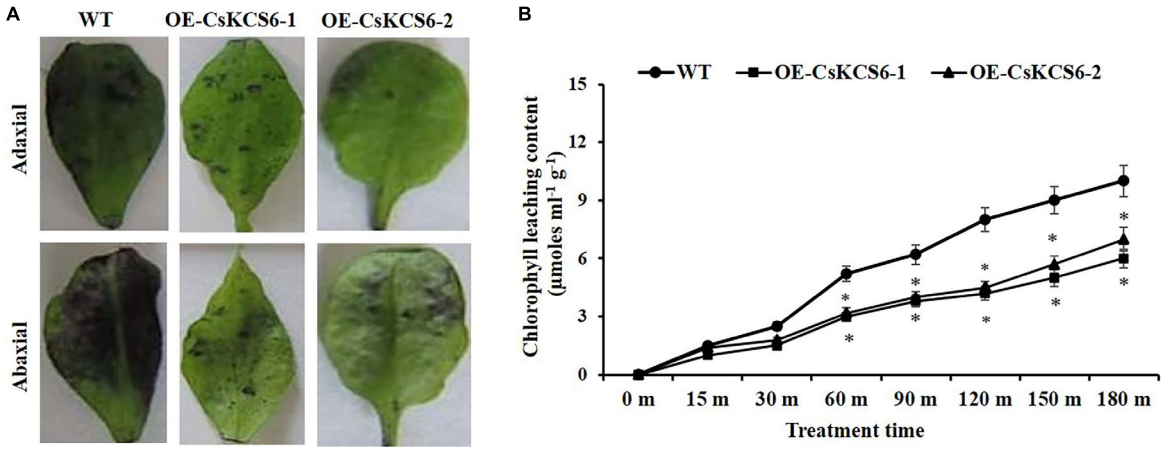

FIGURE 10 | Alterations in cuticle permeability of *CsKCS6* transgenic *Arabidopsis*. **(A)** TB staining, **(B)** chlorophyll leaching content of the WT and transgenic *Arabidopsis* plants after alcohol treatment.

the amino acid sequence of CsKCS6 contained two conserved domains, FAE1-CUT1-RppA and ACP_syn_III_C, which belong to the thiolase-like superfamily. The Cys residue at amino acid position of 225 is the catalytic active site of the condensing enzyme and is highly conserved among different plant species (**Figure 1**). These conserved sites are also present in KCS family proteins from other plant species. In addition, phylogenetic analysis revealed that CsKCS6 clustered with other KCS6 proteins from dicotyledonous plant species, especially CcKCS6, which comes from *Citrus clementine* and is the closest homolog of CsKCS6 (**Figure 2**). The structural features and phylogenetic results of this protein suggested that CsKCS6 belongs to the KCS gene family and might be involved in regulating the synthesis of VLCFAs in citrus.

The expression patterns of KCS family genes have been reported in many studies. For example, tissue-specific expression analysis of 21 KCS family genes in *Arabidopsis* showed that *AtKCS21*, *AtKCS7* and *AtKCS15* were underexpressed in *Arabidopsis* tissues; that *AtKCS18/AtFAE1* and *AtKCS19* were preferentially expressed in the seeds; that *AtKCS10/AtFDH*, *AtKCS4*, *AtKCS9*, *AtKCS11*, *AtKCS20*, *AtKCS2/AtDAISY,* and *AtKCS1* are widely expressed in various tissues of *Arabidopsis*; and that these proteins may be involved in VLCFA synthesis required for growth and development (Suh et al., 2005). However, *AtKCS17* is expressed only in the flowers and siliques (Joubès et al., 2008). It has been reported that *AtKCS6* is highly expressed in the flowers and siliques but not in the roots (Costaglioli et al., 2005; Suh et al., 2005). In agreement with the information in these reports, *CsKCS6* is highly expressed in the flowers of navel orange, especially in the stigmas (**Figure 3**). In our previous study, we reported that the amounts of VLCFAs continuously increased in the epicuticular wax of Newhall navel orange during fruit development. Accordingly, the expression of *CsKCS6* in the flavedo and albedo of Newhall navel orange also increased during fruit development (**Figure 3**). Thus, *CsKCS6* might be involved in the biosynthesis of VLCFAs for the cuticular wax of navel orange (Liu et al., 2015).

Cuticular wax synthesis in plants is induced by various environmental factors, such as light, water deficit and low temperature (Shepherd and Wynne Griffiths, 2006). The expression of many cuticular wax genes, including KCS family genes, also shifted under abiotic stress. For example, the expression levels of *Arabidopsis AtKCS1* and *AtKCS3* were downregulated under darkness and low temperature, and the expression of *AtKCS10* decreased under various kinds of osmotic stress (Joubès et al., 2008). In the present study, the expression level of *CsKCS6* significantly declined under low temperature stress and obviously increased at several time points after high salt, drought and ABA treatment (**Figure 4**). This result was in agreement with the report of Joubès et al. (2008), which indicated that the expression level of Arabidopsis *AtKCS6* was decreased under low temperature stress but increased after high salt and drought treatment. Similar result also reported by Hooker et al. (2002), which suggested that osmotic stress and ABA enhance the transcription of *AtKCS6/AtCER6* (Hooker et al., 2002). Interestingly, the expression levels of *CsKCS6* were fluctuated after high salt, drought and ABA treatments (**Figure 4**). As reviewed by Grundy et al. (2015), the circadian clock controls expression of a large number of genes that are responsive to abiotic stress. Thus, many abiotic stress-responsive genes were found to be expressed rhythmically under diurnal light–dark or temperature cycles. Furthermore, rhythmic expression of abiotic stress-responsive genes under constant conditions was also reported for many plant species, such as Arabidopsis, soybean and barley (Covington et al., 2008; Habte et al., 2014; Marcolino-Gomes et al., 2014). It has been proved that dark can suppress the expression of Arabidopsis *AtKCS6* (Hooker et al., 2002; Joubès et al., 2008). Thus, the *CsKCS6* transcript was probably under the control of circadian clock, leading to the fluctuated changes in *CsKCS6* expression after high salt, drought and ABA treatments.

To further study whether *CsKCS6* participates in the biosynthesis of VLCFAs for cuticular wax and regulates the osmotic stress tolerance of navel orange, transgenic *Arabidopsis* lines ectopic expression *CsKCS6* were generated in this study.

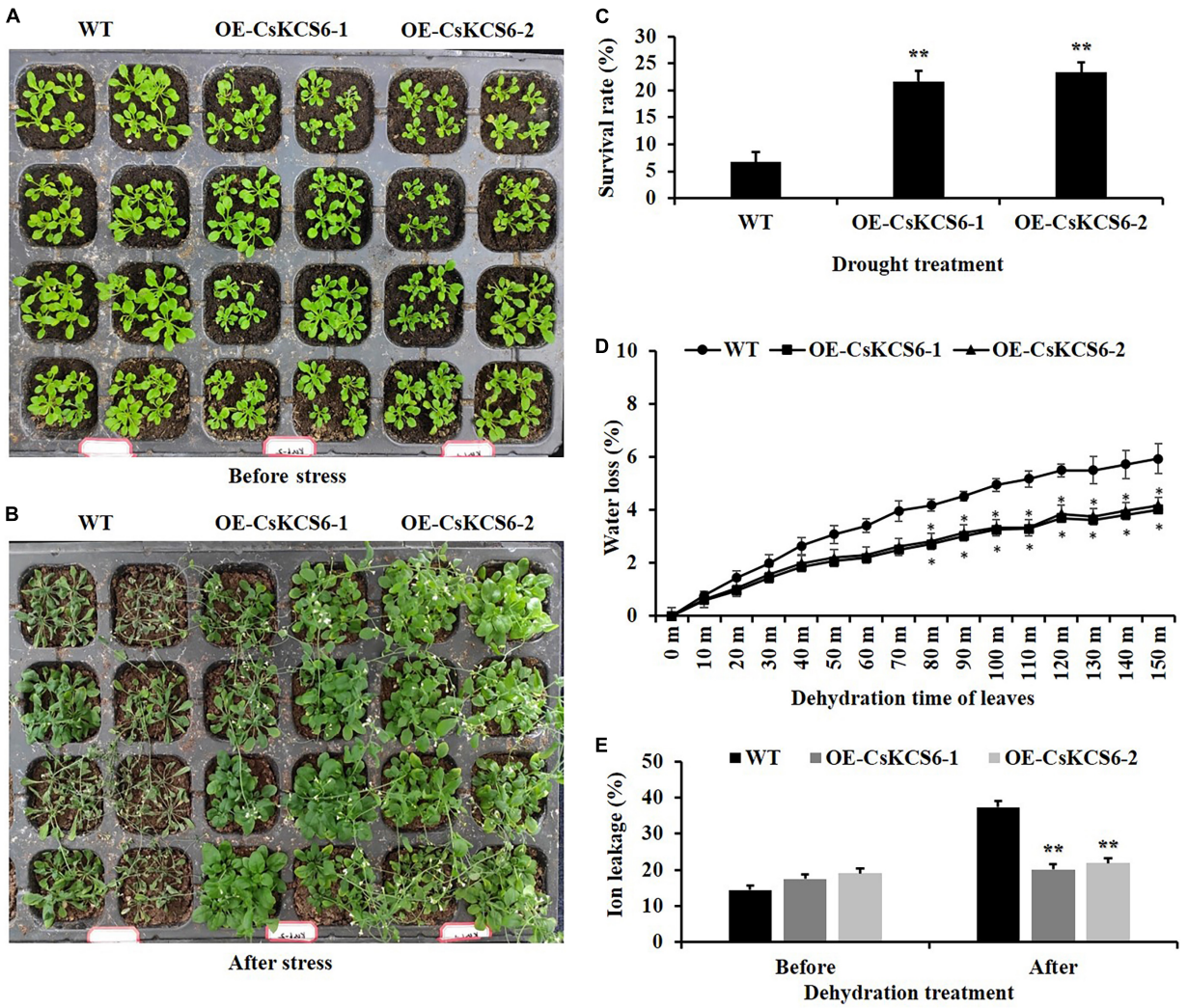

FIGURE 11 | Phenotypes and physiological traits of WT and transgenic *Arabidopsis* lines after drought treatments. **(A,B)** Phenotypes of two genotypes after drought treatment, as well as their **(C)** survival rate, **(D)** water loss rate, and **(E)** ion leakage. Leaves of 6-week-old WT and transgenic plants were collected for measuring the physiological traits. The data are shown as the means ± SE of three biological replicates. The asterisks indicate that the values of the transgenic *Arabidopsis* line are significantly different from the values of the WT (*$P < 0.05$; **$P < 0.01$).

Phenotypic observations and SEM analysis revealed that the density of trichomes on the leaves and stems of transgenic *Arabidopsis* was significantly higher than that of the WT plants (**Figures 5**, **6**, **8**), suggesting *CsKCS6* might be involved in the development of trichomes. To our surprise, although AtKCS16 is proved to catalyze the elongation of C_{34} to C_{38} acyl-CoAs in Arabidopsis leaf trichomes (Hegebarth et al., 2017), none of the *KCS6* homologous genes and other KCS family genes were reported to be related to trichome formation (Fiebig et al., 2000; Hooker et al., 2002; Serra et al., 2009; Weidenbach et al., 2015). The divergence between our result and previous reports is probably attributed to the gene function difference among plant species. Trichomes play an important role in plant resistance to biotic and abiotic stresses (Choi, 2010; Kim et al., 2012). Thus, the increase in trichome numbers in the transgenic *Arabidopsis* plants might enhance their tolerance to abiotic stresses.

Arabidopsis AtCER6 is also named *AtCUT1* and *AtKCS6* (Fiebig et al., 2000). In *cer6* mutants of *Arabidopsis*, wax crystals are nearly undetectable in the stems and siliques due to the loss of *AtCER6* function (Millar et al., 1999; Fiebig et al., 2000). Moreover, overexpression of *AtCER6*/*AtKCS6* in *Arabidopsis* leads to waxless phenotype in stems of transgenic lines (Millar et al., 1999). Surprisingly, in the present study, no significant differences in the structure or total amount of wax were observed on the surfaces of the leaves and stems between the WT and transgenic *Arabidopsis* plants. Similar to our result, although high levels of *AtCER6*/*AtKCS6* expression were observed in the hemizygous 35S-*AtCER6*/*AtKCS6* plants, they did not exhibit higher wax amounts than those in WT plants (Millar et al., 1999). The total amount of cuticular wax in tuber periderms of *StKCS6*-silenced lines was also not significantly different from the wild-type potato (Serra et al., 2009). KCSs catalyze

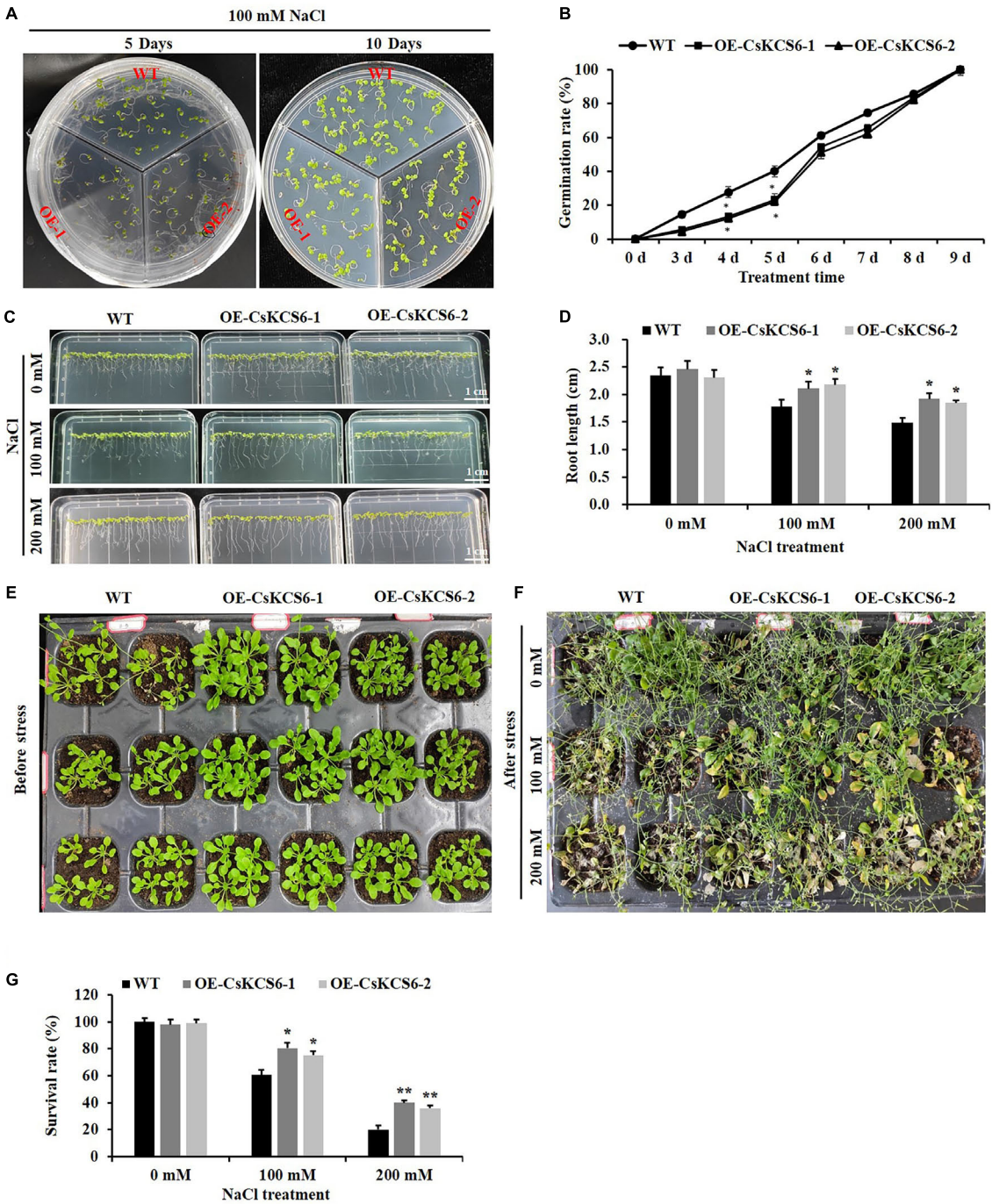

FIGURE 12 | Phenotypes and physiological traits of the WT and transgenic *Arabidopsis* lines after salt treatment. **(A)** Seed germination. T_2 and WT seeds were sown on MS media, with 30 seeds sown per line. **(B)** Germination rates calculated from **(A)**, **(C)** root growth under salt stress treatment. **(D)** Root length (root length ≥ 5 mm) calculated from **(C)**, **(E,F)** phenotypes of two genotype lines after salt treatment. **(G)** Survival. The data are shown as the mean ± SE of three biological replicates. The asterisks indicate significant differences between transgenic *Arabidopsis* lines and WT (*$P < 0.05$; **$P < 0.01$).

the rate-limiting step in VLCFA elongation and have substrate specificity (Joubès et al., 2008). Arabidopsis *AtKCS6* catalyzes the elongation of C_{24} and C_{26} VLCFAs (Jenks et al., 1994; Millar et al., 1999). Tomato *LeCER6* and Potato *StKCS6* are both involved in the biosynthesis of VLCFAs beyond C_{28} (Leide et al., 2007; Serra et al., 2009). Cotton *GhCER6* is responsible for the formation of C_{26} VLCFA (Qin et al., 2007). In agree with these reports, the amounts of VLCFAs with an even-numbered carbon chain length greater than that of C_{24} in the leaves and greater than that of C_{26} in the stems of the

two transgenic lines were significantly higher than those in the WT plants, suggesting *CsKCS6* is involved in the biosynthesis of VLCFAs with chain length beyond C_{24}. In addition to the striking differences in the accumulation of VLCFAs, ectopic expression of *CsKCS6* also decreased the amounts of primary and secondary alcohols, aldehydes and ketones, especially primary alcohols with chain length beyond C_{28} in leaves (decreased by 30%) and aldehydes with chain length longer than C_{26} in stems (decreased by 50%) (**Figures 7**, **9**). The significant decreases of primary alcohols and aldehydes in transgenic plants suggested that either some wax biosynthetic genes might be suppressed by ectopic expression of *CsKCS6* or that a large block in VLCFAs entering the wax biosynthetic pathway might be occurred in transgenic plants. The latter hypothesis was supported by Von Wettstein-Knowles (1979), who suggested that VLCFA channeling was probably occurred in plants so that the substrates destined for specific wax components were not freely changed.

The permeability of the cuticle plays an important role in the adaptation of plants to osmotic stress, which affects the water retention capacity of plants and delays the damage of plants from environmental stress (Yeats and Rose, 2013). Recently, several *KCS* family genes from different plant species were reported to play an important role in regulating cuticle permeability and plant tolerance to abiotic stress. For example, overexpression of *AhKCS1* from a drought tolerant groundnut reduced the cuticle permeability and enhanced the drought tolerance in a susceptible genotype by increasing cuticular wax load in leaves (Lokesh et al., 2019). Overexpression of *BnKCS1-1* and *BnKCS1-2* in *Brassica napus* also increased drought tolerance in transgenic plants by promoting cuticular wax production (Wang et al., 2020). As reviewed by Singh et al. (2018), a number of other genes related to wax biosynthesis also have the function to enhance the resistance to abiotic stress by altering wax composition, such as *WIN1/SHN1*, *DWA1*, *MYB96*, *CER1*, *CER3/WAX2*, *FAR* family genes and so on. In agreement with these reports, a significant decrease in leaf chlorophyll permeability, TB staining, water loss rate, ion leakage and an obvious increase in the root length and survival rate were observed in the transgenic plants under drought and high salt stress (**Figures 10–12**), indicating that ectopic expression of *CsKCS6* can reduce the cuticle permeability and enhance plant tolerance to drought and high salt. The mechanism of *KCS6*-like genes to influence cuticle permeability in tomato (Vogg et al., 2004; Leide et al., 2007) and potato (Serra et al., 2009) is well-established. In detail, for the tomato *lecer6* mutant deficiency in *KCS6*, a decline in aliphatic components such as alkanes with chain length beyond C_{30} and an increase in cyclic triterpenoids lead to the increase in cuticle permeability (Vogg et al., 2004; Leide et al., 2007). Serra et al. (2009) reported that both the significant decrease in aliphatic compounds with chain length beyond C_{28} and total wax coverage in tuber periderm of *StKCS6*-silenced potato should be responsible for the increase of cuticle permeability. Since the wax morphology and the total wax load in the transgenic lines were similar to the WT plants, it is reasonable to deduce that the dramatic increase (about twofold) in VLCFAs with chain length beyond C_{24} in leaves of transgenic plants might be the major reason for the decrease in cuticle permeability. This result further supports the suggestion that cuticular wax composition rather than total wax load predominantly affects the cuticle permeability in plants (Leide et al., 2007; Isaacson et al., 2009; Parsons et al., 2012).

CONCLUSION

In summary, in the present study, the KCS family gene *CsKCS6*, which is mainly highly expressed in flowers of Newhall navel orange, was cloned from this species. Drought, salt, and ABA treatment could increase the transcript levels of *CsKCS6* in leaves of Newhall navel orange. Ectopic expression of *CsKCS6* in *Arabidopsis* promoted a significant increase in the total VLCFA content of the leaves and stems but resulted in no significant change in total wax content. Further study revealed that the drought tolerance and salt tolerance of the transgenic *Arabidopsis* lines were significantly enhanced compared with those of the WT plants. Our results indicate that *CsKCS6* can enhance plant tolerance to drought and high salt stress by regulating the biosynthesis of VLCFAs.

DATA AVAILABILITY STATEMENT

The datasets presented in this study can be found in online repositories. The names of the repository/repositories and accession number(s) can be found in the article/ **Supplementary Material**.

AUTHOR CONTRIBUTIONS

QW, WG, and DL originally formulated the idea. LY, WH, and YL developed methodology. WG performed statistical analyses and wrote the manuscript. All authors edited and approved the final manuscript.

FUNDING

This study was supported by the National Natural Science Foundation of China (Grant Nos. 31660563, 31701896, and 31860544) and by the earmarked fund for Jiangxi Agriculture Research System (Grant No. JXARS-07-cultivation post).

SUPPLEMENTARY MATERIAL

The Supplementary Material for this article can be found online at: https://www.frontiersin.org/articles/10.3389/fpls.2020.564656/full#supplementary-material

Supplementary Figure S1 | Identification of positive transgenic plants by PCR. **(A)** The T_1 generation transgenic lines of *Arabidopsis* were detected by specific primers of *CsKCS6* and *Hyg* genes to obtain positive plants. **(B)** Semi-quantitative detection of the expression level of transgenic *Arabidopsis*.

Supplementary Table S1 | Primer sequences used for *CsKCS6* cloning, expression analysis, vector construction, and transgenic confirmation.

REFERENCES

Bernard, A., Domergue, F., Pascal, S., Jetter, R., and Renne, C. (2012). Reconstitution of plant alkane biosynthesis in yeast demonstrates that Arabidopsis *ECERIFERUM1* and *ECERIFERUM3* are core components of a very long-chain alkane synthesis complex. *Plant Cell* 24, 3106–3118. ne biosynthesis by directly doi: 10.1105/tpc.112.099796

Bourdenx, B., Bernard, A., Domergue, F., Pascal, S., Léger, A., Roby, D., et al. (2011). Overexpression of *Arabidopsis ECERIFERUM1* promotes wax very-long-chain alkane biosynthesis and influences plant response to biotic and abiotic stresses. *Plant Physiol.*156, 29–45.

Chen, W. W., Yu, X. H., Zhang, K. S., Shi, J. X., Sheron, D. O., Zhang, D. B., et al. (2011). *Male sterile2* encodes a plastid-localized fatty acyl carrier protein reductase required for pollen exine development in arabidopsis. *Plant Physiol.* 157, 842–853. doi: 10.1104/pp.111.181693

Choi, Y. E. (2010). Expression profiling of tobacco leaf trichomes identifies genes for biotic and abiotic stresses. *Plant Cell Physiol.* 51, 1627–1637. doi: 10.1093/pcp/pcq118

Costaglioli, P., Joubès, J., Garcia, C., Stef, M., and Arveiler, B. (2005). Profiling candidate genes involved in wax biosynthesis in *Arabidopsis thaliana* by microarray analysis. *Biochim. Biophys. Acta*1734, 247–258. doi: 10.1016/j.bbalip.2005.04.002

Covington, M. F., Maloof, J. N., Straume, M., Kay, S. A., and Harmer, S. L. (2008). Global transcriptome analysis reveals circadian regulation of key pathways in plant growth and development. *Genome Biol.* 9:R130. doi: 10.1186/gb-2008-9-8-r130

Dai, W. S., Wang, M., Gong, X., and Liu, J. H. (2018). The transcription factor fcwrky40 of fortunella crassifolia functions positively in salt tolerance through modulation of ion homeostasis and proline biosynthesis by directly regulating sos2 and p5cs1 homologs. *New Phytol.* 219, 972–989. doi: 10.1111/nph.15240

Fiebig, A., Mayfield, J. A., Miley, N. L., Chau, S., Fischer, R. L., and Preuss, D. (2000). Alterations in *CER6*, a gene identical to *CUT1*, differentially affect long-chain lipid content on the surface of pollen and stems. *Plant Cell* 12, 2001–2008. doi: 10.1105/tpc.12.10.2001

Funa, N., Ohnishi, Y., Ebizuka, Y., and Horinouchi, S. (2002). Alteration of reaction and substrate specificity of a bacterial type III polyketide synthase by site-directed mutagenesis. *Biochem. J.* 367, 781–789. doi: 10.1042/BJ20020953

Grundy, J., Stoker, C., and Carré, I. A. (2015). Circadian regulation of abiotic stress tolerance in plants. *Front. Plant Sci.* 6:48. doi: 10.3389/fpls.2015.00648

Guo, H. S., Zhang, Y. M., Sun, X. Q., Li, M. M., and Xue, J. Y. (2015). Evolution of the *kcs* gene family in plants: the history of gene duplication, sub/neofunctionalization and redundancy. *Mol. Genet. Genomics* 291, 739–752. doi: 10.1007/s00438-015-1142-3

Habte, E., Muller, L. M., Shtaya, M., Davis, S. J., and Von Korff, M. (2014). Osmotic stress at the barley root affects expression of circadian clock genes in the shoot. *Plant Cell Environ.* 37, 1321–1327. doi: 10.1111/pce.12242

Haslam, T. M., and Kunst, L. (2013). Extending the story of very-long-chain fatty acid elongation. *Plant Sci.* 210, 93–107. doi: 10.1016/j.plantsci.2013.05.008

Hegebarth, D., Buschhaus, C., Joubès, J., Thoraval, D., Bird, D., and Jetter, R. (2017). *Arabidopsis* ketoacyl-CoA synthase 16 (KCS16) forms C36 /C38 acyl precursors for leaf trichome and pavement surface wax. *Plant Cell Environ.* 40, 1761–1776. doi: 10.1111/pce.12981

Hooker, T. S., Millar, A. A., and Kunst, L. (2002). Significance of the expression of the *CER6* condensing enzyme for cuticular wax production in *Arabidopsis*. *Plant Physiol.* 129, 1568–1580. doi: 10.1104/pp.003707

Isaacson, T., Kosma, D. K., Matas, A. J., Buda, G. J., and He, Y. (2009). Cutin deficiency in the tomato fruit cuticle consistently affects resistance to microbial infection and biomechanical properties, but not transpirational water loss. *Plant J.* 60, 363–377.

Islam, M. A., Du, H., Ning, J., Ye, H., and Xiong, L. (2009). Characterization of Glossy1-homologous genes in rice involved in leaf wax accumulation and drought resistance. *Plant Mol. Biol.* 70, 443–456. doi: 10.1007/s11103-009-9483-0

James, D. W., Lim, E., Keller, J., Plooy, I., Ralston, E., and Dooner, H. K. (1995). Directed tagging of the *Arabidopsis* FATTY ACID ELONGATION1 (*FAE1*) gene with the maize transposon activator. *Plant Cell* 7, 309–319. doi: 10.1105/tpc.7.3.309

Jenks, M. A., Joly, R. J., Peters, P. J., Rich, P. J., Axtell, J. D., and Ashworth, E. N. (1994). Chemically induced cuticle mutation affecting epidermal conductance to water vapor and disease susceptibility in *Sorghum bicolor* (L.) Moench. *Plant Physiol.* 105, 1239–1245. doi: 10.1104/pp.105.4.1239

Joubès, J., Raffaele, S., Bourdenx, B., Garcia, C., and Laroche-Traineau, J. (2008). The VLCFA elongase gene family in *Arabidopsis thaliana*: phylogenetic analysis, 3D modelling and expression profiling. *Plant Mol. Biol.* 67:547. doi: 10.1007/s11103-008-9339-z

Kim, H. J., Seo, E. Y., Kim, J. H., Cheong, H. J., and Choi, D. I. (2012). Morphological classification of trichomes associated with possible biotic stress resistance in the genus capsicum. *Plant Pathol. J.* 28, 107–113. doi: 10.5423/PPJ.NT.12.2011.0245

Krauss, P., Markstädter, C., and Riederer, M. (1997). Attenuation of UV radiation by plant cuticles from woody species. *Plant Cell Environ.* 20, 1079–1085. doi: 10.1111/j.1365-3040.1997.tb00684.x

Kunst, L., and Samuels, A. L. (2003). Biosynthesis and secretion of plant cuticular wax. *Prog. Lipid Res.* 42, 51–80. doi: 10.1016/S0163-7827(02)00045-0

Lee, S. B., and Suh, M. C. (2013). Recent advances in cuticular wax biosynthesis and its regulation in *Arabidopsis*. *Mol. Plant* 6, 246–249. doi: 10.1093/mp/sss159

Leide, J., Hildebrandt, U., Reussing, K., Riederer, M., and Vogg, G. (2007). The developmental pattern of tomato fruit wax accumulation and its impact on cuticular transpiration barrier properties: effects of a deficiency in a β-ketoacyl-coenzyme A synthase (*LeCER6*). *Plant Physiol.* 144, 1667–1679. doi: 10.1104/pp.107.099481

Liu, D., Yang, L., Wang, Y., Zhuang, X., Liu, C., Liu, S., et al. (2016). Transcriptome sequencing identified wax-related genes controlling the glossy phenotype formation of "ganqi 3," a bud mutant derived from wild-type "newhall" navel orange. *Tree Genet. Genom.* 12:55. doi: 10.1007/s11295-016-1017-8

Liu, D. C., Yang, L., Luo, M., Wu, Q., Liu, S. B., and Liu, Y. (2017). Molecular cloning and characterization of Ptrzpt2-1, a zpt2 family gene encoding a cys2/his2-type zinc finger protein from trifoliate orange (poncirus trifoliata (l.) raf.) that enhances plant tolerance to multiple abiotic stresses. plant science. *Plant Sci.* 263, 66–78. doi: 10.1016/j.plantsci.2017.07.012

Liu, D. C., Yang, L., Zheng, Q., Wang, Y., and Wang, M. (2015). Analysis of cuticular wax constituents and genes that contribute to the formation of 'glossy Newhall', a spontaneous bud mutant from the wild-type 'Newhall' navel orange. *Plant Mol. Biol.* 88, 573–590. doi: 10.1007/s11103-015-0343-9

Liu, D. C., Zeng, Q., Ji, Q. X., Liu, C. F., Liu, S. B., and Liu, Y. (2012). A comparison of the ultrastructure and composition of fruits' cuticular wax from the wild-type 'Newhall'navel orange (*Citrus sinensis* [L.] Osbeck cv. Newhall) and its glossy mutant. *Plant Cell Rep.* 31, 2239–2246. doi: 10.1007/s00299-012-1333-x

Lokesh, U., Venkatesh, B., Kiranmai, K., Nareshkumar, A., Amarnathareddy, V., Rao, G. L., et al. (2019). Overexpression of ß-Ketoacyl CoA Synthase1 gene improves tolerance of drought susceptible groundnut (*Arachis hypogaea* L.) Cultivar K-6 by increased leaf epicuticular wax accumulation. *Front. Plant Sci.* 9:1869. doi: 10.3389/fpls.2018.01869

Marcolino-Gomes, J., Rodrigues, F. A., Fuganti-Pagliarini, R., Bendix, C., Nakayama, T. J., Celaya, B., et al. (2014). Diurnal oscillations of soybean circadian clock and drought responsive genes. *PLoS One* 9:e86402. doi: 10.1371/journal.pone.0086402

Millar, A. A., Clemens, S., Zachgo, S., Giblin, E. M., Taylor, D. C., and Kunst, L. (1999). *CUT1*, an *Arabidopsis* gene required for cuticular wax biosynthesis and pollen fertility, encodes a very-long-chain fatty acid condensing enzyme. *Plant Cell* 11, 825–838. doi: 10.1105/tpc.11.5.825

Parsons, E. P., Popopvsky, S., Lohrey, G. T., Lü, S., Alkalai-Tuvia, S., and Perzelan, Y. (2012). Fruit cuticle lipid composition and fruit post-harvest water loss in an advanced backcross generation of pepper (*Capsicum* sp.). *Physiol. Plant.* 146, 15–25.

Pruitt, R. E., Vielle-Calzada, J. P., Ploense, S. E., Grossniklaus, U., and Lolle, S. J. (2000). *FIDDLEHEAD*, a gene required to suppress epidermal cell interactions in *Arabidopsis*, encodes a putative lipid biosynthetic enzyme. *Proc. Natl. Acad. Sci. U.S.A.* 97, 1311–1316. doi: 10.1073/pnas.97.3.1311

Qin, Y. M., Pujol, F. M., Hu, C. Y., Feng, J. X., Kastaniotis, A. J., Hiltunen, J. K., et al. (2007). Genetic and biochemical studies in yeast reveal that the cotton fibre-specific GhCER6 gene functions in fatty acid elongation. *J. Exp. Bot.* 58, 473–481. doi: 10.1093/jxb/erl218

Riederer, M., and Schneider, G. (1990). The effect of the environment on the permeability and composition of Citrus leaf cuticles. *Planta* 180, 154–165. doi: 10.1007/BF00193990

Rossak, M., Smith, M., and Kunst, L. (2001). Expression of the *FAE1* gene and *FAE1* promoter activity in developing seeds of *Arabidopsis thaliana*. *Plant Mol. Biol.* 46, 717–725. doi: 10.1023/A:1011603923889

Seo, P. J., Xiang, F. N., Qiao, M., Park, J. Y., and Park, C. M. (2009). The *myb96* transcription factor mediates abscisic acid signaling during drought stress response in *Arabidopsis*. *Plant Physiol.* 151, 275–289. doi: 10.2307/40537768

Serra, O., Soler, M., Hohn, C., Franke, R., Schreiber, L., Prat, S., et al. (2009). Silencing of *StKCS6* in potato periderm leads to reduced chain lengths of suberin and wax compounds and increased peridermal transpiration. *J. Exp. Bot.* 60, 697–707. doi: 10.1093/jxb/ern314

Shepherd, T., and Wynne Griffiths, D. (2006). The effects of stress on plant cuticular waxes. *New Phytol.* 171, 469–499. doi: 10.1111/j.1469-8137.2006.01826.x

Sieber, P., Schorderet, M., Ryser, U., Buchala, A., Kolattukudy, P., Métraux, J. P., et al. (2000). Transgenic *Arabidopsis* plants expressing a fungal cutinase show alterations in the structure and properties of the cuticle and postgenital organ fusions. *Plant Cell* 12, 721–737. doi: 10.1105/tpc.12.5.721

Singh, S., Das, S., and Geeta, R. (2018). "Role of cuticular wax in adaptation to abiotic stress: a molecular perspective," in *Abiotic Stress-Mediated Sensing and Signaling in Plants: An Omics Perspective*, eds S. Zargar, and M. Zargar (Singapore: Springer), 155–182.

Suh, M. C., Samuels, A. L., Jetter, R., Kunst, L., and Pollard, M. (2005). Cuticular lipid composition, surface structure, and gene expression in *Arabidopsis* stem epidermis. *Plant Physiol.* 139, 1649–1665. doi: 10.1104/pp.105.070805

Todd, J., Post-Beittenmiller, D., and Jaworski, J. G. (1999). *KCS1* encodes a fatty acid elongase3-ketoacyl-CoA synthase affecting wax biosynthesis in *Arabidopsis thaliana*. *Plant J.* 17, 119–130. doi: 10.1046/j.1365-313X.1999.00352.x

Vogg, G., Fischer, S., Leide, J., Emmanuel, E., Jetter, R., Levy, A. A., et al. (2004). Tomato fruit cuticular waxes and their effects on transpiration barrier properties: functional characterization of a mutant deficient in a very-long-chain fatty acid b-ketoacyl-CoA synthase. *J. Exp. Bot.* 55, 1401–1410. doi: 10.1093/jxb/erh149

Von Wettstein-Knowles, P. M. (1979). "Genetics and biosynthesis of plant epicuticular waxes," in *Advances in Biochemistry and Physiology of Plant Lipids*, eds L. Applequist and C. Liljenberg (Amsterdam: Elsevier), 1–26.

Wang, Y., Jin, S., Xu, Y., Li, S., and Zhang, S. (2020). Overexpression of *BnKCS1-1*, *BnKCS1-2*, and *BnCER1-2* promotes cuticular wax production and increases drought tolerance in *Brassica napus*. *Crop J.* 8, 26–37. doi: 10.1016/j.cj.2019.04.006

Weidenbach, D., Jansen, M., Bodewein, T., Nagel, K. A., and Schaffrath, U. (2015). Shoot and root phenotyping of the barley mutant kcs6 (3-ketoacyl-coa synthase6) depleted in epicuticular waxes under water limitation. *Plant Signal. Behav.* 10:e1003752. doi: 10.1080/15592324.2014.1003752

Xie, Y. P., Chen, P., Yan, Y., Bao, C., and Li, X. (2018). An atypical R2R3 *MYB* transcription factor increases cold hardiness by CBF-dependent and CBF-independent pathways in apple. *New Phytol.* 218, 201–218. doi: 10.1111/nph.14952

Yeats, T. H., and Rose, J. K. (2013). The formation and function of plant cuticles. *Plant Physiol.* 163, 5–20. doi: 10.2307/23598549

Yephremov, A., Wisman, E., Huijser, P., Huijser, C., Wellesen, K., and Saedler, H. (1999). Characterization of the *FIDDLEHEAD* gene of Arabidopsis reveals a link between adhesion response and cell differentiation in the epidermis. *Plant Cell* 11, 2187–2201. doi: 10.1105/tpc.11.11.2187

Zhang, J. Y., Broeckling, C. D., Blancaflor, E. B., Sledge, M. K., Sumner, L. W., and Wang, Z. Y. (2005). Overexpression of *WXP1*, a putative Medicago truncatula AP2 domain-containing transcription factor gene, increases cuticular wax accumulation and enhances drought tolerance in transgenic alfalfa (*Medicago sativa*). *Plant J.* 42, 689–707.

Zhang, J. Y., Broeckling, C. D., Sumner, L. W., and Wang, Z. (2007). Heterologous expression of two Medicago truncatula putative ERF transcription factor genes, *WXP1* and *WXP2*, in Arabidopsis led to increased leaf wax accumulation and improved drought tolerance, but differential response in freezing tolerance. *Plant Mol. Biol.* 64, 265–278. doi: 10.1007/s11103-007-9150-2

Zhang, Y. L., Zhang, C. L., Wang G. L., Wang, Y. X., and Hao, Y. J. (2019a). Apple AP2/EREBP transcription factor *MdSHINE2* confers drought resistance by regulating wax biosynthesis. *Planta* 249, 1627–1643. doi: 10.1007/s00425-019-03115-4

Zhang, Y. L., Zhang, C. L., Wang, G. L., Wang, Y. X., and Hao, Y. J. (2019b). The R2R3 *MYB* transcription factor *MdMYB30* modulates plant resistance against pathogens by regulating cuticular wax biosynthesis. *BMC Plant Biol.* 19:362. doi: 10.1186/s12870-019-1918-4

Zhou, L. J., Zhang, C. L., Zhang, R. F., Wang, G. L., and Hao, Y. J. (2019). The SUMO E3 ligase *MdSIZ1* targets *MdbHLH104* to regulate plasma membrane H+-ATPase activity and iron homeostasis. *Plant Physiol.* 179, 88–106. doi: 10.1111/pce.12978

Conflict of Interest: The authors declare that the research was conducted in the absence of any commercial or financial relationships that could be construed as a potential conflict of interest.

frontiers in Plant Science

ORIGINAL RESEARCH
published: 22 October 2020
doi: 10.3389/fpls.2020.524947

EgMIXTA1, a MYB-Type Transcription Factor, Promotes Cuticular Wax Formation in *Eustoma grandiflorum* Leaves

Lishan Wang[1,2], Wanjie Xue[1,2], Xueqi Li[1,2], Jingyao Li[1,2], Jiayan Wu[1,2], Linan Xie[1,2], Saneyuki Kawabata[3], Yuhua Li[1,2] and Yang Zhang[1,2]**

[1] Key Laboratory of Saline-alkali Vegetation Ecology Restoration, Ministry of Education, College of Life Science, Northeast Forestry University, Harbin, China, [2] College of Life Science, Northeast Forestry University, Harbin, China, [3] Institute for Sustainable Agroecosystem Services, Graduate School of Agriculture and Life Science, The University of Tokyo, Tokyo, Japan

In the aerial plant organs, cuticular wax forms a hydrophobic layer that can protect cells from dehydration, repel pathogen attacks, and prevent organ fusion during development. The *MIXTA* gene encodes an MYB-like transcription factor, which is associated with epicuticular wax biosynthesis to increase the wax load on the surface of leaves. In this study, the *AmMIXTA*-homologous gene *EgMIXTA1* was functionally characterized in the *Eustoma grandiflorum*. *EgMIXTA1* was ubiquitously, but highly, expressed in leaves and buds. We identified the *Eustoma* MIXTA homolog and developed the plants for overexpression. EgMIXTA1-overexpressing plants had more wax crystal deposition on the leaf surface compared to wild-type and considerably more overall cuticular wax. In the leaves of the overexpression line, the cuticular transpiration occurred more slowly than in those of non-transgenic plants. Analysis of gene expression indicated that several genes, such as *EgCER3*, *EgCER6*, *EgCER10*, *EgKCS1*, *EgKCR1*, and *EgCYP77A6*, which are known to be involved in wax biosynthesis, were induced by EgMIXTA1-overexpression lines. Expression of another gene, *WAX INDUCER1/SHINE1*, encoding a transcription factor that stimulates the production of cutin, was also significantly higher in the overexpressors than in wild-type. However, the expression of a lipid-related gene, *EgABCG12*, did not change relative to the wild-type. These results suggest that *EgMIXTA1* is involved in the biosynthesis of cuticular waxes.

Keywords: cuticular wax, lipid biosynthesis, *Eustoma grandiflorum*, *MIXTA* genes, transgenic plants, water loss

OPEN ACCESS

Edited by:
Shiwen Wang,
Northwest A&F University, China

Reviewed by:
Takashi Nakatsuka,
Shizuoka University, Japan
Daoqian Chen,
Fujian Agriculture and Forestry University, China

****Correspondence:***
Yuhua Li
lyhshen@126.com
Yang Zhang
summerzhang@126.com

Specialty section:
This article was submitted to Plant Metabolism and Chemodiversity, a section of the journal Frontiers in Plant Science

Received: *07 January 2020*
Accepted: *22 September 2020*
Published: *22 October 2020*

Citation:
Wang L, Xue W, Li X, Li J, Wu J, Xie L, Kawabata S, Li Y and Zhang Y (2020) EgMIXTA1, a MYB-Type Transcription Factor, Promotes Cuticular Wax Formation in Eustoma grandiflorum Leaves. Front. Plant Sci. 11:524947. doi: 10.3389/fpls.2020.524947

INTRODUCTION

Eustoma grandiflorum (*Raf.*) *Shinn.* is a perennial, herbaceous, ornamental plant, which originated from the southern part of North America (Wang et al., 2011). *E. grandiflorum*, one of the most common potted plants, has very high economic and ornamental value due to its large, attractive, long-stalked flowers, long-lasting in vase flowers (Ecker et al., 1994; Zaccai and Edri, 2002; Uddin et al., 2004; Lena et al., 2009). *E. grandiflorum*, used to produce cut flowers, is vulnerable to plant diseases, insect pest attacks, and require large amounts of water. Hence, considerable efforts were dedicated to screening for drought tolerance, disease, and insect pest resistance.

Cuticular waxes are composed of long chain fatty acids (VLCFAs) and their derivatives, including aldehydes, alkanes, esters, and primary and secondary alcohols (Kunst and Samuels, 2009; Bernard and Joubes, 2013). The cuticular waxes form the outermost barrier to non-stomatic loss of water and play a significant role in responding to environmental stress. Composition, secretion, and synthesis of wax and cutin are modulated during cell expansion (Suh et al., 2005) and vary in different tissues (Yonghua et al., 2007, 2009). Many genes involved in cuticular wax biosynthesis and transportation have been characterized by forward and reverse genetic approaches for understanding the metabolism of plant wax (Hooker et al., 2002; Aharoni et al., 2004; Kim et al., 2013). Some transcription factors (TFs) were also shown to regulate the biosynthesis of cuticle. For example, *Arabidopsis thaliana* WAX INDUCER1/SHINE1 (WIN1/SHN1), which belongs to the TF family of AP2/EREBP type, activates the genes of cuticular wax and cutin biosynthesis (Kannangara et al., 2007). *DECREASE WAX BIOSYNTHESIS* (*DEWAX*), another AP2 TF, represses the expression of cutic wax biosynthesis genes to negatively regulate wax production in Arabidopsis (Go et al., 2014).

The *MIXTA* gene, first identified in *Antirrhinum majus*, encodes a TF an R2R3 MYB, which is a key regulator for the differentiation of epidermal cells into conical cells (Noda et al., 1994). MIXTA and MIXTA-like TFs have been demonstrated to be critical regulators for epidermal cell differentiation across multiple species of plants (Brockington et al., 2013). The MIXTA/MIXTA-like TFs were documented to function as positive regulators for the formation of conical epidermal cells (Noda et al., 1994; Stilio et al., 2010), production of cotton fibers (Walford et al., 2011), trichomes (Gilding and Marks, 2010; Plett et al., 2010), and cuticle development (Oshima et al., 2013; Lashbrooke et al., 2015). The Arabidopsis MIXTA-like orthologs AtMYB16 and AtMYB106 have been shown to control the formation of cuticles, MYB106, and MYB16; loss- and gain-of-function research has shown that they control the expression of the genes of cutin biosynthesis (Oshima et al., 2013). AtMYB96 regulates cutin biosynthesis by directly binding to the promoters of genes involved in cuticular wax biosynthesis (Seo et al., 2011). *Solanum lycopersicum* MIXTA-like (SlMIXTA-like) positively regulates both cuticle and conical epidermal cell formation, and links cutin polymer formation, cuticle assembly, and epidermal cell patterning in the fruit (Lashbrooke et al., 2015). The *Artemisia annua* MIXTA-like protein AaMIXTA1 is a positive regulator of trichome initiation and cuticle development; it forms a regulatory complex leading to increased transcription of *AaHD1* and cuticle development genes (Yan et al., 2018). These studies indicate the involvement of MIXTA-like MYBs in cuticle development.

In this study, we functionally characterize the *E. grandiflorum MIXTA-like 1* (*EgMIXTA1*) gene by investigating the transgenic lines that overexpress *EgMIXTA1*. Our result indicated that *EgMIXTA1* participates in the regulation of cuticular wax biosynthesis genes in *E. grandiflorum*. Moreover, we suggest an essential role for an *EgMIXTA-like* gene and investigate the regulatory relationships between *EgMIXTA1* and other genes involved in the biosynthesis of cuticular wax.

MATERIALS AND METHODS

Plant Materials and Growth Conditions

Seeds of *E. grandiflorum* cv. No. 2003-2-2, were used to generate the *MIXTA1* overexpression lines (OX-1, OX-2, and OX-3) The seeds were rinsed with sterilized water for 10 min, rinsed twice with 70% alcohol for 1 min each, surface sterilized with 3% (v/v) sodium hypochlorite for 10 min, and rinsed with sterilized water five times for 5 min each before sowing on 1.5% agar plates containing Murashige and Skoog (MS) medium. After sowing, the plates were kept at 4°C for 2 days and then incubated under aseptic conditions at 24°C with a photoperiod of 16 h white light (2,000 l×) In order to examine tissue-specific expression patterns, seeds were plated on MS medium with 1.5% sucrose and stratified in darkness for 2 days at 4°C before being transferred to the growth chamber (16 h of light and 8 h of darkness, 22°C). Roots, stems, leaves, petals, and buds were collected and stored at −80°C for further processing.

Cloning of the Full-Length MIXTA1 Gene

Total RNA was extracted from leaves of the aseptic seedlings using TRIzol reagent (Invitrogen, Carlsbad, CA, United States), then treated with DNase I (TaKaRa, Otsu, Shiga, Japan) and re-extracted with TRIzol reagent. Reverse transcription PCR (RT-PCR) was performed using the SuperScript III Reverse Transcriptase (TaKaRa, Otsu, Shiga, Japan). PCR products were purified using the High Pure PCR Product Purification Kit (Invitrogen). A degenerate primer set was designed from protein domains of MIXTA conserved across proteins from related species, namely, *A. majus* (AY821655, AJ006292, X79108, AY661654), *Malus sieversii* (DQ074464), *Gossypium hirsutum* (AF336283), and *Petunia hybrida* (Z13996). Partial fragments of *EgMIXTA1* were amplified from the cDNA library by PCR. Then 5′ rapid amplification of cDNA ends (RACE) and 3′ RACE were performed with gene- and vector-specific primers [MIXTA1F/R, Primer5′ 1st (GSP1) Primer5′ 2nd (GSP2), Primer3′ 1st (GSP1), Primer3′ 2nd (GSP2), Adaptor, Anchor, Primer LF (5′ GSP), Primer LR (3′ GSP), MIXTA1-F/R] (**Supplementary Table 1**).

Generation of Transgenic Plants

The coding sequence of *MIXTA1* from *E. grandiflorum* cv. No. 2003-2-2 cDNA was amplified using a standard RT-PCR protocol. The full-length coding region of *MIXTA1* was cloned into the binary vector pH7WG2D to generate an *MIXTA1* overexpression vector in which *MIXTA1* expression was driven by the CaMV35S promoter. The constructs were introduced into *Agrobacterium tumefaciens* strain LBA4404. Seedlings of *E. grandiflorum* (wild-type) were transformed using the leaf disc transformation method and screened on 0.8% agar plates containing diluted (50% v/v) MS medium and 20 mg/L

kanamycin sulfate. Transgenic lines were selected based on kanamycin resistance.

Real-Time Fluorescence Quantitative PCR Analysis

Total RNA was extracted from *E. grandiflorum* plants using TRIzol reagent (Invitrogen, Carlsbad, CA, United States). Two micrograms of total RNA pooled from three replicate extractions was used for reverse transcription with the PrimeScript First Strand cDNA Synthesis kit (TaKaRa, Tokyo, Japan). The cDNA was then diluted 20-fold, and expression was quantified using the Power SYBR Green PCR Master Mix with the 7500 Real-Time PCR System according to the manufacturer's protocol (Applied Biosystems, Foster City, CA, United States). Amplification was done using the gene-specific primers listed in **Supplementary Table 1**. The quantitative RT-PCR (qRT-PCR) conditions used were 30 s at 95°C, followed by 40 cycles of 5 s at 95°C, 34 s at 60°C, and 15 s at 95°C. The relative quantification method ($2^{-\Delta\Delta CT}$) was used to evaluate quantitative variation between replicates. Data were normalized against the *EgActin* gene. The reactions were performed in biological triplicate using RNA samples extracted from three independent plant samples.

Scanning Electron Microscopy

To observe the cuticular waxes in the transgenic aseptic seedlings, images were captured with a QUANTA 200 scanning electron microscopy (FEI Co., Hillsboro, OR, United States). When the seedlings were at least 5 weeks old, the third true leaves from each transgenic line were analyzed for cuticular wax. Before the observations, the leaves were cut into small pieces (1 cm × 1 cm) and fixed to sample holders, then dehydrated to make the surface of the leaves clean and water free. The samples were sputter-coated with gold particles using an SCD 005 Sputter Coater (Leica Co., Solms, Germany) and examined by scanning electron microscopy at an accelerating voltage of 10 kV.

Immunostaining Analysis

Immunostaining was performed as previously described (Xuhong et al., 2007). Leaves were ground to a fine powder and fixed in ice-cold fixation buffer (4% formaldehyde, 10 mM Tris–HCl, pH 7.5, 10 mM EDTA, and 100 mM NaCl). Then, the sample was suspended in sorting buffer (100 mM Tris–HCl, pH 7.5, 50 mM KCl, 2 mM MgCl, 0.05% Tween 20, and 5% sucrose). Nuclei were sorted using a Falcon® 40 μm Cell Strainer. Nuclei were incubated with antiEgMIXTA1 antibody, washed (10 mM sodium phosphate, pH 7.0, and 143 mM NaCl), incubated with Rhodamine Red-x-conjugated donkey anti-rabbit IgG (1/500 dilution; Alexa Fluor), and washed thoroughly. Images were captured and analyzed using Zeiss Axioskop 2 Plus, and processed using Adobe Photoshop software.

Water Loss Assay

The rate of water loss was estimated using leaves from well-watered 5-week-old plants. The plants were acclimated in the dark for 6 h, then soaked in water for 1 h. Three of the third true leaves were then dried and weighed gravimetrically using a microbalance at the time points indicated.

RESULTS

Identification and Sequence Analysis of the *EgMIXTA1* Gene

The experiments were performed to find the TFs that regulate the synthesis of cuticular waxes and the differentiation of epidermal cells in *E. grandiflorum*. We looked for the MIXTA-like gene encoding sequences in *A. majus* (AY821655, AJ006292, X79108, AY661654), *M. sieversii* (DQ074464), *G. hirsutum* (AF336283), and *P. hybrida* (Z13996) in GeneBank. Based on the conserved domains and RACE technology, we identified the *E. grandiflorum* homolog of the *MIXTA-like* gene and named it *EgMIXTA1*. *EgMIXTA1* has an ORF of 1,128 nucleotides, encoding a polypeptide of 375 amino acids.

Furthermore, the molecular phylogenetic analysis of EgMIXTA1 and Arabidopsis R2R3domain proteins showed that EgMIXTA1 is also closely related to AtMYB16 and AtMYB106 (**Figure 1A**). In previous phylogenetic analyses, it was found that AtMYB16 and AtMYB106 belong to the R2R3 subgroup 9 clade (SBG9); SBG9 members have a well-established relationship with trichome and papillate cell formation (Brockington et al., 2013). Compared with other MIXTA-like genes, EgMIXTA1 and *S. lycopersicum* MIXTA-like are more closely related; EgMIXTA1 shares 59% amino acid identity with *S. lycopersicum* MIXTA-like (Weng et al., 2011; Ying et al., 2019; **Figure 1B**). We were interested in whether EgMIXTA1 has same role in the differentiation of epidermal cells or some other function. Consequently, we examined the function of EgMIXTA1 in *E. grandiflorum* in greater detail.

Expression Patterns of *EgMIXTA1* in *E. grandiflorum*

In order to investigate the spatial expression pattern of *EgMIXTA1*, the levels of *EgMIXTA1* mRNA in different tissues were analyzed. In our study, qRT-PCR revealed that *EgMIXTA1* was ubiquitously expressed in roots, leaves, petals, stems, and flower buds (**Figure 2A**).

Nuclear localization is necessary for TFs to execute their functions, so we used nuclear immunostaining to determine whether EgMIXTA1 accumulates in the nuclei of *E. grandiflorum* leaf tissues. Nuclei isolated from *E. grandiflorum* leaves were stained with DAPI and anti-EgMIXTA1 or a control solution lacking antibodies, followed by incubation in Rhodamine Red-x-conjugated secondary antibody. The Rhodamine Red-x and DAPI signals overlapped in the nuclei stained with anti-EgMIXTA1, indicating that EgMIXTA1 is localized in the nucleus (**Figure 2B**).

Overexpression of *EgMIXTA1* Increases Cuticular Wax Accumulation

To further dissect the biological function of EgMIXTA1, transgenic *E. grandiflorum* plants overexpressing *EgMIXTA1*

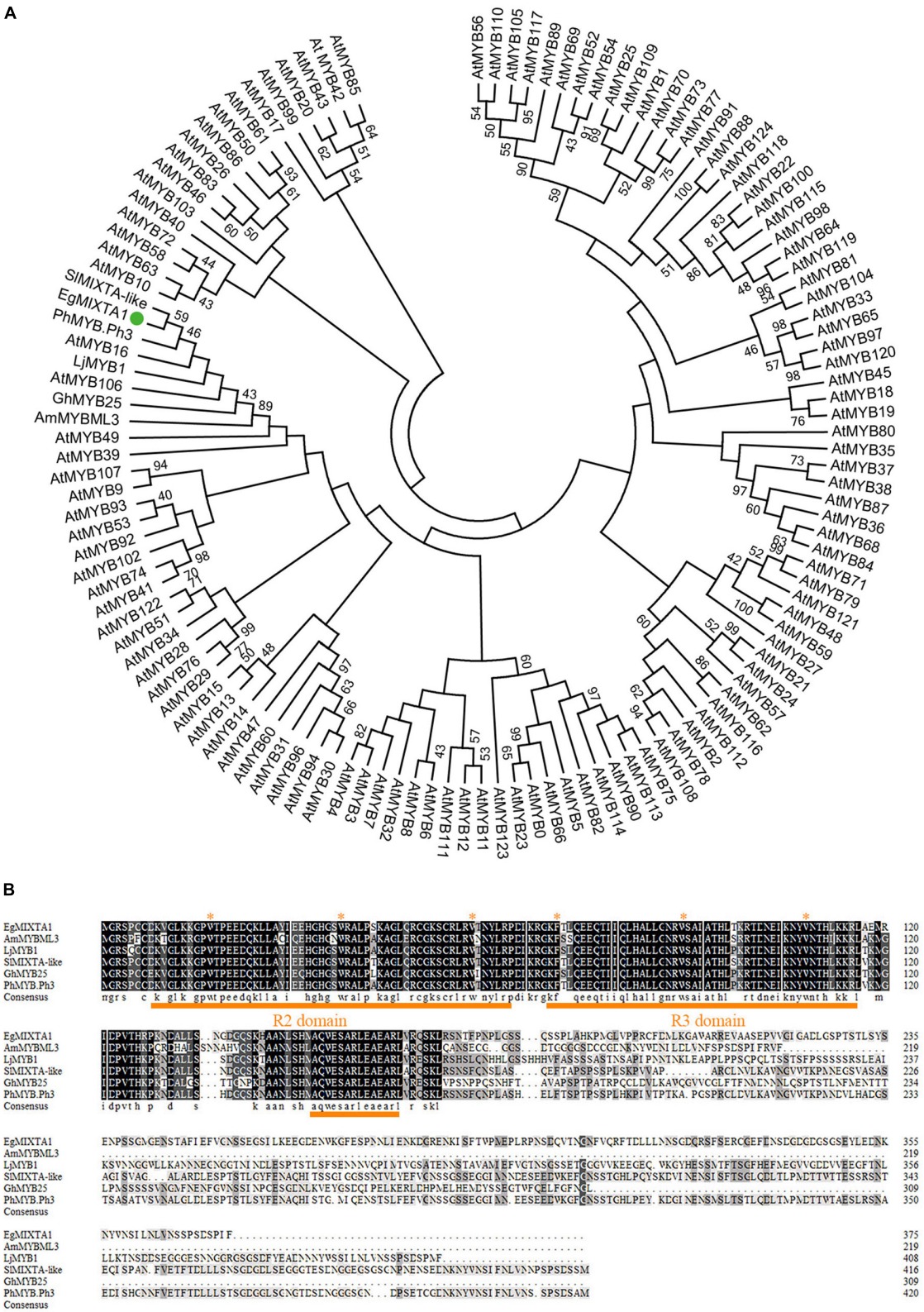

FIGURE 1 | Sequence analysis of EgMIXTA1 homologs. **(A)** Phylogenetic analysis of EgMIXTA1, Arabidopsis R2R3 domain TFs, and other species of MIXTA-like proteins. ClustalW and MEGA7 were used to align the proteins and compute the neighbor-joining tree with significance percentages (bootstrap values = 1,000). **(B)** Amino acid alignment showing the conserved R2R3 MYB domain and subgroup 9 motifs underlined in orange. The highly conserved amino acid residues are marked with red stars.

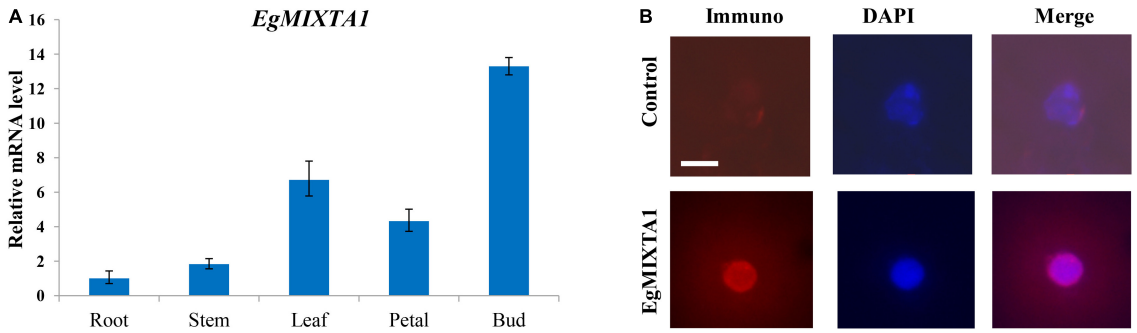

FIGURE 2 | Gene expression pattern of *EgMIXTA1* and nuclear localization of EgMIXTA1 **(A)**. The expression levels of *EgMIXTA1* in roots, stems, leaves, buds, and petals of *E. grandiflorum* were measured by quantitative RT-PCR (qRT-PCR). Actin was used as an internal reference. Data are presented as mean ± SD (n = 3). **(B)** Nuclei isolated from the leaves of 5-week seedlings of *E Eustoma grandiflorum* were probed with anti-EgMIXTA1 or a solution lacking anti-EgMIXTA1 (control), and visualized by staining with DAPI (blue) and Rhodamine Red-x-conjugated donkey-anti-rabbit IgG. Scale bar, 5 μm.

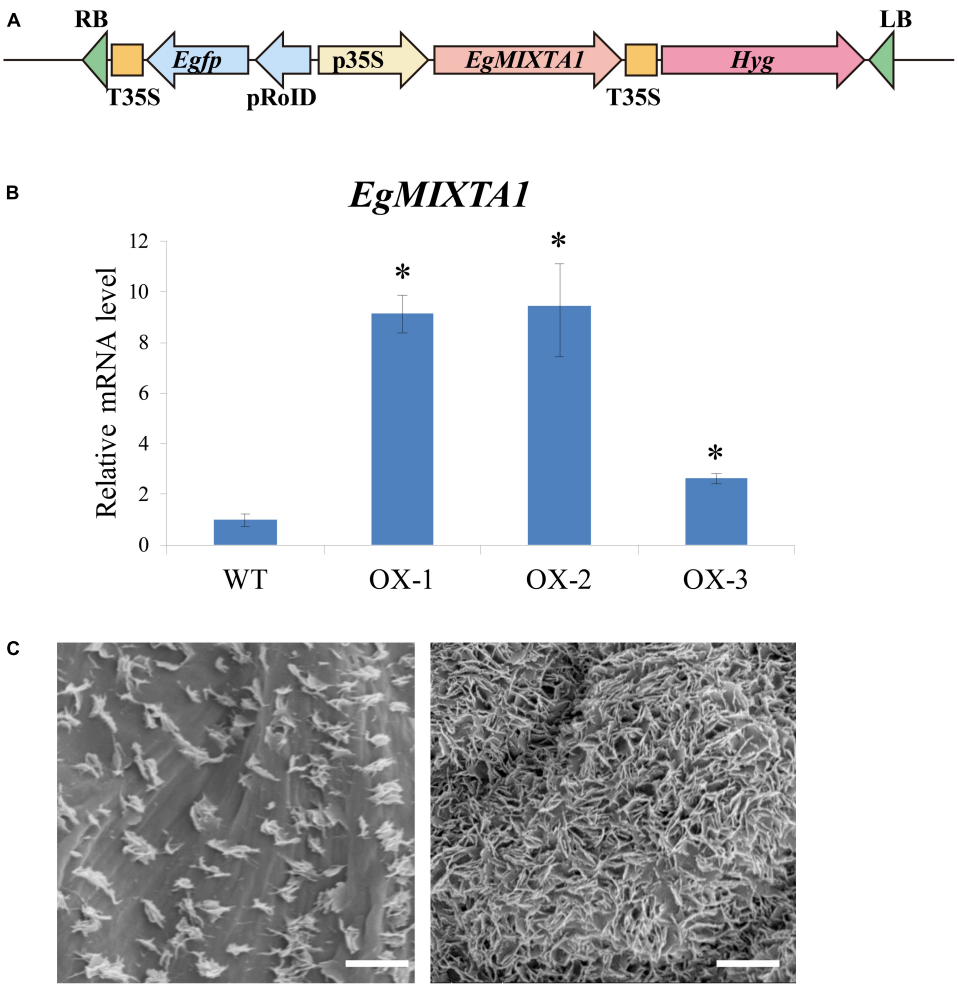

FIGURE 3 | Cuticular wax accumulation in *E. grandiflorum* leaves with altered *EgMIXTA1* expression. **(A)** Schematic diagram of *EgMIXTA1* in the pH7WG2D vector under the control of the CaMV 35S promoter. p35S, CaMV 35S promoter; T-35S, CaMV 35S terminator; pRolD, rolD promoter; Egfp, enhanced green-fluorescent protein; Hyg, hygromycin-resistant gene; RB, T-DNA right border sequence; LB, T-DNA left border sequence. **(B)** Expression levels of *EgMIXTA1* in *EgMIXTA1*-overexpressing plants were measured by qRT-PCR. Total RNA was isolated from leaves of WT and MIXTA1 overexpression lines (OX-1, OX-2, and OX-3), and subjected to qRT-PCR analysis. Actin was used as an internal reference. Student's *t*-test: $^*P < 0.01$. **(C)** Scanning electron microscopy images of epicuticular wax crystals on the leaves of 3-week-old wild-type (left) and *MIXTA1* overexpression lines (right). Scale bar, 5 μm.

under the control of the 35S promoter were generated (**Figure 3A**). Three independent transgenic plants were obtained, and significantly increased levels of *EgMIXTA1* gene expression were detected in independent transgenic lines by qRT-PCR (**Figure 3B**). Scanning electron microscopy analysis showed obvious deposition of epicuticular wax crystals on the leaves of EgMIXTA1 overexpressing lines than wild-type (**Figure 3C**).

These results indicated that high amounts of cuticular waxes accumulated in the leaves of transgenic *E. grandiflorum* plants overexpressing *MIXTA1*.

Expression of Wax Synthesis-Related Genes Is Altered in Leaves of Transgenic *E. grandiflorum* Plants Overexpressing *EgMIXTA1*

Because epicuticular wax deposition was significantly increased in *EgMIXTA1*-overexpressing plants (**Figure 3C**), we asked whether the expression of wax biosynthetic genes was altered in these plants. The biosynthesis of cuticular wax is a complex process, and a number of enzymes related to cuticular wax biosynthesis and transport are involved in wax biosynthesis. C16 and C18 fatty acids are synthesized in the plastids then exported to the cytoplasm, where they are further elongated to VLCFAs through sequential addition of two-carbon units in a reaction catalyzed by fatty acid elongase complexes at the endoplasmic reticulum (Lee and Suh, 2013; Fich et al., 2016; Xue et al., 2017). We investigated the expression patterns of some important genes functioning in wax biosynthetic pathways. The *E. grandiflorum* genes were obtained by performing homologous sequence alignments with *Arabidopsis* genes. We selected six genes that might be involved in cuticular wax biosynthesis: *EgCER3*, *EgCER6*, *EgCER10*, *EgKCS1*, *EgKCR1*, and *EgCYP77A6* (**Figure 4**). We also checked the expression of a gene (*EgABCG12*) putatively involved in lipid transport. A previous study confirmed that the homolog of this gene in Arabidopsis, *ABCG12*, which encodes an ATP-binding cassette (ABC) transporter, is a key component of the export

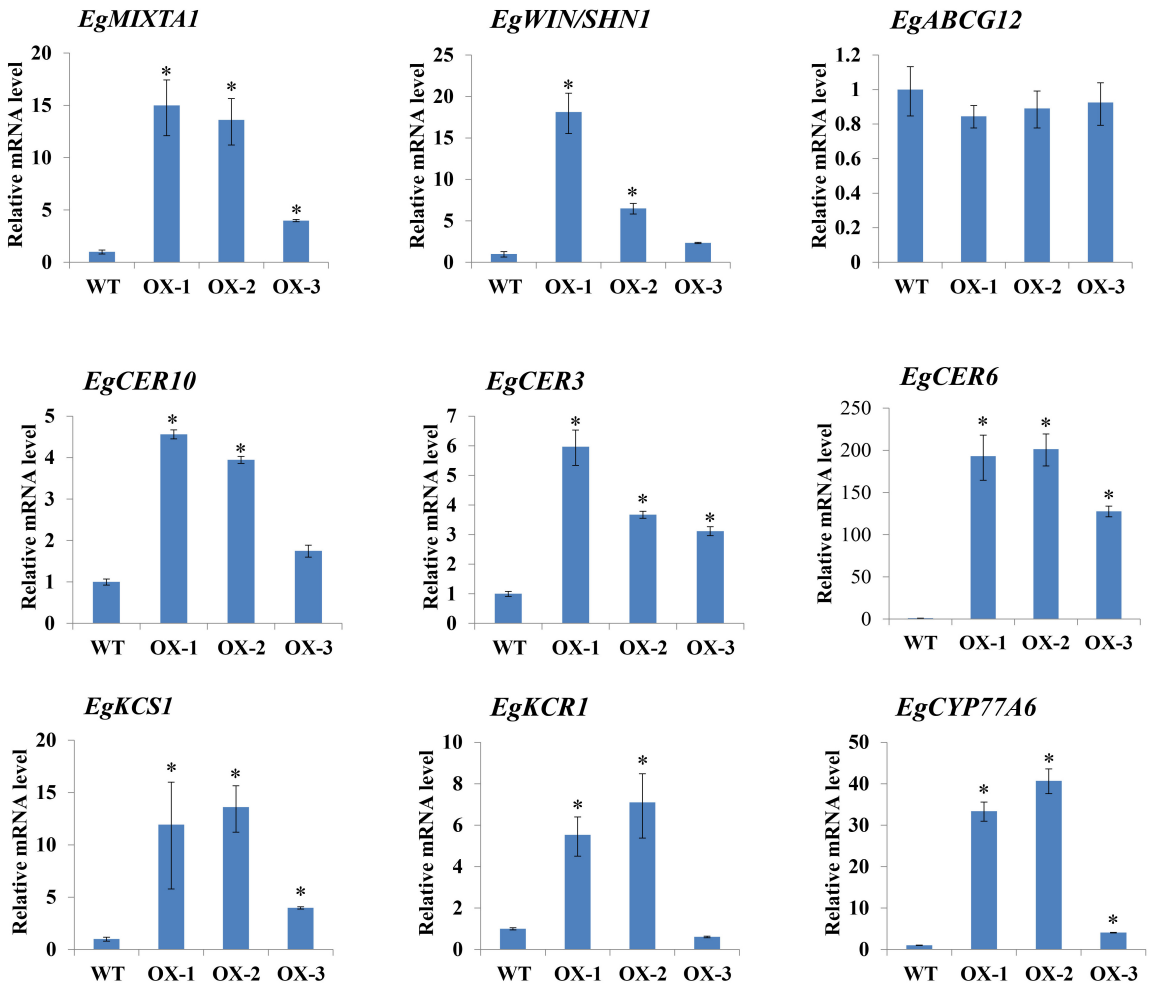

FIGURE 4 | Expression of cuticular wax biosynthetic genes in *EgMIXTA1*-overexpressing plants. qRT-PCR analysis of the expression of genes involved in cutin and wax biosynthesis in the leaves of wild-type (WT) and *EgMIXTA1*-overexpressing plants (OX-1, OX-2, and OX-3). Expression level in the wild-type is set as 1. Actin was used as an internal reference. Student's *t*-test: $^{*}P < 0.01$.

pathway for cuticular lipids (Bird et al., 2007; McFarlane et al., 2010). In addition, we investigated the expression pattern of *WIN1/SHN1*, a TF that induces cutin production in Arabidopsis (Kannangara et al., 2007). Real-time RT-PCR results showed that *EgCER3*, *EgCER6*, *EgCER10*, *EgKCS1*, *EgKCR1*, *EgCYP77A6*, and *EgWIN1* were upregulated in *EgMIXTA1*-overexpressing plants compared with non-transgenic plants. However, no significant changes in the transcript levels of *EgABCG12* were observed. This result revealed that overexpression of *EgMIXTA1* activated the expression of *E. grandiflorum* wax biosynthetic genes, which consequently caused an increase in cuticular wax biosynthesis and accumulation in transgenic *E. grandiflorum* plants.

EgMIXTA1-Overexpressing Plants Lose Water More Slowly Than the Wild-Type

Cuticular wax is the outermost layer that protects plants from water loss, and there is a lot of evidence showing that cuticular wax accumulation is closely associated with the water loss rate (Aharoni et al., 2004; Wang et al., 2018). We examined whether cuticular wax accumulation is linked to water loss by measuring cuticular transpiration. Five-week-old plants were dark acclimated for 6 h to ensure stomatal closure and soaked in water for 1 h in the dark to equilibrate the water content. Compared with wild-type leaves, transpiration occurred more slowly in the leaves of *EgMIXTA1*-overexpressing plants (**Figure 5**). The results showed that the elevated accumulation of cuticular waxes contributes to a reduction in water loss.

DISCUSSION

Plant cuticular wax covers the outer surface of aerial plant tissues. Many different studies have demonstrated that the plant cuticle plays an important role in limiting water loss and protecting plants from ultraviolet radiation and pathogen attacks (Kunst, 2003; Fich et al., 2016). Many *Arabidopsis* genes involved in wax synthesis, transport, and export, and in regulating the biosynthetic pathway have been identified. For example, *KCR1* encodes a β-ketoacyl-CoA reductase enzyme and is a candidate fatty acid elongase (Beaudoin et al., 2009), and *ECERIFERUM3* (*CER3*) is involved in the alkane-forming pathway (Chen et al., 2003). There are several lines of evidence from previous reports indicating that cuticular wax biosynthesis is regulated at the transcriptional level. For example, significant upregulation of the *WSD1*, *KCS2/DAISY*, *CER1*, *CER2*, *FAR3*, and *ECR* genes was observed in the leaves of transgenic Arabidopsis plants overexpressing MYB94 (Lee and Suh, 2015). In the activation-tagged myb96-1D mutant, a group of genes encoding cuticular wax biosynthetic enzymes, including *KCS1*, *KCS2*, *KCS6*, *KCR1*, *CER1*, and *CER3*, were greatly upregulated. In addition, the dominant active form of MYB106 (35S:MYB106-VP16) increased the expression of *WIN1/SHN1* and wax biosynthetic genes. In this study, we cloned the *EgMIXTA1* gene, which encodes a MIXTA-like R2R3-MYB TF, and generated transgenic plants overexpressing this gene. Overexpression of *EgMIXTA1* increased the expression of the wax biosynthetic genes (**Figure 4**).

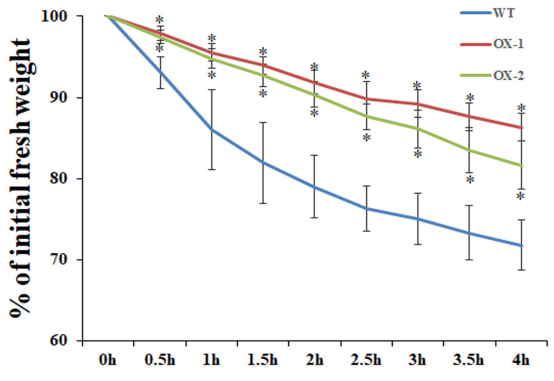

FIGURE 5 | Water loss rate in the leaves of wild-type (WT), *35S:MIXTA1* (OX-1), and *35S:MIXTA1* (OX-2) plants. Leaves at the same developmental stage were excised and weighed at various time points after detachment. The water loss rate is shown as the percentage of initial fresh weight at each time point. The bars indicate the SE of three individual plants per genotype, and the asterisks denote significant differences from the wild-type (Student's *t*-test, $^*P < 0.05$).

MIXTA and MIXTA-like TFs have been shown to be key regulators of epidermal cell differentiation and cuticle biosynthesis. *A. majus*, a *mixta* mutant, in which conical cells become flat, shows alterations in petal color intensity (Noda et al., 1994). In Arabidopsis, the MIXTA-like genes AtMYB16 and AtMYB106 were shown to regulate epidermal cell morphology and cuticle development (Oshima et al., 2013). In this experiment, through scanning electron microscopy pictures, we observed that no epidermal hair was observed on the wild-type leaves of *E. grandiflorum*, and the same results were also shown after overexpression. At the same time, no changes were found in the morphology of the epidermal cells. In addition to the increase in cuticular wax, it is possible that EgMIXTA1 in the *E. grandiflorum* leaves mainly regulates the biosynthesis and transport of wax crystal. Unfortunately, we failed to observe changes in the morphological differentiation status and cuticular wax of *E. grandiflorum* petal epidermal cells after overexpression. In our study, EgMIXTA1 was demonstrated to function quite similarly to the MIXTA-like MYB TFs in determining cuticular wax formation in *E. grandiflorum* leaves (**Figure 3C**). It has been documented that biosynthesis and accumulation of cuticular waxes are closely linked with drought resistance responses. Under water deficit conditions, cuticular wax accumulation significantly increases. In roses, drought stress caused a 9–15% increase in wax load on leaves exposed to drought during development (Jenks et al., 2001). In tobacco, the total wax load increased 1.5- to 2.5-fold under periodic dehydration stress. In addition, a high-wax-producing *Dianthus spiculifolius* mutant with increased cuticular wax accumulation exhibited stronger drought resistance (Zhou et al., 2018). Our results demonstrate that EgMIXTA1 regulates cuticular wax deposition and decrease water loss (**Figure 5**).

Eustoma grandiflorum, which belongs to the Gentianaceae family, is becoming increasingly popular for use in cut flower

production because it has large flowers, long stems, and an extended vase life (Davies et al., 1993). We found that elevated accumulation of cuticular waxes contributes to a reduction in water loss in *E. grandiflorum* (**Figure 5**). We did not conduct an experiment to elucidate the phenotype change and drought stress tolerance in the naturally growing conditions or the fresh-cut vase life. Our subsequent research will also verify this. The subsequent research will help in production and application. Based on this observation, increasing the accumulation of cuticular waxes may be important in reducing water loss and possibly delaying senescence and extending the vase life of cut *E. grandiflorum* flowers.

DATA AVAILABILITY STATEMENT

The datasets generated for this study are available on request to the corresponding author.

AUTHOR CONTRIBUTIONS

LW and JW carried out the experiments and data analysis and drafted the manuscript. YL and YZ provided guidance on experimental design and drafting the manuscript. WX, XL, JL, LX, and SK provided help in carrying out the experiments and modifying the manuscript. All authors contributed to the article and approved the submitted version.

FUNDING

This research was financially supported by a grant from the National Natural Science Foundation of China (Grant Nos. 31772339, and 31872139), Natural Science Foundation of Heilongjiang Province of China (Grant No. C2016008), the Fundamental Research Fund for Central Universities (Grant No. 2572019AA24), and Heilongjiang Touyan Innovation Team Program (Tree Genetics and Breeding Innovation Team).

SUPPLEMENTARY MATERIAL

The Supplementary Material for this article can be found online at: https://www.frontiersin.org/articles/10.3389/fpls.2020.524947/full#supplementary-material

Supplementary Table 1 | Primer sequences used in this paper.

REFERENCES

Aharoni, A., Dixit, S., Jetter, R., Thoenes, E., Van, A. G., and Pereira, A. (2004). The SHINE clade of AP2 domain transcription factors activates wax biosynthesis, alters cuticle properties, and confers drought tolerance when overexpressed in *Arabidopsis*. *Plant Cell* 16, 2463–2480. doi: 10.1105/tpc.104.022897

Beaudoin, F., Wu, X., Li, F., Haslam, R. P., Markham, J. E., Zheng, H., et al. (2009). Functional characterization of the *Arabidopsis* β-ketoacyl-coenzyme a reductase candidates of the fatty acid elongase. *Plant Physiol.* 150, 1174–1191. doi: 10.1104/pp.109.137497

Bernard, A., and Joubes, J. (2013). *Arabidopsis* cuticular waxes: advances in synthesis, export and regulation. *Prog. Lipid Res.* 52, 110–129. doi: 10.1016/j.plipres.2012.10.002

Bird, D., Beisson, F., Brigham, A., Shin, J., Greer, S., Jetter, R., et al. (2007). Characterization of *Arabidopsis* ABCG11/WBC11, an ATP binding cassette (ABC) transporter that is required for cuticular lipid secretion. *Plant J.* 52, 485–498. doi: 10.1111/j.1365-313X.2007.03252.x

Brockington, S. F., Alvarezfernandez, R., Landis, J. B., Alcorn, K., Walker, R. H., Thomas, M. M., et al. (2013). Evolutionary analysis of the MIXTA gene family highlights potential targets for the study of cellular differentiation. *Mol. Biol. Evol.* 30, 526–540. doi: 10.1093/molbev/mss260

Chen, X., Goodwin, S. M., Boroff, V. L., Liu, X., and Jenks, M. A. (2003). Cloning and characterization of the WAX2 gene of *Arabidopsis* involved in cuticle membrane and wax production. *Plant Cell* 15, 1170–1185. doi: 10.1105/tpc.010926

Davies, K. M., Bradley, J. M., Schwinn, K. E., Markham, K. R., and Podivinsky, E. (1993). Flavonoid biosynthesis in flower petals of five lines of lisianthus (*Eustoma grandiflorum* Grise.). *Plant Sci.* 95, 67–77. doi: 10.1016/0168-9452(93)90080-j

Ecker, R., Barzilay, A., and Osherenko, E. (1994). The genetic relations between length of time to germination and seed dormancy in lisianthus *(Eustoma grandiflorum*). *Euphytica* 80, 125–128. doi: 10.1007/bf00039307

Fich, E. A., Segerson, N. A., and Rose, J. K. (2016). The plant polyester cutin: biosynthesis, structure, and biological roles. *Annu. Rev. Plant Biol.* 67, 207–233. doi: 10.1146/annurev-arplant-043015-111929

Gilding, E. K., and Marks, M. D. (2010). Analysis of purified glabra3-shapeshifter trichomes reveals a role for NOECK in regulating early trichome morphogenic events. *Plant J.* 64, 304–317. doi: 10.1111/j.1365-313x.2010.04329.x

Go, Y. S., Kim, H., Kim, H. J., and Suh, M. C. (2014). *Arabidopsis* cuticular wax biosynthesis is negatively regulated by the DEWAX gene encoding an AP2/ERF-type transcription factor. *Plant Cell* 26, 1666–1680. doi: 10.1105/tpc.114.123307

Hooker, T. S., Millar, A. A., and Kunst, L. (2002). Significance of the expression of the CER6 condensing enzyme for cuticular wax production in *Arabidopsis*. *Plant Physiol.* 129, 1568–1580. doi: 10.1104/pp.003707

Jenks, M. A., Andersen, L., Teusink, R. S., and Williams, M. H. (2001). Leaf cuticular waxes of potted rose cultivars as affected by plant development, drought and paclobutrazol treatments. *Physiol. Plant* 112, 62–70. doi: 10.1034/j.1399-3054.2001.1120109.x

Kannangara, R., Branigan, C., Liu, Y., Penfield, T., Rao, V., Mouille, G., et al. (2007). The transcription factor WIN1/SHN1 regulates Cutin biosynthesis in *Arabidopsis thaliana*. *Plant Cell* 19, 1278–1294. doi: 10.1105/tpc.106.047076

Kim, J., Jung, J. H., Lee, S. B., Go, Y. S., Kim, H. J., Cahoon, R., et al. (2013). *Arabidopsis* 3-ketoacyl-coenzyme a synthase9 is involved in the synthesis of tetracosanoic acids as precursors of cuticular waxes, suberins, sphingolipids, and phospholipids. *Plant Physiol.* 162, 567–580. doi: 10.1104/pp.112.210450

Kunst, L. (2003). Biosynthesis and secretion of plant cuticular wax. *Prog. Lipid Res.* 42, 51–80. doi: 10.1016/s0163-7827(02)00045-0

Kunst, L., and Samuels, L. (2009). Plant cuticles shine: advances in wax biosynthesis and export. *Curr. Opin. Plant Biol.* 12, 721–727. doi: 10.1016/j.pbi.2009.09.009

Lashbrooke, J., Adato, A., Lotan, O., Alkan, N., Tsimbalist, T., Rechav, K., et al. (2015). The tomato MIXTA-like transcription factor coordinates fruit epidermis conical cell development and cuticular lipid biosynthesis and assembly. *Plant Physiol.* 169, 2553–2571. doi: 10.1104/pp.15.01145

Lee, S. B., and Suh, M. C. (2013). Recent advances in cuticular wax biosynthesis and its regulation in *Arabidopsis*. *Mol. Plant* 6, 246–249. doi: 10.1093/mp/sss159

Lee, S. B., and Suh, M. C. (2015). Cuticular wax biosynthesis is up-regulated by the MYB94 transcription factor in *Arabidopsis*. *Plant Cell Physiol.* 56, 48–60. doi: 10.1093/pcp/pcu142

Lena, S., Dalia Rav, D., Irit, D., Uri, Y., Shimon, P., Rahel, L., et al. (2009). Cultural methods and environmental conditions affecting gray mold and its management in lisianthus. *Phytopathology* 99, 557–570.

McFarlane, H. E., Shin, J. J., Bird, D. A., and Samuels, A. L. (2010). *Arabidopsis* ABCG transporters, which are required for export of diverse cuticular lipids, dimerize in different combinations. *Plant Cell* 22, 3066–3075. doi: 10.1105/tpc.110.077974

Noda, K., Glover, B. J., Linstead, P., and Martin, C. (1994). Flower colour intensity depends on specialized cell shape controlled by a Myb-related transcription factor. *Nature* 369:661. doi: 10.1038/369661a0

Oshima, Y., Shikata, M., Koyama, T., Ohtsubo, N., Mitsuda, N., and Ohme-Takagi, M. (2013). MIXTA-like transcription factors and WAX INDUCER1/SHINE1 coordinately regulate cuticle development in *Arabidopsis* and *Torenia fournieri*. *Plant Cell* 25, 1609–1624. doi: 10.1105/tpc.113.110783

Plett, J. M., Wilkins, O., Campbell, M. M., Ralph, S. G., and Regan, S. (2010). Endogenous overexpression of Populus MYB186 increases trichome density, improves insect pest resistance, and impacts plant growth. *Plant J.* 64, 419–432. doi: 10.1111/j.1365-313x.2010.04343.x

Seo, P. J., Lee, S. B., Suh, M. C., Park, M. J., Go, Y. S., and Park, C. M. (2011). The MYB96 transcription factor regulates cuticular wax biosynthesis under drought conditions in *Arabidopsis*. *Plant Cell* 23, 1138–1152. doi: 10.1105/tpc.111.083485

Stilio, V. S., Di Cathie, M., Schulfer, A. F., and Connelly, C. F. (2010). An ortholog of MIXTA-like2 controls epidermal cell shape in flowers of Thalictrum. *New Phytol.* 183, 718–728. doi: 10.1111/j.1469-8137.2009.02945.x

Suh, M. C., Samuels, A. L., Jetter, R., Kunst, L., Pollard, M., Ohlrogge, J., et al. (2005). Cuticular lipid composition, surface structure, and gene expression in *Arabidopsis* stem epidermis. *Plant Physiol.* 139, 1649–1665. doi: 10.1104/pp.105.070805

Uddin, A. F. M. J., Hashimoto, F., Miwa, T., Ohbo, K., and Sakata, Y. (2004). Seasonal variation in pigmentation and anthocyanidin phenetics in commercial Eustoma flowers. *Sci. Horticult.* 99, 103–115. doi: 10.1016/j.scienta.2003.07.002

Walford, S. A., Wu, Y., Llewellyn, D. J., and Dennis, E. S. (2011). GhMYB25-like: a key factor in early cotton fibre development. *Plant J.* 65, 785–797. doi: 10.1111/j.1365-313x.2010.04464.x

Wang, Q., Zhang, Y., Kawabata, S., and Li, Y. (2011). Double fertilization and embryogenesis of *Eustoma grandiflorum*. *J. Japanese Soc. Horticult. Sci.* 80, 351–357. doi: 10.2503/jjshs1.80.351

Wang, Z., Tian, X., Zhao, Q., Liu, Z., Li, X., Ren, Y., et al. (2018). The E3 Ligase DROUGHT HYPERSENSITIVE negatively regulates cuticular wax biosynthesis by promoting the degradation of transcription factor ROC4 in Rice. *Plant Cell* 30, 228–244. doi: 10.1105/tpc.17.00823

Weng, L., Tian, Z., Feng, X., Li, X., Xu, S., Hu, X., et al. (2011). Petal development in *Lotus japonicus*. *J. Integr. Plant Biol.* 53, 770–782. doi: 10.1111/j.1744-7909.2011.01072.x

Xue, D., Zhang, X., Lu, X., Chen, G., and Chen, Z. H. (2017). Molecular and evolutionary mechanisms of cuticular wax for plant drought tolerance. *Front. Plant Sci.* 8:621. doi: 10.3389/fpls.2017.00621

Xuhong, Y., John, K., Xiaoying, Z., Dror, S., Maskit, M., Hongyun, Y., et al. (2007). *Arabidopsis* cryptochrome 2 completes its posttranslational life cycle in the nucleus. *Plant Cell* 19, 3146–3156. doi: 10.1105/tpc.107.053017

Yan, T., Li, L., Xie, L., Chen, M., Shen, Q., Pan, Q., et al. (2018). A novel HD-ZIP IV/MIXTA complex promotes glandular trichome initiation and cuticle development in *Artemisia annua*. *New Phytol.* 218, 567–578. doi: 10.1111/nph.15005

Ying, S., Su, M., Wu, Y., Zhou, L., and Zhang, Y. (2019). Trichome regulator SlMX1 directly manipulates primary metabolism in tomato fruit. *Plant Biotechnol. J.* 18, 354–363. doi: 10.1111/pbi.13202

Yonghua, L., Fred, B., Koo, A. J. K., Isabel, M., Mike, P., and John, O. (2007). Identification of acyltransferases required for cutin biosynthesis and production of cutin with suberin-like monomers. *Proc. Natl. Acad. Sci. U.S.A.* 104, 18339–18344. doi: 10.1073/pnas.0706984104

Yonghua, L. B., Mike, P., Vincent, S., Franck, P., John, O., and Fred, B. (2009). Nanoridges that characterize the surface morphology of flowers require the synthesis of cutin polyester. *Proc. Natl. Acad. Sci. U.S.A.* 106, 22008–22013. doi: 10.1073/pnas.0909090106

Zaccai, M., and Edri, N. (2002). Floral transition in lisianthus (*Eustoma grandiflorum*). *Sci. Horticult.* 95, 333–340. doi: 10.1016/s0304-4238(02)00057-2

Zhou, A., Liu, E., and Jiao, L. (2018). Characterization of increased cuticular wax mutant and analysis of genes involved in wax biosynthesis in *Dianthus spiculifolius*. *Horticult. Res.* 5:40.

Conflict of Interest: The authors declare that the research was conducted in the absence of any commercial or financial relationships that could be construed as a potential conflict of interest.

frontiers in Plant Science

ORIGINAL RESEARCH
published: 14 December 2020
doi: 10.3389/fpls.2020.611897

Phospholipid:Diacylglycerol Acyltransferase1 Overexpression Delays Senescence and Enhances Post-heat and Cold Exposure Fitness

Kamil Demski†, Anna Łosiewska, Katarzyna Jasieniecka-Gazarkiewicz, Sylwia Klińska and Antoni Banaś*

Intercollegiate Faculty of Biotechnology, University of Gdańsk and Medical University of Gdańsk, Gdańsk, Poland

OPEN ACCESS

Edited by:
Krzysztof Zienkiewicz, Nicolaus Copernicus University in Toruń, Poland

Reviewed by:
Thierry Chardot, INRA Centre Versailles-Grignon, France
Joaquín J. Salas, Instituto de la Grasa (IG), Spain

***Correspondence:**
Kamil Demski
kamil.demski@slu.se

†Present address:
Kamil Demski, Department of Plant Breeding, Swedish University of Agricultural Sciences, Alnarp, Sweden

Specialty section:
This article was submitted to Plant Metabolism and Chemodiversity, a section of the journal Frontiers in Plant Science

Received: *29 September 2020*
Accepted: *26 November 2020*
Published: *14 December 2020*

Citation:
Demski K, Łosiewska A, Jasieniecka-Gazarkiewicz K, Klińska S and Banaś A (2020) Phospholipid:Diacylglycerol Acyltransferase1 Overexpression Delays Senescence and Enhances Post-heat and Cold Exposure Fitness. Front. Plant Sci. 11:611897. doi: 10.3389/fpls.2020.611897

In an alternative pathway to acyl-CoA: diacylglycerol acyltransferase (DGAT)-mediated triacylglycerol (TAG) synthesis from diacylglycerol, phospholipid:diacylglycerol acyltransferase (PDAT) utilizes not acyl-CoA but an acyl group from sn-2 position of a phospholipid, to form TAG. The enzyme's activity *in vitro* matches DGAT's in a number of plant species, however its main function in plants (especially in vegetative tissue) is debatable. In the presented study, we cultivated *PDAT1*-overexpressing, *pdat1* knockout and wild-type lines of *Arabidopsis thaliana* through their whole lifecycle. *PDAT1* overexpression prolonged Arabidopsis lifespan in comparison to wild-type plants, whereas knocking out *pdat1* accelerated the plant's senescence. After subjecting the 3-week old seedlings of the studied lines (grown *in vitro*) to 2-h heat stress (40°C) and then growing them for one more week in standard conditions, the difference in weight between wild-type and *PDAT*1-overexpressing lines increased in comparison to the difference between plants grown only in optimal conditions. In another experiment all lines exposed to 2-week cold stress experienced loss of pigment, except for *PDAT*1-overexpressing lines, which green rosettes additionally weighed 4 times more than wild-type. Our results indicate that plants depleted of *PDAT1* are more susceptible to cold exposure, while *PDAT1* overexpression grants plants a certain heat and cold resilience. Since it was shown, that lysophospholipids may be intertwined with stress response, we decided to also conduct *in vitro* assays of acyl-CoA:lysophosphatidylcholine acyltransferase (LPCAT) and acylCoA:lysophosphatidylethanolamine acyltransferase (LPEAT) activity in microsomal fractions from the *PDAT1*-overexpressing Arabidopsis lines in standard conditions. The results show significant increase in LPEAT and LPCAT activity in comparison to wild-type plants. *PDAT1*-overexpressing lines' rosettes also present twice as high expression of *LPCAT2* in comparison to control. The presented study shows how much heightened expression of *PDAT1* augments plant condition after stress and extends its lifespan.

Keywords: PDAT, *Arabidopsis thaliana*, plant stress, plant senescence, LPEAT, LPCAT, heat-shock, cold stress

INTRODUCTION

Triacylglycerols (TAG) are a plant's way of storing high-dense energy, being twice as energy-efficient as equivalent mass of carbohydrates or protein (Xu and Shanklin, 2016). Those most-abundant neutral lipids are found in almost all plant tissues and have multiple functions in plants (Stumpf and Conn, 1988; Kaup et al., 2002; Kim et al., 2002; Theodoulou and Eastmond, 2012; Fan et al., 2013a,b). Recently, stress conditions were shown to promote TAG synthesis in plants by providing fatty acids from autophagy of cellular organelles (Su et al., 2020).

Triacylglycerol had been considered to be only synthesized in Kennedy pathway from acyl-CoA and diacylglycerol (DAG) by DGAT enzyme (acyl-CoA:diacylglycerol acyltransferase; Kennedy, 1961). However, in the year 2000 an enzyme was discovered, which was able to form TAG not by utilizing acyl-CoA, but by taking an acyl group from a phospholipid (most of the time phosphatidylcholine or phosphatidylethanolamine) and transferring it to the sn-3 position of DAG. This enzyme has been known ever since as phospholipid:diacylglycerol acyltransferase (PDAT; Banaś et al., 2000; Dahlqvist et al., 2000).

For the last 20 years, since its discovery, PDAT has been studied to a certain extent. The enzyme's expression was confirmed in a number of plant species, including model organism *Arabidopsis thaliana*, *Vernonia galamensis*, *Euphorbia lagascae*, *Stokesia levis*, *Ricinus communis*, *Glycine max* and *Linum usitatissimum* among others (Ståhl et al., 2004; Mhaske et al., 2005; Li et al., 2010; Pan et al., 2013).

In plants, the exact contribution to TAG synthesis of PDAT-type enzymes in relation to DGAT enzymes remains elusive. PDAT role might vary depending on the plant species studied. In seeds of sunflower (*Helianthus annuus*), for example, PDAT's role in TAG formation is dwarfed by DGAT's role in the same process. The opposite is true for safflower (*Carthamus tinctorius*) in which seeds PDAT's part in TAG accumulation matches, or even borders on surpassing DGAT's part (Banaś et al., 2013).

Complementary role of DGAT and PDAT enzymes was also researched in Arabidopsis. In *A. thaliana pdat1* knockout lines *DGAT1* expression increases. Contrary, in Arabidopsis *dgat1* knockout lines, PDAT1 takes over as the primary contributor to TAG synthesis. Double mutants, depleted of both *dgat1* and *pdat1*, are not viable (Zhang et al., 2009).

The studies of PDAT's activity illustrated that the enzyme may play a crucial role in plants, especially in those accumulating polyunsaturated or unusual fatty acids (Brown et al., 2012). Arabidopsis overexpressing *PDAT1* and *PDAT2* from linseed was enriched in PUFA (Pan et al., 2013). In *Ricinus communis* (producing hydroxy ricinoleic acid) or in *Crepis palaestina* (producing epoxy vernolic acid) PDAT preferentially utilized phospholipid's ricinoleoyl or vernoyl groups to acylate sn-3 position of DAG (Dahlqvist et al., 2000). The transfer of oxygenated fatty acids directly from a membrane-bound phospholipid and not from the acyl-CoA pool could be connected with plant's stress response (Mhaske et al., 2005).

Phospholipid:diacylglycerol acyltransferase enzymes are grouped into two families of PDAT1 and PDAT2 enzymes (Ståhl et al., 2004). The number of isoforms of each PDAT and their expression patterns differ between plant species (Yuan et al., 2017a; Chellamuthu et al., 2019). Moreover, different *PDAT* isoforms' expression is upregulated during different stress conditions (Yuan et al., 2017a).

Phospholipid:diacylglycerol acyltransferase's role during plant stress response seems to be significant. In *Camelina sativa PDAT*'s expression grew 2 to 5-fold during various stress conditions (Yuan et al., 2017b). Also, PDAT was shown to be crucial to plant basal thermotolerance through TAG synthesis. Arabidopsis *pdat*-depleted mutants were not able to accumulate TAG after subjecting them to heat stress (Mueller et al., 2017).

In this study, we decided to investigate PDAT's role in *Arabidopsis thaliana* further. Cultivation of the following Arabidopsis lines in pot cultures: *PDAT1*-overexpressing, *pdat1* knockout and wild-type lines resulted in the discovery of PDAT1's delaying effect on plant's senescence. We then decided to test our lines in stress conditions. Heat-shock experiments revealed that *PDAT1*'s expression increases in heat-stressed Arabidopsis, and high-temperature treatment elevates the already increased weight of *PDAT1*-overexpressing plants. While testing cold stress we found loss of pigment in wild-type and knockout lines (which were still smaller than wild-type), but *PDAT1*-overexpressing lines retained chlorophyll in most plants and its rosette leaves were quadruple the weight of wild-type ones. We concluded that *PDAT1* overexpression equips Arabidopsis with a measurable heat and cold resilience. *In vitro* assays of acyl-CoA:lysophosphatidylcholine acyltransferase (LPCAT) and acyl-CoA:lysophosphatidylethanolamine acyltransferase (LPEAT) activity in microsomal fractions from the *PDAT1*-overexpressing Arabidopsis were also conducted with results showing a significant increase in LPLAT activity in comparison to wild-type plants, with an additional doubling of *LPCAT*2 expression detected in *PDAT1*-overexpressing plants. The implications of our findings on better understanding PDAT1's role in plant stress mechanism are expanded on in the Discussion.

MATERIALS AND METHODS

Plant Material

Our wild-type/control Arabidopsis was *Arabidopsis thaliana* ecotype Columbia-0 (Col-0). Knockout mutants of *pdat1* are homozygotes of T-DNA insertion mutant lines SALK_065334 (*pdat1* KO1) and SALK_032261 (*pdat1* KO2), which were obtained from the Arabidopsis Biological Resource Center (The Ohio State University). PCR screening for *pdat1* homozygotes was performed using primers detailed in **Supplementary Table 1**. Genomic DNA for the PCR was isolated from 4-week old leaves by phenol extraction method (Sambrook et al., 1989) and the reaction was performed using Taq DNA Polymerase (Thermo Fisher Scientific).

AtPDAT1 (At5g13640) overexpression lines were kindly provided by Anders S. Carlsson in pART27 vector, with *AtPDAT1* being expressed under the 35S Cauliflower Mosaic Virus promoter (CaMV; Ståhl et al., 2004; Banaś et al., 2014).

Plant Lifecycle Analysis

Lifecycle events of *pdat1* knockout mutant, *PDAT1*-overexpressing, and wild-type lines were recorded simultaneously during plant development. All of the studied lines were grown together in a growth chamber at 23°C. The applied photoperiod consisted of 16 h of light (120 μmol photons m^{-2} s^{-1}) and 8 h of dark. The relative humidity was at 60%. Lifecycle events were recorded on 6 or more different plants for each line.

In vitro Plant Cultivation

The seeds of tested Arabidopsis lines were surface-sterilized by immersion in ethanol (70%, 2 min) followed by 1 min wash in distilled water and immersion in calcium hypochlorite (4%, 10 min). After that, the seeds were washed with distilled water (4 times) and planted on plates containing: 1% agar, 0.33× Murashige-Skoog medium (MS) and 1% sucrose. The seeds were sown on agar on a straight line in an upper part of the plate (up to 10 seeds per plate) and put in 4°C for 48 h vernalization. After that the plates were placed in the growth chamber vertically. After the needed amount of time (depending on the experiment) the rosette leaves and roots were separated and weighed. Under all temperature conditions the plants were grown with 16 h light (120 μmol photons m^{-2} s^{-1})/8 h dark photoperiod. For optimal growth condition measurements, the plates were placed for 4 weeks in 23°C. For heat stress measurements, the plates where placed for 3 weeks in 23°C, then for 2 h in 40°C (in MLR-352H Climate Chamber, Panasonic; humidity set at 60%). Now, depending on the experimental destination they were either placed for 2 h back into 23°C (for relative expression measurements) or placed for an additional week back into 23°C (for fresh weight measurements, lipid extraction). For cold stress measurements, the plants were put into growth chamber with 23°C for 2 weeks and then for additional 2 weeks into cold chamber (4°C), after which the fresh weight was measured.

Lipid Extraction and Analysis

Three 4-week-old rosettes of *in vitro* cultivated Arabidopsis were weighed and subjected to a Bligh and Dyer lipid extraction (Bligh and Dyer, 1959). One-fifth of the chloroform extract was transmethylated in 2 ml solution of 2% H_2SO_4 dissolved in dry methanol (45 min, 90°C), extracted to heptane with 50 nmol of heptadecanoic acid (internal standard) and then directly analyzed with GC-FID (Shimadzu GC-2010) utilizing 60 m × 0,25 mm BPX70 column (SGE Analytical Science). The rest of the chloroform extract was separated on TLC plate (silica gel 60; Merck) in heptane:diethyl ether:acetic acid (70:30:1) mobile phase. TAG spots were visualized under UV light after staining by 0.05% primuline solution and later scraped off. Silica gel samples containing TAG lipid group were from then on processed as described above for the one-fifth of the chloroform extract.

Microsomal Fraction Isolation

To obtain microsomal fraction from roots and rosettes, the seeds of tested Arabidopsis lines were sterilized and placed on MS plates as described above (only spread throughout the plate and not in a straight line). After 2 weeks of cultivation in 23°C, they were transferred into flasks containing 0.5× MS medium and 1% sucrose and grown with gentle shaking (80 rpm) for three more weeks. For all 5 weeks *in vitro* Arabidopsis lines were cultivated under the same light conditions as pot-cultivated plants (16 h light/8 h dark). The roots from approximately 20 plants were then carefully separated from leaves and homogenized separately in a glass homogenizers with homogenization buffer (0.1 M potassium phosphate buffer with 7.2 pH, 0.33 M sucrose, 1 mg/ml BSA and catalase 1000 units/ml) in a cold room (4°C) in ice. After homogenates were ready they were filtered through two-layer Miracloth and centrifuged at 20 000 × *g* for 12 min. The supernatants were filtered through two-layer Miracloth and centrifuged again, this time at 100 000 × *g* for 100 min. The supernatants were disposed of and the obtained pellets (containing microsomal fraction) were suspended in 0.1 M potassium phosphate buffer (pH 7.2). Aliquots of each suspension were used to measure microsomal protein content via Pierce™ BCA Protein Assay Kit (Thermo Fisher Scientific) and analyze phosphatidylcholine (PC) content as previously described by Klińska et al. (2019). PC content is equivalent to membrane concentrations in microsomal fractions. We show how both values relate to each other in **Supplementary Table 4**.

Enzyme Assays

For conducting enzyme assays we have utilized substrates both employed by the enzymes and with proven *in vitro* activity (Ståhl et al., 2004; Banaś et al., 2014; Jasieniecka-Gazarkiewicz et al., 2017). For LPCAT activity tests, following optimization, 5 nmol of exogenous sn-1-18:1-lysophosphatidylcholine and 5 nmol of exogenous [^{14}C]18:2-CoA were used with aliquots of microsomal fractions equivalent to 0.05 nmol (both roots and rosettes) of endogenous PC (0.022 μg of microsomal protein). The reaction components were diluted in 100 μl of 100 mM potassium buffer (pH 7.2). Addition of microsomal fraction was treated as the beginning of the reaction, which lasted for 30 min, and was conducted in 30°C. The reaction was terminated by addition of 375 μl of chloroform:methanol (1:2; v:v), 5 μl of glacial acetic acid, 125 μl of chloroform and 125 μl of water. Chloroform fraction was separated by centrifugation and transferred to a new tube. Extracts were then separated on silica gel 60 plates (Merck) utilizing thin-layer chromatography (TLC) principles in a glass chamber containing chloroform:methanol:acetic acid:water (90:15:10:2,5; v:v:v:v). The product of the reaction ([^{14}C]-PC was visualized and quantified with electronic autoradiography (Instant Imager, Packard Instrument Co.).

AcylCoA:lysophosphatidylethanolamine acyltransferase activity tests were conducted and assessed in similar fashion, only instead of sn-1-18:1-lysophosphatidylcholine, sn-1-18:1-lysophosphatidylethanolamine was used, and microsomal fraction concentration went up to 0.5 nmol (0.22 μg of microsomal protein for both roots and rosettes) of endogenous PC per assay. The desired product was not [^{14}C]-PC, but [^{14}C]-PE.

Phospholipid:diacylglycerol acyltransferase activity assays were conducted in a slightly different manner. 18 h before the planned activity assays aliquots of 12 nmol of microsomal fractions were lyophilized (Heto PowerDry LL3000 Freeze Dryer, Thermo Electron Corporation). 5 nmol of sn-1-18:1-sn-2-[^{14}C]18:2-PE and 5 nmol of sn-1,2-18:1-diacylglycerol for each assay were diluted in benzene and added to lyophilized microsomal fraction. The benzene was then evaporated under nitrogen, and 100 µl of 100 mM potassium buffer (pH 7.2) was added (beginning of the reaction). The reaction lasted for 2 h in 30°C. The reaction was terminated as described above for LPCAT activity. Reagent-containing chloroform extracts were separated by TLC on silica gel 60 plates with solvent system of hexane:diethyl ether:acetic acid (70:30:1; v:v:v:v). The product, which was [^{14}C]-TAG, was visualized and quantified with electronic autoradiography.

Relative Expression Analysis

Before the experiments, primers for qPCR were designed (**Supplementary Table 2**) for the following genes: *ACT2* (At3g18780), *PP2A* (At1g69960), *LPCAT1* (At1g12640), *LPCAT2* (At1g63050), *LPEAT1* (At1g80950), *LPEAT2* (At2g45670), *PDAT1* (At5g13640), *ATG8a* (At4g16520). Heat-stressed or non-stressed leaves of 3-week-old Arabidopsis grown *in vitro* were flash-frozen in liquid nitrogen. Total RNA was extracted from samples with GeneMatrix Universal RNA Purification Kit (EurX). RNA was then incubated with dsDNase (Thermo Fisher Scientific) to remove genomic DNA and then cDNA was synthesized with Maxima First Strand cDNA Synthesis Kit for RT-qPCR (Thermo Fisher Scientific). Maxima SYBR Green/ROX qPCR Master Mix (2×; Thermo Fisher Scientific) was used for qPCR analysis. qPCR measurements were conducted in QuantStudio™ 3 Real-Time PCR System (Applied Biosystems). All procedures were performed according to the manufacturers' instructions. The acquired results were analyzed employing the $2^{-\Delta\Delta CT}$ algorithm (Winer et al., 1999).

RESULTS

AtPDAT1 Overexpression Prolongs *A. thaliana* Flowering and Delays Senescence

We began our journey into investigating *At*PDAT1 by studying phenotypic differences between selected *pdat1* knockout mutants and *PDAT1*-overexpressing lines, as well as wild-type *Arabidopsis thaliana*. After 48 h vernalization, the seeds were planted into soil and observed while growing under assigned standard conditions (23°C, 16 h light/8 h dark photoperiod, 60% humidity). Key plant lifecycle events which were examined under utmost scrutiny were: appearance of the first flower buds (known as 0 DAF – day after flowering), opening of the first flower, yellowing of the first rosette leaf, yellowing of the last leaf in the rosette and cessation of flowering (all flowers of the plant becoming siliques). The obtained results are presented in **Figure 1** and **Supplementary Table 3**.

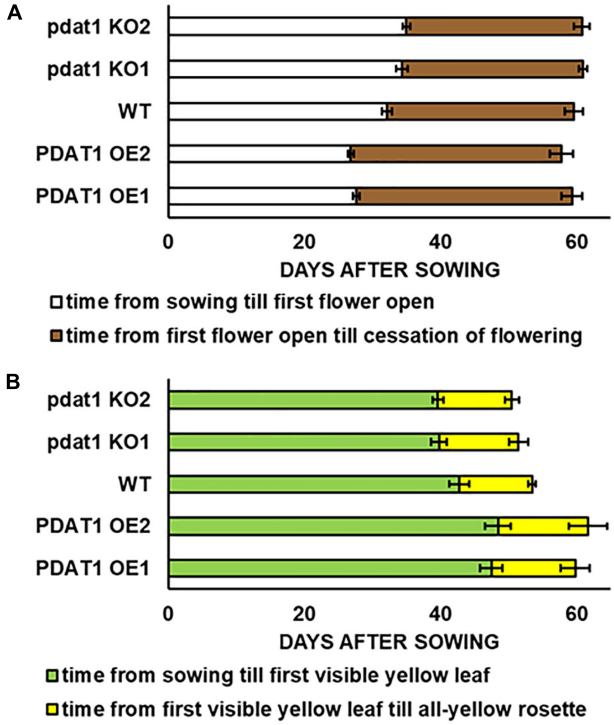

FIGURE 1 | Differences in length of *Arabidopsis thaliana* lifecycle stages: time of flowering **(A)** and rosette senescence **(B)**, measured in days after sowing between wild-type (WT), *PDAT1*-overexpressing lines (PDAT1 OE1 and OE2) and *pdat1* knockout lines (pdat1 KO1 and KO2). Error bars indicate standard deviations (SD) between biological replicates ($n = 6$).

Contrary to our expectations, there was no drastic difference between wild-type and *pdat1* knockout lines generative lifecycle events. Wild-type and mutant lines went through the main milestones in flower development at similar points in time (they occurred at similar days after sowing), from first appearance of flower buds, through first flower opening to cessation of flowering, understood as all flowers on a single plant becoming siliques. *PDAT1*-overexpressing lines, on the other hand, began flowering significantly earlier than control, but ceased to produce flowers around the same time as wild-type and mutant lines. Their generative lifecycle was thus effectively longer. The wild-type plants were also visibly smaller than *PDAT1*-overexpressing plants (**Figure 2**).

Both the knocking-out and overexpression of *PDAT1*, influenced the advancement of Arabidopsis leaves yellowing (**Figure 1**). Lines with knockout of *pdat1*, entered senescence earlier than wild-type and had an all-yellow leaves rosette sooner. Overexpression of the gene, on the other hand, retarded plant aging and resulted in *PDAT1*-overexpressing plants going through the appearance of the first yellow leaf in the rosette at average 5 or 6 days later than wild-type (depending on the *PDAT1*-overexpressing line) and exhibiting an all-yellow leaves rosette 6 or 8 days after wild-type, on average. Therefore, *PDAT1* expression level acts on Arabidopsis senescence and lifespan.

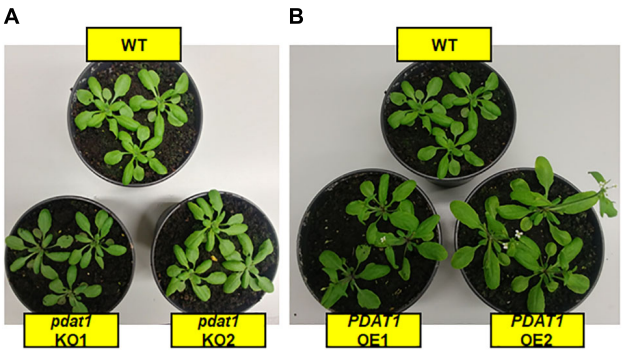

FIGURE 2 | Cultivation of studied *Arabidopsis thaliana* lines in pots, 4 weeks after sowing. Panel **(A)** shows *pdat1* knockout lines in comparison to wild-type control, while panel **(B)** shows the same wild-type control with *PDAT1*-overexpressing lines.

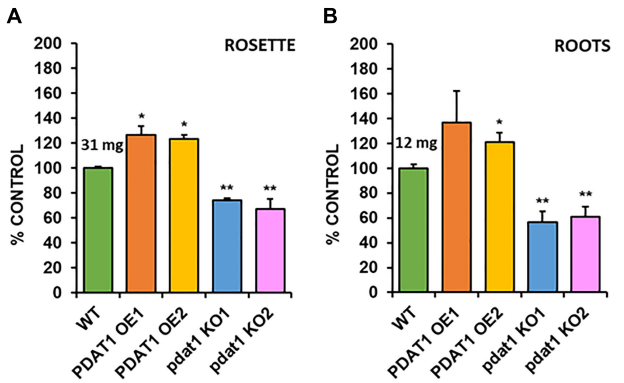

FIGURE 3 | Differences in rosette **(A)** and root **(B)** fresh weight of *Arabidopsis thaliana* seedlings between wild-type (WT, treated as control), *PDAT1*-overexpressing lines (PDAT1 OE1 and OE2) and *pdat1* knockout lines (pdat1 KO1 and KO2). The measurements were taken 4 weeks after planting seeds *in vitro*. Mean weight of each control is written above the bar representing it. Error bars indicate standard deviations (SD) between 3 average weights of 3 groups of 10 pooled seedlings ($n = 3$). Single asterisks (*) indicate significant difference between means in comparison to control (WT) in a two-tailed Student's *t*-test at $p < 0.05$ and double asterisks (**) at $p < 0.01$.

Overexpression and Knockout of *AtPDAT1* Influence Plant Rosette and Root Weight *in vitro*

In order to check the effect, which both *PDAT1* overexpression and *pdat1* knockout would have on plant size (weight), we cultivated *A. thaliana* lines *in vitro* in assigned standard conditions, described in the previous chapter. Subsequently, we measured the fresh weight of their rosettes and roots after 4 weeks had passed (**Supplementary Figure 1** contains photos of the cultivation at 3 weeks). The rosettes of *PDAT1*-overexpressing Arabidopsis lines weighed significantly more than wild-type control (126 and 123% of the control weight; **Figure 3A**). Clear difference was also observed in *pdat1* mutants, which weighed 67 and 74% of control weight, depending on the mutant line. The differences were also significant in roots (**Figure 3B**), especially between *pdat1* knockout plants and control, since the *pdat1* mutant Arabidopsis had significantly lower root weight at 56 and 61% of the weight of control's roots. No trends in regard to total fatty acid composition were observed (**Supplementary Figure 2**). In TAG there was a slight decrease in molar proportion of 18:3 in *pdat1* knockout lines (**Supplementary Figure 3**), which would be in accordance with PDAT1's specificity toward unsaturated fatty acids.

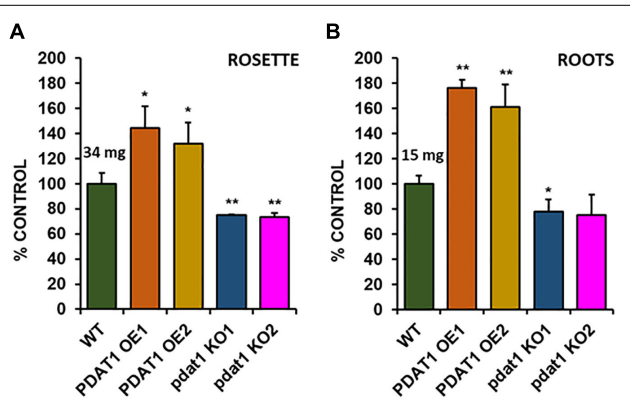

FIGURE 4 | Comparison of wild-type (WT), *PDAT1*-overexpressing (PDAT1 OE1 and OE2) and *pdat1* knockout lines (pdat1 KO1 and KO2), when exposed to 2 h 40°C heat stress at 3-week-old and then placed for one more week in standard conditions. Fresh weight of either rosettes **(A)** or roots **(B)** is compared. Mean weight of each control (WT) is written above the bar representing it. Error bars indicate standard deviations (SD) between 3 average weights of 3 groups of 10 pooled seedlings ($n = 3$). Single asterisks (*) indicate significant difference between means in comparison to control (WT) in a two-tailed Student's *t*-test at $p < 0.05$ and double asterisks (**) at $p < 0.01$.

AtPDAT1 Influences Arabidopsis Fitness When Subjected to Stress Factors

Because of the previous experiment's outcome we decided to test the investigated Arabidopsis lines in stress conditions, to see, if *PDAT1* overexpression or knockout were influencing plant's resilience to hostile environmental conditions. The first series of experiments we designed focused on short-term heat stress. In our experiment 3-week-old Arabidopsis seedlings grown *in vitro* in optimal temperature (23°C) were exposed to heat for 2 h (40°C, 60% humidity). After the shock treatment, plants were placed back into optimal temperature, where they recovered for 7 days (**Supplementary Figure 4**). Then we proceeded to measure the fresh weight of all investigated plants' rosettes (**Figure 4A**) and roots (**Figure 4B**).

Rosettes of wild-type (**Figure 4A**) experienced a small boost in comparison with 4-week-old seedlings, grown only in optimal temperature (**Figure 3A**). Heat-shocked knockout lines' rosettes also weighed more than those grown in optimal temperature, but their weight in relation to the stressed control mirrored optimal conditions. However, that was not true for root measurements (**Figure 4B**). The weight of *pdat1* mutant roots constituted more percentage of the control than their

unstressed counterparts in previous experiment – 78 and 75% of control's root weight in comparison to 56 and 61% in optimal conditions. The biggest change comparing to unstressed Arabidopsis *in vitro* growth occurred in *PDAT1*-overexpressing plants' roots. The difference between them and control grew 40% in case of both overexpressing lines in comparison to optimal conditions. The weight divergence between wild-type and PDAT1-overexpressing plants increased also in case of rosettes (by 18% and 9% for particular lines). Total fatty acid composition was not affected by changes observed in the studied lines (**Supplementary Figure 5**). What distinguished the heat-shocked plants from the non-stressed ones was the TAG content, which increased in all of the studied lines (**Figure 5**). However, we could not discern any trends between the wild-type, the overexpressing lines and the mutant lines. Similarly, to non-stressed Arabidopsis, TAG of knockout lines contained lower mole percent of 18:3 in comparison to other studied plants (**Supplementary Figure 6**).

After short-term heat stress, we decided to subject our Arabidopsis lines to prolonged cold exposure. We selected 4°C as our testing cold temperature. Knowing, the plants would not germinate in 4°C, we first cultivated them in optimal temperature for 2 weeks (*in vitro*) and then placed them in the cold chamber for the next 2 weeks. Both wild-type control and *pdat1* knockout reacted extremely to the stress factor, experiencing arrested growth and loss of pigment (**Figures 6A–C**). *PDAT1*-overexpressing lines were the most resilient, continuing to grow, with most or all of the rosette leaves preserving the green color. The measured fresh weight of rosette leaves and roots reflected that (**Figures 6D,E**). While both rosettes and roots of the *pdat1* mutant lines weighed significantly less than control's rosettes and roots, the *PDAT1*-overexpressing lines' rosettes weighed on average 3.75 and 4.2 times more and roots average weight was 5.41 and 7.06 times more than their wild-type counterparts.

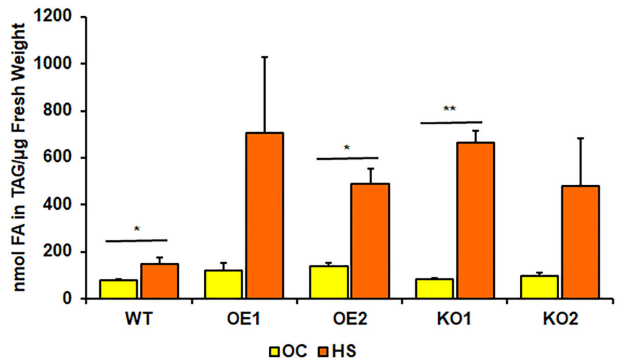

FIGURE 5 | Comparison of triacylglycerol (TAG) content in rosettes of wild-type (WT), *PDAT1*-overexpressing lines (OE1 and OE2) and *pdat1* knockout lines (KO1 and KO2), measured as nmol of all fatty acids in the TAG fraction per µg of fresh weight. The comparison was made between 4-week-old Arabidopsis seedlings grown only in optimal conditions (OC) and seedlings which were subjected to 2-h heat-shock at 40°C 3 weeks after sowing (HS). Error bars indicate standard deviations (SD) between 3 means of biological replicates ($n = 3$). Asterisks indicate significant difference in TAG content between means of the same line in optimal conditions (OC) and after heat stress (HS) in a two-tailed Student's *t*-test. Single asterisks (*) indicate significant difference at $p < 0.05$ and double asterisks (**) at $p < 0.01$.

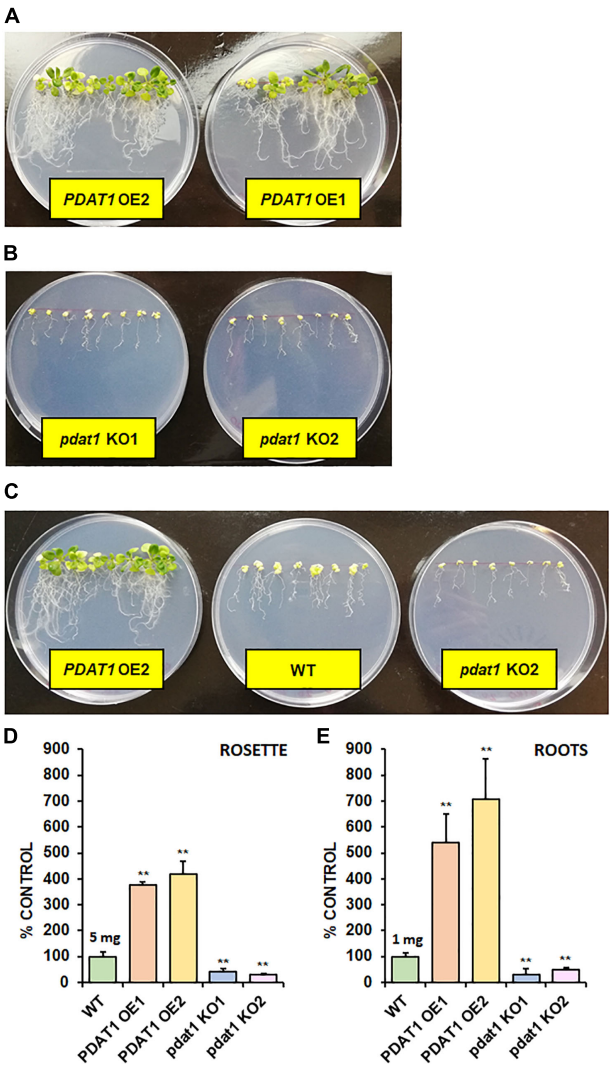

FIGURE 6 | The effect of 2-week 4°C cold stress on 4-week-old seedlings of *Arabidopsis thaliana* lines cultivated *in vitro*. Panel **(A)** presents two *PDAT1*-overexpressing lines, panel **(B)** presents two *pdat1* knockout lines, and panel **(C)** presents, from left to right: *PDAT1*-overexpressing line (*PDAT1* OE2), wild-type control (WT) and *pdat1* knockout line (*pdat1* KO2). Diameter of the Petri dishes used is 90 mm. Fresh weight of the cold-subjugated Arabidopsis lines was in both rosettes **(D)** and roots **(E)**. Mean weight of each control (WT) is written above the bar representing it. Error bars indicate standard deviations (SD) between 3 average weights of 3 groups of 10 pooled seedlings ($n = 3$). Single asterisks (*) indicate significant difference between means in comparison to control (WT) in a two-tailed Student's *t*-test at $p < 0.05$ and double asterisks (**) at $p < 0.01$.

Heat Stress Stimulates *PDAT1* Expression in Arabidopsis

Some of the Arabidopsis plants, which were subjected to short-term heat stress were not given 1 week to recover, but their rosettes were instead harvested 2 h after the high-temperature

treatment and used for relative expression measurements. For comparison, relative expression was also measured in rosettes of 3-week-old seedlings, which were grown with heat-stressed plants, but not exposed to 2 h in 40°C.

Taking into the account just wild-type lines, it turns out, that *PDAT1* is expressed more than three times more in rosettes of seedlings, which were cultivated in 40°C for 2 h (**Figures 7A,B**) in comparison to non-stressed wild-type. It means, that enduring a short period of heat exposure triggers tripling of *PDAT1* expression in Arabidopsis plants.

Investigated *PDAT1*-overexpressing lines exhibited a monumental increase in *PDAT1* relative expression in comparison to wild-type (**Figures 7C,D**), just in optimal conditions. The increase of *PDAT1* expression between *PDAT1*-overexpressing lines in optimal conditions versus the same lines after heat stress was noticeable and statistically significant in one *PDAT1*-overexpressing line in reference to *ACT2* and in both lines in reference to *PP2A* (**Figures 7A,B**).

ATG8a Post-heat-Stress Expression Is Not Conditional on *PDAT1* Expression

Since plant stress response stimulates autophagocytic process, we decided to measure relative expression levels of *ATG8a* gene,

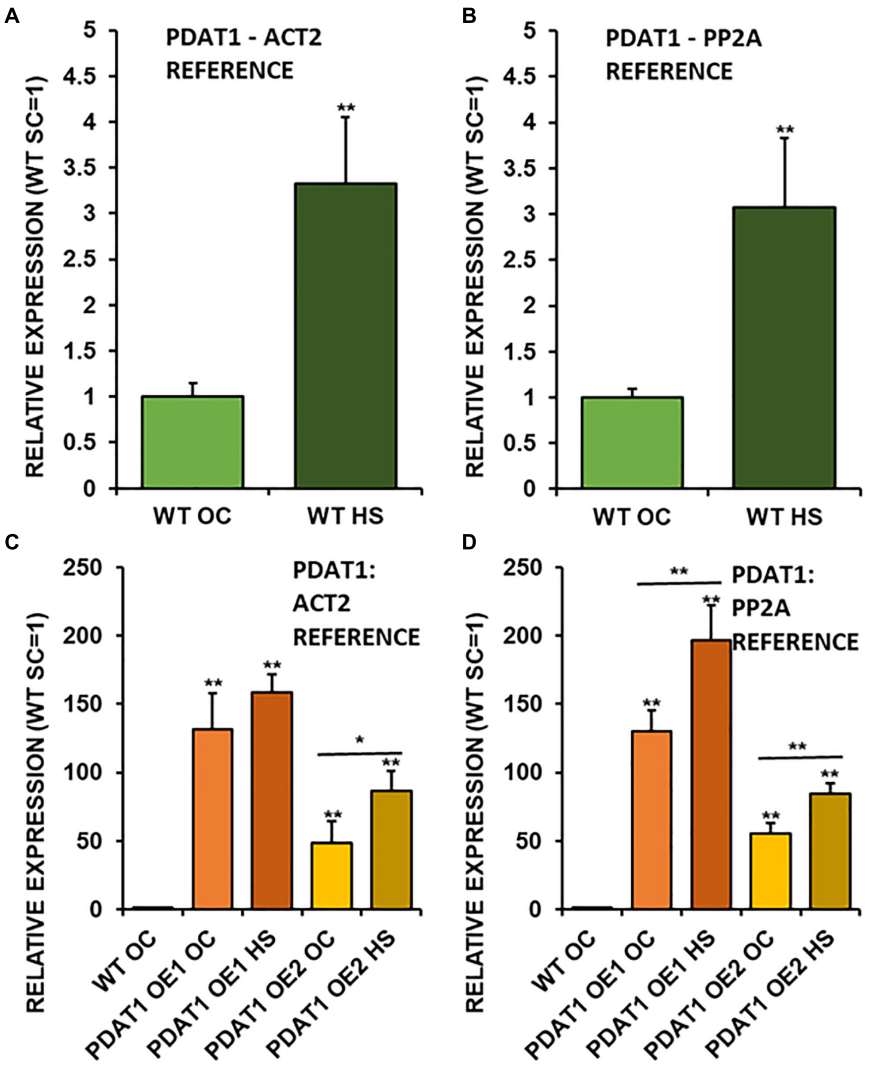

FIGURE 7 | Relative expression of *AtPDAT1* in 3-week old rosettes of *Arabidopsis thaliana* in comparison to *ACT2* housekeeping gene **(A,C)** and *PP2A* housekeeping gene **(B,D)** as determined by RT-qPCR. First two charts **(A,B)** present difference in *AtPDAT1* expression between wild-type (WT) in optimal conditions (OC) and wild-type after heat stress (HS). Charts **(C,D)** present how relative *AtPDAT1* expression in wild-type in optimal conditions (WT OC) compares to *AtPDAT1* relative expression in *AtPDAT1*-overexpressing lines in optimal conditions (PDAT1 OE1 SC, PDAT1 OE2 SC) and *AtPDAT1*-overexpressing lines after heat stress (PDAT1 OE1 HS, PDAT1 OE2 HS). Error bars indicate standard deviations (SD) between biological replicates ($n = 3$). Double asterisks (**) above error bars indicate significant difference between means in comparison to control (WT OC) in a two-tailed Student's *t*-test at $p < 0.01$. Single asterisks (*) or double asterisks (**) above horizontal lines above two columns representing the same Arabidopsis line subjected to different growth conditions indicate significant difference between means of the results in in a two-tailed Student's *t*-test at $p < 0.05$ and $p < 0.01$, respectively.

which encodes a protein regarded as essential in autophagy (Bu et al., 2020). *ATG8*a expression levels were measured in wild-type plants, *PDAT1*-overexpressing plants and pdat1 knockout mutants, both those cultivated only in optimal temperature for 3 weeks and those exposed to 2 h heat stress with 2 additional hours after shock treatment.

ATG8a relative expression was on the same level and not statistically different in any of the lines cultivated without heat-shock treatment (**Figure 8**). In comparison, all *ATG8*a expression levels in every Arabidopsis line subjected to high temperature were significantly multiple times higher than optimal-temperature-only wild-type control. The highest *ATG8a* relative expression in heat-exposed plants was found in *PDAT1*-overexpressing line 2 followed by expression in *pdat1* knockout mutant line 2, then wild-type, then *pdat1* knockout line 1 with the lowest ATG8a expression after heat exposure presented by *PDAT1*-overexpressing line 1. Expression in all plants subjected to heat-shock was on similar level. Based on those results, it seems that *PDAT1* overexpression or knockout in *A. thaliana* does not correlate with higher or lower expression of autophagy-related *ATG8a* gene, neither in standard growth conditions nor after 2 h following the exposure to high-temperature stress.

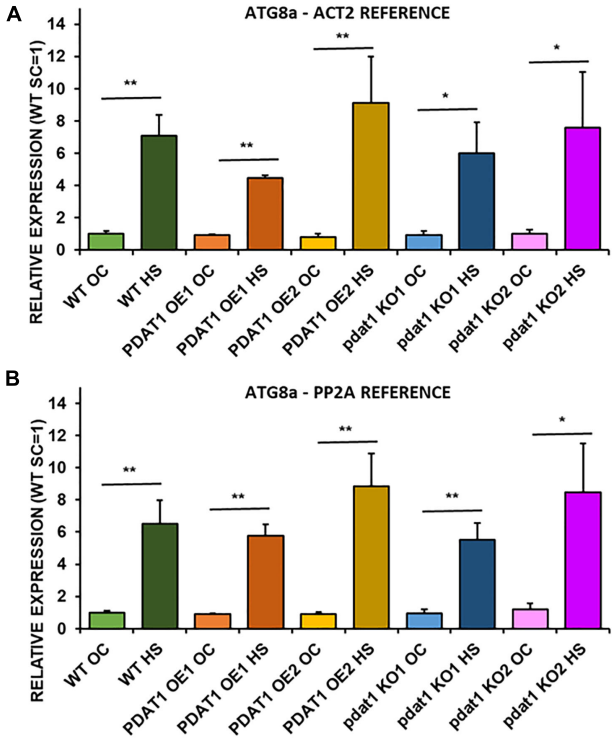

FIGURE 8 | Relative expression of *ATG8a* in 3-week old rosettes of *Arabidopsis thaliana* in comparison to *ACT2* housekeeping gene **(A)** and *PP2A* housekeeping gene **(B)** as determined by RT-qPCR. WT indicates wild-type line (control), PDAT1 OE1 indicates *AtPDAT1*- overexpressing line 1, PDAT1 OE2 indicates *AtPDAT1*- overexpressing line 2, pdat1 KO1 indicates line 1 with *pdat1* knockout and pdat1 KO2 indicates line 2 with *pdat1* knockout. OC refers to seedlings grown only in optimal conditions, whereas HS refers to seedlings, which were subjected to 2 h heat stress. Error bars indicate standard deviations (SD) between biological replicates ($n = 3$). Asterisks indicate significant difference in relative *ATG8a* expression between means of the same line in optimal conditions (OC) and after heat stress (HS) in a two-tailed Student's *t*-test. Single asterisks (*) indicate significant difference at $p < 0.05$ and double asterisks (**) at $p < 0.01$.

AtPDAT1 Overexpression Lines Present Higher LPLAT Activity in Microsomal Fractions

Phospholipid:diacylglycerol acyltransferase enzymes are intertwined with LPLAT enzymes, since products of forward reactions of LPLAT enzymes are substrates for PDAT in DAG acylation and one of the products of PDAT action (LPL) is a substrate of LPLAT enzymes. For that reason, we decided to conduct *in vitro* assays using microsomal fractions from rosettes and roots of wild-type and *PDAT1*-overexpressing Arabidopsis cultures. First, we measured PDAT endogenous activity in root microsomal fractions from both wild-type control and *PDAT1*-overexpressing lines to confirm that those lines showed higher enzyme activity *in vitro*. PDAT1 activity in roots (**Figure 9A**; **Supplementary Figure 7A**) correlated with *PDAT1* relative expression measurements in rosettes, even though plants for both experiments were grown in different conditions (**Figures 7C,D**). *PDAT1* overexpression in roots was confirmed in its endogenous enzyme activity, which was 6.7 and 3.1-fold higher in *PDAT1*-overexpressing lines than in wild-type control.

With higher activity in *PDAT1* OE confirmed, we advanced to LPLAT activity measurements. Since phosphatidylcholine (PC) and phosphatidylethanolamine (PE) are the most abundant phospholipids in plants, we concentrated on LPCAT and LPEAT activity of the microsomal fractions. We measured the analyzed enzyme's activity as amount of product (an appropriate phospholipid) *de novo* synthesized in an *in vitro* reaction utilizing the amount of microsomal fraction containing 1 mg of microsomal protein during 1 h. Of the two LPLAT, LPCAT turned out to be the more active enzyme in microsomal fractions from both wild-type and *PDAT1*-overexpressing line (after optimizing reactions we used aliquots of root microsomal fraction equivalent to 0.05 nmol of endogenous PC for LPCAT assays and equivalent to 0.5 nmol of endogenous PC for LPEAT assays). LPCAT was significantly more active in *PDAT1*-overexpressing line 1 roots (7.7 times) and rosettes (by 27%) and *PDAT1*-overexpressing line 2 (6.3 times) roots and rosettes (by 52%) (**Figures 9B,D**; **Supplementary Figures 7B,D**). Our preliminary studies of microsomal LPLAT activity in wild-type and *PDAT1*-overexpressing line 2 (**Supplementary Figure 8**) showed higher LPCAT activity in rosettes of PDAT1-overexpressing line 2 and lower LPCAT activity in the same line in roots. However, LPCAT activity was always higher in comparison to wild-type control.

The investigated LPEAT activity was also higher in microsomal fraction from PDAT1-overexpressing lines in both rosettes and roots (**Figures 9C,E**; **Supplementary Figures 7C,E**). The increase in LPEAT activity in rosettes was more pronounced reaching twice the activity of control in both PDAT1-overexpressing lines.

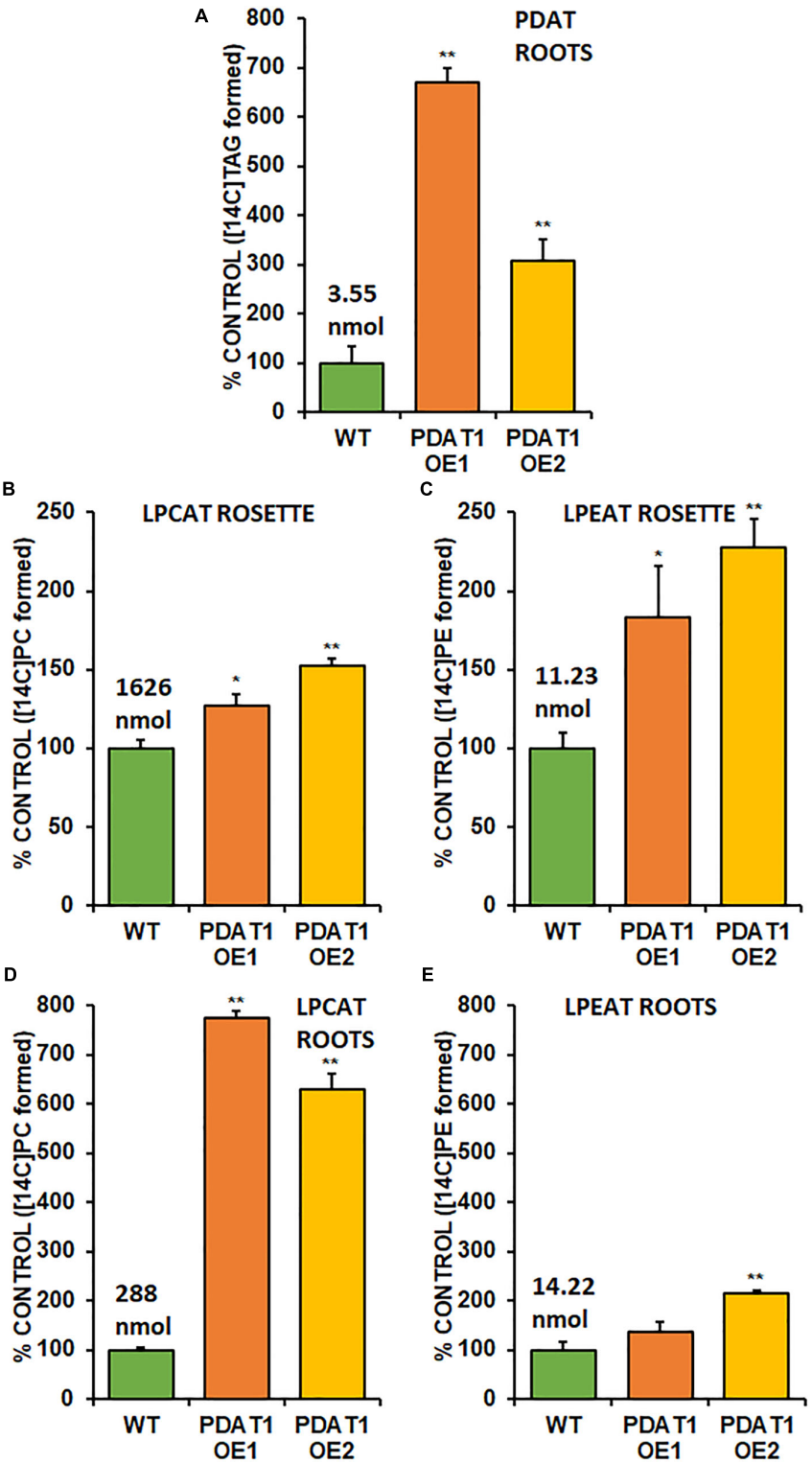

FIGURE 9 | Endogenous enzyme activity measured *in vitro* in root **(A,B,C)** and rosette **(D,E)** microsomal fractions from Arabidopsis wild-type control (WT) and *PDAT1*-overexpressing lines (PDAT1 OE1 and PDAT1 OE2). Comparison of enzyme activity of PDAT **(A)**, LPCAT **(B,D)**, and LPEAT **(C,E)** between the two lines. Values above the WT bars correspond to 100% activity for each chart measured as nmol of [14C] enzymatic activity product (TAG for PDAT, PC for LPCAT and PE for LPEAT) synthesized during 1 h reaction, utilizing microsomal fraction equivalent to 1 mg of microsomal protein. Error bars indicate standard deviations (SD) between biological replicates ($n = 3$). Single (*) or double (**) asterisks indicate significant difference between means in comparison to control (WT) in a two-tailed Student's *t*-test at $p < 0.05$ or at $p < 0.01$, respectively.

AtLPCAT2 Expression Doubles in *AtPDAT1* Overexpression Lines

Knowing how *PDAT1* overexpression affects LPLAT activity *in vitro*, we proceeded to analyze the relative expression of two *LPCAT* and two *LPEAT* isoenzymes (*LPCAT1*, *LPCAT2*, *LPEAT1* and *LPEAT2*) in rosettes of 3-week-old plants cultivated in optimal growth conditions *in vitro*, as well as in rosettes of 3-week-old plants harvested after 2 h heat stress, followed by 2 h in optimal conditions.

We first measured relative expression of *LPCAT1* in both optimal and heat-shock conditions throughout all lines investigated in this study (**Figure 10**). The expression of this gene did not change in any lines in non-stressed plants except for it being lower than control in *PDAT1*-overexpressing line 1 with *PP2A* as a reference. In stress conditions, a significant difference was found between *PDAT1*-overexpressing line 1 and WT with one of the reference genes (*ACT2*). Those differences, however, were not much lower than in WT and they were not found to be significant with the other reference gene nor were they confirmed by expression measured in *PDAT1*-overexpressing line 2. The second *LPCAT* isoenzyme's expression turned out to be much more diverse (**Figure 11**). In optimal conditions *LPCAT2* expression was more than two times higher than control in both studied *PDAT1*-overexpressing lines, and with both reference genes. It was also significantly lower in *pdat1* mutant line 1 with both *ACT2* and *PP2A*. Expression of *LPCAT2* grew in all the lines in stress conditions, and was still significantly higher in *PDAT1*-overexpressing lines than in wild-type. *LPEAT1* relative expression (**Figure 12**) showed no difference between the lines in neither plants subjected to non-stress and stress conditions. The enzyme's expression increased, however, between plants grown in optimal conditions and plants that endured heat-shock treatment, in all the studied lines. Its isoenzyme, *LPEAT2*, did not have increased expression in *PDAT1*-overexpressing lines neither (**Figure 13**). In stress conditions *LPEAT2* expression was slightly (yet significantly with *PP2A*) lower after heat-shock than in optimal conditions. Non-stressed *pdat1* mutant lines were exhibiting marginal increase in *LPEAT2* expression.

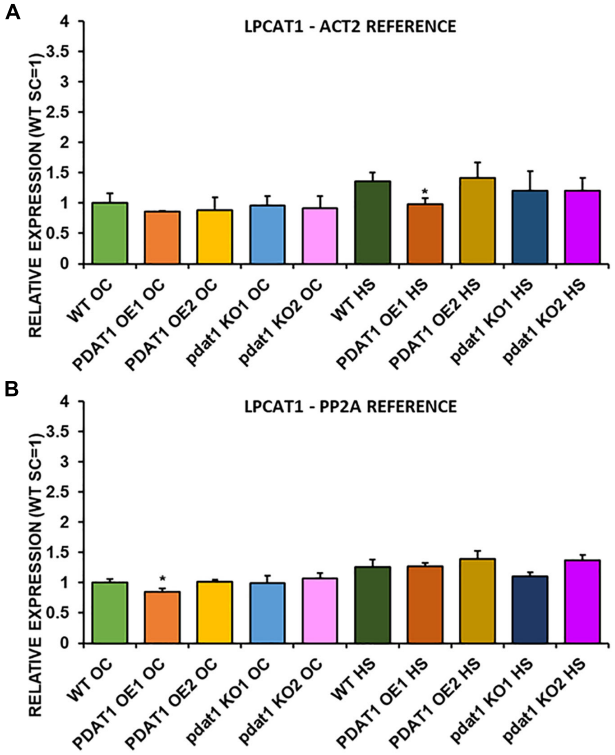

FIGURE 10 | Relative expression of *LPCAT1* in 3-week old rosettes of *Arabidopsis thaliana* in comparison to *ACT2* housekeeping gene **(A)** and *PP2A* housekeeping gene **(B)** as determined by RT-qPCR. WT indicates wild-type line (control), PDAT1 OE1 indicates *AtPDAT1*- overexpressing line 1, PDAT1 OE2 indicates *AtPDAT1*- overexpressing line 2, pdat1 KO1 indicates line 1 with *pdat1* knockout and pdat1 KO2 indicates line 2 with *pdat1* knockout. OC refers to seedlings grown only in optimal conditions, whereas HS refers to seedlings, which were subjected to 2 h heat stress. Error bars indicate standard deviations (SD) between biological replicates ($n = 3$). Single asterisks (*) above error bars indicate significant difference at $p < 0.05$ in a two-tailed Student's *t*-test between means of the tested line and the wild-type line grown in the same conditions (OC or HS).

DISCUSSION

Phospholipid:diacylglycerol acyltransferase (PDAT) still remains somewhat of an enigma within the enzymes involved in plant lipid biosynthesis. One of the reasons we decided to investigate it was to lift the veil on its mystery a bit more, to further our understanding of PDAT's role in plant metabolism. The enzyme's main function was naturally assumed to be connected with its enzymatic activity – production of TAG. However, hitherto reports on *PDAT* overexpression in Arabidopsis lead to a certain ambiguity. There are publications suggesting that *PDAT* overexpression in Arabidopsis translates to higher TAG content (Fan et al., 2013a,b). Transient expression of *PDAT* from *C. sativa* has also led to increase in TAG production in tobacco leaves (Yuan et al., 2017a). However, there are also publications demonstrating lack of TAG production increase in Arabidopsis' seeds with *PDAT* overexpression (Ståhl et al., 2004; Banaś et al., 2014). In this study, we have found that TAG content in leaves increased in all of the studied lines after heat-shock. Increased TAG accumulation in the stressed plant leave tissue was shown before (Yang and Benning, 2018). However, there were no outright tendencies as to TAG accumulation and *PDAT1* overexpression and knockout. In stressed *pdat1* mutant lines DGAT enzymes may overcompensate for lack of PDAT1 activity, which would be in agreement with previous findings (Zhang et al., 2009).

Amongst the mixed reports concerning *PDAT* overexpression affecting TAG content, it was shown that even when *PDAT* overexpression in Arabidopsis did not result in elevated TAG levels, it produced plants with increased growth rate and weight in comparison to wild-type (Banaś et al., 2014). Progeny of those *PDAT1* overexpression plants were used in our study and resulted in plants, which were visibly bigger than wild-type control. What is more, T-DNA insert *pdat1* mutants genotyped and selected by us, which did not express the studied gene, were

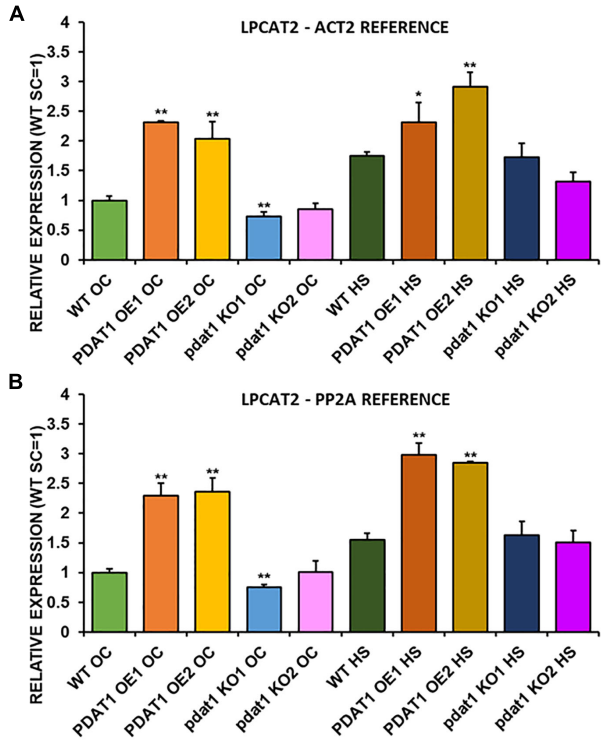

FIGURE 11 | Relative expression of *LPCAT2* in 3-week old rosettes of *Arabidopsis thaliana* in comparison to *ACT2* housekeeping gene **(A)** and *PP2A* housekeeping gene **(B)** as determined by RT-qPCR. WT indicates wild-type line (control), PDAT1 OE1 indicates *AtPDAT1*- overexpressing line 1, PDAT1 OE2 indicates *AtPDAT1*- overexpressing line 2, pdat1 KO1 indicates line 1 with *pdat1* knockout and pdat1 KO2 indicates line 2 with *pdat1* knockout. OC refers to seedlings grown only in optimal conditions, whereas HS refers to seedlings, which were subjected to 2 h heat stress. Error bars indicate standard deviations (SD) between biological replicates ($n = 3$). Single (*) and double (**) asterisks above error bars indicate significant difference at $p < 0.05$ and at $p < 0.01$, respectively, in a two-tailed Student's *t*-test between means of the tested line and the wild-type line grown in the same conditions (OC or HS).

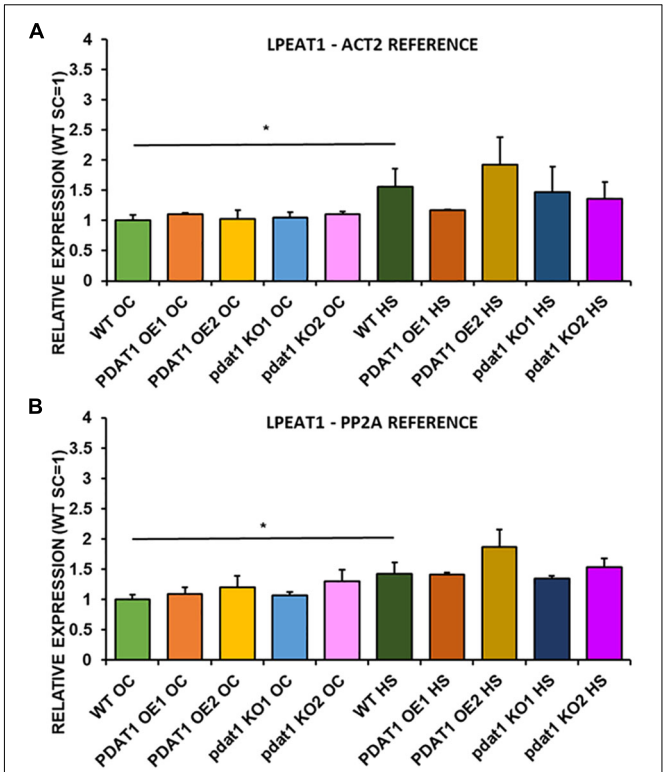

FIGURE 12 | Relative expression of *LPEAT1* in 3-week old rosettes of *Arabidopsis thaliana* in comparison to *ACT2* housekeeping gene **(A)** and *PP2A* housekeeping gene **(B)** as determined by RT-qPCR. WT indicates wild-type line (control), PDAT1 OE1 indicates *AtPDAT1*- overexpressing line 1, PDAT1 OE2 indicates *AtPDAT1*- overexpressing line 2, pdat1 KO1 indicates line 1 with *pdat1* knockout and pdat1 KO2 indicates line 2 with *pdat1* knockout. OC refers to seedlings grown only in optimal conditions, whereas HS refers to seedlings, which were subjected to 2 h heat stress. Error bars indicate standard deviations (SD) between biological replicates ($n = 3$). Single (*) asterisks above horizontal lines indicate significant difference in a two-tailed Student's *t*-test at $p < 0.05$ between means of the results two columns at the border of the horizontal line represent.

smaller than wild-type. This phenomenon resulted in heightened rosette and root fresh weights of *PDAT1*-overexpressing line and lower equivalent weights of *pdat1* mutant organs, in comparison to control. The level of *PDAT1* expression in a particular Arabidopsis line correlated with the plants aging rate with *PDAT1* overexpression resulting in a plant lifecycle with delayed senescence, whereas *pdat1* knockout aged faster. One possible explanation of *PDAT1*'s role in aging process may be connected to lysophosphatidylethanolamines (LPE). PDAT as a TAG-producing enzyme preferentially utilizes PC and PE as substrates (**Figure 14**). When PDAT transfers an acyl group from the above-mentioned phospholipids to DAG, what is left as by-products are lysophospholipids: lysophosphatidylcholine (LPC) and LPE. LPE have been long known as plant senescence retardants (Farag and Palta, 1993). Addition of exogenous LPE induces expression of phenylalanine ammonia lyase and acid invertase, pathogenesis-related proteins, which in turn results in anabolic lignin formation and its deposition to cell walls (Cowan, 2009; Hong et al., 2009). *PDAT1* overexpression introduced in Arabidopsis might have resulted in an increase of LPE amount in those plants, which caused its elicitor action, leading to the observed delayed senescence. The opposite might have been true for *pdat1* mutant, which might have had lower LPE amount than wild-type cultivated in the same environmental conditions. Different LPE amounts in different lines may have also contributed to the changes observed in the fresh weight measurements of 4-week-old plants *in vitro*.

One of the proposed possible roles of PDAT in plant metabolism concerns the enzyme being an acyl group donor utilizing membrane phospholipids (PC and PE). PDAT would thus be responsible for regulating the fatty acid composition of cytosolic membrane lipids – which is linked with plant reaction to stress factors (Dahlqvist et al., 2000; Banaś et al., 2014). PDAT's connection with plant stress response is what we have explored in our research. When we subjected our tested lines to short-term heat exposure followed by a period of 1-week recovery, we

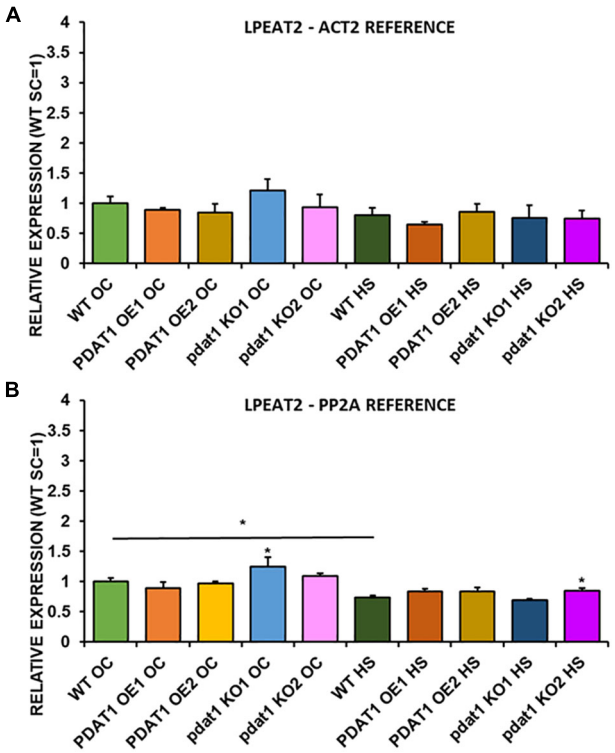

FIGURE 13 | Relative expression of *LPEAT2* in 3-week old rosettes of *Arabidopsis thaliana* in comparison to *ACT2* housekeeping gene **(A)** and *PP2A* housekeeping gene **(B)** as determined by RT-qPCR. WT indicates wild-type line (control), PDAT1 OE1 indicates *AtPDAT1*- overexpressing line 1, PDAT1 OE2 indicates *AtPDAT1*- overexpressing line 2, pdat1 KO1 indicates line 1 with *pdat1* knockout and pdat1 KO2 indicates line 2 with *pdat1* knockout. OC refers to seedlings grown only in optimal conditions, whereas HS refers to seedlings, which were subjected to 2 h heat stress. Error bars indicate standard deviations (SD) between biological replicates ($n = 3$). Single (*) asterisks above error bars indicate significant difference at $p < 0.05$ in a mean difference two-sided test between the tested line and wild-type line grown in the same conditions (OC or HS). Single (*) asterisks above horizontal lines indicate significant difference in a two-tailed Student's *t*-test at $p < 0.05$ between means of the results two columns at the border of the horizontal line represent.

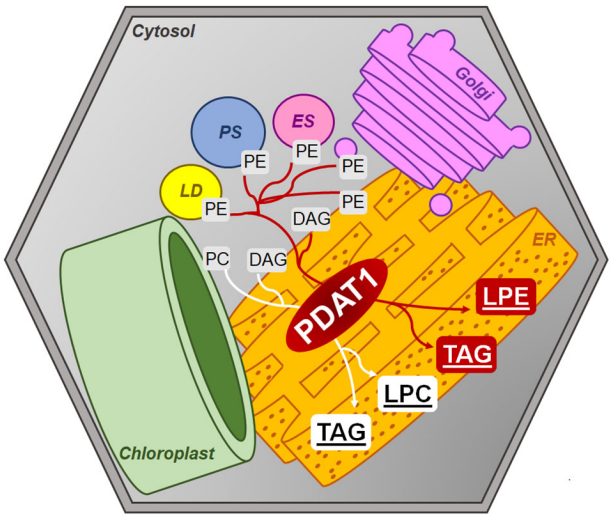

FIGURE 14 | Postulated PDAT1 enzymatic action within plant cells' cytosolic membranes. DAG, diacylglycerol; ER, endoplasmic reticulum; ES, endosome; Golgi, Golgi apparatus; LD, lipid droplet; LPC, lysophosphatidylcholine; LPE, lysophosphatidylethanolamine; PC, phosphatidylcholine; PE, phosphatidylethanolamine; PS, peroxisome; TAG, triacylglycerol.

noticed a growth boost in *PDAT1*-overexpressing line and wild-type control in comparison to plants of similar age, which were not exposed to the heat shock. This may be due to activation of the stress response mechanisms of plants, which were set off by the 2-h submission to adverse temperature. Knockout lines of *pdat1* in our study exhibited increase in root mass after stress, but not much difference in rosette weight in comparison to control in particular temperature. In previous reports concerning *pdat1* knockout lines response to heat stress, heat has been found to impede *pdat1* knockout mutants in Arabidopsis from accumulating TAG after stress (Mueller et al., 2017). We also show that short exposure to high temperature increases *PDAT1* expression in wild-type plants by at least a 3-fold. It was shown that CaMV 35S promoter-driven expression of a transgene can increase in *Nicotiana benthamiana* leaves after exposing them to short-term 50°C stress, but the increase went down after several hours and constituted at most 1.33 of the relative expression in non-stressed leaves (Boyko et al., 2010). In our study *PDAT1* expression also increases in *PDAT1*-overexpressing lines after heat-treatment, despite the already present *PDAT1* mRNA abundance due to overexpression. This may partly correlate to further weight increase of *PDAT1*-overexpressing lines after high temperature stress. By far the biggest difference in fresh weight between the studied Arabidopsis lines was observed, when 2-week-old seedlings were transferred to a cold chamber and grown there for two additional weeks. Both the wild-type and the *pdat1* mutant did not endure the harmful conditions well, being much smaller than plants grown in optimal conditions and losing pigment, which would foil their ability to bounce back, if transferred back to 23°C. Still, *pdat1* mutants' leaves and roots weighed less than the wild-type, which means they were even less tolerant to the cold than the control. The *PDAT1*-overexpressing lines were much less sensitive to the cold, with their rosettes weighing four times as much and roots weighing five to seven times as much as the wild-type. Most of the *PDAT1*-overexpressing plants retained the green color, an indication of their kept ability to photosynthesize carbohydrates, which would possibly enable them to recover, if they were placed back in optimal conditions. The importance of *PDAT1* in cold stress has been previously reported in *Camelina sativa* (Yuan et al., 2017a). Low temperatures induced increased *PDAT1* expression by 6-fold (Yuan et al., 2017b), with particular isoforms expression, *CsPDAT1*-A and *CsPDAT1*-C, increasing by 3.5-fold and 2.5-fold, respectively (Yuan et al., 2017a). We have to remember, however, that our experiments were conducted *in vitro* and may not reflect how well *PDAT1* overexpression would facilitate better plant stress response in the natural environment. Further studies have to be performed to resolve these doubts.

As was mentioned above, LPE and LPC are the by-products of PDAT activity. Both are utilized by LPEAT and LPCAT enzymes to synthesize phospholipids. Thus, we had suspected, that in plants with *PDAT1* overexpression we would observe higher activity of LPEAT and LPCAT (being expressed more because of additional substrates available for their enzymatic action). There were no previous reports concerning this topic. Our research shows that indeed *PDAT1* overexpression in Arabidopsis leads to an increase in LPEAT and LPCAT activity in both rosette and root microsomal fractions. The increase in LPCAT activity in rosettes in comparison to control was not as profound as in other cases (but still statistically significant in *PDAT1*-overexpressing line 2) in the presented results, but our preliminary studies showed that activity to be 2.5 times higher. The differences may be due to different microsomal preparations used (that being said, microsomal fractions of a particular set of all the lines were prepared at the same time). The heightened microsomal LPCAT activity in *PDAT1*-overexpressing lines corresponds well with the double increase in *AtLPCAT2* relative expression calculated for the same lines. We also measured *LPEAT* expression *in vitro* and discovered that the relative expression of both *LPEAT* isoenzymes in the investigated *PDAT1*-overexpressing lines did not differ much from the control, which does not confirm the observed increase in microsomal LPEAT activity. This may be due to the different methods of cultivating plants for microsomal preparations and difference in the plants' age.

It was suggested, that PE-producing LPEAT enzymes may be connected with the regulation of the autophagy intensity (Jasieniecka-Gazarkiewicz et al., 2017). We decided to test, whether *PDAT1* overexpression or knockout would trigger increase or decrease in autophagocytic response, since PE is a major substrate for PDAT. *ATG8a* expression levels, which were measured in all lines subjected and not subjected to heat shock, are considered one of the markers for intensity of plant autophagy. Our findings showed that increase of *ATG8a* relative expression levels after high temperature exposure did not correlate with *PDAT1*-overexpression or *pdat1* knockout in Arabidopsis. These findings may mean that *PDAT1* overexpression's role in increasing plant fitness after stress does not have to be outright connected with plant autophagocytic response.

The precise reason why *PDAT1* accentuates plant stress response needs to be elucidated further, but its overexpression certainly increases plant's endurance through disadvantageous environmental conditions. Our research opens possibilities for genetic modification of crops to be more resilient to adverse environment through increased PDAT1 activity. Investigation of PDAT1's effect on different plant species should continue, in order to assess the benefits of such genetic modifications.

DATA AVAILABILITY STATEMENT

The original contributions presented in the study are included in the article/**Supplementary Material**, further inquiries can be directed to the corresponding author/s.

AUTHOR CONTRIBUTIONS

KD, KJ-G, and AB conceived and designed the research. AŁ, KD, and SK conducted the experiments. KD and AB analyzed the data. KD wrote the original draft of the manuscript. All authors reviewed and edited the final version.

FUNDING

The project was financed by the National Science Centre (NCN), Poland. Project number: UMO-2017/25/B/NZ3/00721.

ACKNOWLEDGMENTS

The authors would like to thank Anders S. Carlsson for providing *AtPDAT1* overexpression lines and Maciej Wróblewski for his help with preliminary research.

SUPPLEMENTARY MATERIAL

The Supplementary Material for this article can be found online at: https://www.frontiersin.org/articles/10.3389/fpls.2020.611897/full#supplementary-material

REFERENCES

Banaś, A., Dahlqvist, A., Ståhl, U., Lenman, M., and Stymne, S. (2000). The involvement of phospholipid:diacylglycerol acyltransferases in triacylglycerol production. *Biochem. Soc. Trans.* 28, 703–705. doi: 10.1042/BST0280703

Banaś, W., Carlsson, A. S., and Banaś, A. (2014). Effect of overexpression of PDAT gene on *Arabidopsis* growth rate and seed oil content. *J. Agric. Sci.* 6, 65–79. doi: 10.5539/jas.v6n5p65

Banaś, W., Sanchez Garcia, A., Banaś, A., and Stymne, S. (2013). Activities of acyl-CoA:diacylglycerol acyltransferase (DGAT) and phospholipid:diacylglycerol acyltransferase (PDAT) in microsomal preparations of developing sunflower and safflower seeds. *Planta* 237, 1627–1636. doi: 10.1007/s00425-013-1870-8

Bligh, E. G., and Dyer, W. J. (1959). A rapid method of total lipid extraction and purification. *Can. J. Biochem. Physiol.* 37, 911–917. doi: 10.1139/o59-099

Boyko, A., Molinier, J., Chatter, W., Laroche, A., and Kovalchuk, I. (2010). Acute but not chronic exposure to abiotic stress results in transient reduction of expression levels of the transgene driven by the 35S promoter. *N. Biotechnol.* 27, 71–77. doi: 10.1016/j.nbt.2009.09.007

Brown, A. P., Kroon, J. T. M., Swarbreck, D., Febrer, M., Larson, T. R., Graham, I. A., et al. (2012). Tissue-specific whole transcriptome sequencing in castor, directed at understanding triacylglycerol lipid biosynthetic pathways. *PLoS One* 7:e30100. doi: 10.1371/journal.pone.0030100

Bu, F., Yang, M., Guo, X., Huang, W., and Chen, L. (2020). Multiple functions of ATG8 family proteins in plant autophagy. *Front. Cell Dev. Biol.* 8:466. doi: 10.3389/fcell.2020.00466

Chellamuthu, M., Kumaresan, K., Subramanian, S., and Muthumanickam, H. (2019). Functional analysis of sesame diacylglycerol acyltransferase and phospholipid: diacylglycerol acyltransferase genes using in silico and *in vitro*

approaches. *Plant Mol. Biol. Report.* 37, 146–156. doi: 10.1007/s11105-019-01144-7

Cowan, A. K. (2009). Plant growth promotion by 18:0-lyso-phosphatidylethanolamine involves senescence delay. *Plant Signal. Behav.* 4, 324–327. doi: 10.4161/psb.4.4.8188

Dahlqvist, A., Ståhl, U., Lenman, M., Banaś, A., Lee, M., Sandager, L., et al. (2000). Phospholipid:diacylglycerol acyltransferase: an enzyme that catalyzes the acyl-CoA-independent formation of triacylglycerol in yeast and plants. *Proc. Natl. Acad. Sci. U.S.A.* 97, 6487–6492. doi: 10.1073/pnas.120067297

Fan, J., Yan, C., and Xu, C. (2013a). Phospholipid:diacylglycerol acyltransferase-mediated triacylglycerol biosynthesis is crucial for protection against fatty acid-induced cell death in growing tissues of *Arabidopsis*. *Plant J. Cell Mol. Biol.* 76, 930–942. doi: 10.1111/tpj.12343

Fan, J., Yan, C., Zhang, X., and Xu, C. (2013b). Dual role for phospholipid:diacylglycerol acyltransferase: enhancing fatty acid synthesis and diverting fatty acids from membrane lipids to triacylglycerol in *Arabidopsis* leaves. *Plant Cell* 25, 3506–3518. doi: 10.1105/tpc.113.117358

Farag, K. M., and Palta, J. P. (1993). Use of lysophosphatidylethanolamine, a natural lipid, to retard tomato leaf and fruit senescence. *Plant Physiol.* 87, 515–524. doi: 10.1111/j.1399-3054.1993.tb02501.x

Hong, J. H., Chung, G. H., and Cowan, A. K. (2009). Lyso-phosphatidylethanolamine-enhanced phenylalanine ammonia-lyase and insoluble acid invertase in isolated radish cotyledons. *Plant Growth Regul.* 57, 69–78. doi: 10.1007/s10725-008-9323-2

Jasieniecka-Gazarkiewicz, K., Lager, I., Carlsson, A. S., Gutbrod, K., Peisker, H., Dörmann, P., et al. (2017). Acyl-CoA:lysophosphatidylethanolamine acyltransferase activity regulates growth of *Arabidopsis*. *Plant Physiol.* 174, 986–998. doi: 10.1104/pp.17.00391

Kaup, M. T., Froese, C. D., and Thompson, J. E. (2002). A role for diacylglycerol acyltransferase during leaf senescence. *Plant Physiol.* 129, 1616–1626. doi: 10.1104/pp.003087

Kennedy, E. P. (1961). Biosynthesis of complex lipids. *Fed. Proc.* 20, 934–940.

Kim, H. U., Hsieh, K., Ratnayake, C., and Huang, A. H. C. (2002). A novel group of oleosins is present inside the pollen of *Arabidopsis*. *J. Biol. Chem.* 277, 22677–22684. doi: 10.1074/jbc.M109298200

Klińska, S., Jasieniecka-Gazarkiewicz, K., and Banaś, A. (2019). Acyl-CoA:lysophosphatidylcholine acyltransferases (LPCATs) of *Camelina sativa* seeds: biochemical properties and function. *Planta* 250, 1655–1670. doi: 10.1007/s00425-019-03248-6

Li, R., Yu, K., and Hildebrand, D. F. (2010). DGAT1, DGAT2 and PDAT expression in seeds and other tissues of epoxy and hydroxy fatty acid accumulating plants. *Lipids* 45, 145–157. doi: 10.1007/s11745-010-3385-4

Mhaske, V., Beldjilali, K., Ohlrogge, J., and Pollard, M. (2005). Isolation and characterization of an *Arabidopsis thaliana* knockout line for phospholipid: diacylglycerol transacylase gene (At5g13640). *Plant Physiol. Biochem.* 43, 413–417. doi: 10.1016/j.plaphy.2005.01.013

Mueller, S. P., Unger, M., Guender, L., Fekete, A., and Mueller, M. J. (2017). Phospholipid:diacylglycerol acyltransferase-mediated triacylglyerol synthesis augments basal thermotolerance. *Plant Physiol.* 175, 486–497. doi: 10.1104/pp.17.00861

Pan, X., Siloto, R. M. P., Wickramarathna, A., Mietkiewska, E., and Weselake, R. J. (2013). Identification of a pair of phospholipid:diacylglycerol acyltransferases from developing flax (*Linum usitatissimum* L.) seed catalyzing the selective production of trilinolenin. *J. Biol. Chem.* 288, 24173–24188. doi: 10.1074/jbc.M113.475699

Sambrook, J., Fritsch, E. E., and Maniatis, T. (1989). *Molecular Cloning: A Laboratory Manual*. Cold Spring Harbor, NY: Cold Spring Harbor Laboratory Press.

Ståhl, U., Carlsson, A. S., Lenman, M., Dahlqvist, A., Huang, B., Banaś, W., et al. (2004). Cloning and functional characterization of a phospholipid:diacylglycerol acyltransferase from *Arabidopsis*. *Plant Physiol.* 135, 1324–1335. doi: 10.1104/pp.104.044354

Stumpf, P. K., and Conn, E. E. (1988). *The Biochemistry of Plants: A Comprehensive Treatise*. New York, NY: Elsevier.

Su, T., Li, X., Yang, M., Shao, Q., Zhao, Y., Ma, C., et al. (2020). Autophagy: an intracellular degradation pathway regulating plant survival and stress response. *Front. Plant Sci.* 11:164. doi: 10.3389/fpls.2020.00164

Theodoulou, F. L., and Eastmond, P. J. (2012). Seed storage oil catabolism: a story of give and take. *Curr. Opin. Plant Biol.* 15, 322–328. doi: 10.1016/j.pbi.2012.03.017

Winer, J., Jung, C. K., Shackel, I., and Williams, P. M. (1999). Development and validation of real-time quantitative reverse transcriptase-polymerase chain reaction for monitoring gene expression in cardiac myocytes *in vitro*. *Anal. Biochem.* 270, 41–49. doi: 10.1006/abio.1999.4085

Xu, C., and Shanklin, J. (2016). Triacylglycerol metabolism, function, and accumulation in plant vegetative tissues. *Annu. Rev. Plant Biol.* 67, 179–206.

Yang, Y., and Benning, C. (2018). Functions of triacylglycerols during plant stress and development. *Curr. Opin. Biotechnol.* 49, 191–198. doi: 10.1016/j.copbio.2017.09.003

Yuan, L., Mao, X., Zhao, K., Ji, X., Ji, C., Xue, J., et al. (2017a). Characterisation of phospholipid: diacylglycerol acyltransferases (PDATs) from *Camelina sativa* and their roles in stress responses. *Biol. Open* 6, 1024–1034. doi: 10.1242/bio.026534

Yuan, L., Mao, X., Zhao, K., Sun, Y., Ji, C., Xue, J., et al. (2017b). Spatio-temporal expression and stress responses of DGAT1, DGAT2 and PDAT responsible for TAG biosynthesis in *Camelina sativa*. *Emirates J. Food Agric.* 29, 274–284. doi: 10.9755/ejfa.2016-10-1420

Zhang, M., Fan, J., Taylor, D. C., and Ohlrogge, J. B. (2009). DGAT1 and PDAT1 acyltransferases have overlapping functions in *Arabidopsis* triacylglycerol biosynthesis and are essential for normal pollen and seed development. *Plant Cell* 21, 3885–3901. doi: 10.1105/tpc.109.071795

Conflict of Interest: The authors declare that the research was conducted in the absence of any commercial or financial relationships that could be construed as a potential conflict of interest.

frontiers in Plant Science

ORIGINAL RESEARCH
published: 04 February 2021
doi: 10.3389/fpls.2020.590928

Effect of Intermittent Warming on the Quality and Lipid Metabolism of Blueberry (*Vaccinium corymbosum* L., cv. Duke) Fruit

Hongyu Dai[1†], Yajuan Wang[2†], Shujuan Ji[1], Ximan Kong[1], Fan Zhang[1], Xin Zhou[1] and Qian Zhou[1]*

[1] College of Food, Shenyang Agricultural University, Shenyang, China, [2] College of Plant Protection, Shenyang Agricultural University, Shenyang, China

OPEN ACCESS

Edited by:
Lina Yin,
Northwest A&F University, China

Reviewed by:
Hetong Lin,
Fujian Agriculture and Forestry University, China
Hui Wang,
Fujian Agriculture and Forestry University, China

****Correspondence:***
Qian Zhou
66zhouqian@syau.edu.cn;
66zhouqian@sina.com

† These authors have contributed equally to this work and share first authorship

Specialty section:
This article was submitted to Plant Metabolism and Chemodiversity, a section of the journal Frontiers in Plant Science

Received: *24 August 2020*
Accepted: *21 December 2020*
Published: *04 February 2021*

Citation:
Dai H, Wang Y, Ji S, Kong X, Zhang F, Zhou X and Zhou Q (2021) Effect of Intermittent Warming on the Quality and Lipid Metabolism of Blueberry (Vaccinium corymbosum L., cv. Duke) Fruit. Front. Plant Sci. 11:590928. doi: 10.3389/fpls.2020.590928

The change of lipid metabolism is a key point of blueberry fruit after refrigeration. This study was conducted to evaluate the effects of intermittent warming (IW) of "DuKe" blueberry fruit on its shelf life at 20 ± 0.5°C following 30 days of refrigeration. IW-treated fruit showed higher contents of phosphatidylcholine, linoleic acid, and oleic acid but lower contents of phosphatidic acid and palmitic acid compared to controls. Protective effects on the cell membrane were also reflected as inhibition of the activity of phospholipase D and lipoxygenase. The blueberry fruit showed a lower decay and pitting incidence with higher firmness than control. Interestingly, IW increased C-repeat binding transcription factor gene expression, which can induce the expression of genes related to hypothermia tolerance in plant cells at low temperature. These results indicate that IW can prevent damage to the membrane lipids, which occurs by senescence at a low temperature of blueberry fruit.

Keywords: blueberry, storage, intermittent warming, lipid metabolism, fruit quality

INTRODUCTION

Blueberry (*Vaccinium* spp.) is a kind of popular fruits because of high levels of nutrients (Wang S. Y. et al., 2018). The maintenance of quality is important to guarantee the economic success of fruits such as blueberry (Montecchiarini et al., 2019). However, the post harvest life of blueberry fruit is short. Therefore, it is necessary to improve the storage quality of fresh blueberry fruit using efficient strategies.

Intermittent warming (IW) is a convenient and environment-friendly strategy for delaying senescence and relieving chilling injury (CI) during low-temperature storage. For example, The IW treatment during cold storage can alleviate the peel browning of "Nanguo" pears (Wang J. W. et al., 2018). Fernández-Trujillo and Artés (1997) applied intermittent heating during storage of peach fruit, which effectively maintained the firmness and color of peach fruit. The role of IW treatment in reducing fruit chilling has been widely demonstrated, but few studies have evaluated the relationship between membrane lipid changes, cold stress, and IW treatment after low-temperature storage.

Membrane integrity is important for maintaining the quality of blueberry fruit during storage. The types and contents of unsaturated fatty acids and membrane lipids play important

roles in lipid metabolism (Lyons, 1973; Marangoni et al., 1996). Lipids on the cell membrane are mainly phospholipids, glycolipids, and cholesterol. Phospholipid is the most important component, and its double-layer structure ensures the stability of various physiological reactions in the fruit. Phospholipids in plants are complex (Kong et al., 2018). However, phosphatidic acid (PA), phosphatidylcholine (PC), phosphatidylglycerol (PG), phosphatidylethanolamine (PE), phosphatidylserine (PS), and phosphatidylinositol (PI) are commonly present. Senescence and some abiotic stressors cause degradation of phospholipids on the cell membrane, damage to the structure and integrity of the cell membrane, and disruption of the compartments within the cell. Phospholipids not only function as a barrier between cells and the outside environment but also are extremely important signal molecules, which is critical for the conversion of fatty acids (Manoharan et al., 1990). Any shift in the compositions of phospholipid and fatty acid during storage may damage the structural integrity of the cell membrane system (Lin et al., 2016), during which the enzymes phospholipase D (PLD) and lipoxygenase (LOX) play a major role. In short, PLD initiates the hydrolysis of phospholipids, after which LOX catalyzes the oxygenation of polyunsaturated fatty acids. Attack by the peroxidation products results in loss of compartmentalization of the cell membrane system (Cai et al., 2015). In addition to changes in the saturation levels of fatty acids, the composition and content of phospholipids also change to a certain extent at cold temperatures (Tarazona et al., 2015).

Based on our previous studies on the changes of membrane lipid in blueberry fruits during cold storage, we found that after 30 days of refrigeration, the pitting incidence increased significantly, and the linoleic acid content decreased significantly on day 4 of shelf life at room temperature (Wang Y. J. et al., 2019). Therefore, this study aimed to analyze the changes of membrane lipid of blueberry fruits during shelf life after a 30-day refrigeration and we have chosen the data at day 4 of the shelf life as the main object to analyze the differences of fatty acid content and membrane lipid composition between the IW-treated fruit and the controls. In addition, for clarifying the changes of enzyme activities of PLD and LOX better, we have chosen two representative genes, *VcLOX1* and *VcPLD*β, based on our previous studies. We also found that some phenomena in fruit during low-temperature storage were similar to the results of CI in the previous study. Some transcription factors such as C-repeat binding transcription factors (CBFs) have a vital role in plants involved in response to low temperature (Gilmour et al., 2004; Zhao et al., 2016). It was reported that the ectopic expression of CBFs can increase the freezing tolerance of transgenic Arabidopsis (Yamaguchi-Shinozaki and Shinozaki, 2006). Some studies also showed that treatments such as salicylic acid and eugenol fumigation increased the tolerance of grape and eggplant fruit to cold stress by increasing the gene expression of CBFs (Aazami and Mahna, 2017; Huang et al., 2019). Based on the study of the role of CBF in plant cold resistance, we determined *VcCBF* gene expression levels in this study.

The purpose of this study was to investigate the effect of IW treatment on "DuKe" blueberry at room temperature after refrigeration. The membrane lipid composition and fatty acid content of IW-treated fruit on day 4 of the shelf life after a 30-day refrigeration (0 ± 0.5°C) were examined. The firmness, decay incidence, pitting incidence, electrolyte leakage, malondialdehyde (MDA) concentration, and proline concentration at days 0, 2, 4, 6, and 8 of refrigeration were evaluated to determine the influence of cell membrane damage. Moreover, the enzyme activities of LOX and PLD and gene expression of *VcLOX1*, *VcPLD*β, and *VcCBF* during the shelf life were evaluated.

MATERIALS AND METHODS

Fruit Material and Treatments

Samples of blueberry fruit (*Vaccinium* spp. "DuKe") without mechanical injury or disease were harvested at commercial maturity (firmness about 2.0–2.5 N, total soluble solids about 7–8%, purple surface area larger than red area) from Shenyang, Liaoning Province, China (41.8°N, 123.4°E).

After 10 h of pre-cooling at 0 ± 0.5°C, the fruit was randomly divided into two groups; each group was composed of 20 kg fruit and transplanted into plastic boxes. The fruit of each box contains 125 g. The control group was stored at 0 ± 0.5°C, while another group was treated with IW by exposing to 20 ± 0.5°C for 1 day every 10 days during refrigeration. Both groups were stored for 30 days and then placed for 8 days at room temperature (20 ± 0.5°C) and 80% RH.

Fruit from both groups were sampled for analysis at 0, 2, 4, 6, and 8 days during the shelf life. Three replicates of fruit from both groups at each sampling point were collected to determine the firmness, decay index, pitting incidence, and electrolyte leakage. The fresh samples were frozen in liquid nitrogen and stored at −80°C until use for the measurement of fatty acid, membrane lipid composition, MDA concentration, proline concentration, enzyme activity, and gene expression. Three independent replicates were conducted.

Measurement of Decay Incidence

Decay incidence was expressed as percentage of the total number (Am) of blueberry fruits in each group. Three independent replicates were measured, and 100 fruit per replication were taken for analysis. Decay incidence was shown as follows: decay incidence = An/Am × 100%, where An is the number of blueberries with decay and Am is the total numbers.

Measurement of Pitting Incidence

Three independent replicates were measured, and 100 fruit per replication were taken for analysis.

The pitting incidence of the sample was calculated according to the following equation: pitting incidence = An/Am × 100%, where An is the number of blueberries with pitting and Am is the total numbers.

Measurement of Firmness

Fruit firmness of 10 fruit at each sampling point for each treatment was measured using a CT3 texture analyzer (Brookfield Engineering Laboratories, Inc., United States) with the TA39

rod probe. The penetration rate was 0.5 mm s^{-1}, and the final penetration depth was 5 mm. The result was expressed in newton (N).

Measurement of Electrolyte Leakage, MDA, and Proline Concentration

Electrolyte leakage measurements were performed following Zhu et al. (2009) using 15 disks with 1-mm thickness and 10-mm diameter from five fruits. Electrolyte leakage was expressed as relative conductivity (%).

Extraction of MDA content was according to Wang Y. J. et al. (2019). Blueberry tissue (1 g FW) from three blueberry fruit per replication has been taken for analysis. The MDA concentration (μmol g^{-1}) was calculated according to the equation: $[6.45 \times (A532 - A600) - 0.56 \times A450] \times 5$.

The values of *A*532, *A600*, and *A*450 are the absorbance of the sample at 532, 600, and 450 nm.

Proline content was measured according to the method of Zhao et al. (2009) with slight modifications. Briefly, 2 g (FW) tissue from three blueberry fruit was suspended in 2 mL of 30 g L^{-1} sulfosalicylic acid and transferred into a test tube quickly. Subsequently, the tube was heated in a 100°C water bath for 10 min and cooled to room temperature and then centrifuged at 10,000 × *g* for 15 min. Then, 2 mL of the supernatant was mixed with a mixture of glacial acetic acid and ninhydrin. After that, the mixture was heated in a 100°C water bath for 30 min until red. After quickly cooling, 4 mL of toluene was added into the tube, which was shaken for 30 s and then allowed to stand still for a while. The absorbance was read at 520 nm using the UV 5100 spectrophotometer (METASH). The content was calculated according to the standard curve and expressed as μg g^{-1}.

Analysis of Membrane Lipid Composition

Membrane lipid extraction was performed according to Welti et al. (2002) with some modifications. The fruit of the harvest day, the control group, and the treatment group were used as the samples for determination (fresh sample, control sample, and IW-treated sample). Blueberry tissues cut from the same position from eight fruits were transferred into 3 mL of pre-heated dimethylcarbinol, containing 0.01% butylated hydroxytoluene (BHT), and incubated in a 75°C water bath for 15 min. Then, 1.5 mL of chloroform and 0.6 mL of ultrapure water were added into the tube successively and centrifuged for 1 h at 150 *g* min^{-1}. The extract was transferred into the glass tube. The lipid extraction was repeated with 4 mL of $CHCl_3$/MeOH (2:1, v/v) (containing 0.01% BHT) for 30 min at 150 *g* min^{-1} and then transferred again. The steps were repeated until the samples became discolored. After that, the extracted solutions were combined, followed by addition of 1 mL of 1 mol L^{-1} KCl and centrifugation at 500 × *g* for 5 min; the water phase was discarded. 2 mL of ultrapure water was added to the extract and centrifuged at 500 × *g* for 5 min, and the water phase was discarded. The solvent was evaporated under a stream of N_2, stored at −80°C.

Membrane lipids were measured by the method as Xiao et al. (2010) described.

Analysis of Fatty Acid Content

Blueberry tissue (5.0 g FW) from 15 fruits, whose enzymes were inactivated in the oven (100°C, 10 min) and cooled to room temperature (20°C), was used as samples for follow steps.

Fatty acids were extracted using the method of Zhang and Tian (2010) and assayed as described by Wang Y. J. et al. (2019).

The fatty acids were qualitatively analyzed using the NIST/WILEY MS Search 2.0 standard database.

Analysis of Enzyme Activity

Blueberry tissue (5 g FW) from 15 fruits was fully ground to homogenate in 5 mL precooled phosphate buffer (0.1 mol L^{-1} $Na_2HPO_4 \cdot 12H_2O$, 0.1 mol L^{-1} $NaH_2PO_4 \cdot 2H_2O$) and centrifuged at 8,300 × *g* and 4°C for 20 min to collect the culture fluid to determine PLD activity according to the instructions provided in the Plant Phospholipase D ELISA Kit (Shangle, China). The PLD activity was expressed as μg L^{-1} FW.

Blueberry tissue (5 g FW) from 15 fruits was fully ground to homogenate in 5 mL precooled 0.01 mol L^{-1} phosphate buffer (pH 6.8) and centrifuged at 12,000 × *g* and 4°C for 20 min to collect the culture fluid to determine the LOX activity according to the instructions provided in the Plant Lipoxygenase ELISA Kit (Shangle, China). The LOX activity was expressed as μg L^{-1} FW.

RNA Isolation, cDNA Synthesis, and Real-Time q-PCR Assays

Blueberry tissue (100 mg FW) from three fruits was ground into powder in liquid nitrogen and transferred into a 1.5-mL RNase-Free tube for total RNA extraction of each treatment and time point.

Total RNA extraction, synthesis of cDNA, and qRT-PCR were performed according to the kit instructions of OminiPlant RNA Kit (CWBIO, China), HiFiScript cDNA Synthesis Kit (CWBIO, China), and UItraSYBR Mixture (Low Rox) Kit (CWBIO, China), respectively. The gene-specific primers used for RT-PCR (*VcPLD*β, *VcLOX1*, and *VcCBF*) designed using Primer Premier 5.0 are shown in **Table 1**. The sample of blueberry fruit on the harvest day was used as the mock sample (not shown in this article) following the $2^{-\Delta\Delta Ct}$ method.

Statistical Analyses

All of the statistical analyses were conducted using SPSS 20.0 (SPSS Inc., Chicago, IL, United States). Data were analyzed by one-way analysis of variance (ANOVA). Means were analyzed

TABLE 1 | Primers for real-time q-PCR analysis.

Gene	Forward primer (5′–3′)	Reverse primer (5′–3′)
Actin	5′-ACTACCATCCACT CTATCACCG-3′	5′-AACACCTTACCAACAGCCTTG-3′
*VcPLD*β	5′-TCAGCTTACGTCG TTATTCCTATGTG-3′	5′-ACGGTTGCCAAGACAGTAGAAGTTC-3′
VcLOX1	5′-GGATCACCATGAT GCGCTAA-3′	5′-ATGGCTTCAGTGTTCCGTCA-3′
VcCBF	5′-GCCTCTCGTCCTG CCGTATTAATG-3′	5′-TCCAGGTCAGGAATCAACAAGCAG-3′

using Duncan's multiple-range tests. All of the differences were considered significant at $p < 0.05$.

RESULTS

Changes in Decay Incidence, Pitting Incidence, and Fruit Firmness During the Shelf Life of Refrigerated Blueberry Fruit at Room Temperature

From day 0 to day 8 at room temperature after a 30-day refrigeration, the decay incidence (%) of the blueberry fruit increased quickly in both two groups (**Figure 1A**). At 2, 4, 6, and 8 days of the shelf life, there were significant differences between IW-treated and control fruit ($p < 0.05$). The decay incidence was more than 67% in control fruit the last day; in contrast, it was only 43% in IW-treated fruit, indicating that the treatment reduced fruit loss by more than 20%.

There was a sharp increase in pitting incidence during the shelf life at room temperature, and the incidence of pitting in control fruit was higher than that in IW-treated fruit (**Figure 1B**). IW treatment significantly alleviated the occurrence of pitting incidence until day 6 ($p < 0.05$). In particular, the incidence of pitting in IW-treated fruit was detected to be 11 and 10% lower than that of control fruit on days 2 and 4, respectively.

During the whole shelf life at room temperature, the firmness exhibited a normal softening pattern in both two groups (**Figure 1C**). After a 30-day refrigeration, the firmness of the IW-treated fruit was significantly higher than that of the control at 0, 4, and 6 days ($p < 0.05$).

Changes in Electrolyte Leakage, MDA Concentration, and Proline Concentration During the Shelf Life of Refrigerated Blueberry Fruit at Room Temperature

The electrolyte leakage of both two groups increased steadily during the shelf life after the 30-day refrigeration (**Figure 2A**). Compared with the control group, the electrolyte leakage of

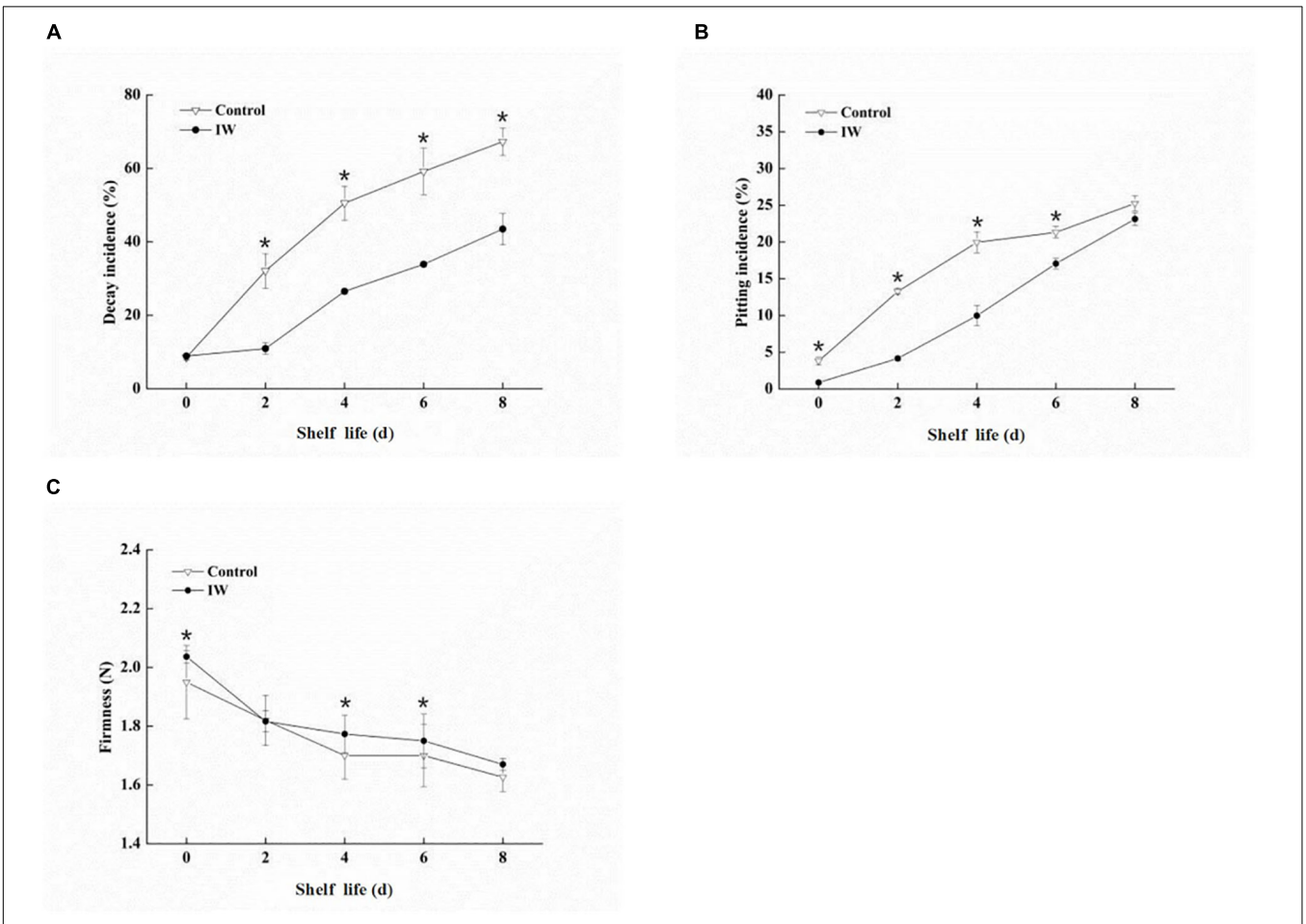

FIGURE 1 | Effect of intermittent warming on decay incidence **(A)**, pitting incidence **(B)**, and firmness **(C)** of blueberry fruit during shelf life at room temperature after a 30-day refrigeration. Mean ± SE of three replicate experiments are shown. Asterisks indicate significant differences between control and IW-treated fruit (*$p < 0.05$).

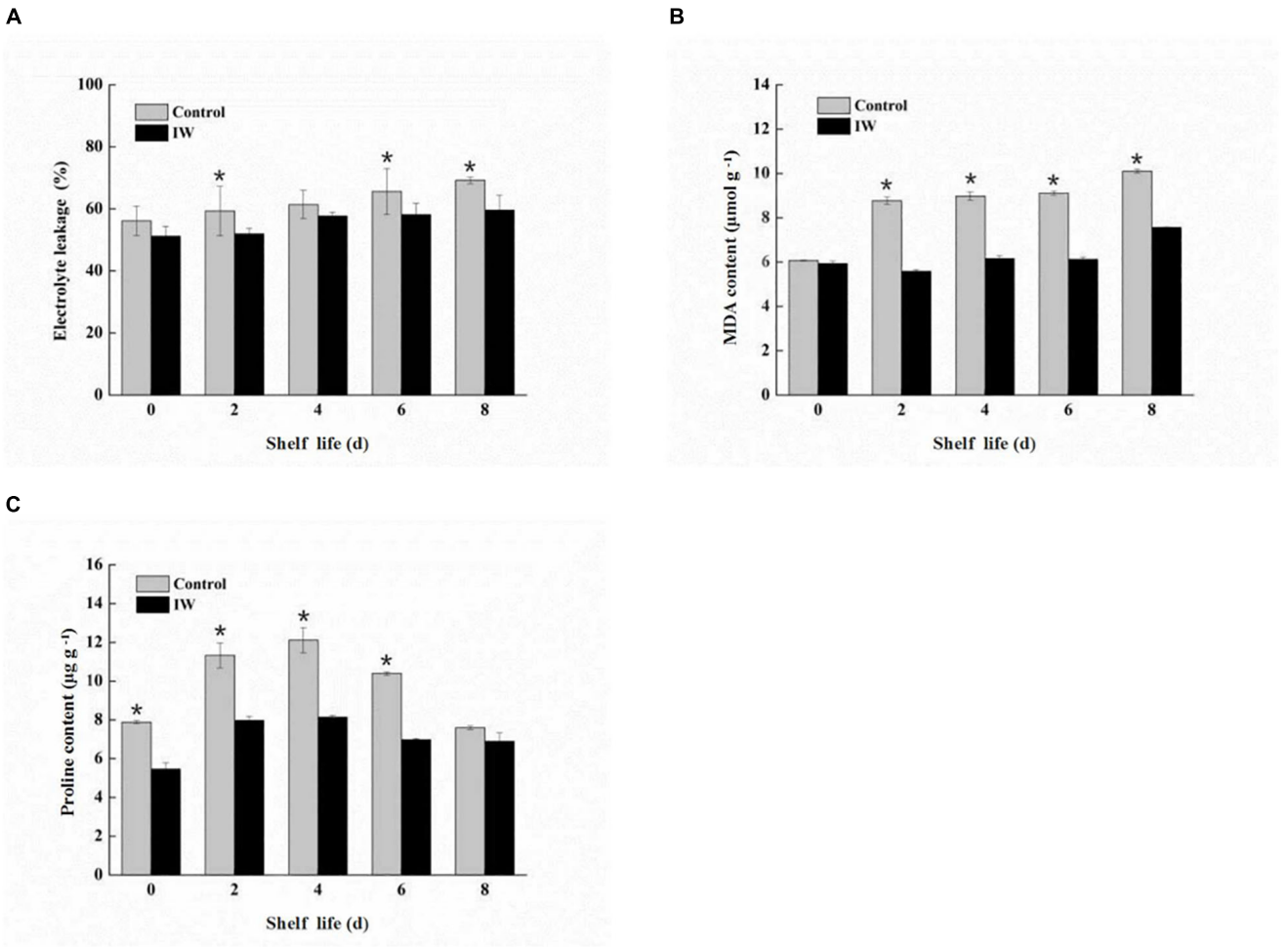

FIGURE 2 | Effect of intermittent warming on electrolyte leakage **(A)**, MDA content **(B)**, and proline content **(C)** of blueberry fruit during shelf life at room temperature after 30 days refrigeration. Mean ± SE of three replicate experiments are shown. Asterisks indicate significant differences between control and IW-treated fruit (*$p < 0.05$).

IW-treated fruit was maintained at a lower level; especially at 2, 6, and 8 days, the differences between the two groups were significant ($p < 0.05$).

At the beginning of the shelf life, there were no significant differences between the fruit of two groups (**Figure 2B**), and both of two increased steadily. However, the MDA concentrations in IW-treated fruit were significantly lower than those in control fruit from 2 to 8 days ($p < 0.05$).

During the entire shelf life, the proline concentrations of IW-treated fruit were increased in the first 4 days of shelf life and then decreased, and the peak appeared in 4 days. The level of control fruit showed a similar trend to IW-treated fruit. Proline concentrations of IW treatment were lower than control, and the differences between the two groups were significantly different at 0, 2, 4, and 6 days ($p < 0.05$) (**Figure 2C**).

Compared with the control fruit, the accumulation of membrane lipid peroxidation markers in the treatment group was significantly reduced ($p < 0.05$), indicating that the stability and integrity of the cell membrane were well protected.

Effects on Membrane Lipid Content on Day 4 of the Shelf Life at Room Temperature of Refrigerated Blueberry Fruit

We identified two categories of galactolipids [monogalactosyldiacylglycerol (MGDG) and digalactosyldiacylglycerol (DGDG)], six categories of phospholipids [PA, PC, PE, PG, PI, and PS], and three categories of lyso-phosphatides [lyso-phosphatidylcholine (LPC), lyso-phosphatidylethanolamine (LPE), and lyso-phosphatidylglycerol (LPG)].

The total lipid contents were 153.8, 157.7, and 151.5 nmol mg^{-1} DW in fresh, control, and IW-treated samples, respectively (**Figure 3A**). The contents of DGDG were significantly higher in control fruit than in fresh fruit ($p < 0.05$), whereas the

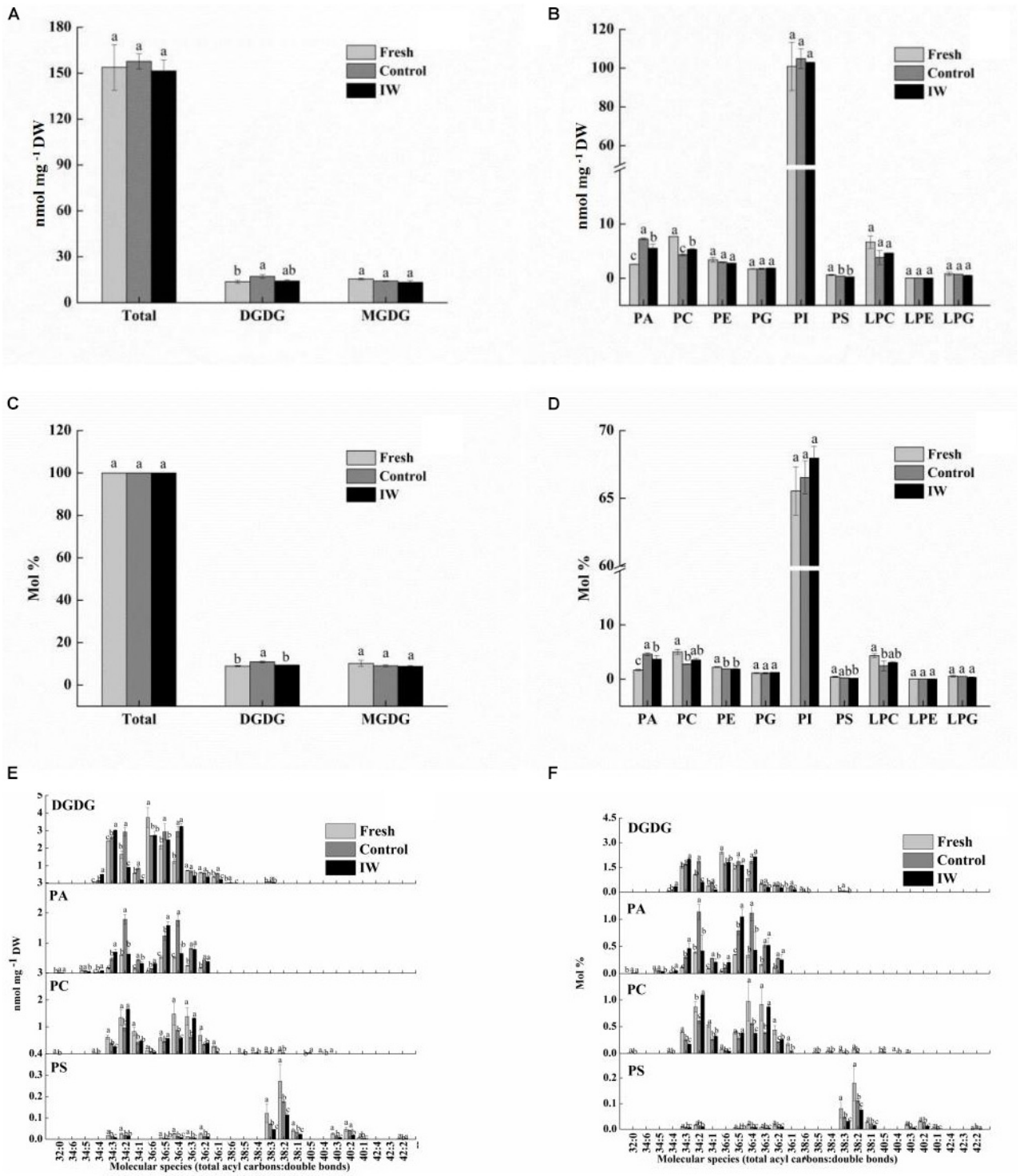

FIGURE 3 | Effect of intermittent warming on membrane lipid content of blueberry fruit at the day 4 during shelf life at room temperature after 30-day refrigeration. **(A)** Total lipid and glycolipid composition changes during shelf life, **(B)** phospholipid composition changes during shelf life, **(C)** total lipid and glycolipid proportion changes during shelf life, **(D)** phospholipid proportion changes during shelf life, **(E)** main glycolipid and phospholipid molecular species composition changes during shelf life, and **(F)** main glycolipid and phospholipid molecular species proportion changes during shelf life. Mean ± SE of three replicate experiments are shown. The letters a, b, and c show significant differences according to the independent samples *t*-test ($p < 0.05$) at each time point.

contents in IW-treated fruit were not. Compared to fresh fruit, the contents of PS and PC in control fruit and IW-treated were significantly decreased ($p < 0.05$) (**Figure 3B**); the contents of PC in IW-treated fruit were higher than in controls. In contrast, the contents of PA were increased after refrigeration, and they were significantly lower in IW-treated fruit ($p < 0.05$). The relative change is shown in **Figures 3C,D**.

The differences in the contents of PA came from the increases in 34:2 and 36:4 PA. Some of the PC and PS contents decreased significantly, such as 34:2 and 36:3 PC and 36:4 and 38:2 PS (**Figures 3E,F**). Under low-temperature stress, the structure of non-bilayer lipid MGDG is easy to transform into DGDG with a relatively stable structure and the increase of DGDG content indicated that the fruit was subjected to low-temperature stress. In this study, there are five main molecular species of DGDG, including 34:2, 34:3, 36:4, 36:5, and 36:6. Higher levels of molecular species of 34: 3-, 36: 4-, and 36:5-DGDG occurred along with a lower level of 36:6 DGDG in control and IW-treated fruit than in fresh fruit. However, the main components affecting the difference of DGDG content between control and IW-treated fruit may be 34:2 DGDG (**Figures 3E,F**).

Effects on Fatty Acid Content and the Index of Unsaturated Fatty Acid at Day 4 During Shelf Life of Refrigerated Blueberry Fruit at Room Temperature

Five major fatty acids were detected, namely, palmitic acid and stearic acid as saturated fatty acids, oleic acid as monounsaturated fatty acid, and linoleic acid and linolenic acid as polyunsaturated fatty acids.

At day 4 of the shelf life following a 30-day refrigeration, the content of stearic acid and linolenic acid in IW-treated fruit was higher than controls, although the difference was not significant (**Figure 4**). The content of palmitic acid was significantly lower ($p < 0.05$). At the same time, the content of oleic acid and linoleic acid was significantly higher than controls ($p < 0.05$). Overall, the relative content of saturated fatty acids in the control blueberry fruit was 26.88%, which was more than 6% higher than that in the IW-treated fruit (20.32%). As shown in **Table 2**, both the indexes of unsaturated fatty acid (IUFA) and unsaturated fatty acid/saturated fatty acid (UFA/FA) in control fruit were lower than those in IW-treated fruit ($p < 0.05$).

TABLE 2 | Effect of intermittent warming on index of unsaturated fatty acid of blueberry fruit at the day 4 of shelf life at room temperature after 30 days refrigeration.

	IUFA	UFA/FA
Control	122.797	1.993
IW	131.716*	2.682*

Values are meaning ± SD. Asterisks indicate significant differences between control and IW-treated fruit ($p < 0.05$, **$p < 0.01$).*

Changes in the Enzyme Activity and Expression Level of Genes of Refrigerated Blueberry Fruit at Room Temperature

The activity of PLD was increased in both two groups after a 30-day refrigeration, and its levels were lower in IW-treated fruit than in the control fruit (**Figure 5A**). Significant differences in activity were observed ($p < 0.05$) during the first 6 days post refrigeration. IW treatment suppressed the increase in PLD activity during the period post refrigeration. The expression levels of *VcPLD*β showed similar trends in the two groups, and the levels were significantly lower in IW-treated fruit than in the control fruit ($p < 0.05$) (**Figure 5B**). However, in control fruit, levels of *VcPLD*β were peaked at day 6, while in IW-treated fruit, they peaked at day 8. Therefore, IW treatment delayed the peak of the expression of *VcPLD*β.

The LOX activity in IW-treated fruit showed the same trend as in control fruit, and the levels in these fruit were similar at day 6 and day 8 after a 30-day refrigeration (**Figure 5C**). The level in IW-treated fruit during the first 4 days was lower than in controls, and the difference in levels was significant ($p < 0.05$). Compared to the control, IW treatment could decrease the level of LOX activity and delay its peak activity. There was no significant change in the expression levels of *VcLOX1* in IW-treated fruit post refrigeration (**Figure 5D**). At the same time, the expression level in the control increased slowly and was higher than that in IW-treated fruit; differences

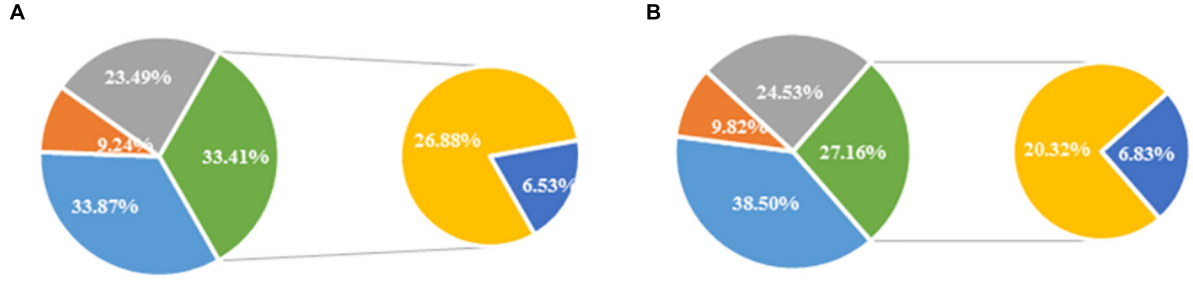

FIGURE 4 | The fatty acid content of blueberry fruit at the day 4 of shelf life at room temperature after 30 days refrigeration in control **(A)** and intermittent warming **(B)**. Mean ± SE of three replicate experiments are shown.

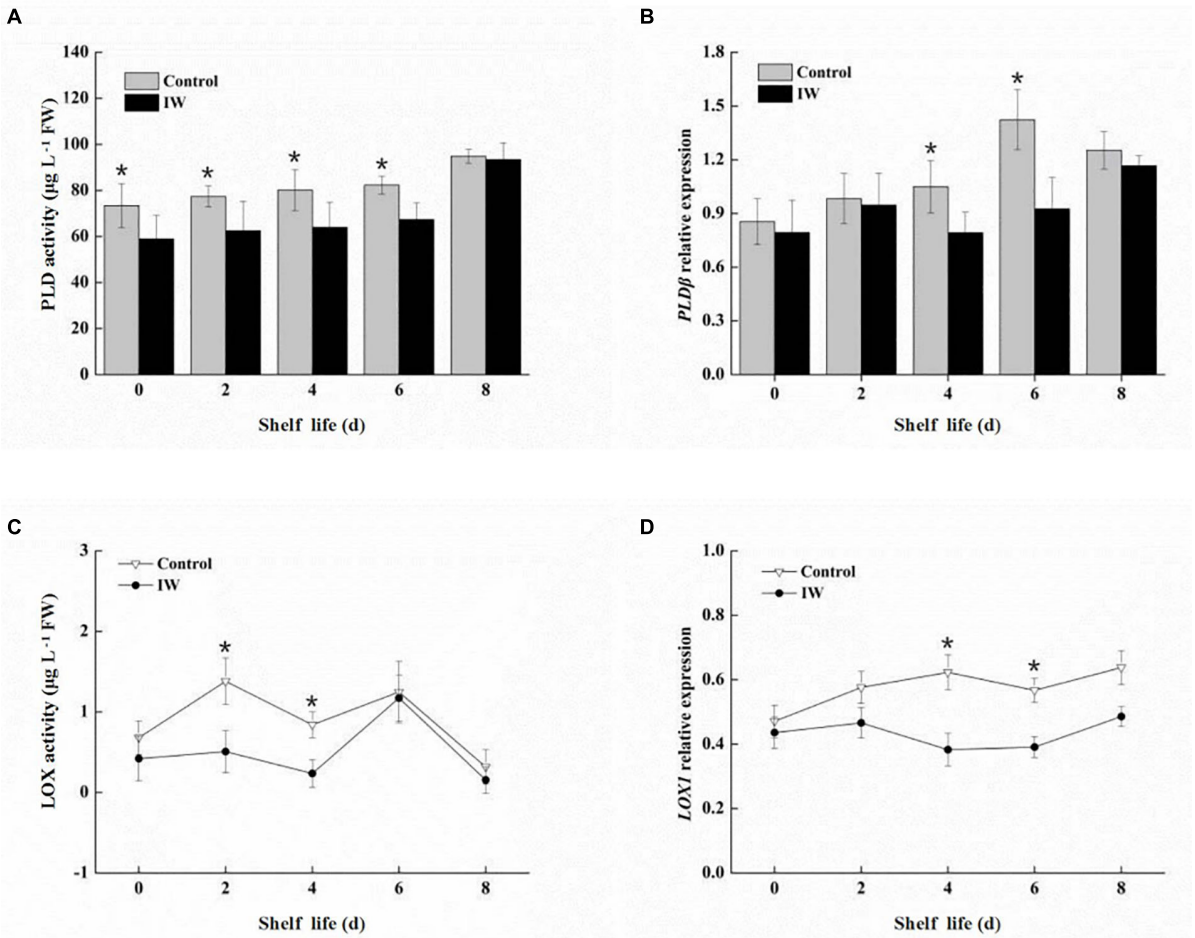

FIGURE 5 | Effect of intermittent warming on PLD activity **(A)**, gene expression of *VcPLD*β **(B)**, LOX activity **(C)**, and gene expression of *VcLOX1* **(D)** in blueberry fruit at room temperature after a 30-day refrigeration. Mean ± SE of three replicate experiments are shown. Asterisks indicate significant differences between control and IW-treated fruit (*$p < 0.05$).

in expression levels were significant at day 4 and day 6 ($p < 0.05$).

Changes in the Expression Levels of *VcCBF* Post Refrigeration of Blueberry Fruit at Room Temperature

The highest expression of *VcCBF* was observed at day 6 and at day 4 in control fruit and IW-treated fruit, respectively, after a 30-d refrigeration (**Figure 6**). The expression level in IW-treated fruit was significantly higher than that in controls at day 2, and the difference in the expression levels between the two groups was significant ($p < 0.01$).

DISCUSSION

Low-temperature storage is a common solution to the problem of off-season fruit supply (Sanchez-Bel et al., 2012). However, it is also associated with certain limitations; one of them is the damage of cell membranes. For example, pears and longan fruit are prone to browning after low-temperature storage (Wang J. W. et al., 2018; Zhang et al., 2019), whereas the main symptoms which showed damage due to low-temperature storage in peppers are surface pitting, seed darkening, and so on (Hardenburg et al., 1990). For blueberry, one of the main consequences of low-temperature damage is the pitting of the fruit. The development of pitting in blueberry fruit during low-temperature storage is rapid and damage to cellular membranes (Zhou et al., 2014). IW is widely used to maintain the quality of fruit during storage and has been demonstrated to be effective for fruits such as bell peppers (Kong et al., 2018), peach fruit (Xi et al., 2012), and apple fruit (Alwan and Watkins, 1999). In this study, IW treatment delayed the incidence of pitting in "DuKe" blueberry fruit after a 30-day low-temperature storage (**Figure 1B**) and maintained a higher degree of firmness and lower incidence of fruit decay (**Figures 1A,C**).

These functions appear to be mediated by effects on membrane components. As a key point of fruit ripening and senescence before the component content and enzyme activity

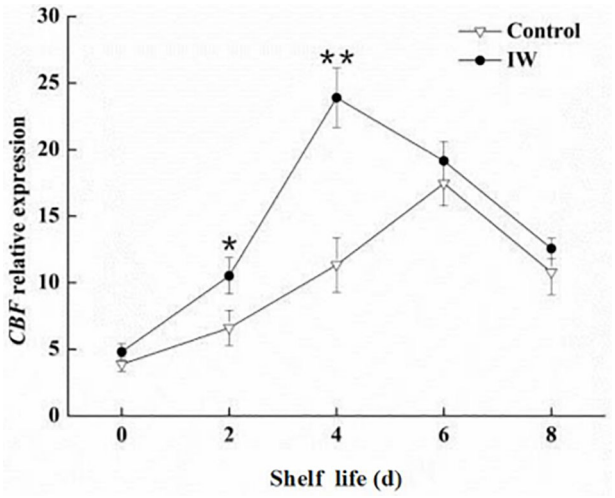

FIGURE 6 | Effect of intermittent warming on the gene expression of *VcCBF* of blueberry fruit at room temperature after a 30-day refrigeration. Mean ± SE of three replicate experiments are shown. Asterisks indicate significant differences between control and IW-treated fruit (*$p < 0.05$, **$p < 0.01$).

changes of the cell wall, the change of membrane integrity and membrane penetrability deserve attention (Maalekuu et al., 2006; Meyer and Terry, 2010). Phospholipids, as the principle component of the plasma membrane, maintain cellular fluidity and permeability and play an important role in the maintenance of regular physiological metabolism. As a major phospholipid, PC undergoes hydrolysis and transfer under the action of PLD during fruit senescence, producing PA and another phospholipid, resulting in changes in cell membrane structure and function (Aktas et al., 2014). Intermittent temperature treatment effectively inhibits the degradation of PC, which means that the cell membrane structure can be better protected from damage. Phosphatidic acid can provide some substrates for lipid peroxidation by participating in a series of reactions (Jia and Li, 2015). The collapse of the membrane system caused by cell senescence causes a strong accumulation of PA and further promotes membrane lipid peroxidation. In the present study, IW maintained the stability of the cell membrane by delaying the increase of DGDG and PA and inhibiting the decrease of PC, PE, and LPC (**Figure 3**). The inhibitory effect of intermittent temperature treatment on PC degradation and PA accumulation was significant, indicating that this treatment can reduce the accumulation of MDA and maintain the stability of the membrane system.

Phospholipids are linked to a variety of unsaturated fatty acid chains, which together form the cell membrane. The fatty acid components of the cell membrane play a predominant role in cell signaling and defense mechanisms (Liu et al., 2011). Yao et al. (2018) found that the CI index showed significantly negative correlations with the contents of linoleic acid and linolenic acid but significantly positive correlations with stearic acid and palmitic acid during storage. The study of García-Pastor et al. (2020) showed that the MeJa treatment reduced external and internal CI symptoms in pomegranate husk likely by reducing UFA losses and enhancing the UFA/SFA ratio. It has also been reported that the GB treatment can alleviate the CI of peach fruit by increasing the levels of unsaturated fatty acids and the degree of unsaturation (Wang L. et al., 2019). During storage, cell senescence leads to lipid peroxidation, which reduces fatty acid unsaturation, resulting in decreased cell membrane fluidity and structural and functional destruction. Intermittent warming effectively maintained high relative USFA content by delaying the increase in palmitic acid content and inhibiting the decrease of linoleic acid and oleic acid content and reducing the loss of unsaturated fatty acids, thereby reducing the accumulation of membrane lipid peroxidation products, maintaining the fluidity and stability of cell membranes (**Figure 4** and **Table 2**). Similarly, Xi et al. (2012) reported that the IW treatment could improve aroma quality by maintaining higher levels of unsaturated fatty acids in peach fruit.

The degradation of structural membrane lipids is the main cause of cell membrane loss, and PLD and LOX are two major degrading enzymes participating in this process. The activity of PLD can serve as an indicator of the intensity of hydrolysis, while LOX is a key factor in membrane lipid peroxidation (Zhang et al., 2010; Chen et al., 2011; Sirikesorn et al., 2013; Lin et al., 2016). Phosphatidic acid, released *via* catalysis by PLD, provided substrates for reactions catalyzed by LOX (Xu et al., 2016). Here, PA content in IW-treated fruit was significantly lower than that in the control, a trend also observed for the content of PLD and LOX. Intermittent warming significantly inhibited the activity of PLD and LOX as well as gene expression in the fruit, thus delaying membrane degradation (**Figure 5**). A similar result can be found in the research from Wang J. W. et al. (2018).

Electrolyte leakage can be used to monitor the degree of water and ion leakage due to cell rupture (Sharom et al., 1994; Marangoni et al., 1996). Malondialdehyde is a product of membrane lipid peroxidation, which is indicative of the level of membrane oxidative damage. Moreover, the content of proline is also closely related to membrane lipids (Wise and Naylor, 1987; Iba, 2002). In the present study, lower electrolyte leakage, MDA concentration, and proline concentration were observed in IW-treated fruit (**Figure 2**). This result showed that the IW treatment could maintain the quality of blueberry fruit by delaying membrane lipid peroxidation.

An interesting phenomenon is that we observed that some changes in control fruit were similar to the results of CI in the previous study. It was reported that the C-repeat binding transcription factor can induce the expression of genes related to hypothermia tolerance in plant cells at low temperature (Gilmour et al., 1998; Fowler and Thomashow, 2002; Ma et al., 2014). Some studies found that the *CBF* expression was positively correlated with the cold resistance of plants such as tomato and kiwifruit (Zhao et al., 2009; Ma et al., 2014). Moreover, this transcription factor participates in the control of the ABA-independent anti-cold pathway (Wong et al., 2006). We therefore determined the *VcCBF* expression level in the two groups of fruit. IW advanced the peak in *VcCBF* expression and also increased the expression levels (**Figure 6**), consequently improving the cold resistance of blueberry fruit while LOX activity and MDA content in treatment group were significantly lower than those in the control group.

These results suggest some connection between low-temperature storage of blueberry fruit and CI. IW treatment could improve the *VcCBF* expression level and maintain membrane stability. However, this relationship needs to be further discussed in future work and there are still some deficiencies in the study. In the future, we will explore the effect of different varieties of blueberry, other treatments combined with IW on low-temperature storage of blueberry fruit, and the role of the *VcCBF* gene in this process.

CONCLUSION

In conclusion, IW effectively delayed the softening of blueberry fruit and significantly delayed the incidence of pitting and decay, maintaining the storage quality of the fruit. The higher IUFA and UFA/FA content and the lower PA content in IW-treated fruit facilitated the maintenance of cellular fluidity and permeability; IW treatment also alleviated cell membrane damage by inhibiting the increased expression of *VcPLD*β and *VcLOX1*. Moreover, the gene expression level of *VcCBF* was increased in the IW-treated fruit. These results provided an experimental basis for future research as well as improved production practices for blueberry storage. In future work, we plan to study the relationship between the change in *CBF* expression and blueberry fruit quality during cold storage.

DATA AVAILABILITY STATEMENT

The original contributions presented in the study are included in the article/supplementary material, further inquiries can be directed to the corresponding author/s.

AUTHOR CONTRIBUTIONS

HD and YW prepared the fruit materials, participated in the physiological measurements, and participated in the statistical analyses. HD drafted the manuscript. SJ and XZ supervised the research. XK and FZ participated in the statistical analyses. QZ designed the experiment and proposed and supervised the research. All authors contributed to the article and approved the submitted version.

FUNDING

This work was supported by China Postdoctoral Science Foundation (grant number 2018M640260), Guidance Plan of Liaoning Natural Science Foundation (grant number 2019-ZD-0715), and the National Natural Science Foundation of China (grant number 31501534).

REFERENCES

Aazami, M. A., and Mahna, N. (2017). Salicylic acid affects the expression of *VvCBF4* gene in grapes subjected to low temperature. *J. Genet. Eng. Biotechnol.* 15, 257–261. doi: 10.1016/j.jgeb.2017.01.005

Aktas, M., Danne, L., Möller, P., and Narberhaus, F. (2014). Membrane lipids in *Agrobacterium tumefaciens*: biosynthetic pathways and importance for pathogenesis. *Front. Plant Sci.* 5:109. doi: 10.3389/fpls.2014.00109

Alwan, T. F., and Watkins, C. B. (1999). Intermittent warming effects on superficial scald development of 'Cortland', 'Delicious' and 'Law Rome' apple fruit. *Postharvest Biol. Technol.* 16, 203–212. doi: 10.1016/S0925-5214(99)00017-4

Cai, J. H., Chen, J., Lu, G. B., Zhao, M., Tian, S. P., and Qin, G. Z. (2015). Control of brown rot on jujube and peach fruits by trisodium phosphate. *Postharvest Biol. Technol.* 99, 93–98. doi: 10.1016/j.postharvbio.2014.08.003

Chen, Y. H., Lin, H. T., Lin, Y. F., Zhang, J. N., and Zhao, Y. F. (2011). Effects of *Phomopsis longanae* Chi infection on browning and active oxygen metabolism in pericarp of harvested longan fruits. *Sci. Agricult. Sin.* 44, 4858–4866. doi: 10.3864/j.issn.0578-1752.2011.23.012

Fernández-Trujillo, J. P., and Artés, F. (1997). Keeping quality of cold stored peaches using intermittent warming. *Food Res. Int.* 30, 441–450. doi: 10.1016/S0963-9969(97)00069-0

Fowler, S., and Thomashow, M. F. (2002). *Arabidopsis* transcriptome profiling indicates that multiple regulatory pathways are activated during cold acclimation in addition to the CBF cold response pathway. *Plant Cell* 14, 1675–1690. doi: 10.1105/tpc.003483

García-Pastor, M. E., Serrano, M., Guillén, F., Zapata, P. J., and Valero, D. (2020). Preharvest or a combination of preharvest and postharvest treatments with methyl jasmonate reduced chilling injury, by maintaining higher unsaturated fatty acids, and increased aril colour and phenolics content in pomegranate. *Postharvest Biol. Technol.* 167:111226. doi: 10.1016/j.postharvbio.2020.111226

Gilmour, S. J., Fowler, S. G., and Thomashow, M. F. (2004). *Arabidopsis* transcriptional activators CBF1, CBF2, and CBF3 have matching functional activities. *Plant Mol. Biol.* 54, 767–781. doi: 10.1023/b:plan.0000040902.06881.d4

Gilmour, S. J., Zarka, D. G., Stockinger, E. J., Salazar, M. P., and Thomashow, M. F. (1998). Low temperature regulation of the *Arabidopsis* CBF family of AP2 transcriptional activators as an early step in cold-induced COR gene expression. *Plant J.* 16, 433–442. doi: 10.1046/j.1365-313x.1998.00310.x

Hardenburg, R. E., Watada, A. E., and Yang, C. Y. (1990). The Commercial Storage of Fruits, Vegetables, and Florist and Nursery Stocks. *Agriculture Handbook* 66, 14–16.

Huang, Q., Qian, X., Jiang, T., and Zheng, X. (2019). Effect of eugenol fumigation treatment on chilling injury and CBF gene expression in eggplant fruit during cold storage. *Food Chem.* 292, 143–150. doi: 10.1016/j.foodchem.2019.04.048

Iba, K. (2002). Acclimative response to temperature stress in higher plants:approaches of gene engineering for temperature tolerance. *Annu. Rev. Plant Biol.* 53, 225–245. doi: 10.1146/annurev.arplant.53.100201.160729

Jia, Y., and Li, W. (2015). Characterisation of lipid changes in ethylene-promoted senescence and its retardation by suppression of phospholipase D in *Arabidopsis* leaves. *Front. Plant Sci.* 6:1045. doi: 10.3389/fpls.2015.01045

Kong, X. M., Wei, B. D., Gao, Z., Zhou, Y., Shi, F., Zhou, X., et al. (2018). Changes in membrane lipid composition and function accompanying chilling injury in bell peppers. *Plant Cell Physiol.* 59, 167–178. doi: 10.1093/pcp/pcx171

Lin, Y. F., Lin, H. T., Lin, Y. X., Zhang, S., Chen, Y. H., and Jiang, X. J. (2016). The roles of metabolism of membrane lipids and phenolics in hydrogen peroxide-induced pericarp browning of harvested longan fruit. *Postharvest Biol. Technol.* 111, 53–61. doi: 10.1016/j.postharvbio.2015.07.030

Liu, H., Song, L., You, Y., Li, Y., Duan, X., Jiang, Y., et al. (2011). Cold storage duration affects litchi fruit quality, membrane permeability, enzyme activities and energy charge during shelf time at ambient temperature. *Postharvest Biol. Technol.* 60, 24–30. doi: 10.1016/j.postharvbio.2010.11.008

Lyons, J. M. (1973). Chilling injury in plants. *Annu. Rev. Plant Physiol.* 24, 445–466. doi: 10.1146/annurev.pp.24.060173.002305

Ma, Q. S., Suo, J. T., Huber, D. J., Dong, X. Q., Han, Y., Zhang, Z. K., et al. (2014). Effect of hot water treatments on chilling injury and expression of a new C-repeat binding factor (CBF) in'Hongyang'kiwifruit during low temperature storage. *Postharvest Biol. Technol.* 97, 102–110. doi: 10.1016/j.postharvbio.2014.05.018

Maalekuu, K., Elkind, Y., Leikin-Frenkel, A., Lurie, S., and Fallik, E. (2006). The relationship between water loss, lipid content, membrane integrity and LOX activity in ripe pepper fruit after storage. *Postharvest Biol. Technol.* 42, 248–255. doi: 10.1016/j.postharvbio.2006.06.012

Manoharan, K., Prasad, R., and Guhamukherjee, S. (1990). Senescence-related lipid changes in callus culures of *Datura innoxia*. *Phytochemistry* 29, 2529–2531. doi: 10.1016/0031-9422(90)85181-e

Marangoni, A. G., Palma, T., and Stanley, D. W. (1996). Membrane effects in postharvest physiology. *Postharvest Biol. Technol.* 7, 193–217. doi: 10.1016/0925-5214(95)00042-9

Meyer, M. D., and Terry, L. A. (2010). Fatty acid and sugar composition of avocado, cv. Hass, in response to treatment with an ethylene scavenger or 1-methylcyclopropene to extend storage life. *Food Chem.* 121, 1203–1210. doi: 10.1016/j.foodchem.2010.02.005

Montecchiarini, M. L., Margarita, E., Moralesa, L., Rivadeneirab, M. F., Bellob, F., and Gollánb, A. (2019). Proteomic and metabolomic approaches unveil relevant biochemical changes in carbohydrate and cell wall metabolisms of two blueberry (*Vaccinium corymbosum*) varieties with different quality attributes. *Plant Physiol. Biochem.* 136, 230–244. doi: 10.1016/j.plaphy.2018.12.019

Sanchez-Bel, P., Egea, I., Sanchez-Ballesta, M. T., Martinez-Madrid, C., Fernandez-Garcia, N., Romojaro, F., et al. (2012). Understanding the mechanisms of chilling injury in bell pepper fruits using the proteomic approach. *J. Proteom.* 75, 5463–5478. doi: 10.1016/j.jprot.2012.06.029

Sharom, M., Willemot, C., and Thompson, J. E. (1994). Chilling injury induces lipid phase changes in membranes of tomato fruit. *Plant Physiol.* 105, 305–308. doi: 10.1104/pp.105.1.305

Sirikesorn, L., Ketsa, S., and van Doorn, W. G. (2013). Low temperature-induced water-soaking of *Dendrobium* inflorescences: relation with phospholipase D activity, thiobarbaturic-acid staining membrane degradation products, and membrane fatty acid composition. *Postharvest Biol. Technol.* 80, 47–55. doi: 10.1016/j.postharvbio.2013.01.007

Tarazona, P., Kirstin, F., and Ivo, F. (2015). An enhanced plant lipidomics method based on multiplexed liquid chromatography-mass spectrometry reveals additional insights into cold- and drought-induced membrane remodeling. *Plant J.* 84, 621–633. doi: 10.1111/tpj.13013

Wang, J. W., Lv, M., Li, G. D., Jiang, Y. G., Fu, W. W., Zhang, L., et al. (2018). Effect of intermittent warming on alleviation of peel browning of 'Nanguo' pears by regulation energy and lipid metabolisms after cold storage. *Postharvest Biol. Technol.* 142, 99–106. doi: 10.1016/j.postharvbio.2017.12.007

Wang, L., Bokhary, S. U. F., Xie, B., Hu, S., Jin, P., and Zheng, Y. (2019). Biochemical and molecular effects of glycine betaine treatment on membrane fatty acid metabolism in cold stored peaches. *Postharvest Biol. Technol.* 154, 58–69. doi: 10.1016/j.postharvbio.2019.04.007

Wang, S. Y., Zhou, Q., Zhou, X., Wei, B. D., and Ji, S. J. (2018). The effect of ethylene absorbent treatment on the softening of blueberry fruit. *Food Chem.* 246, 286–294. doi: 10.1016/j.foodchem.2017.11.004

Wang, Y. J., Ji, S. J., Dai, H. Y., Kong, X. M., Hao, J., Wang, S. Y., et al. (2019). Changes in membrane lipid metabolism accompany pitting in blueberry during refrigeration and subsequent storage at room temperature. *Front. Plant Sci.* 10:829. doi: 10.3389/fpls.2019.00829

Welti, R., Li, W., Li, M., Sang, Y., Biesiada, H., and Zhou, H. E. (2002). Profiling membrane lipids in plant stress responses. *J. Biol. Chem.* 277, 31994–32002. doi: 10.1074/jbc.m205375200

Wise, R. R., and Naylor, A. W. (1987). Chilling-enhanced photophylls, chilling-enhanced photooxidation-the peroxidative destruction of lipids during chilling injury tophotosynthesis and ultrastructure. *Plant Physiol.* 83, 272–277. doi: 10.1104/pp.83.2.272

Wong, C. E., Li, Y., Labbe, A., Guevara, D., Nuin, P., Whitty, B., et al. (2006). Transcriptional profiling implicates novel interactions between abiotic stress and hormonal responses in *Thellungiella*, a close relative of *Arabidopsis*. *Plant Physiol.* 140, 1437–1450. doi: 10.1104/pp.105.070508

Xi, W. P., Zhang, B., Shen, J. Y., Sun, C. D., Xu, C. J., and Chen, K. S. (2012). Intermittent warming alleviated the loss of peach fruit aroma-related esters by regulation of AAT during cold storage. *Postharvest Biol. Technol.* 74, 42–48. doi: 10.1016/j.postharvbio.2012.07.003

Xiao, S., Gao, W., Chen, Q. F., Chan, S. W., Zheng, S. X., and Ma, J. (2010). Overexpression of *Arabidopsis* Acyl-CoA binding protein ACBP3 promotes starvation-induced and age-dependent leaf senescence. *Plant Cell* 22, 1463–1482. doi: 10.1105/tpc.110.075333

Xu, J. N., Cao, Q., Deng, L. L., Yao, S., Wang, W. H., and Zeng, K. (2016). Mechanisms of membrane lipid metabolism in citrus fruit at low ripening stage in response to oleocellosis. *Food Sci.* 37, 262–270.

Yamaguchi-Shinozaki, K., and Shinozaki, K. (2006). Transcriptional regulatory networks in cellular responses and tolerance to dehydration and cold stresses. *Annu. Rev. Plant Biol.* 57 781–803. doi: 10.1146/annurev.arplant.57.032905.105444

Yao, W., Xu, T., Farooq, S. U., Jin, P., and Zheng, Y. (2018). Glycine betaine treatment alleviates chilling injury in zucchini fruit (*Cucurbita pepo* L.) by modulating antioxidant enzymes and membrane fatty acid metabolism. *Postharvest Biol. Technol.* 144, 20–28. doi: 10.1016/j.postharvbio.2018.05.007

Zhang, B., Xi, W. P., Wei, W. W., Shen, J. Y., Ferguson, I., and Chen, K. S. (2010). Changes in aroma-related volatiles and gene expression during low temperature storage and subsequent shelf-life of peach fruit. *Postharvest Biol. Technol.* 60, 7–16. doi: 10.1016/j.postharvbio.2010.09.012

Zhang, C., and Tian, S. (2010). Peach fruit acquired tolerance to low temperature stress by accumulation linolenic acid and N-acylphosphatidylethanolamine in plasma membrane. *Food Chem.* 120, 864–872. doi: 10.1016/j.foodchem.2009.11.029

Zhang, S., Lin, H. T., Lin, M. S., Lin, Y. F., Chen, Y. H., Wang, H., et al. (2019). *Lasiodiplodia theobromae* Griff. & Maubl. Reduced energy status and ATPase activity and its relation to disease development and pericarp browning of harvested longan fruit. *Food Chem.* 275, 235–245. doi: 10.1016/j.foodchem.2018.09.105

Zhao, C., Zhang, Z., Xie, S., Si, T., Li, Y., and Zhu, J. K. (2016). Mutational evidence for the critical role of *CBF* transcription factors in cold acclimation in *Arabidopsis*. *Plant Physiol.* 171:2744. doi: 10.1104/pp.16.00533

Zhao, D. Y., Shen, L., and Fan, B. (2009). Ethylene and cold participate in the regulation of *LeCBFl* gene expression in postharvest tomato fruitsf. *FEBS Lett.* 583, 3329–3334. doi: 10.1016/j.febslet.2009.09.029

Zhou, Q., Ma, C., Cheng, S. C., Wei, B. D., Liu, X. Y., and Ji, S. J. (2014). Changes in antioxidative metabolism accompanying pitting development in stored blueberry fruit. *Postharvest Biol. Technol.* 88, 88–95. doi: 10.1016/j.postharvbio.2013.10.003

Zhu, L. Q., Jie, Z., Zhu, S. H., and Guo, L.-H. (2009). Inhibition of browning on the surface of peach slices by short-term exposure to nitric oxide and ascorbic acid. *Food Chem.* 114, 174–179. doi: 10.1016/j.foodchem.2008.09.036

Conflict of Interest: The authors declare that the research was conducted in the absence of any commercial or financial relationships that could be construed as a potential conflict of interest.

frontiers in Plant Science

ORIGINAL RESEARCH
published: 08 March 2021
doi: 10.3389/fpls.2021.653997

The Oleic/Linoleic Acid Ratio in Olive (*Olea europaea* L.) Fruit Mesocarp Is Mainly Controlled by *OeFAD2-2* and *OeFAD2-5* Genes Together With the Different Specificity of Extraplastidial Acyltransferase Enzymes

M. Luisa Hernández[1]†, M. Dolores Sicardo[1], Angjelina Belaj[2] and José M. Martínez-Rivas[1]**

[1] Instituto de la Grasa (IG-CSIC), Campus Universidad Pablo de Olavide, Seville, Spain, [2] IFAPA Centro Alameda del Obispo, Córdoba, Spain

OPEN ACCESS

Edited by:
Krzysztof Zienkiewicz, Nicolaus Copernicus University in Toruń, Poland

Reviewed by:
Adrian Troncoso, University of Technology Compiegne, France
Jaruswan Warakanont, Kasetsart University, Thailand

***Correspondence:**
M. Luisa Hernández
mhjimenez@us.es
José M. Martínez-Rivas
mrivas@ig.csic.es

†Present address:
M. Luisa Hernández, Departamento de Bioquímica Vegetal y Biología Molecular/Instituto de Bioquímica Vegetal y Fotosíntesis, Universidad de Sevilla-CSIC, Seville, Spain

Specialty section:
This article was submitted to Plant Metabolism and Chemodiversity, a section of the journal Frontiers in Plant Science

Received: 15 January 2021
Accepted: 15 February 2021
Published: 08 March 2021

Citation:
Hernández ML, Sicardo MD, Belaj A and Martínez-Rivas JM (2021) The Oleic/Linoleic Acid Ratio in Olive (Olea europaea L.) Fruit Mesocarp Is Mainly Controlled by OeFAD2-2 and OeFAD2-5 Genes Together With the Different Specificity of Extraplastidial Acyltransferase Enzymes. Front. Plant Sci. 12:653997. doi: 10.3389/fpls.2021.653997

Fatty acid composition of olive oil has an important effect on the oil quality to such an extent that oils with a high oleic and low linoleic acid contents are preferable from a nutritional and technological point of view. In the present work, we have first studied the diversity of the fatty acid composition in a set of eighty-nine olive cultivars from the Worldwide Olive Germplasm Bank of IFAPA Cordoba (WOGBC-IFAPA), and in a core collection (Core-36), which includes 28 olive cultivars from the previously mentioned set. Our results indicate that oleic and linoleic acid contents displayed the highest degree of variability of the different fatty acids present in the olive oil of the 89 cultivars under study. In addition, the independent study of the Core-36 revealed two olive cultivars, Klon-14 and Abou Kanani, with extremely low and high linoleic acid contents, respectively. Subsequently, these two cultivars were used to investigate the specific contribution of different fatty acid desaturases to the linoleic acid content of mesocarp tissue during olive fruit development and ripening. Fatty acid desaturase gene expression levels, together with lipid analysis, suggest that not only *OeFAD2-2* and *OeFAD2-5* but also the different specificities of extraplastidial acyltransferase enzymes are responsible for the variability of the oleic/linoleic acid ratio in olive cultivars. All this information allows for an advancement in the knowledge of the linoleic acid biosynthesis in different olive cultivars, which can impact olive breeding programs to improve olive oil quality.

Keywords: ***Olea europaea*** **L., olive, linoleic acid, oleic acid, fatty acid desaturase, gene expression, lipid analysis**

INTRODUCTION

Olea europaea L. was one of the first plants to be cultivated for oil production. The olive tree is one of the most important and widespread fruit trees in the Mediterranean basin and, nowadays, is the second most important oil fruit crop cultivated worldwide (Baldoni et al., 2009). Most olive production is destined for olive oil, which is obtained only by mechanical procedures from the

olive fruit, with a major contribution of the olive mesocarp to its final composition (Connor and Fereres, 2005). Global olive oil production and consumption have been growing considerably in recent decades thanks to its remarkable organoleptic, technological, and nutritional properties, which are ultimately determined by the metabolites present in the olive oil (Rallo et al., 2018). Among these metabolites, fatty acids that are esterifying triacylglycerols (TAG), which are the major components, are what largely determine the technological and nutritional properties of olive oil (Salas et al., 2000). Oleic acid is the main fatty acid in olive oil and accounts for 55–83% of total fatty acid content. Olive oil also contains variable amounts of linoleic acid (3–21%) and linolenic acid (<1%). The relative content of these fatty acids, which depends mainly on the cultivar, but also on pedoclimatic and management conditions (Beltrán et al., 2004), is an important quality attribute, and it is used to verify the authenticity of olive oil (IOOC, 2001). Noticeably, oleic acid reduces the risk of cardiovascular diseases (Sales-Campos et al., 2013) and suppresses tumorigenesis of inflammatory diseases (Yamaki et al., 2005). Conversely, the excessive linoleic acid intake, due to the high proportion of seed oils in the diet, is associated with a higher risk of hypertension and cardiovascular and carcinogenic diseases (Vos, 2003). Concerning the technological properties, the autoxidative stability of oleic acid is 10-fold higher than that of linoleic acid (O'Keefe et al., 1993). Therefore, olive oils with high oleic and low linoleic acid content are better from a nutritional and technological point of view. Accordingly, the generation of new olive cultivars producing oils with high oleic/linoleic acid ratio is a priority in olive breeding programs.

In higher plants, *de novo* fatty acid synthesis starts in the plastid, yielding primarily palmitoyl-ACP and stearoyl-ACP (Harwood, 2005). Still in the plastid, stearoyl-ACP is desaturated by a soluble stearoyl-ACP desaturase (SAD) to produce oleoyl-ACP, which is the main product of the plastidial fatty acid biosynthesis. These fatty acids are then incorporated into the two glycerolipids pathways that exist in plants: the prokaryotic and eukaryotic pathways. In "18:3 plants", such as olive, phosphatidylglycerol is the only glycerolipid synthesized in the plastid by the prokaryotic pathway, while the rest of glycerolipids are synthesized in the endoplasmic reticulum (ER) or the plastid using a diacylglycerol (DAG) backbone synthesized in the ER, like the case of galactolipids (Browse and Somerville, 1991). Storage lipids are synthesized in the ER in oil-accumulating tissues via the Kennedy pathway (Gunstone et al., 2007), as well as alternative acyl-CoA-independent mechanism, such as those involving phospholipid:diacylglycerol acyltransferase (PDAT) (Dahlqvist et al., 2000) or diacylglycerol:diacylglycerol transacylase (DGTA) activities (Stobart et al., 1997). In both glycerolipids pathways, desaturation of fatty acids is performed by a series of integral membrane enzymes called fatty acid desaturases. Two sets of ω6 and ω3 membrane-bound fatty acid desaturases have been described, which differ in their cellular localization, lipid substrates, and electron donor system (Shanklin and Cahoon, 1998). The plastidial ω6 and ω3 desaturases (FAD6 and FAD7/8, respectively) are located in the chloroplast, while the microsomal ω6 and ω3 desaturases (FAD2 and FAD3, respectively) are localized in the ER. In the case of ER fatty acid desaturases, two pathways have been reported for the reversible entry of unsaturated fatty acids in phosphatidylcholine (PC) as lipid substrate for further desaturation: an acyl-editing mechanism involving the acyl-CoA pool and the lysophosphastidylcholine acyltransferase (LPCAT) enzyme; and the synthesis of PC from DAG catalysed by the CDP choline:DAG choline phosphotransferase (CPT) and/or PC:DAG choline phosphotransferase (PDCT) enzymes (Bates et al., 2009).

In olive, four genes encoding the soluble SAD have been described: *OeSAD1* (Haralampidis et al., 1998), *OeSAD2*, *OeSAD3* (Parvini et al., 2016), and *OeSAD4* (Contreras et al., 2020). Regarding membrane bound desaturases, five genes encoding microsomal oleate desaturases (*OeFAD2-1* to *OeFAD2-5*) have been isolated and characterized by Hernández et al., 2005, 2009, 2020, whereas only one *OeFAD6* gene has been described so far (Banilas et al., 2005; Hernández et al., 2011). Additionally, four members of the olive linoleate desaturase gene family have been characterized, two microsomal (*OeFAD3A*, Banilas et al., 2007; *OeFAD3B*, Hernández et al., 2016) and two plastidial (*OeFAD7-1*, Poghosyan et al., 1999; *OeFAD7-2*, Hernández et al., 2016).

In previous studies, we have characterized the olive fatty acid desaturase genes involved in the unsaturated fatty acid composition of olive oil in the two main cultivars for olive oil production such as Picual and Arbequina (Hernández et al., 2005, 2009, 2016, 2020; Parvini et al., 2016). However, the genetic control of its variability among olive cultivars is still poorly understood. For this reason, we extended the study to the cultivars of a previously developed core collection (Core-36) with a wide genetic diversity (Belaj et al., 2012), which allowed the identification of two olive cultivars with highly contrasting linoleic acid content: Klon-14 and Abou Kanani. These two cultivars were further used to determine the expression levels of genes encoding fatty acid desaturases in their mesocarp tissues during olive fruit development and ripening, in order to investigate their involvement in the regulation of the oleic and linoleic acid content. In addition, lipid analysis has been carried out to examine the possible implication of other genes and enzymes of the lipid biosynthetic pathway. Our data shed light on the understanding of the transcriptional and metabolic mechanisms that control the oleic/linoleic acid ratio in olive cultivars, to improve olive oil quality.

MATERIALS AND METHODS

Plant Material

A total of 89 cultivars from the Worldwide Olive Germplasm Bank of Cordoba (WOGBC-IFAPA) located at the Andalusian Institute of Agricultural and Fisheries Research and Training (IFAPA), "Alameda del Obispo," in Cordoba (Spain) were included in this work (**Supplementary Table 1**). The study was also extended to the 36 cultivars (**Supplementary Table 2**) corresponding to a previously established core collection (Core-36) (Belaj et al., 2012), which included 28 cultivars from the 89 selected from the WOGBC. Trees, two per accession, were cultivated in the same agroclimatic conditions at the

experimental orchards of IFAPA (Alameda del Obispo, Córdoba, Spain) at 6 m × 5 m spacing, using standard culture practices (Gómez-Gálvez et al., 2020). In order to obtain representative samples of the olive fruits from all parts of the olive trees, fruits were harvested by hand all around from two trees per cultivar, mixed and spliced into three different pools, that constitute three different biological replicate, for oil fatty acid analysis and mesocarp developmental studies.

For olive oil extraction, fruit samples from the 89 cultivars from the WOGBC-IFAPA were harvested during the seasons 2008/2009 and 2009/2010, while samples from the Core-36 were harvested during season 2011/2012. The harvest was carried out at the turning stage (28–31 weeks after flowering [WAF]), and oil was extracted consecutively.

In the case of developmental studies, mesocarp tissue were harvested from the selected cultivars, Klon-14 and Abou Kanani, at different WAF corresponding to different developmental stages of the olive fruit: green (20 WAF); yellowish (24 WAF); turning or veraison (28 WAF) and purple or mature (31 WAF). Immediately after harvesting, olive mesocarp was frozen in liquid nitrogen and stored at −80°C until its use.

Olive Oil Extraction

Oil was extracted from olive fruits using a laboratory oil extraction plant (Abencor, Comercial Abengoa, SA, Seville, Spain) that mimics the industrial virgin olive oil (VOO) production at a laboratory scale according to Martínez et al. (1975). Fruit crushing was carried out with a stainless steel hammer mill working at 3000 rpm and a 5 mm sieve. The Abencor thermo-beater was used for the malaxation step for 30 min at 28°C. Finally, paste centrifugation was performed in a basket centrifuge for 1 min at 3500 rpm. Oils were decanted, filtered through paper, and stored under a nitrogen atmosphere at −20°C until analysis.

Lipid and Fatty Acid Analysis

Olive fruit mesocarp tissue was heated at 70°C for 30 min with isopropanol to inactivate endogenous lipase activity. Lipids were extracted as described by Hara and Radin (1978) and lipid separation was carried out by thin layer chromatography (Hernández et al., 2008).

Fatty acid methyl esters of the different olive oil extracted and the lipid preparations obtained from the olive mesocarp at different stages of development were produced by acid-catalyzed transmethylation (Garcés and Mancha, 1993) and analyzed by gas chromatography (Román et al., 2015). Heptadecanoic acid was used as internal standard to calculate the lipid and fatty acid content in the samples. Results are expressed either in mol percent of the different fatty acids or in μg of fatty acid per mg of FW and are presented as means ± SD of three biological replicates.

Total RNA Isolation and cDNA Synthesis

Total RNA isolation was performed as described by Hernández et al. (2005) using 1.5 g of frozen olive mesocarp. RNA quality verification, removal of contaminating DNA, and cDNA synthesis were carried out according to Hernández et al. (2009).

Quantitative Real-Time PCR

The expression levels of the olive fatty acid desaturase genes were determined by quantitative real-time PCR (qRT-PCR) using a CFX Connect real-time PCR System and iTaq Universal SYBR Green Supermix (BioRad, California, United States) as previously described (Hernández et al., 2019). Primers for gene-specific amplification (**Supplementary Table 3**) were previously described for *OeSAD* genes (Parvini et al., 2016), for *OeFAD2* and *OeFAD6* genes (Hernández et al., 2009, 2020), and *OeFAD3* and *OeFAD7* genes (Hernández et al., 2016). The housekeeping olive ubiquitin2 gene (*OeUBQ2* and AF429430) was used as an endogenous reference to normalize (Hernández et al., 2009). The relative expression level of each gene was calculated using the equation $2^{-\Delta Ct}$ where $\Delta Ct = (Ct_{GOI} - Ct_{UBQ2})$ (Livak and Schmittgen, 2001; Pfaffl, 2004). This method gave us the advantage to make comparisons in the level of gene expression across developmental stages, cultivars, and genes. The data are presented as means ± SD of three biological replicates, each having two technical replicates per 96-well plate.

RESULTS AND DISCUSSION

Variability of Oleic and Linoleic Acid Content in an Olive Cultivar Core Collection (Core-36)

In accordance with previous studies in olive (León et al., 2018), the fatty acid analysis of 89 olive cultivars showed a high level of diversity conserved in the WOBGC-IFAPA located in Córdoba (Spain). As expected, oleic acid was the most abundant fatty acid, followed by palmitic and linoleic acids (**Supplementary Table 1**). This variability could be explained only by the genetic component, since the culture conditions, fruit ripeness, and oil extraction conditions were fixed, further confirming that the genotype is the major source of variability for olive oil fatty acid composition (Ripa et al., 2008). To further explore the diversity in the oleic/linoleic acid ratio in different olive cultivars, we decided to analyze the fatty acid composition of a Core-36, which holds most of the genetic diversity found in the WOGBC-IFAPA (Belaj et al., 2012) (**Supplementary Table 2**). Thus, among the most abundant fatty acids, the highest degree of variability in the fatty acid profile was found for the oleic and linoleic acid percentage in the oils of the Core-36, in such a way that the coefficient of variation for the oleic/linoleic acid ratio was 66.48% (**Supplementary Table 4**). The mean percentages of oleic and linoleic acids were 66.84 and 12.35%, respectively, being these values very similar to the ones found in cultivated material (León et al., 2018). The variability intervals of oleic and linoleic acids ranged from 46.24–79.15% and 3.34–27.12%, respectively, being the cultivars Picual and Abou Kanani the ones with the most contrasting linoleic acid percentage (**Figure 1**). Interestingly, these variability ranges were slightly lower than those observed for oleic and linoleic acids in the segregating progeny of the cross between Picual and Arbequina cultivars (50.6–81.9% and 2.9–23.1%, respectively) (Hernández et al., 2017). In addition, the oleic/linoleic acid ratio was inversely proportional to the

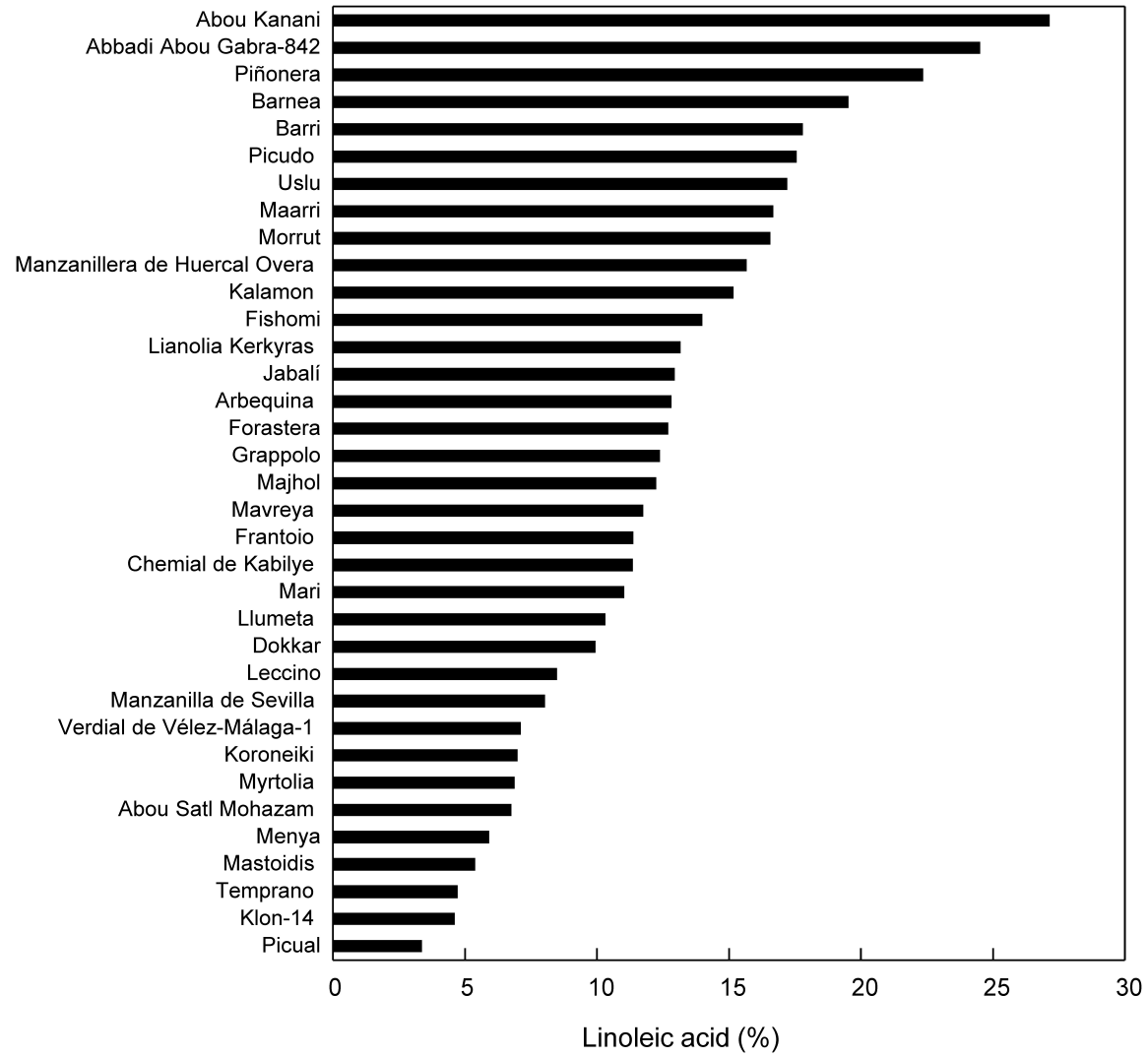

FIGURE 1 | Linoleic acid percentage in the oils of the Core-36. Olive fruits were hand-harvested at the turning stage during the season 2011/2012. Oil extraction and fatty acid analysis were determined as described in materials and methods. Data represent the mean of three biological replicates. In all the cases SD < 3% of mean values.

linoleic acid content (**Supplementary Table 2**), clearly indicating that the variability of linoleic acid content found in the Core-36 oils is mainly caused by different varietal capacities of oleate desaturase enzymes. High variability was also found between the saturated/unsaturated ratio, mainly due to the differences found in palmitic acid content, with the highest (23.70%) and the lowest (9.68%) levels detected in cultivars Dokkar and Majhol-152, respectively (**Supplementary Table 2**). A high level of variability of the Core-36 has also been previously reported for the VOO phenolic and volatile fractions (García-Rodríguez et al., 2017; García-Vico et al., 2017), and tocopherol composition (Pérez et al., 2019). Therefore, our results confirm the evidence that cultivar differences in the fatty acid composition of olive oils are due to the genetic component (Tous et al., 2005; De la Rosa et al., 2013; Montaño et al., 2016). The Core-36 analyzed in this study facilitates the evaluation and utilization of its genetic diversity to understand the mechanism underlying fatty acid desaturation in olive for crop improvement.

OeFAD2-2 and *OeFAD2-5* Are the Main Genes Controlling the Oleic/Linoleic Acid Ratio in Olive Mesocarp

Previously, we have investigated the specific contribution of each olive oleate desaturase gene to the linoleic acid content in the olive oil using "Picual" and "Arbequina," because these are the two main cultivars for olive oil production (Hernández et al., 2009, 2016, 2020; Parvini et al., 2016). In this work, we decided to select two olive cultivars with high contrasting amounts of linoleic acid, with the aim of investigating the genotypic differences in olive mesocarp fatty acid desaturation. Specifically, we chose cultivars Klon-14, with a low linoleic acid content

(4.58%), and Abou Kanani, with high linoleic acid levels (27.12%) (**Figure 1**) for a comparative molecular and metabolic analysis during olive fruit development and ripening.

As shown in **Figure 2**, oil accumulation in olive mesocarp during development and ripening increased in both cultivars studied, in parallel to the oleic, linoleic, and linolenic acids content (**Figure 3**). Besides, the amount of oleic acid in "Klon-14" mesocarp was much higher than in "Abou Kanani," reaching up to 80 μg/mg FW at the matured stage. In contrast, linoleic acid levels increased moderately in "Klon-14" mesocarp during the olive fruit development and ripening, while in "Abou Kanani" they increased abruptly during the developing period, reaching a maximum at the turning stage. These patterns of linoleic acid accumulation observed in Klon-14 and Abou Kanani cultivars were respectively similar, to those reported for "Picual," "Koroneiki" and "Mari," and for "Arbequina" and "Shengeh" (Hernández et al., 2009; Parvini et al., 2015). Regarding linolenic acid, its content was considerably low in both cultivars studied, although slightly higher in "Klon-14" mesocarp. This result was different from those reported by Hernández et al. (2016), in which "Arbequina," the cultivar with a higher linoleic acid content, also showed higher level of linolenic acid, particularly during the olive fruit developing period.

Subsequently, we determined the expression levels of olive fatty acid desaturase genes responsible for the biosynthesis of oleic (*OeSAD*), linoleic (*OeFAD2* and *OeFAD6*), and linolenic acid (*OeFAD3* and *OeFAD7*). The relative transcript abundance analysis of olive *SAD* genes showed that *OeSAD2* gene expression levels were the highest throughout the olive mesocarp development and ripening in both cultivars studied (**Figure 4**). These data point to the *OeSAD2* gene as the main candidate for oleic acid production in the olive mesocarp. In contrast, *OeSAD1*, and especially *OeSAD3*, exhibited lower expression levels compared to *OeSAD2*. These data are in agreement with previous studies in other olive cultivars (Parvini et al., 2016; Contreras et al., 2020), further confirming that *OeSAD2* is the main gene that contributes to the oleic acid synthesis in the olive mesocarp and, therefore, to its content in the olive oil.

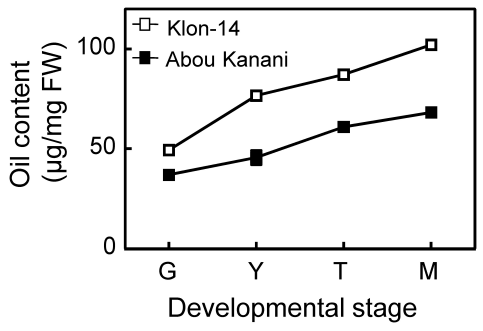

FIGURE 2 | Oil content in the mesocarp tissue of Klon-14 and Abou Kanani cultivars at different stages of development. Lipid content was determined as described in materials and methods. Data are presented as means ± SD of three biological replicates. G, Green; Y, yellowish; T, turning; M, matured.

The higher *OeSAD2* gene expression levels observed in "Abou Kanani" compared to "Klon-14" mesocarp (**Figure 4**) did not correlate with the total oil content, which was higher in Klon-14 cultivar (**Figure 2**). These results are consistent with those reported by Parvini et al. (2016) in Picual and Arbequina cultivars, indicating that in olive, the *SAD2* gene, which seems to be mainly responsible for oleic acid synthesis, was not directly associated with TAG accumulation. In contrast, a full correlation between expression levels of a *SAD* gene and oil accumulation has been reported in many plant species (Cummins et al., 1993; Liu et al., 2009; Shilman et al., 2011; Li et al., 2014; Kilaru et al., 2015).

On the other hand, Parvini et al. (2015) proposed that the higher oleic/linoleic ratio in Mari mesocarp, in comparison to Shengeh, was due to the higher expression levels of *OeSAD2* gene, together with lower *OeFAD2-2* expression levels. However, this hypothesis was discarded in a later study by Parvini et al. (2016), who observed the highest *OeSAD2* expression level in Arbequina and Manzanilla cultivars, which are characterized by low and high oleic/linoleic acid ratio, respectively. The results obtained in the present study agree with Parvini et al. (2016) since "Abou Kanani" mesocarp, which showed higher *OeSAD2* expression levels (**Figure 4**), exhibit a lower oleic/linoleic acid ratio (**Supplementary Table 2**), supporting the hypothesis that olive *SAD2* gene is not primarily involved in the control of the linoleic acid content in the olive mesocarp.

Regarding oleate desaturase genes (*FAD2* and *FAD6*), *OeFAD2-2* and *OeFAD2-5* showed the highest expression levels in Klon-14 and Abou Kanani cultivars (**Figures 5**, **6A**). In addition, we could observe a correlation between the *OeFAD2-2* and *OeFAD2-5* gene expression levels (**Figure 5**) and the linoleic acid content (**Figure 3**) in "Klon-14" and "Abou Kanani" mesocarp, particularly during the ripening period. Furthermore, the higher transcript levels detected for these two *FAD2* genes in "Abou Kanani" mesocarp compared with "Klon-14" (**Figure 5**) agree with the high linoleic acid content observed for the mesocarp tissue from "Abou Kanani" relative to that of "Klon-14" (**Figure 3**). All these results indicate that *OeFAD2-2* and *OeFAD2-5* are the main genes responsible for the linoleic acid synthesis in the olive mesocarp and, therefore, for the linoleic acid content of olive oil. This conclusion is in keeping with that described for other olive cultivars, either in the case of *OeFAD2-2* (Hernández et al., 2009; Parvini et al., 2015; Contreras et al., 2020), or *OeFAD2-5* (Hernández et al., 2020). The fact that the mesocarp tissue possesses two genes involved in the oleic acid desaturation may be to assure the linoleic acid biosynthesis all over the prolonged developmental period of olive fruit that takes approximately 35–40 weeks (Hernández et al., 2020).

Our whole data strongly support the hypothesis that the linoleic acid content is essentially determined by the olive cultivar, which is ultimately controlled by the *OeFAD2-2* and *OeFAD2-5* gene expression levels. Additionally, these results point to *OeFAD2-2* and *OeFAD2-5* as good candidate genes for the co-localized QTLs for oleic and linoleic acids, as well as for monounsaturated and polyunsaturated fatty acids, and the oleic/linoleic acid ratio, identified in a linkage map of a "Picual" × "Arbequina" progeny (Hernández et al., 2017). This information could be particularly useful for the development of

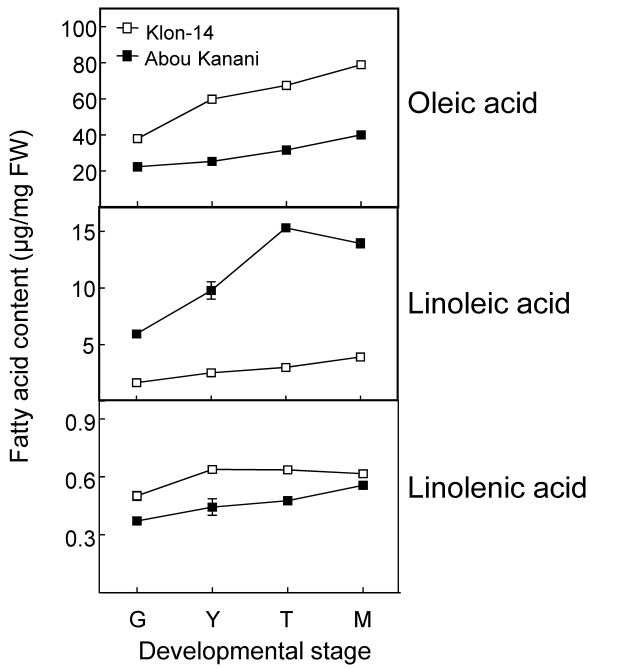

FIGURE 3 | Oleic, linoleic, and linolenic acid contents in the mesocarp tissue of Klon-14 and Abou Kanani cultivars at different stages of development. Fatty acid content was determined as described in materials and methods. Data are presented as means ± SD of three biological replicates. G, Green; Y, yellowish; T, turning; M, matured.

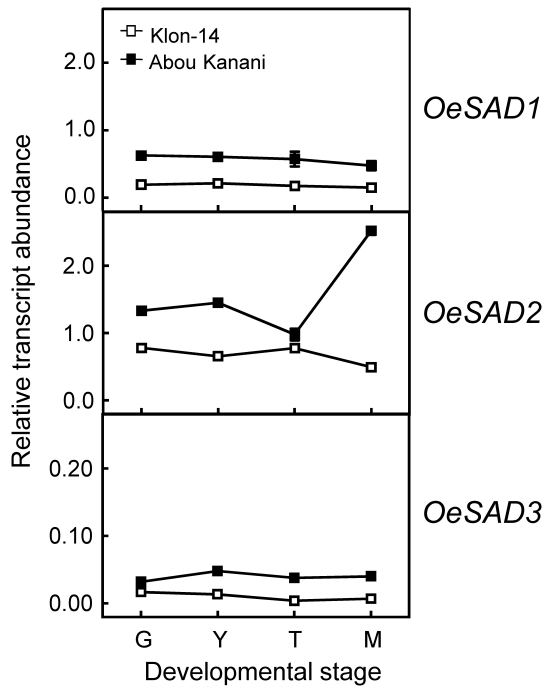

FIGURE 4 | Relative transcript abundance of olive *SAD* genes in the mesocarp tissue of Klon-14 and Abou Kanani cultivars at different stages of development. The relative transcript abundance was determined by qRT-PCR as described under materials and methods. Data are presented as means ± SD of three biological replicates. G, Green; Y, yellowish; T, turning; M, matured.

molecular markers for the high oleic/low linoleic character, to increase the efficiency of breeding programs for the selection of new and improved olive cultivars.

Concerning linoleate desaturases, the analysis of their gene expression levels during "Klon-14" and "Abou Kanani" mesocarp development and ripening revealed that *OeFAD3A* and *OeFAD3B* gene transcripts were undetectable at the stages studied, while *OeFAD7-1* and *OeFAD7-2* increased all along the development and ripening period, particularly in "Abou Kanani" mesocarp (**Figure 6B**). Analogous expression patterns for olive *FAD3* and *FAD7* genes have been reported before for the mesocarp tissue of "Koroneiki" (Poghosyan et al., 1999; Banilas et al., 2007), "Canino," "Frantoio," and "Moraiolo" (Matteuci et al., 2011), and "Picual" and "Arbequina" (Hernández et al., 2016). These data indicate that *OeFAD7*, and not *OeFAD3*, could be the main genes responsible for the linolenic acid content in the mesocarp and, therefore, in the olive oil. In fact, Hernández et al. (2016) postulated that in olive mesocarp, the linoleic acid synthesized in the ER by *OeFAD2* genes is transferred to the chloroplast where *OeFAD7-1* and *OeFAD7-2* genes are responsible for its desaturation to produce linolenic acid, which is then exported again to the ER to be incorporated into TAG. Alternatively, olive FAD7 enzymes can act on ER lipids while located in chloroplast as it has been proposed for FAD7 in *Chlamydomonas reinhardtii* (Nguyen et al., 2013). Although the specific mechanism by which trafficking of fatty acids out of and into the chloroplast has not yet been elucidated, the most recent advances suggest that lipid transport is achieved by multiple mechanisms which include membrane contact sites with specialized protein machinery, such as TGD complexes (LaBrant et al., 2018). It is interesting to point out the higher expression levels of *OeFAD7* genes observed in "Abou Kanani" mesocarp compared to "Klon-14" (**Figure 6A**), with "Abou Kanani" exhibiting lower levels of linolenic acid (**Figure 3**). Similar results were reported in Picual and Arbequina cultivars, where the higher *OeFAD7* genes expression levels detected in "Picual" mesocarp did not correspond with a higher amount of linolenic acid. One possible explanation could be that the linoleate desaturation in olive mesocarp may be subjected to post-transcriptional regulation. In soybean cellular cultures, *FAD7* regulation by light is carried out by post-translational regulatory mechanisms (Collados et al., 2006). On the other hand, the explanation may lie in the mechanism involved in the transport of fatty acids across the chloroplast membrane, which remains to be completely elucidated.

Cultivar Differences in LPCAT Specificity Could Play a Significant Role in Determining the Linoleic Acid Content of TAG Molecules

With the aim of further investigation of the metabolic pathways for the biosynthesis and accumulation of linoleic acid in olive mesocarp, we analyzed the fatty acid composition in

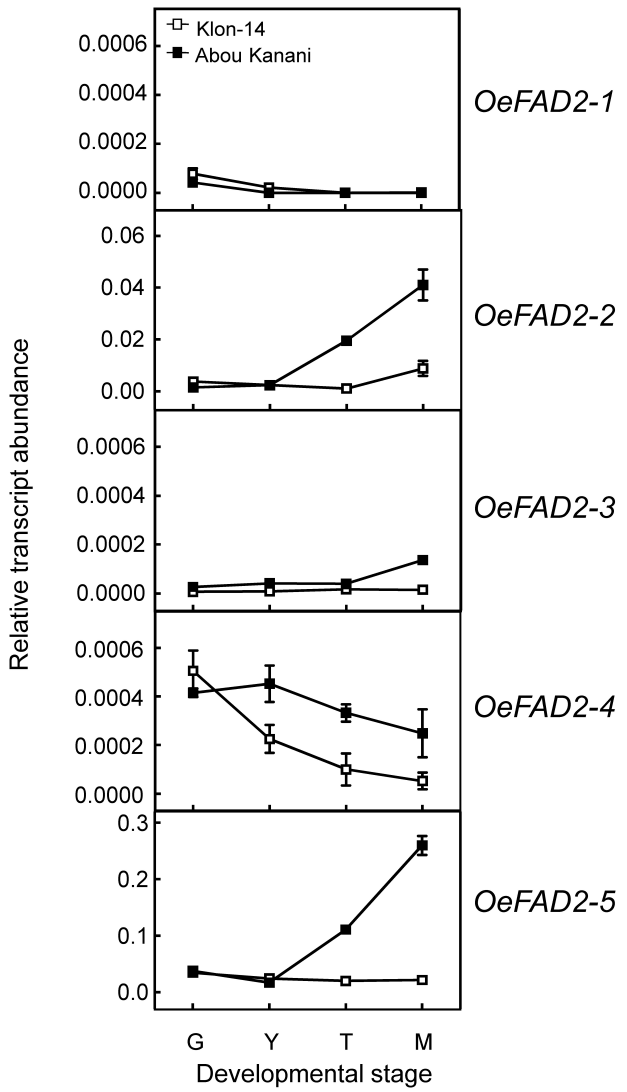

FIGURE 5 | Relative transcript abundance of olive *FAD2* genes in the mesocarp tissue from Klon-14 and Abou Kanani cultivars at different stages of development. The relative transcript abundance was determined by qRT-PCR as described under materials and methods. Data are presented as means ± SD of three biological replicates. G, Green; Y, yellowish; T, turning; M, matured.

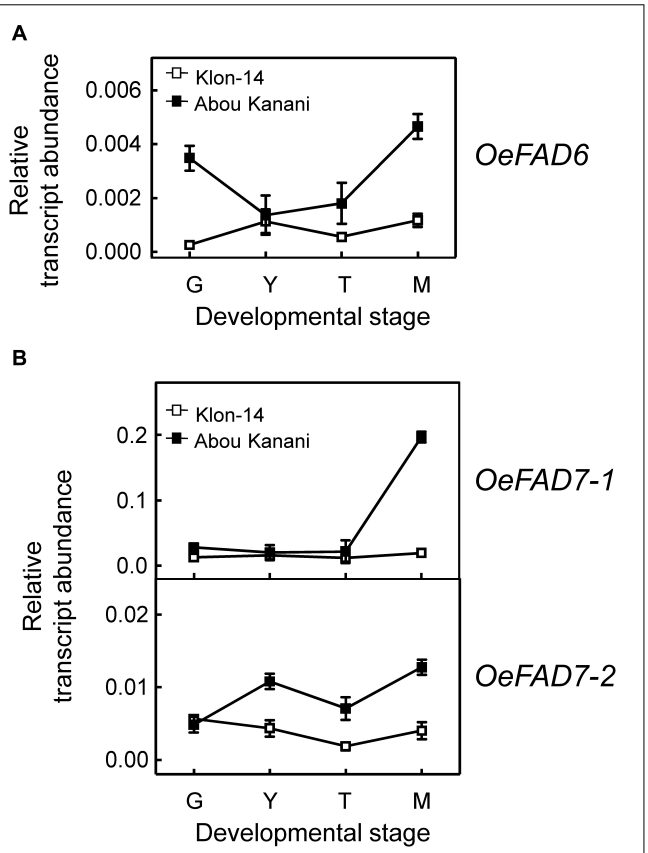

FIGURE 6 | Relative transcript abundance of olive *FAD6* **(A)** and *FAD7* **(B)** genes in the mesocarp tissue from Klon-14 and Abou Kanani cultivars at different stages of development. The relative transcript abundance was determined by qRT-PCR as described under materials and methods. Data are presented as means ± SD of three biological replicates. G, Green; Y, yellowish; T, turning; M, matured.

different lipid classes from "Klon-14" and "Abou Kanani" mesocarp at different stages of olive fruit development and ripening. The linoleic acid percentage in DAG and TAG was considerably higher in "Abou Kanani" than in "Klon-14" mesocarp (**Figure 7A**), in agreement with the high linoleic acid levels found in "Abou Kanani" oil (**Figure 1**). In addition, while the increase of linoleic acid in neutral lipids in "Klon-14" mesocarp was slow and gradual during the olive fruit development and ripening, in "Abou Kanani" mesocarp the linoleic acid increased sharply from the beginning of fruit development in both, DAG, and TAG (**Figure 7A**). These results correlate quite well with *OeFAD2-2* and *OeFAD2-5* genes expression levels in both cultivars (**Figure 5**), further confirming the role of these two genes in the production of linoleic acid in the olive mesocarp.

Furthermore, the analysis of linoleic acid content in phospholipids revealed clear differences between both cultivars (**Figure 7B**). Interestingly, the percentage of linoleic acid was low (∼4%) and did not change significantly in any of the phospholipids studied in "Klon-14" mesocarp during development and ripening. In contrast, in "Abou Kanani" mesocarp, the linoleic acid increased considerably during the olive fruit development and ripening, reaching up to 20% of total fatty acid, particularly in PC, which showed the highest values (**Figure 7B**). This increase in PC linoleic acid levels was accompanied by a reduction in oleic acid (**Supplementary Table 5**), indicating a high rate of oleate desaturation in this cultivar.

The parallel tendency detected in the linoleic acid content in PC and PA, unchanged in "Klon-14" and increased in "Abou Kanani," points to the acyl-editing mechanism catalyzed by LPCAT and further incorporation to the Kennedy pathway as the main entry route of linoleic acid synthesized in PC into *de novo*

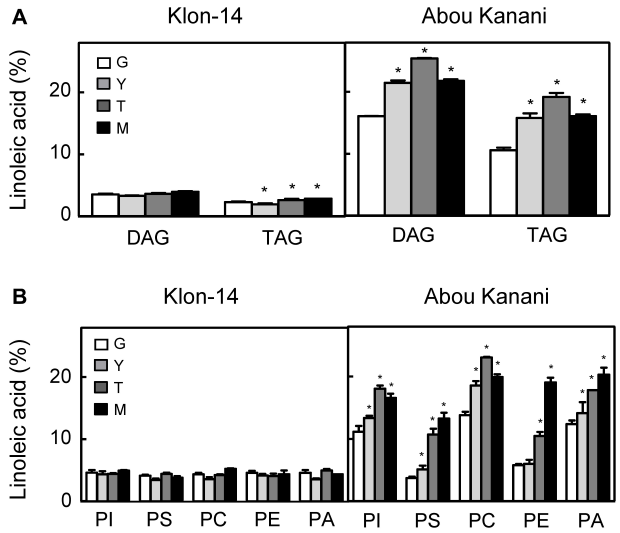

FIGURE 7 | Linoleic acid percentage in neutral lipids **(A)** and phospholipids **(B)** from "Klon-14" and "Abou Kanani" mesocarp tissue at different stages of development. The linoleic acid percentage was determined as described under materials and methods. Data are presented as means ± SD of three biological replicates. G, Green; Y, yellowish; T, turning; M, matured. *Indicates significantly different ($P < 0.05$) to G stage by two-way ANOVA with a Bonferroni *post hoc* test.

DAG, versus the CPT and/or PDCT pathway that produce PC-derived DAG as substrate for TAG synthesis (Bates, 2016). The observation that the linoleic acid metabolism differs in different olive cultivars has been previously reported by Hernández et al. (2020) in "Picual" and "Arbequina." Interestingly, in all cultivars studied so far, a similar trend in linoleic acid content in PC and PA has been observed (**Figure 7B**; Hernández et al., 2020), highlighting the role of LPCAT in olive mesocarp lipid metabolism.

On the other hand, it is likely that in the case of "Abou Kanani" mesocarp, the high degree of desaturation of oleic to linoleic acid allows the accumulation of this fatty acid in all lipid classes, including TAG. However, in "Klon-14" mesocarp it seems that the scenario is different. The observation that the linoleic acid slightly increased in TAG while did not change in phospholipids (**Figure 7**) indicates that the small amount of linoleic acid that is synthesized in PC, due to the low *OeFAD2-2* and *OeFAD2-5* genes expression levels (**Figure 5**), is incorporated into TAG. Differently, in "Picual" and "Arbequina" mesocarp, a distinct preference of DGAT enzyme for linoleoyl-CoA has been proposed to explain the accumulation of this fatty acid in phospholipids or TAG, respectively (Hernández et al., 2020).

However, the most striking observation was that the oleic acid content decreased in PC in "Klon-14" mesocarp, while there is an increase in palmitic and stearic acids (**Supplementary Table 6**). These results could be explained by a decrease in oleic acid production due to the low *SAD2* expression levels detected in this cultivar (**Figure 4**). However, this hypothesis is not plausible since the total oleic acid content increased in "Klon-14" mesocarp during the olive fruit development and ripening (**Figure 3**). An alternative explanation could be a reduced incorporation of oleic acid into PC. This phospholipid is the major site of acyl-editing, and LPCAT enzyme is responsible for the partition of newly synthesized fatty acid between the acyl-CoA pool and PC. Therefore, LPCAT plays a major role in supplying oleate to the PC pool for desaturation (Wang et al., 2012). Although the substrate specificity of the acyltransferases of the Kennedy pathway is one of the determining factors of TAG composition (Ohlrogge and Browse, 1995; Jeppson et al., 2019), Menard et al. (2018) reported that natural variation in a gene encoding the acyl-editing enzyme LPCAT influences TAG composition in Arabidopsis seed. Therefore, the low *OeFAD2-2* and *OeFAD-5* genes expression levels, together with a decreased incorporation of oleic acid into PC by LPCAT, could explain the low linoleic acid levels found in "Klon-14" oil.

CONCLUSION

The oleic and linoleic acid contents exhibit the highest degree of variability in the fatty acid composition of olive oils from the Core-36 olive cultivar collection. Gene expression data in olive mesocarp during development and ripening from two olive cultivars with contrasting amounts of linoleic acid suggest that *OeFAD2-2* and *OeFAD2-5* genes play a key role in the variability of the oleic/linoleic acid ratio in olive cultivars. In addition, the different fatty acid profile of individual lipids in both cultivars suggests that differences in the specifities of extraplastidial acyltransferase enzymes could be also involved in the control of the oleic/linoleic acid ratio in olive. The present study highlights the importance of cultivar collections not only for the selection of optimal parents for breeding programs but also as a key source of plant material to carry out basic research. Finally, all this information will allow the development of molecular markers to be used in the marker-assisted selection of new olive cultivars that produce oils with high oleic and low linoleic contents, increasing the efficiency of olive breeding programs to obtain VOO with improved quality.

DATA AVAILABILITY STATEMENT

The original contributions presented in the study are included in the article/**Supplementary Material**, further inquiries can be directed to the corresponding author/s.

AUTHOR CONTRIBUTIONS

MLH managed and performed the harvest of plant material, carried out RNA isolation and cDNA synthesis, analyzed the data, and drafted the manuscript. MDS performed the harvest of plant material and qRT-PCR and lipid analysis. AB contributed to the selection and collection of the plant materials and to the manuscript revision. JM-R conceived and designed the study, analyzed the data, and contributed to manuscript revision. All authors discussed, commented, and approved the final version of the manuscript.

FUNDING

This work was supported by the Spanish Ministry of Science and Innovation through Research Grants AGL2011-24442, AGL2014-55300-R, AGL2017-87871-R (AEI/FEDER, UE), and by OLEAGEN Project funded by the Fundación Genoma España, Junta de Andalucía through IFAPA and Corporación Tecnológica de Andalucía (CTA). The WOGBC-IFAPA has been maintained by different national projects (RFP 2013-00005-00-00 and RFP 2017-00007-00-00) funded by INIA, as well as by project PR. CRF. CRF2019.004 is partly funded by the European Agricultural Fund for Rural Development (EAFRD). MLH was the recipient of a contract from the JAE-Postdoctoral CSIC program (Spain).

ACKNOWLEDGMENTS

We acknowledge support of the publication fee by the CSIC Open Access Publication Support Initiative through its Unit of Information Resources for Research (URICI).

SUPPLEMENTARY MATERIAL

The Supplementary Material for this article can be found online at: https://www.frontiersin.org/articles/10.3389/fpls.2021.653997/full#supplementary-material

REFERENCES

Baldoni, L., Cultrera, N. G., Mariotti, R., Ricciolini, C., Arcioni, S., Vendramin, G. G., et al. (2009). A consensus list of microsatellite marker for olive genotyping. *Mol. Breed.* 24, 213–231. doi: 10.1007/s11032-009-9285-8

Banilas, G., Moressis, A., Nikoloudakes, N., and Hatzopoulos, P. (2005). Spatial and temporal expressions of two distinct oleate desaturases from olive (*Olea europaea* L.). *Plant Sci.* 168, 547–555. doi: 10.1016/j.plantsci.2004.09.026

Banilas, G., Nikiforiadis, A., Makariti, I., Moressis, A., and Hatzopoulos, P. (2007). Discrete roles of a microsomal linoleate desaturase gene in olive identified by spatiotemporal transcriptional analysis. *Tree Physiol.* 27, 481–490. doi: 10.1093/treephys/27.4.481

Bates, P. D. (2016). Understanding the control of acyl flux through the lipid metabolic network of plant oil biosynthesis. *Biochim. Biophys. Acta* 1861, 1214–1225. doi: 10.1016/j.bbalip.2016.03.021

Bates, P. D., Durrett, T. P., Ohlrogge, J. B., and Pollard, M. (2009). Analysis of acyl fluxes through multiple pathways of triacylglycerol synthesis in developing soybean embryos. *Plant Physiol.* 150, 55–72. doi: 10.1104/pp.109.137737

Belaj, A., Dominguez-Garcia, M. C., Atienza, S. G., Martin-Urdiroz, N., de la Rosa, R., Satovic, Z., et al. (2012). Developing a core collection of olive (*Olea europaea* L.) based on molecular markers (DArTs, SSRs, SNPs) and agronomic traits. *Tree Genet. Genomes* 8, 365–378. doi: 10.1007/s11295-011-0447-6

Beltrán, G., del Río, C., Sánchez, S., and Martínez, L. (2004). Influence of harvest date and crop yield on the fatty acid composition of virgin olive oils from cv. *Picual. J. Agric. Food Chem.* 52, 3434–3440. doi: 10.1021/jf049894n

Browse, J., and Somerville, C. (1991). Glycerolipid synthesis: biochemistry and regulation. *Annu. Rev. Plant Physiol.* 42, 467–506. doi: 10.1146/annurev.pp.42.060191.002343

Collados, R., Andreu, V., Picorel, R., and Alfonso, M. (2006). A light-sensitive mechanism differently regulates transcription and transcript stability of ω3 fatty-acid desaturases (FAD3, FAD7 and FAD8) in soybean photosynthetic cell suspensions. *FEBS Lett.* 580, 4934–4940. doi: 10.1016/j.febslet.2006.07.087

Connor, D. J., and Fereres, E. (2005). The physiology of adaptation and yield expression in olive. *Horticult. Rev.* 34, 155–229. doi: 10.1002/9780470650882.ch4

Contreras, C., Mariotti, R., Mousavi, S., Baldoni, L., Guerrero, C., Roka, L., et al. (2020). Characterization and validation of olive *FAD* and *SAD* gene families: expression analysis in different tissues and during fruit development. *Mol. Biol. Rep.* 47, 4345–4355. doi: 10.1007/s11033-020-05554-9

Cummins, I., Hill, M. J., Ross, J. H. E., Hobbs, D. H., Watson, M. D., and Murphy, D. J. (1993). Differential, temporal and spatial expression of genes involved in storage oil and oleosin accumulation in developing rapeseed embryos: implications for the role of oleosins and the mechanism of oil-body formation. *Plant Mol. Biol.* 23, 1015–1027. doi: 10.1007/bf00021816

Dahlqvist, A., Stahl, U., Lenman, M., Banas, A., Lee, M., Sandager, L., et al. (2000). Phospholipid:diacylglycerol acyltransferase: an enzyme that catalyzes the acyl-CoA-independent formation of triacylglycerol in yeast and plants. *Proc. Natl. Acad. Sci. U S A.* 97, 6487–6492. doi: 10.1073/pnas.120067297

De la Rosa, R., Talhaoui, N., Rouis, H., Velasco, L., and Leòn, L. (2013). Fruit characteristics and fatty acid composition in advanced olive breeding selections along the ripening period. *Food Res. Int.* 54, 1890–1896. doi: 10.1016/j.foodres.2013.08.039

Garcés, R., and Mancha, M. (1993). One-step lipid extraction and fatty acid methyl esters preparation from fresh plant tissues. *Anal. Biochem.* 211, 139–143. doi: 10.1006/abio.1993.1244

García-Rodríguez, R., Belaj, A., Romero-Segura, C., Sanz, C., and Pérez, A. G. (2017). Exploration of genetic resources to improve the functional quality of virgin olive oil. *J. Funct. Food* 38, 1–8. doi: 10.1016/j.jff.2017.08.043

García-Vico, L., Belaj, A., Sánchez-Ortiz, A., Martínez-Rivas, J. M., Pérez, A. G., and Sanz, C. (2017). Volatile compound profiling by HS-SPME/GC-MS-FID of a core olive cultivar collection as a tool for aroma improvement of virgin olive oil. *Molecules* 22:141. doi: 10.3390/molecules22010141

Gómez-Gálvez, F. J., Vega-Macias, V., Hidalgo-Moya, J. C., Hidalgo-Moya, J. J., and Rodríguez-Jurado, D. (2020). Application to soil of disinfectants through irrigation reduces *Verticillium dahliae* in the soil and verticillium wilt of olive. *Plant Pathol.* 69, 272–283. doi: 10.1111/ppa.13114

Gunstone, F. D., Harwood, J. L., and Dijkstra, A. J. (2007). *The Lipid Handbook*. New York, NY: CRC Press.

Hara, A., and Radin, N. S. (1978). Lipid extraction of tissues with a low-toxicity-solvent. *Anal. Biochem.* 90, 420–426. doi: 10.1016/0003-2697(78)90046-5

Haralampidis, K., Sánchez, J., Baltrusch, M., Heinz, E., and Hatzopoulos, P. (1998). Temporal and transient expression of stearoyl-ACP carrier protein desaturase gene during olive fruit development. *J. Exp. Bot.* 49, 1661–1669. doi: 10.1093/jexbot/49.327.1661

Harwood, J. L. (2005). "Fatty acid biosynthesis," in *Plant Lipids*, ed. D. J. Murphy (Oxfork: Blackwell Publishing), 27–101.

Hernández, M. L., Belaj, A., Sicardo, M. D., León, L., de la Rosa, R., Martín, A., et al. (2017). Mapping quantitative trait loci controlling fatty acid composition in olive. *Euphytica* 213:7. doi: 10.1007/s10681-016-1802-3

Hernández, M. L., Guschina, I. A., Martínez-Rivas, J. M., Mancha, M., and Harwood, J. L. (2008). The utilization and desaturation of oleate and linoleate during glycerolipid biosynthesis in olive (*Olea europaea* L.) callus cultures. *J. Exp. Bot.* 59, 2425–2435. doi: 10.1093/jxb/ern121

Hernández, M. L., Mancha, M., and Martínez-Rivas, J. M. (2005). Molecular cloning and characterization of genes encoding two microsomal oleate desaturases (FAD2) from olive. *Phytochemistry* 66, 1417–1426. doi: 10.1016/j.phytochem.2005.04.004

Hernández, M. L., Padilla, M. N., Mancha, M., and Martínez-Rivas, J. M. (2009). Expression analysis identifies *FAD2-2* as the olive oleate desaturase gene mainly responsible for the linoleic acid content in virgin olive oil. *J. Agric. Food Chem.* 57, 6199–6206. doi: 10.1021/jf900678z

Hernández, M. L., Padilla, M. N., Sicardo, M. D., Mancha, M., and Martínez-Rivas, J. M. (2011). Effect of different environmental stresses on the expression of oleate desaturase genes and fatty acid composition in olive fruit. *Phytochemistry* 72, 178–187. doi: 10.1016/j.phytochem.2010.11.026

Hernández, M. L., Sicardo, M. D., Alfonso, M., and Martínez-Rivas, J. M. (2019). Transcriptional regulation of stearoyl-acyl carrier protein desaturase genes in response to abiotic stresses leads to changes in the unsaturated fatty acids composition of olive mesocarp. *Front. Plant Sci.* 10:251. doi: 10.3389/fpls.2019.00251

Hernández, M. L., Sicardo, M. D., and Martínez-Rivas, J. M. (2016). Differential contribution of endoplasmic reticulum and chloroplast ω-3 fatty acid desaturase genes to the linolenic acid content of olive (*Olea europaea*) fruit. *Plant Cell Physiol.* 57, 138–151. doi: 10.1093/pcp/pcv159

Hernández, M. L., Sicardo, M. D., Arjona, P. M., and Martínez-Rivas, J. M. (2020). Specialized functions of olive *FAD2* gene family members related to fruit development and the abiotic stress response. *Plant Cell Physiol.* 61, 427–441. doi: 10.1093/pcp/pcz208

IOOC (2001). *IOOC Trade standard applying to olive and olive pomance oil. COI/T.15/NC no. 2/Rev. 10.*

Jeppson, S., Demski, K., Carlsson, A. S., Zhu, L.-H., Banas, A., Stymne, S., et al. (2019). *Crambe hispanica* Subsp. *abyssinica* diacylglycerol acyltransferase specificities towards diacylglycerols and acyl-CoA reveal combinatorial effects that greatly affect enzymatic activity and specificity. *Front. Plant Sci.* 10:1442. doi: 10.3389/fpls.2019.01442

Kilaru, A., Cao, X., Dabbs, P. B., Sung, H.-J., Rahman, M. M., Thrower, N., et al. (2015). Oil biosynthesis in a basal angiosperm: transcriptome analysis of *Persea americana* mesocarp. *BMC Plant Biol.* 15:203.doi: 10.1186/s12870-015-0586-2

LaBrant, E., Barnes, A. C., and Roston, R. L. (2018). Lipid transport required to make lipids of photosynthetic membranes. *Photosynt. Res.* 138, 345–360. doi: 10.1007/s11120-018-0545-5

León, L., de la Rosa, R., Velasco, L., and Belaj, A. (2018). Using wild olives in breeding programs: implications on oil quality composition. *Front. Plant Sci.* 9:232. doi: 10.3389/fpls.2018.00232

Li, C., Miao, H., Wei, L., Zhang, T., Han, X., and Zhang, H. (2014). Association mapping of seed oil and protein content in *Sesamum indicum* L. using SSR markers. *PLoS One* 9:e105757. doi: 10.1371/journal.pone.0105757

Liu, Z. J., Yang, X. H., and Fu, Y. (2009). SAD, a stearoyl-acyl carrier protein desaturase highly expressed in high-oil maize inbred lines. *Russ. J. Plant Physiol.* 56, 709–715. doi: 10.1134/s1021443709050185

Livak, K. J., and Schmittgen, T. D. (2001). Analysis of relative gene expression data using real-time quantitative PCR and the $2^{-\Delta\Delta Ct}$ method. *Methods* 25, 402–408. doi: 10.1006/meth.2001

Martínez, J. M., Munoz, E., Alba, J., and Lanzon, A. (1975). Report about the use of the 'Abencor' analyser. *Grasas Aceites* 26, 379–385.

Matteuci, M., D'Angeli, S., Errico, S., Lamanna, G., Perrotta, G., and Altamura, M. M. (2011). Cold affects the transcription of fatty acid desaturases and oil quality in the fruit of *Olea europaea* L. genotypes with different cold hardiness. *J. Exp. Bot.* 62, 3403–3420. doi: 10.1093/jxb/err013

Menard, G., Bryant, F. M., Kelly, A. A., Craddock, C. P., Lavagi, I., Hassani-Pak, K., et al. (2018). Natural variation in acyl editing is a determinant of seed storage oil composition. *Sci. Rep.* 8:17346. doi: 10.1038/s41598-018-35136-6

Montaño, A., Hernández, M., Garrido, I., Llerena, J. L., and Espinosa, F. (2016). Fatty acid and phenolic compound concentrations in eight different monovarietal virgin olive oils from Extremadura and the relationship with oxidative stability. *Int. J. Mol. Sci.* 17:1960. doi: 10.3390/ijms17111960

Nguyen, H. M., Cuiné, S., Beyly-Adriano, A., Légeret, B., Billon, E., Auroy, P., et al. (2013). The green microalga *Chlamydomonas reinhardtii* has a single *ω*-3 fatty acid desaturase that localizes to the chloroplast and impacts both plastidic and extraplastidic membrane lipids. *Plant Physiol.* 163, 914–928. doi: 10.1104/pp.113.223941

O'Keefe, V. A., Wiley, V. A., and Knauft, D. A. (1993). Comparison of oxidative stability of high- and normal-oleic peanut oils. *J. Am. Oil Chem. Soc.* 70, 489–492. doi: 10.1007/bf02542581

Ohlrogge, J., and Browse, J. (1995). Lipid biosynthesis. *Plant Cell* 7, 957–970.

Parvini, F., Sicardo, M. D., Hosseini-Mazinani, M., Martínez-Rivas, J. M., and Hernández, M. L. (2016). Transcriptional analysis of stearoyl-acyl carrier protein desaturase genes from olive *(Olea europaea*) in relation to the oleic acid content of the virgin olive oil. *J. Agric. Food Chem.* 64, 7770–7781. doi: 10.1021/acs.jafc.6b02963

Parvini, F., Zeinanloo, A. A., Ebrahimie, E., Tahmasebi-Enferadi, S., and Hosseini-Mazinani, M. (2015). Differential expression of fatty acid desaturases in Mari and Shengeh olive cultivars during fruit development and ripening. *Eur. J. Lipid Sci. Technol.* 117, 523–531. doi: 10.1002/ejlt.201400327

Pérez, A. G., León, L., Pascual, M., de la Rosa, R., Belaj, A., and Sanz, C. (2019). Analysis of olive (*Olea europaea* L.) genetic resources in relation to the content of vitamin E in virgin olive oil. *Antioxidants* 8:242. doi: 10.3390/antiox8080242

Pfaffl, M. W. (2004). "Quantification strategies in real-time PCR," in *A–Z of Quantitative PCR*, ed. S. A. Bustin (La Jolla: International University Line), 87–112.

Poghosyan, Z. P., Haralampidis, K., Martsinkowskaya, A. I., Murphy, D. J., and Hatzopoulos, P. (1999). Developmental regulation and spatial expression of a plastidial fatty acid desaturase from *Olea europaea*. *Plant Physiol. Biochem.* 37, 109–119. doi: 10.1016/S0981-9428(99)80072-2

Rallo, L., Díez, C. M., Morales-Sillero, A., Miho, H., Priego-Capote, F., and Rallo, P. (2018). Quality of olives: a focus on agricultural preharvest factors. *Sci. Hort.* 233, 491–509. doi: 10.1016/j.scienta.2017.12.034

Ripa, V., De Rose, F., Caravita, Parise, M. R., Perri, E., Rosati, S., et al. (2008). Qualitative evaluation of olive oils from new olive selections and effects of genotype and environment on oil quality. *Adv. Hort. Sci.* 22, 95–103.

Román, A., Hernández, M. L., Soria-García, A., López-Gomollón, S., Lagunas, B., Picorel, R., et al. (2015). Non-redundant contribution of the plastidial FAD8 ω-3 desaturase to glycerolipid unsaturation at different temperatures in Arabidopsis. *Mol. Plant* 8, 1599–1611. doi: 10.1016/j.molp.2015.06.004

Salas, J. J., Sánchez, J., Ramli, U. S., Manaff, A. M., Williams, M., and Harwood, J. L. (2000). Biochemistry of lipid metabolism in olive and other oil fruits. *Prog. Lipid Res.* 39, 151–180. doi: 10.1016/s0163-7827(00)00003-5

Sales-Campos, H., Reis, de Souza, P., Crema Peghini, B., Santana, da Silva, J., et al. (2013). An overview of the modulatory effects of oleic acid in health and disease. *Mini Rev. Med. Chem.* 13, 201–210. doi: 10.2174/13895571380480 5193

Shanklin, J., and Cahoon, E. B. (1998). Desaturation and related modifications of fatty acids. *Ann. Rev. Plant Physiol.* 49, 611–641. doi: 10.1146/annurev.arplant. 49.1.611

Shilman, F., Brand, Y., Brand, A., Hedvat, I., and Hovav, R. (2011). Identification and molecular characterization of homeologous Δ9-stearoyl acyl carrier protein desaturase 3 genes from the allotetraploid peanut (*Arachis hypogaea*). *Plant Mol. Biol. Rep.* 29, 232–241. doi: 10.1007/s11105-010-0226-9

Stobart, K., Mancha, M., Lenman, M., Dahlqvist, A., and Stymne, S. (1997). Triacylglycerols are synthesised and utilized by transacylation reactions in microsomal preparations of developing safflower (*Carthamus tinctorius* L.) seeds. *Planta* 203, 58–66. doi: 10.1007/s004250050165

Tous, J., Uceda, M., Romero, A., Beltrán, G., Días, I., and Jiménez, A. (2005). "Composición del Aceite," in *Variedades de Olivo en España (Libro II: Variabilidad y Selección)*, eds L. Rallo, D. Barranco, J. M. Caballero, C. del Río, A. Martín, J. Tous, et al. (Madrid: Junta de Andalucía).

Vos, E. (2003). Linoleic acid, "vitamin F6"; is the Western World getting too much? Probably. *Lipid Technol.* 15, 81–84.

Wang, L., Shen, W., Kazachkov, M., Chen, G., Chen, Q., Carlsson, A. S., et al. (2012). Metabolic interactions between the Lands cycle and the Kennedy pathway of glycerolipid synthesis in Arabidopsis developing seeds. *Plant Cell* 24, 4652–4669. doi: 10.1105/tpc.112.104604

Yamaki, T., Nagamine, I., Fukumoto, T., Yano, T., Miyahara, M., and Sakurai, H. (2005). High oleic peanut oil modulates promotion stage in lung tumorigenesis of mice treated with methyl nitrosourea. *Food Sci. Technol. Res.* 11, 231–235. doi: 10.3136/fstr.11.231

Conflict of Interest: The authors declare that the research was conducted in the absence of any commercial or financial relationships that could be construed as a potential conflict of interest.

frontiers in Plant Science

ORIGINAL RESEARCH
published: 15 March 2021
doi: 10.3389/fpls.2021.635327

The Adjustment of Membrane Lipid Metabolism Pathways in Maize Roots Under Saline–Alkaline Stress

Xiaoxuan Xu[1,2†], Jinjie Zhang[1†], Bowei Yan[3], Yulei Wei[1], Shengnan Ge[1], Jiaxin Li[1], Yu Han[1], Zuotong Li[1], Changjiang Zhao[1] and Jingyu Xu[1]**

[1] Key Lab of Modern Agricultural Cultivation and Crop Germplasm Improvement of Heilongjiang Province, Heilongjiang Engineering Technology Research Center for Crop Straw Utilization, College of Agriculture, Heilongjiang Bayi Agricultural University, Daqing, China, [2] Beijing Hortipolaris Co., Ltd., Beijing, China, [3] Institute of Industrial Crops, Heilongjiang Academy of Agricultural Sciences, Harbin, China

OPEN ACCESS

Edited by:
Agnieszka Zienkiewicz, Nicolaus Copernicus University in Toruń, Poland

Reviewed by:
Patrick J. Horn, East Carolina University, United States
Kamil Demski, Swedish University of Agricultural Sciences, Sweden

***Correspondence:**
Changjiang Zhao
zhaocj15@126.com
Jingyu Xu
xujingyu2003@hotmail.com

† These authors have contributed equally to this work

Specialty section:
This article was submitted to Plant Metabolism and Chemodiversity, a section of the journal Frontiers in Plant Science

Received: 30 November 2020
Accepted: 09 February 2021
Published: 15 March 2021

Citation:
Xu X, Zhang J, Yan B, Wei Y, Ge S, Li J, Han Y, Li Z, Zhao C and Xu J (2021) The Adjustment of Membrane Lipid Metabolism Pathways in Maize Roots Under Saline–Alkaline Stress. Front. Plant Sci. 12:635327. doi: 10.3389/fpls.2021.635327

Plants are frequently confronted by diverse environmental stress, and the membrane lipids remodeling and signaling are essential for modulating the stress responses. Saline–alkaline stress is a major osmotic stress affecting the growth and development of crops. In this study, an integrated transcriptomic and lipidomic analysis was performed, and the metabolic changes of membrane lipid metabolism in maize (*Zea mays*) roots under saline–alkaline stress were investigated. The results revealed that phospholipids were major membrane lipids in maize roots, and phosphatidylcholine (PC) accounts for approximately 40% of the total lipids. Under 100 mmol $NaHCO_3$ treatment, the level of PC decreased significantly (11–16%) and the parallel transcriptomic analysis showed an increased expression of genes encoding phospholipase A and phospholipase D/non-specific phospholipase C, which suggested an activated PC turnover under saline–alkaline stress. The plastidic galactolipid synthesis was also activated, and an abnormal generation of C34:6 galactolipids in 18:3 plants maize implied a plausible contribution from the prokaryotic pathway, which could be partially supported by the up-regulated expression of three putative plastid-localized phosphatidic acid phosphatase/lipid phosphate phosphatase. A comprehensive gene–metabolite network was constructed, and the regulation of membrane lipid metabolism under saline–alkaline stress in maize was discussed.

Keywords: maize (*Zea mays*), lipid metabolism, lipidome, transcriptome, saline–alkaline stress

INTRODUCTION

Cell membrane is the first parclose of defense for plants to cope with the external environmental stimuli, and its fluidity and stability are critical for the survival of cells and even whole plants under various stress conditions (Sulian et al., 2020). In plants and other organisms, the structure and properties of membrane are determined by a complex mixture of lipid species with different head group structures, fatty acid (FA) lengths, and unsaturation (Mikami and Murata, 2003; Li N. et al., 2016).

Plasma membranes of plant cells are mainly composed of glycerolipids. Phospholipids dominate the extraplastidic glycerolipids, including phosphatidylcholine (PC), phosphatidylethanolamine

(PE), phosphatidic acid (PA), phosphatidylinositol (PI), and phosphatidylserine (PS), whereas the major components of the plastidic membrane are monogalactosyldiacylglycerol (MGDG), digalactosyldiacylglycerol (DGDG), phosphatidyl glycerol (PG), and sulfoquinovosyl diacylglycerol (SQDG) (Benning, 2009). Studies have shown that the physical properties of the membrane can be altered by changing the relative amount of each lipid class (Botella et al., 2017). The metabolic changes of membrane lipids are closely related to the stress responses of plant, and frequent lipid remodeling has been observed in membrane lipids under various stress conditions (Gu et al., 2017). Narasimhan et al. (2013) found that the increase of PA would affect root growth and proliferation through its effect on vesicle transport and cytoskeletal recombination under the condition of P and N defects. Studies have been shown that phospholipase D (PLD) and non-specific phospholipase C (NPC), which direct dephosphorylation of endoplasmic reticulum (ER) PC into PA and diacylglycerol (DAG), respectively, involved in lipid remodeling (Nakamura et al., 2009).

The synthesis of glyceroglycolipids has two different pathways, which are compartmentalized in two different subcellular spaces and work synergistically (Li-Beisson et al., 2013; Li Q. et al., 2016). One pathway is the eukaryotic pathway, also known as the ER pathway, which is implemented in the ER, and the other is the prokaryotic pathway, also known as the plastidic pathway, which is localized in the plastid envelope (Li-Beisson et al., 2013). Numerous previous studies have shown that the balance of prokaryotic and eukaryotic pathways of lipid synthesis in *Arabidopsis* is associated with abiotic stress, and the contribution of the enhanced eukaryotic pathway to lipid synthesis can be observed under various abiotic stress conditions (Nakamura et al., 2009; Moellering and Benning, 2011; Higashi et al., 2015; Li et al., 2015). Previous biochemical and molecular biology studies have shown the synergistic regulation of the key enzymes involved in these two pathways (Shen et al., 2010). In *Arabidopsis*, light and temperature stimulation promotes their interaction, and marked changes in FA molecular species of the membrane lipids occurred (Burgos et al., 2011; Szymanski et al., 2014; Li et al., 2015). In maize (*Zea mays*), low temperature stress induced the expression of lipid related genes in the eukaryotic pathway and led to enhanced flow of lipids products to plastids/chloroplasts (Gu et al., 2017).

Saline–alkaline stress is a major osmotic stress affecting the growth and development of crops. Previous study revealed that salinity could induce membrane structure and lipid changes in maize mesophyll and bundle sheath chloroplasts (Omoto et al., 2016). In this study, the combined analysis of transcriptome and lipidome was conducted to investigate the transcriptional regulation of lipid metabolism in the root of maize under saline–alkaline stress and to provide a better understanding of saline–alkaline stress response mechanism in major field crops.

Abbreviations: DAG, Diacylglycerol; DGAT, diacylglycerol acyltransferase; DGD, digalactosyl diacylglycero synthase; DGDG, digalactosyldiacylglycerol; DGK, diacylglycerol kinase; DGL, diacylglycerol lipase; FAD, fatty acid desaturase; GPAT, glycerol-3-phosphate acyltransferase; LPAAT, lysophosphatidyl acyltransferase; LPP, lipid phosphate phosphatase; MGD, monogalactosyl diacylglycerol synthase; MGDG, monogalactosyldiacylglycerol; NPC, non-specific phospholipase C; PA, phosphatidic acid; PAH, phosphatidate phosphohydrolase; PAP, phosphatidic acid phosphatase; PC, phosphatidylcholine; PE, phosphatidylethanolamine; PG, phosphatidyl glycerol; PI, phosphatidylinositol; PLA, phospholipase A; PLC, phospholipase C; PLD, phospholipase D; PS, phosphatidylserine; SQDG, sulfoquinovosyl diacylglycerol; TAG, triacylglycerol.

MATERIALS AND METHODS

Plant Treatments and Sampling

The seeds of inbred maize variety He 344 were selected and disinfected with 1% sodium hypochlorite for 30 min and then were washed with tap water and rinsed with distilled water for three times. The seeds were soaked in nutrient solution 6–8 h for germination. When the buds were 0.5 cm long, they were placed in perforated plates and cultured in 1/2 Hoagland nutrient solution (LEAGEN) in an artificial chamber (KUANSONS, 22°C, 16 h light/8-h dark, 250 μmol m^{-2} s^{-1} photosynthetic photon flux density and 60–65% relative humidity). The maize seedlings grown to the "two leaves and one heart" stage (around 2 weeks old) were treated with 1/2 Hoagland nutrient solution supplemented with 100 mmol $NaHCO_3$, and the control group was left in the 1/2 Hoagland nutrient solution, and then the root tissues of maize seedlings were sampled at 24 and 72 h after treatment, respectively.

Transcriptomic Analysis and Quantitative Reverse Transcriptase–Polymerase Chain Reaction Validation

The total RNA of the maize root tissues was extracted using TRIZOL reagent (Invitrogen). The construction of cDNA library was started from the synthesis of two cDNA strands, followed by the purification of double-stranded cDNA and the enrichment of cDNA library by polymerase chain reaction (PCR) amplification (TOYOBO). The Illumina HiSeq 2000 platform was used for the RNA-seq sequencing of the constructed library (BioMarker). The obtained unigene sequences were aligned with the protein databases NR, NT, SwissProt, KEGG, COG, and GO using Blast software[1] (*E*-value $< 1.0E^{-5}$) for the best feature annotation. The differentially expressed genes (DEGs) were determined, and the significant DEGs were further screened out based on the criteria of $Log_2FC \geq 1.5$ or ≤ -1.5 (false discovery rate ≤ 0.01). The RNA-seq data have been submitted to the online SRA (sequential read file) database with accession number SRP307694.

Quantitative reverse transcriptase (RT)–PCR analysis was performed to verify the validity of RNA-seq data. The gene primers were designed by Primer 5 software. Maize *actin* (*GRMZM2G126010*) and *GAPDH* (*GRMZM2G155348*) genes were used as internal controls. The extracted RNA samples were reverse transcribed according to the instructions of ReverTra Ace qPCR RT Master Mix with gDNA remover reverse transcription kit (TOYOBO). Fluorescence quantitative PCR reactions were performed according to the instructions of THUNDERBIRD SYBR qPCR mixture real-time quantification kit (TOYOBO).

[1] http://blast.ncbi.nlm.nih.gov/Blast.cgi

Each reaction was repeated three times, and three biological replicates were set up for each sample (see **Supplementary Figure S1** for details).

Membrane Lipid Extraction and Analysis

After treatment with $NaHCO_3$ (100 mmol) at different time points, root samples from 2 week-old maize seedlings were collected from five plants in different pots (samples from plants without $NaHCO_3$ treatment were used as control), and the lipidomic analysis was conducted in six replicates. The extraction of total plant lipids was modified based on previous reports (Narayanan et al., 2016). Approximately 200 mg of fresh root tissues was quickly immersed in a 50 mL glass tube (Teflon lining, threaded cap) containing 3 mL of 0.01% BHT (SIGMA) in hot isopropanol solution (75°C). After cooling to room temperature, 1.5 mL of chloroform and 0.6 mL of water were added and vortexed for 1 h. The extract was then placed in a new tube, and 4 mL of chloroform/methanol (2:1) containing 0.01% BHT was added. The mixture was shaken for 30 min, and the extraction process was repeated several times until the tissues turned white. One milliliter of 1 M KCl was added to the mixed extract, and then the new mixture was centrifuged, and the supernatant was discarded. The extract was washed again with 2 mL of water, and supernatant was discarded, and the remaining lipid extract was fully vaporized under a nitrogen blower. The dried lipid samples were stored at −80°C.

For FA compositional analyses, the extracts were dissolved in 1 mL of chloroform and precise amounts of internal standards, obtained and quantified as previously described (Welti et al., 2002). Unfractionated lipid extracts were introduced by continuous infusion into the Essential Science Indicators (ESI) source on a triple quadrupole MS/MS (API4000, ABSciex, Framingham, MA, United States). Samples were introduced using an autosampler (LCMini PAL, CTC Analytics AG, Zwingen, Switzerland) fitted with the required injection loop for the acquisition time and presented to the ESI needle at 30 μL min^{-1} (Narayanan et al., 2016). The precursor and neutral loss scans were applied to obtain polar lipid profiles. The sample is introduced into the electrospray ionization source, further generation of lipid molecular ions, including PC-, lysoPC-, PE-, and lysoPE-positive $[M + H]^+$ ions; MGDG-, DGDG-, PG-, PI-, PA-, and PS-positive $[M + NH_4]^+$ ions; and lysoPG-negative $[M\text{-}H]^-$ ions. A series of peak values of lipid content were detected by electrospray ionization. The peaks on the spectra are quantified in comparison to a group of internal standards. Mass spectrometry lipid analysis was performed at the Kansas Lipidomics Research Center (KLRC, United States) using electrospray ionization mass spectrometry.

The data for each lipid molecular species were normalized and displayed as mol% of the total lipids analyzed. Lipidomics results were expressed as values (mol%) = mean 5 ± standard deviation, three biological replicates for each set of data, and statistical analysis was performed by SPSS Statistic 21.0 with a significant level set to $a = 0.05$.

Transmembrane Structure and Subcellular Location Analysis

The analysis of the structural domain of the maize ZmPAPs was through the Phytozome v13.0 database and the SMART website, and the transmembrane structure information of the maize ZmPAP gene was obtained through the Expasy online prediction website[2]. The protein sequences of ZmPAPs were submitted to WOLF PORST[3] to predict the subcellular location of the ZmPAP proteins.

Statistical Analysis

All statistical analyses were conducted with SPSS statistics 21.0 (SPSS Inc.). Five to six biological replicates for lipidomic data and three biological replicates for gene expression data were subjected for the calculation. The significance levels were calculated using Student *t*-test method. $^*P < 0.05$ and $^{**}P < 0.01$ represent difference significance levels.

RESULTS

Lipids Metabolic Changes in Maize Roots Under Saline–Alkaline Stress

To investigate the changes of membrane lipids in maize root under $NaHCO_3$ treatment (100 mmol), lipidomic analysis was conducted to analyze the various glycerolipids content and their FA composition. A total of 11 glycerolipids were detected by ESI-MS/MS, including six types of phospholipids (PC, PE, PA, PI, PS, and PG), two types of galactolipids (MGDG and DGDG), and three classes of lysophospholipids (LPG, LPC, and LPA).

As shown in **Figure 1**, phospholipids are the main membrane lipids in maize root tissues, which account for approximately 70% of the total components. PC was the most abundant lipid species, accounting for more than 40% of all lipids, and the remaining phospholipid species account for another 30%. The proportion of the galactolipids MGDG and DGDG is approximately 20% of the total membrane lipids, with each accounting for 10%, respectively. The levels of three lysophospholipids (LPG, LPC, and LPA) were relatively low. Under saline–alkaline stress (100 mmol $NaHCO_3$ treatment), the molar percentage of most phospholipid species was declined. The level of PC decreased around 11 and 16% after 24 and 72 h treatment, respectively, in comparison with the control. PA and PS also decreased in various degrees. The reduction of PA is 15 and 26% at 24 and 72 h time points, respectively, and PS decreased more than 50% at both time points. In contrast, the level of PI was elevated about 1.3–1.5 times under $NaHCO_3$ treatment. The level of the plastidic phospholipid PG was increased, especially at the 72 h time point, which was 30% higher than the control. Regarding the galactolipids, the percentage of DGDG decreased significantly under $NaHCO_3$ stress, which reduced 20 and 39% at 24 and 72 h, respectively. Although the content of lysophospholipids was low, the levels of LPG, LPC, and LPE were observed to be increased, and LPC showed a significant increase at the 72 h time point.

[2]https://web.expasy.org/protscale/

[3]https://wolfpsort.hgc.jp/

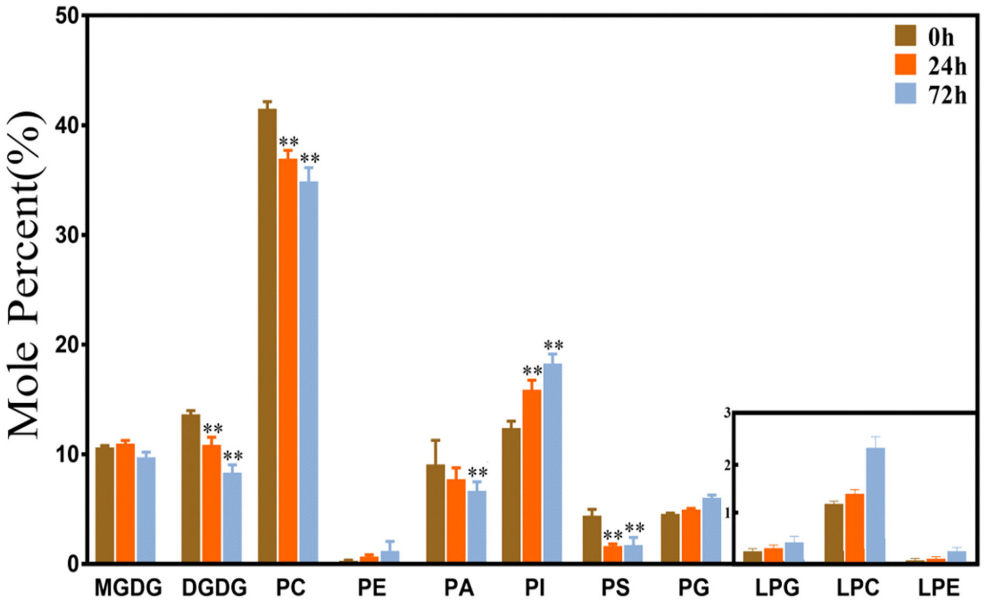

FIGURE 1 | Changes of glycerolipids species in maize roots under $NaHCO_3$ (100 mmol). MGDG, monogalactosyldiacylglycerol; DGDG, digalactosyldiacylglycerol; PC, phosphatidylcholine; PE, phosphatidylethanolamine; PA, phosphatidic acid; PI, phosphatidylinositol; PS, phosphatidylserine. PG, phosphatidylglycerol; LPG, Lyso-PC; LPC, Lyso-PC; LPA, Lyso-PC. Values (mol%) are means 5 ± standard deviation (SD), three biological replicates for each set of data. "∗∗" indicated that the value was significantly different from the control ($P < 0.01$).

The Changes of Fatty Acid Molecular Species Under Saline–Alkaline Stress

The profiles of the FA molecules of the two side chains of the glycerolipids were also determined by lipidomic analysis. The molecular species are represented by the total number of carbon atoms vs. the total number of double bonds. As shown in **Figure 2**, the glycerolipids in maize root tissues have distinct FA profiles, which are particularly enriched in C34 and C36 molecules (the total number of acyl carbon atoms), and relatively higher molar percentage of C34:2 and C36:4 (the total number of acyl carbon atoms: double bonds) was observed. Most of the extraplastidic phospholipids classes (PC, PE, PA, and PS) were composed of similar proportion of C36 and C34 molecular species, whereas in the plastidic phospholipid PG, C34 molecules (especially C34:2) were dominant. Under saline–alkaline stress (100 mmol $NaHCO_3$ treatment), the molar percentage of C34:2 and C36:4 molecules in the major phospholipids (PC, PA, PS, and PG) were decreased, whereas the percentage of C36:2, C36:5, and C34:3 was increased to varied degrees.

As shown in **Figure 3**, the plastidic galactolipids MGDG and DGDG were mainly composed of C34 and C36 molecules, and C36 molecules were obviously dominant in MGDG. Under saline–alkaline stress (100 mmol $NaHCO_3$ treatment), the molar percentage of C36 molecules decreased, whereas that of C34 molecules increased significantly in both MGDG and DGDG. In MGDG, the level of C34 was around two times higher than that of control after 24 h of $NaHCO_3$ treatment and approximately three times higher after 72 h treatment in comparison with the control. It is worth noting that the level of polyunsaturated C34 molecules, including that of C34:4, C34:5, C34:6, was found tremendously elevated under $NaHCO_3$ treatment (3–6-fold). In DGDG, the increase in the level of C34:4, C34:5, C34:6 under saline–alkaline stress was also obvious.

Transcriptomic Analysis of Maize Roots Under Saline–Alkaline Stress

In order to investigate the molecular regulation of lipid metabolism in maize root tissues, the transcriptome was analyzed by means of Illumina RNA-seq. RNA was prepared from maize root samples collected from 2 week-old seedlings, after treatment with 100 mmol $NaHCO_3$ for 0 (control), 24 and 72 h. Real-time PCR analysis was performed on a number of DEGs to validate the RNA-seq data. The results showed that all six tested genes exhibited similar expression profiles, which proved the reliability of the transcriptome data (**Supplementary Figure S1**). The RNA-seq data have been submitted to the online SRA database with an accession number of SRP307694.

The obtained unigene sequences were aligned with the NR, NT, SwissProt, KEGG, COG, and GO protein databases. As shown in **Figure 4A**, in the "24 h vs. 0 h" comparison group, a total of 4,761 DEGs ($Log_2FC \geq 1.5$ or ≤ -1.5) were annotated and characterized into 136 metabolic pathways, among which the "carbohydrate metabolism," "amino acid metabolism," and "lipid metabolism" are the three most enriched metabolic pathways, and the lipid metabolism-related DEGs accounted for 10% in total DEGs. In the "72 h vs. 0 h" comparison group (**Figure 4B**), a total of 5,623 DEGs associated with 153 metabolic pathways were annotated, and approximately 9% of which are involved in lipid metabolism pathways.

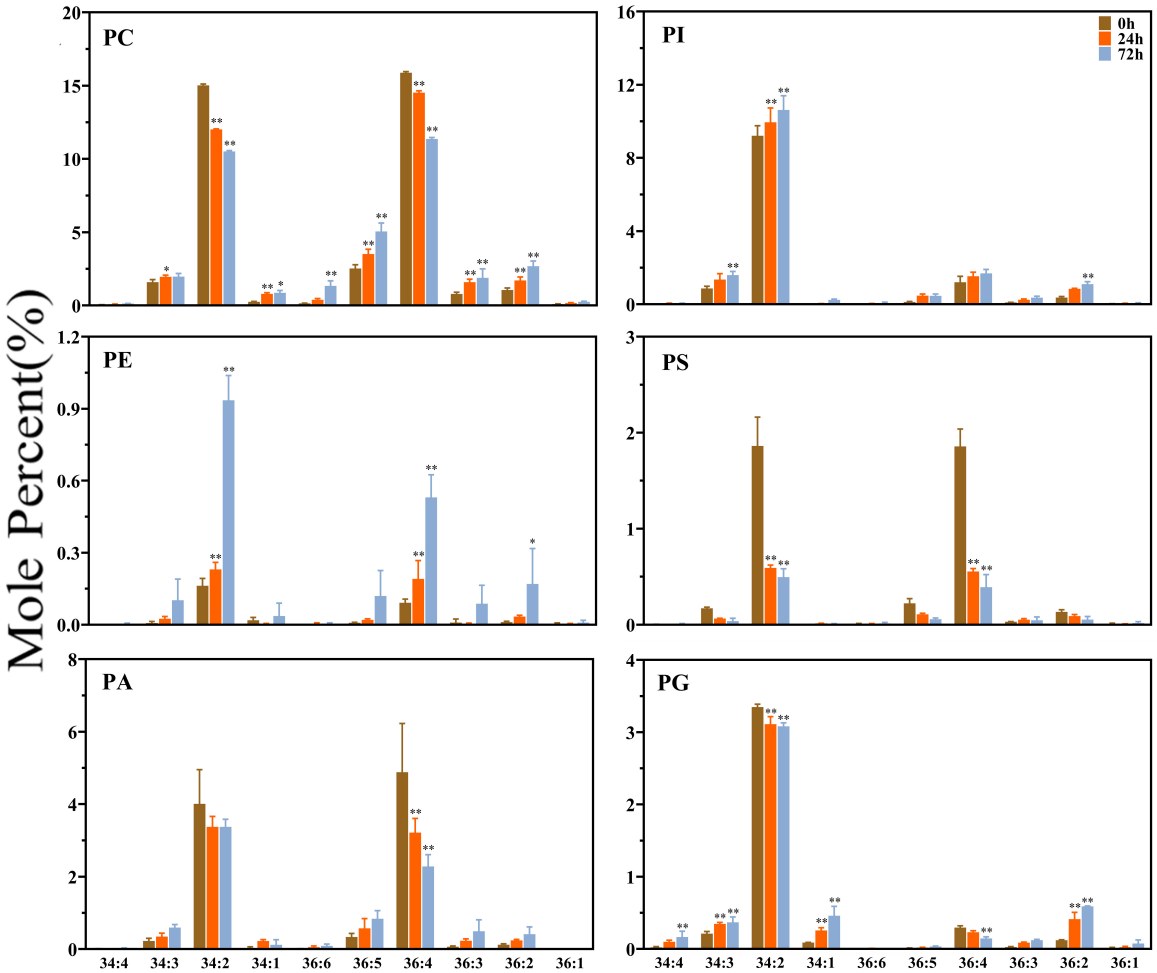

FIGURE 2 | Changes in diacyl lipid molecular species of major phospholipids in maize roots under $NaHCO_3$ (100 mmol). Major phospholipids: PC, phosphatidylcholine; PE, phosphatidylethanolamine; PA, phosphatidic acid; PI, phosphatidylinositol; PS, phosphatidylserine. PG, phosphatidylglycerol. Values (mol%) are means 5 ± standard deviation (SD), three biological replicates for each set of data. "∗" indicated that the value was significantly different from the control ($P < 0.05$). "∗∗" indicated that the value was significantly different from the control ($P < 0.01$).

The DEGs were determined, and their differential enrichment in different comparison groups is analyzed. As shown in **Figure 4C**, a total of 26,435 up-regulated genes and 29,048 down-regulated genes were obtained in the entire transcriptome. In the "24 h vs. 0 h" comparison group, there were 8,887 up-regulated genes and 7,166 down-regulated genes. In the "72 h vs. 0 h" group, the largest number of DEGs was obtained, and the up-regulated genes and down-regulated genes were 10,416 and 12,215, respectively. In the "72 h vs. 24 h" group, there were 7,132 up-regulated genes and 9,667 down-regulated genes, respectively. In general, the down-regulated DEGs in maize roots under saline–alkaline stress were slightly more than the up-regulated ones. In the three-group joint analysis, the number of the up-regulated DEGs was 603, which was 322 fewer than the 925 down-regulated DEGs. We also compared the distribution of DEGs related to lipid metabolism, and 387 up-regulated DEGs and 621 down-regulated genes were annotated in the transcriptome data, and their distribution was consistent with the overall trend of the transcriptome (**Figure 4D**). In the "24 h vs. 0 h" comparison group, 171 genes were up-regulated, and 68 genes were down-regulated. In the "72 h vs. 0 h" group, 173 genes were found up-regulated and 197 genes were down-regulated. In the "72 h vs. 24 h" group, 43 genes were up-regulated, and 356 genes were down-regulated.

Differential Responses of Lipid Metabolism and Signaling Pathways in Maize Roots Under Saline–Alkaline Stress

Based on previously published *Arabidopsis* lipid gene database and related literature (Li-Beisson et al., 2013; Troncoso-Ponce et al., 2013; Botella et al., 2017), and combined with GO and KEGG annotation, lipid-related DEGs genes were recruited from maize root transcriptome data. A total of 609 lipid-related genes were further classified into specific pathways.

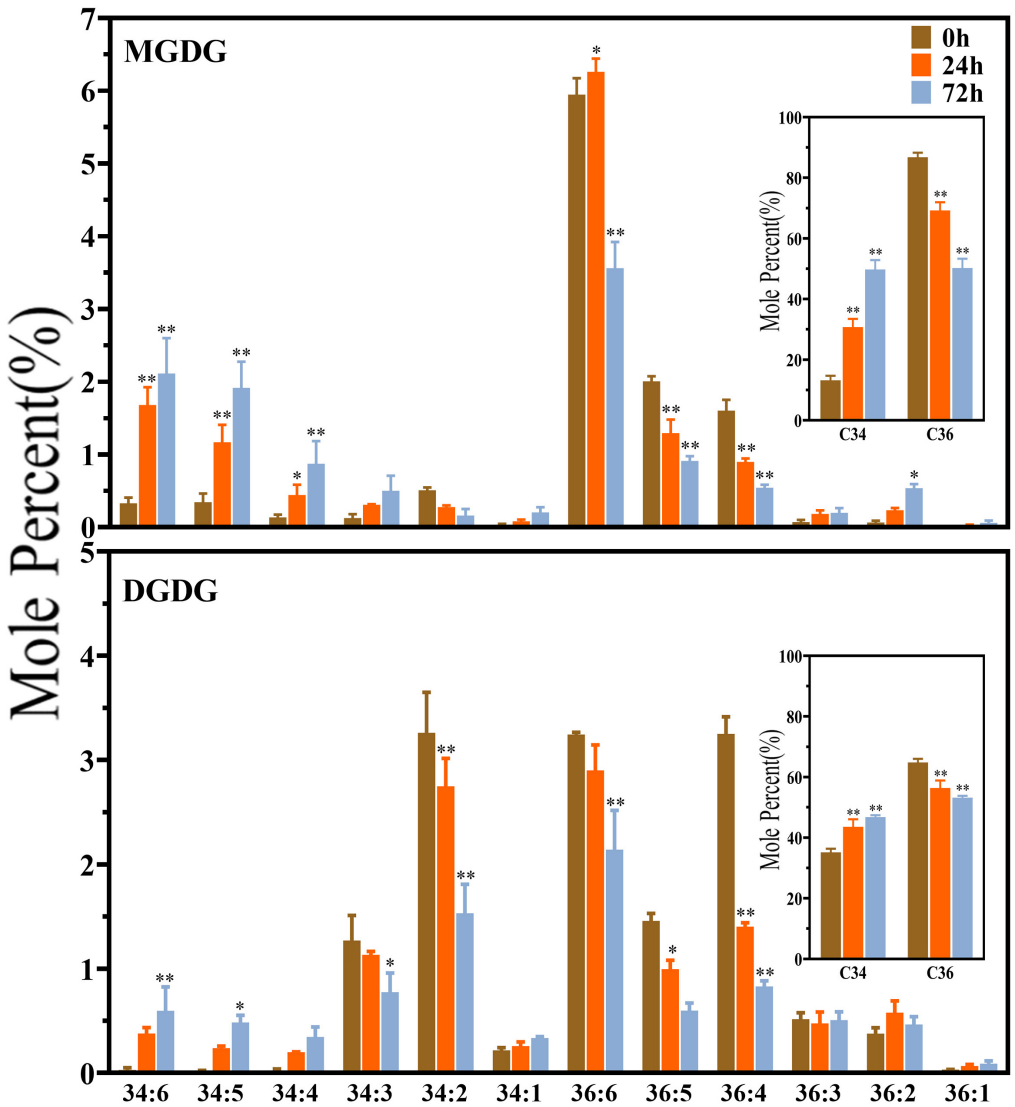

FIGURE 3 | Changes in diacyl lipid molecular species of major plastidic galactolipids in maize roots under $NaHCO_3$ (100 mmol). MGDG, monogalactosyldiacylglycerol; DGDG, digalactosyldiacylglycerol. Values (mol%) are means 5 ± standard deviation (SD), three biological replicates for each set of data. "∗" indicated that the value was significantly different from the control ($P < 0.05$). "∗∗" indicated that the value was significantly different from the control ($P < 0.01$).

Figure 5 shows the number of genes involved in each lipid metabolism pathway. The results revealed that under saline–alkaline stress (100 mmol $NaHCO_3$ treatment), various lipid-related pathways were stimulated (**Figure 5**). In the "24 h vs. 0 h" group, genes involved in the "eukaryotic galactolipid and sulfolipid synthesis," "phospholipid signaling," and "prokaryotic galactolipid, sulfolipid, and phospholipid synthesis" pathways exhibited significant up-regulation, with DEG distribution of 5-up/0-down and 8-up/2-down, 15-up/6-down and 67-up/50-down, and 7-up/1-down and 36-up/16-down ($Log_2FC \geq 1.5$ or ≤ -1.5), respectively. The differential expression of genes involved in the "sphingolipid biosynthesis" pathway was 8-up/5-down in "24 h vs. 0 h" and 32-up/23-down in "72 h vs. 0 h" ($Log_2FC \geq 1.5$ or ≤ -1.5) comparison groups. Genes involved in the "fatty acid synthesis" pathway were significantly down-regulated in both "24 h vs. 0 h" and "72 h vs. 0 h" groups, respectively. The transcriptional regulation of genes involved in the "eukaryotic phospholipid synthesis and editing" and "fatty acid elongation and wax biosynthesis" were different in both "24 h vs. 0 h" and "72 h vs. 0 h" groups, whereas the genes involved in "eukaryotic phospholipid synthesis and editing" were mostly down-regulated (16-up/28-down) in "72 h vs. 0 h" group. The DEGs in "fatty acid elongation and wax biosynthesis" were 35-up/9-down and 57-up/77-down in "24 h vs. 0 h" and "72 h vs. 0 h" groups, respectively. In the "triacylglycerol synthesis and degradation" and "oxylipin metabolism" pathway, a large number of genes were up-regulated under saline–alkaline stress. These results indicated that the transcriptions of genes involved

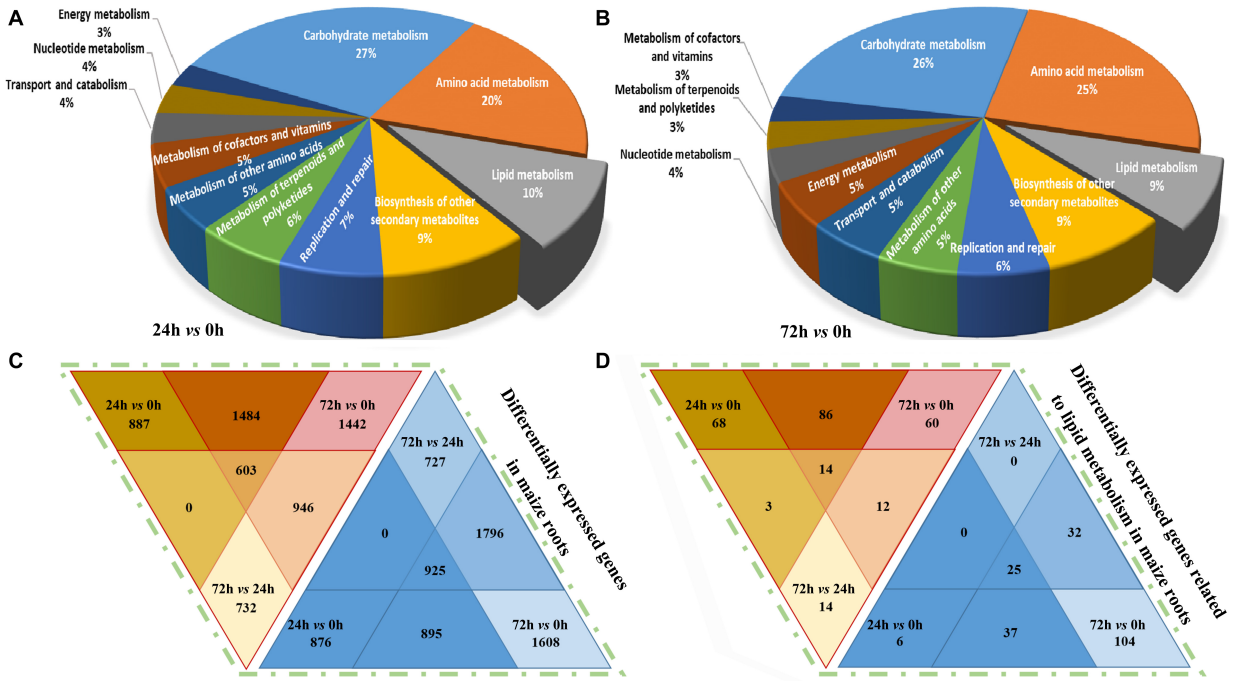

FIGURE 4 | KEGG classification and DEGs ($Log_2FC \geq 1.5$ or ≤ -1.5) distribution analysis in maize roots transcriptome under $NaHCO_3$ (100 mmol). **(A,B)** Kyoto Encyclopedia of Genes and Genomes (KEGG) pathway analysis with pie chart showing the distribution of metabolism-related differentially expressed genes (DEGs) identified in the maize roots' transcriptome. **(A)** 24 h vs. 0 h, **(B)** 72 h vs. 0 h. **(C,D)** Venn diagram showing differentially expressed genes in maize roots transcriptome. **(C)** Differentially expressed genes in maize. **(D)** Differentially expressed genes related to lipid metabolism in maize roots. The color scale indicates the expression value: red indicates high level; blue indicates low level.

in phospholipid and galactolipid metabolism pathways were activated under saline–alkaline stress.

Analysis of Significant DEGs Involved in Lipid Metabolism Under Saline–Alkaline Stress

As revealed in the previous part, it was evident that the metabolism of phospholipids and galactolipids was activated at the transcriptional level under saline–aline–alkaline stress. The expression profiles of a number of key genes involved in the major membrane lipid metabolism processes were illustrated in **Figure 6** (see **Supplementary Table S3** for a complete list). The *de novo* synthesis of triacylglycerol (TAG) in the ER is accomplished *via* three steps acylation of glycerol-3-phosphate (also known as the Kennedy pathway), which is also the necessary way leading to the synthesis of PC. Under saline–alkaline stress, genes involved in this pathway were apparently up-regulated, including some glycerol-3-phosphate acyltransferase (GPAT) and lysophosphatidyl acyltransferase (LPAAT) isoforms, and most of the diacylglycerol acyltransferase (DGAT) and phospholipids: diacylglycerol acyltransferase isoforms. It is worth noting that in another branch of the *de novo* synthesis of the PC (free choline to CDP choline), both the choline kinase and the choline phosphate cytidine transferase isoforms were down-regulated, which indicated that the *de novo* synthesis of PC was weakened.

PC and PE could be hydrolyzed by PLD and NPC to generate PA and DAG. In this study, three PLDs were up-regulated and three were down-regulated under 72 h saline–alkaline stress, and three NPCs were up-regulated, which means that both PLD and phospholipase C (PLC) pathways were partially triggered under saline–alkaline stress (**Supplementary Table S3**). The formation of PA and DAG *via* PA phosphatase (PAP)/lipid phosphate phosphatase (LPP) is a critical step for the synthesis of plastidic membrane lipids (MGDG and DGDG). Among the eight PAP/LPP orthologs, six putative membrane-bound and plastid-localized PAPs were induced by saline–alkaline (see **Supplementary Table S3** for predicting transmembrane structure and subcellular localization). After 72 h of saline–alkaline stress treatment, the most highly induced LPP3 has a Log_2FC of 3.67, which is an ortholog of AtLPPδ (AT3G58490). Another major pathway for PC degradation is mediated by phospholipase A (PLA) to form PLC. Two PLA2 genes were drastically up-regulated (Log_2FC is from 3.05 to 5.46), which might be associated with the degradation of PC under saline–alkaline stress.

Monogalactosyldiglyceride synthase (MGD) and digalactosyldiglyceride synthase (DGD) are key enzymes responsible for the biosynthesis of plastidic galactolipids MGDG and DGDG. These genes were all up-regulated in the "24 h vs. 0 h" saline–alkaline stress treatment, but the changes were not significant. The up-regulation of *DGD2* was more notable at "72 h vs. 0 h" group, which has a Log_2FC of 2.02. Fatty acid desaturase

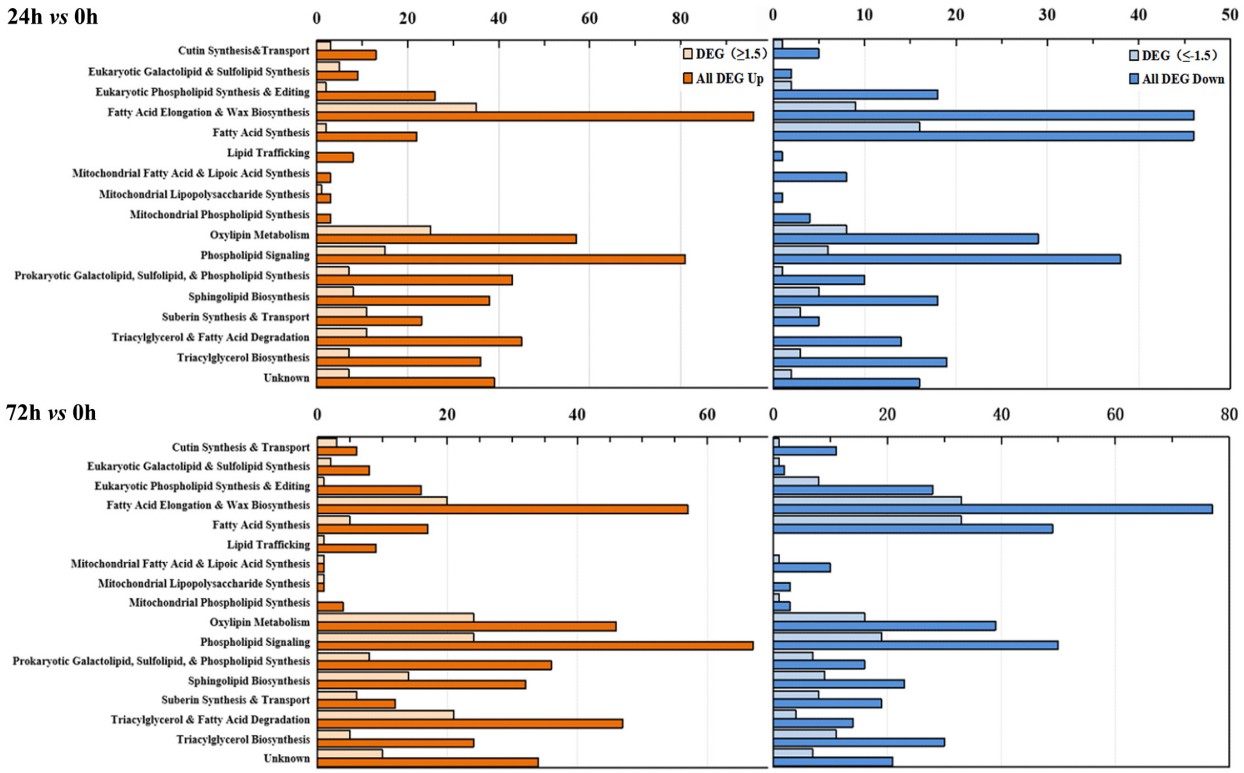

FIGURE 5 | Functional categorization of lipid-related genes from maize roots transcriptome of under $NaHCO_3$ stress (100 mmol). Genes involved in lipid metabolism were compiled from the *Arabidopsis* lipid gene database (Beisson et al., 2003) and categorized into different pathways. The upper panel is "24 h vs. 0 h," and the lower panel is "72 h vs. 0 h." Yellow columns represent down-regulated genes, and blue columns represent up-regulated genes. In each category, the light-colored column represents the significantly differentially expressed genes (DEGs, $Log_2FC \geq 1.5$ or ≤ -1.5), and the dark-colored column represents the total differentially expressed genes (DEGs). The number of the genes in each category was displayed in the *x*-axis (the ones on the upper *x*-axis indicate the DEGs, $Log_2FC \geq 1.5$ or ≤ -1.5).

(FAD) is involved in the desaturation of phospholipids and galactolipids in plants (Welti et al., 2002), including PC acyl editing enzymes FAD2 and FAD3, PG acyl editing enzyme FAD4, and galactolipids desaturases FAD6, FAD7, and FAD8. Most of the genes encoding these FADs showed a slight induction in the "24 h vs. 0 h" group, whereas in the "72 h vs. 0 h" group, the plastidic FAD4, FAD7, and FAD8 were obviously up-regulated. The genes encoding a group of lipases that catalyze the hydrolysis of phospholipids and galactolipids to release free FAs were also up-regulated, including four diacylglycerol lipase (DGL) genes.

Combined Analysis of Membrane Lipid Metabolic Changes in Maize Roots Under Saline–Alkaline Stress

To interpret the regulation of metabolic changes of membrane lipids in maize roots under saline–alkaline stress, a combined analysis of transcriptome and lipidome was conducted, and a gene–metabolite network was constructed (**Figure 7**). In the ER compartment, genes encoding the main catalytic enzymes in the Kennedy pathway, such as GPAT, LPAAT, PAH, and DGAT, showed a significant up-regulation under saline–alkaline stress. PC is the most abundant phospholipids in maize root tissue, which is initially synthesized by transferring P-choline from CDP-choline to DAG in ER. The ER-generated PC is also an essential precursor to generate PA and DAG, through the hydrolyzing reaction mediated by PLD and/or NPC/DGK. Under saline–alkaline stress, a number of genes involved in PC degradation were obviously up-regulated, including PLD, NPC, and PAP. In addition, two PLA2 genes, mediating PC degradation to form PLC, were drastically up-regulated. These findings suggested enhanced PC turnover under saline–alkaline stress, which might explain the decreased PC content as revealed by lipidomic analysis.

As an important intermediate product of lipid metabolism and a bearer of lipid signals, PA can be produced in different subcellular through a variety of ways. In the inner plastid membrane, it is produced through a unique prokaryotic pathway and converted to DAG under the dephosphorylation of the plastid PAP. The transcriptomic data showed that three putative plastid-localized PAP/LPP genes were significantly up-regulated, which might correlate to the significant decrease in PA content. The galactolipid MGDG in the outer plastid membrane is produced by the MGD using DAG as the substrate, and DGDG could be produced from MGDG by DGD. In the transcription level, the synthesis of DGDG was partially activated through the

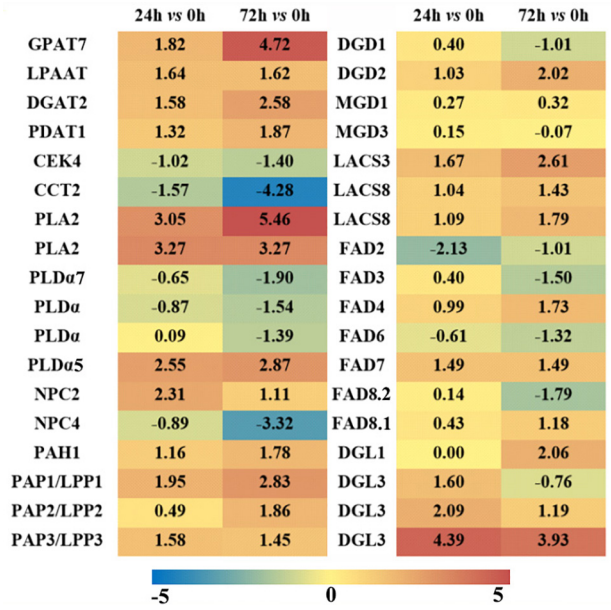

FIGURE 6 | Differentially expressed genes (DEGs, $Log_2FC \geq 1.5$ or ≤ -1.5) involved in major lipid metabolism pathways in maize roots under $NaHCO_3$ (100 mmol). A heatmap was constructed to illustrate the differential expression profiles of significant lipid related DEGs in "24 h vs. 0 h" and "72 h vs. 0 h" comparison groups. The number in each color block represents the Log_2(fold change) of the corresponding genes, and the negative number represents down-regulated DEGs. The color scale was provided. Red color indicates higher expression level, and blue color indicates lower expression level.

up-regulated DGD2 under saline–alkaline stress. The expression of DGL genes, which converts glycerolipids (DGDG and PC) into free FAs, increased significantly, resulting in enhanced degradation of membrane lipids.

In plants, there are two pathways for the production of galactolipids: one is the eukaryotic pathway in the ER, and the other is the prokaryotic pathway in the plastid/chloroplast. Maize as an 18:3 plant, its galactolipid synthesis is completely dependent on the eukaryotic pathway, which is mainly reflected by the dominating C36:6 (two 18:3 acyl chains) molecular species in their galactolipids MGDG and DGDG. In this study, an increased level of C34:4, C34:5. C34:6 under saline–alkaline stress was observed, which implied that the saline–alkaline stress might be able to trigger the prokaryotic pathway to produce the C34 galactolipids.

Transcription of Lipid Transport and Transcriptional Factors in Maize Roots Under Saline–Alkaline Stress

The DEGs related to lipid transport and transcriptional factors were screened, and their differential expression profiles were presented by a heatmap (**Figure 8**, and the detailed information is on **Supplementary Table S4**). In plants, although the synthesis of FAs occurs in chloroplasts, the synthesis of different kinds of lipids occurs in different compartments, thus requiring lipid transport between different organelles (Li N. et al., 2016). In our RNA-seq data, most of the genes encoding trigalatosyldiacylglycerol proteins were up-regulated under saline–alkaline, but not significantly up-regulated. ATP-binding box is a type of protein that outputs lipids from the plasma membrane, and the most up-regulated ATP-binding cassette G transporters showed a Log_2FC 5.72 in the "72 h vs. 0 h" group. In addition, two DEGs encoding Acyl-CoA binding protein (ACBP5), which associates with the transfer of FAs out of the plastid, were both down-regulated. Long-chain fatty acyl-CoA synthetase (LACS3) is associated with FAs and lipid transport, and the Log_2FC of LACS3 was 1.67 and 2.61 in the "24 h vs. 0 h" and "72 h vs. 0 h" groups, respectively. These results suggested that the lipid transport among different organelles might be important for the lipid remodeling in maize roots under saline–alkaline stress.

In the transcriptome data, the DEGs encoding transcriptional factors were also screened out, and 48 transcriptional factor families were determined with a total of 674 transcriptional factors. The transcriptional factors closely related to lipid metabolism are demonstrated in **Figure 8**. The maize WRI1 was up-regulated in "24 h vs. 0 h" group and significantly down-regulated in "72 h vs. 0 h" group. This is consistent with our findings that a large number of genes were up-regulated during FA and TAG synthesis in the "24 h vs. 0 h" group, whereas some genes were down-regulated in the "72 h vs. 0 h" group. Other related transcriptional factors exhibited varied degrees of activated expression under saline–alkaline condition, particularly some members from bZIP and Dof families, which might be associated with the transcriptional regulation of FA and/or lipid metabolism under saline–alkaline stress.

DISCUSSION

As the most widely planted crop in the world, maize is sensitive to saline–alkaline stress, and its production is largely limited in the salinized areas. Salinity stress could cause changes in cell membrane permeability, resulting in membrane lipid structure and membrane protein damage, which affects the normal physiological function of the cell membrane (Greenway and Munns, 1980). The root tissues of crops directly contact with the soil thus would first sense the saline–alkaline stress. In this study, maize root tissues were used as the research materials, and combined transcriptomic and lipidomic analyses were conducted to investigate the regulation of membrane lipid metabolism under saline–alkaline stress.

Lipidomic analysis has played an important role in revealing the changes of membrane lipid metabolism in crops under various abiotic stresses, including wheat under low- and high-temperature stress (Li Q. et al., 2016; Narayanan et al., 2016) and maize under cold stress (Gu et al., 2017). There is only scarce information on the lipid metabolic changes in plant response to saline–alkaline stress (Guo et al., 2019). In this study, lipidomic analysis by UPLC/MS detected a large number of lipids including the major phospholipids, lysophospholipids, and plastidic galactolipids. In maize roots, PC was the most abundant lipid species, whereas the level of PC decreased significantly

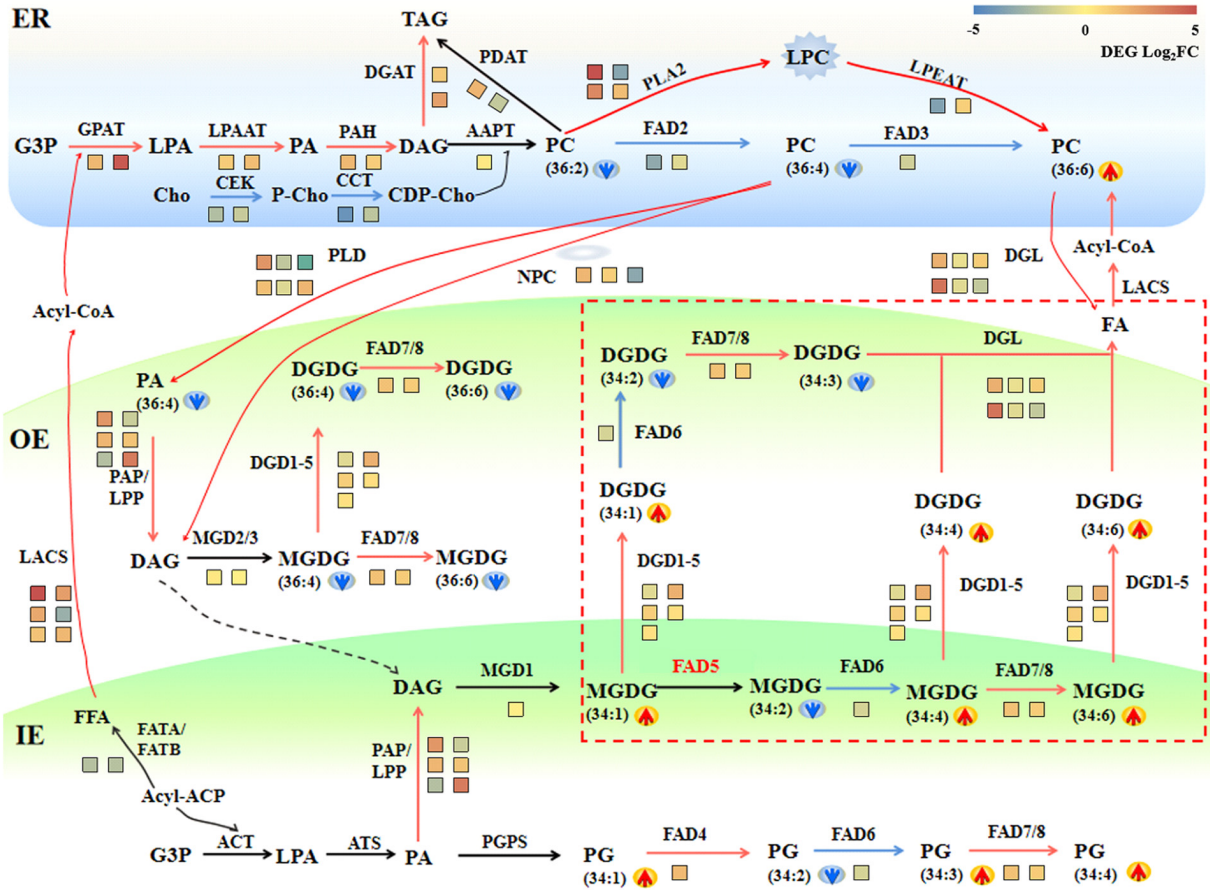

FIGURE 7 | A schematic diagram of gene–metabolite network demonstrates lipid metabolism in maize roots under 72 h $NaHCO_3$ (100 mmol). The glycerolipid synthesis pathways were depicted, and the involving genes and lipid metabolites were symbolized. The relative change of lipid molecular species was marked as arrows. Red and blue arrows indicate increased and decreased lipid metabolites, respectively. The relative expression levels of selected genes (72 h vs. 0 h) were marked as heat-map icons. The color scale of the heatmap was provided. Red color indicates higher expression level, and blue color indicates lower expression level. The red lines represent activated steps by $NaHCO_3$ (100 mmol). ER, endoplasmic reticulum; OE, outer envelope. IE, inner envelope.

under saline–alkaline stress (100 mmol $NaHCO_3$ treatment). As illustrated in the gene–metabolite network (**Figure 8**), PC degradation was enhanced through both PLA pathways, as evidenced by up-regulated PLA2 genes and increased PLC level, and the PLD and NPC/DGK pathway as supported by the up-regulated expression of a number of PLD and NPC isoforms. Our previous studies have revealed that the degradation of PC under low temperature conditions is mainly through the PLD pathway in maize leaf tissues (Gu et al., 2017). The hydrolyzation of PC mediated by PLD and NPC/DGK pathway produced PA and DAG, respectively, which are important intermediates in lipid metabolism (Canonne et al., 2011; Botella et al., 2017). In plants, PLD is directly hydrolyzed by phospholipid PC to produce PA, and NPC catalyzed reaction directly produces DAG (Hurlock et al., 2015; Li et al., 2015; Narayanan et al., 2016).

Although the plastidic galactolipids MGDG and DGDG are not dominating in membrane lipids in maize roots, they are important for maintaining the integrity of plastid membrane lipids (Narasimhan et al., 2013). In plant cells, there are two completely independent pathways for galactolipid synthesis, including the plastid/prokaryotic pathway and the ER/eukaryotic pathway (Frentzen et al., 1983; Browse et al., 1986). Plants that produce galactolipids through both prokaryotic and eukaryotic pathways are called 16:3 plants, which contain almost equal proportion of C34:6 and C36:6 in their MGDG and DGDG; plants that produce glycerolipids only through eukaryotic pathways are called 18:3 plants, which feature dominating C36:6 in their MGDG and DGDG (Ohlrogge and Browse, 1995; Li-Beisson et al., 2013). Our previous study revealed dominating C36:6 (two 18:3 acyl chains) molecular species in maize galactolipids (MGDG and DGDG); therefore, maize is proven to be a 18:3 plant whose synthesis of glycerolipids is almost entirely dependent on the eukaryotic pathway (Gu et al., 2017).

These two pathways are synergistic, and the glycerolipid metabolism pathways between the ER eukaryotic pathway and the plastid prokaryotic pathway could be adjusted with changes in the external environment (Li et al., 2015). In this study, the galactolipids DGDG decreased significantly, and MGDG did not change a lot under saline–alkaline. DGDG has been reported to be a major chloroplast bilayer lipid and plays an important role in

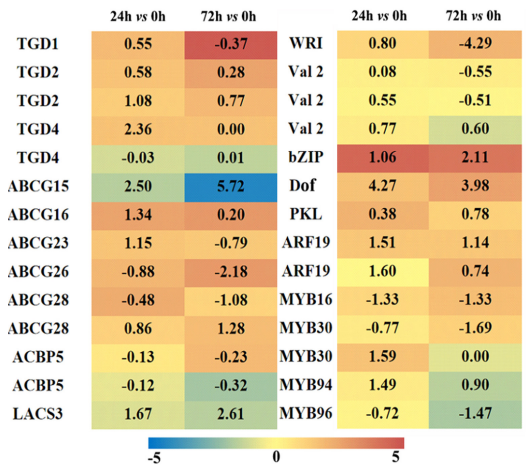

FIGURE 8 | Heatmap of lipid-associated transporters and transcription factors differentially expressed in maize roots under $NaHCO_3$ (100 mmol). A heatmap was constructed to illustrate the differential expression profiles of significant lipid related DEGs in "24 h vs. 0 h" and "72 h vs. 0 h" comparison groups. The number in each color block represents the Log_2(fold change) of the corresponding genes, and the negative number represents down-regulated DEGs. The color scale was provided. Red color indicates higher expression level, and blue color indicates lower expression level.

maintaining membrane integrity under stress (Li et al., 2015; Lin et al., 2016; Zheng et al., 2016). The significant decrease in DGDG might indicate the damaging effect of saline–alkaline stress on cell membrane. The parallel transcriptomic analysis revealed that a large number of the genes involved in the phospholipid and galactolipid pathways were significantly up-regulated, indicating the activated membrane lipid metabolism in maize roots under salinity condition (**Figure 9**).

It is worth noting that, under saline–alkaline stress, the number of C34 molecules, including that of C34:4, C34:5. C34:6, was found tremendously elevated (3–6-fold) in the galactolipids MGDG and DGDG. As maize has been proven to be a typical 18:3 plant, this new finding implied one possibility that saline–alkaline stress might be able to trigger the prokaryotic pathway to produce the C34 galactolipids. The low PAP enzyme activity in the chloroplast has been suggested to be the reason for the dysfunction of prokaryotic pathway in 18:3 plants (Frentzen et al., 1983; Heinz and Roughan, 1983). The formation of PA and DAG *via* PAP/LPP is a critical step for the synthesis of plastidic membrane lipids (MGDG and DGDG) (Eastmond et al., 2010). Previous research on the PAP family revealed two soluble PAHs, which had no transmembrane domain and were distinct from the non-soluble nature of their homologs AtPAH1&2 (Nakamura et al., 2007; Eastmond et al., 2010; Craddock et al., 2015). In *Arabidopsis*, in addition to the aforementioned soluble PAHs, there is a group of membrane-bound LPPs, some of which have been considered to be plastidic PAP (Pierrugues et al., 2001; Nakamura et al., 2009). In our transcriptome data, a total of 8 PAP/LPP orthologs were identified, and six of which represent membrane-bound and putative plastid-localized PAPs (see **Supplementary Table S3** for predicting

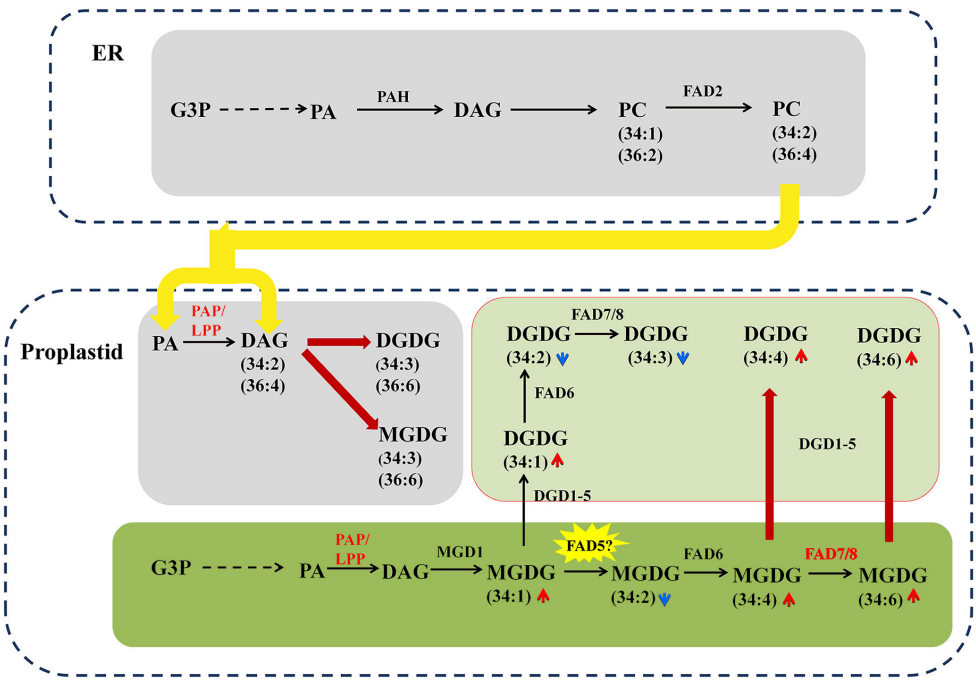

FIGURE 9 | The proposed interaction and intermediates exchange between phospholipids pathway and galactolipid pathway in maize under $NaHCO_3$ (100 mmol). The glycerolipid synthesis pathways were depicted, and the involving genes and lipid metabolites were symbolized. The relative change of lipid molecular species was marked as arrows. Red and blue arrows indicate increased and decreased lipid metabolites, respectively. The colored and bold lines represent activated steps by $NaHCO_3$ (100 mmol).

transmembrane structure and subcellular localization). Under saline–alkaline stress, three putative plastid-localized PAP/LPPs were significantly induced, and the most highly induced LPP3 had a Log_2FC of 3.67, which is an ortholog of AtLPPδ (AT3G58490) (Nakamura et al., 2007). It appeared that the activated expression of PAP/LPP genes could partially restore the function of prokaryotic pathway in plastids, resulting the remarkable remodeling of membrane lipids in response to saline–alkaline stress.

FADs are involved in the desaturation of glycerolipids in plants (Welti et al., 2002). FAD5–8 catalyze the unsaturation of FA substrates esterified to plastidial lipids, which result in high linolenic (18:3) lipid species and are responsible for the generation of C34:6 molecules (Dunn et al., 2004). Under saline–alkaline stress, the increased expression of FAD7 and FAD8 was observed, which might be another contributor to the elevated level of C34:6 MGDG and DGDG (**Figure 9**). FAD5 required for the desaturation of C34:1 MGDG to C34:2 MGDG was not found in our transcriptome data, which may await further study.

In this study, the combined lipidomic and transcriptomic analysis revealed the activation of phospholipid and galactolipid metabolism pathways in response to saline–alkaline stress on both biochemical and transcriptional levels and the modular regulation of metabolite accumulation and gene expression. An increased level of C34 galactolipids under saline–alkaline stress implied that the saline–alkaline stress might be able to trigger the prokaryotic pathway. As the information on explicating the mechanism underlying the lipid regulation in18:3 plants has been lacking, this study shed a light on understanding the regulation of glycerolipid metabolism in 18:3 plants and for deciphering the roles of lipid remodeling in saline–alkaline stress response in major field crops.

DATA AVAILABILITY STATEMENT

The datasets presented in this study can be found in online repository SRA/NCBI (Sequence Read Archive/National Center for Biotechnology Information) with accession number SRP307694.

AUTHOR CONTRIBUTIONS

XX and JZ performed the experiments and prepared the manuscript. YW, SG, and YH prepared the samples. JZ, BY, JL, and ZL analyzed the data. JX and CZ conceived the experiments and revised the manuscript. All authors contributed to the article and approved the submitted version.

FUNDING

This work was supported by the grants from the National key research and development program of China (2016YFD0101002); National Transgenic Science and Technology Program (2019ZX08010-001); Natural Science Foundation of Heilongjiang Province (ZD2020C007); and Heilongjiang Bayi Agricultural University graduate student innovation fund projects (YJSCX2019-Y15).

ACKNOWLEDGMENTS

We kindly acknowledge Dr. Ruth Welti and Mary Roth (Kansas Lipidomics Research Center) for their help with lipidomic analysis, and Dr. Liying Song (Harbin Botai Bio-tech Co., Ltd.) for her assistance in bioinformatics analysis.

SUPPLEMENTARY MATERIAL

The Supplementary Material for this article can be found online at: https://www.frontiersin.org/articles/10.3389/fpls.2021.635327/full#supplementary-material

Supplementary Figure 1 | Quantitative RT-PCR verification of differentially expressed genes of roots of maize seedlings under $NaHCO_3$ stress (100 mmol).

Supplementary Table 1 | The original data of major lipids.

Supplementary Table 2 | Differentially expressed genes in maize roots transcriptome under $NaHCO_3$ (100 mmol).

Supplementary Table 3 | The differentially expressed genes (DEGs, $Log_2FC \geq 1.5$ or ≤ -1.5) were further screened out from the total lipid related genes.

Supplementary Table 4 | The differentially expressed lipid-related transporters and transcriptional factors in maize roots under $NaHCO_3$ stress (100 mmol).

Supplementary Table 5 | The subcellular localization and transmembrane structure prediction of related genes.

Supplementary Table 6 | Primers used for quantitative real-time PCR.

REFERENCES

Beisson, F., Koo, A. J., Ruuska, S., Schwender, J., Pollard, M., Thelen, J. J., et al. (2003). *Arabidopsis* genes involved in acyl lipid metabolism. A 2003 census of the candidates, a study of the distribution of expressed sequence tags in organs, and a web-based database. *Plant Physiol.* 132, 681–697. doi: 10.1104/pp.103.022988

Benning, C. (2009). Mechanisms of lipid transport involved in organelle biogenesis in plant cells. *Annu. Rev. Cell Dev. Biol.* 25, 71–91. doi: 10.1146/annurev.cellbio.042308.113414

Botella, C., Jouhet, J., and Block, M. A. (2017). Importance of phosphatidylcholine on the chloroplast surface. *Prog. Lipid Res.* 65, 12–23. doi: 10.1016/j.plipres.2016.11.001

Browse, J., Warwick, N., Somerville, C. R., and Slack, C. R. (1986). Fluxes through the prokaryotic and eukaryotic pathways of lipid synthesis in the '16:3' plant *Arabidopsis thaliana*. *Biochem. J.* 235, 25–31. doi: 10.1042/bj2350025

Burgos, A., Szymanski, J., and Seiwert, B. (2011). Analysis of short-term changes in the *Arabidopsis thaliana* glycerolipidome in response to temperature and light. *Plant J.* 66, 656–668. doi: 10.1111/j.1365-313X.2011.04531.x

Canonne, J., Solène, F.-N., and Rivas, S. (2011). Phospholipases in action during plant defense signaling. *Plant Signal. Behav.* 6, 13–18. doi: 10.4161/psb.6.1.14037

Craddock, C. P., Adams, N., Bryant, F. M., Kurup, S., and Eastmond, P. J. (2015). Phosphatidic acid phosphohydrolase regulates phosphatidylcholine biosynthesis in *Arabidopsis* by phosphatidic acid-mediated activation of ctp:phosphocholine cytidylyltransferase activity. *Plant Cell* 27, 1251–1264. doi: 10.1105/tpc.15.00037

Dunn, T. M., Lynch, D. V., Michaelson, L. V., and Napier, J. A. (2004). A post-genomic approach to understanding sphingolipid metabolism in *Arabidopsis thaliana*. *Ann. Bot.* 93, 483–497. doi: 10.1093/aob/mch071

Eastmond, P. J., Quettier, A.-L., Kroon, J. T. M., Craddock, C., Adams, N., and Slabas, A. R. (2010). Phosphatidic acid phosphohydrolase1 and 2 regulate phospholipid synthesis at the endoplasmic reticulum in *Arabidopsis*. *Plant Cell* 22, 2796–2811. doi: 10.1105/tpc.109.071423

Frentzen, M., Heinz, E., Mckeon, T. A., and Stumpf, P. K. (1983). Specificities and selectivities of glycerol-3-phosphate acyltransferase and monoacylglycerol-3-phosphate acyltransferase from pea and spinach chloroplasts. *Eur. J. Biochem.* 129, 629–636. doi: 10.1111/j.1432-1033.1983.tb07096.x

Greenway, H., and Munns, R. A. (1980). Mechanisms of salt tolerance in nonhalophytes. *Annu. Rev. Plant Physiol.* 31, 149–190. doi: 10.1146/annurev.pp.31.060180.001053

Gu, Y., He, L., Zhao, C., Wang, F., Yan, B., Gao, Y., et al. (2017). Biochemical and transcriptional regulation of membrane lipid metabolism in maize leaves under low temperature. *Front. Plant Sci.* 8:2053. doi: 10.3389/fpls.2017.02053

Guo, Q., Liu, L., and Barkla, B. J. (2019). Membrane lipid remodeling in response to salinity. *Int. J. Mol. Sci.* 20:4264. doi: 10.3390/ijms20174264

Heinz, E., and Roughan, P. G. (1983). Similarities and differences in lipid metabolism of chloroplasts isolated from 18:3 and 16:3 plants. *Plant Physiol.* 72, 273–279. doi: 10.1104/pp.72.2.273

Higashi, Y., Okazaki, Y., Myouga, F., Shinozaki, K., and Saito, K. (2015). Landscape of the lipidome and transcriptome under heat stress in *Arabidopsis thaliana*. *Sci. Rep.* 5:10533. doi: 10.1038/srep10533

Hurlock, A. K., Roston, R. L., Wang, K., and Benning, C. (2015). Lipid trafficking in plant cells. *Traffic* 15, 915–932. doi: 10.1111/tra.12187

Li, N., Xu, C., Li-Beisson, Y., and Philippar, K. (2016). Fatty acid and lipid transport in plant cells. *Trends Plant Ence* 21, 145–158. doi: 10.1016/j.tplants.2015.10.011

Li, Q., Shen, W., Zheng, Q., Fowler, D. B., and Zou, J. (2016). Adjustments of lipid pathways in plant adaptation to temperature stress. *Plant Signal. Behav.* 11:e1058461. doi: 10.1080/15592324.2015.1058461

Li, Q., Zheng, Q., Shen, W., Cram, D., Fowler, D. B., Wei, Y., et al. (2015). Understanding the biochemical basis of temperature-induced lipid pathway adjustments in plants. *Plant Cell* 27, 86–103. doi: 10.1105/tpc.114.134338

Li-Beisson, Y., Shorrosh, B., Beisson, F., Andersson, M. X., and Ohlrogge, J. (2013). Acyl-lipid metabolism. *Arabidopsis Book* 11:e0161. doi: 10.1199/tab.0161

Lin, Y. T., Chen, L. J., Herrfurth, C., Feussner, I., and Li, H. M. (2016). Reduced biosynthesis of digalactosyldiacylglycerol, a major chloroplast membrane lipid, leads to oxylipin overproduction and phloem cap lignification in *Arabidopsis*. *Plant Cell* 28, 219–232. doi: 10.1105/tpc.15.01002

Mikami, K., and Murata, N. (2003). Membrane fluidity and the perception of environmental signals in cyanobacteria and plants. *Prog. Lipid Res.* 42, 527–543. doi: 10.1016/s0163-7827(03)00036-5

Moellering, E. R., and Benning, C. (2011). Galactoglycerolipid metabolism under stress: a time for remodeling. *Trends Plant Sci.* 16, 98–107. doi: 10.1016/j.tplants.2010.11.004

Nakamura, Y., Koizumi, R., Shui, G., Shimojima, M., Wenk, M. R., Ito, T., et al. (2009). *Arabidopsis lipins* mediate eukaryotic pathway of lipid metabolism and cope critically with phosphate starvation. *Proc. Natl. Acad. Sci. U.S.A.* 106, 20978–20983. doi: 10.1073/pnas.0907173106

Nakamura, Y., Tsuchiya, M., and Ohta, H. (2007). Plastidic phosphatidic acid phosphatases identified in a distinct subfamily of lipid phosphate phosphatases with prokaryotic origin. *J. Biol. Chem.* 282, 29013–29021. doi: 10.1074/jbc.M704385200

Narasimhan, R., Wang, G., Li, M., Roth, M., Welti, R., and Wang, X. (2013). Differential changes in galactolipid and phospholipid species in soybean leaves and roots under nitrogen deficiency and after nodulation. *Phytochemistry* 96, 81–91. doi: 10.1016/j.phytochem.2013.09.026

Narayanan, S., Prasad, P. V., and Welti, R. (2016). Wheat leaf lipids during heat stress: II. Lipids experiencing coordinated metabolism are detected by analysis of lipid co-occurrence. *Plant Cell Environ.* 39, 608–617. doi: 10.1111/pce.12648

Ohlrogge, J., and Browse, J. (1995). Lipid biosynthesis. *Plant Cell* 7, 957–970. doi: 10.1105/tpc.7.7.957

Omoto, E., Iwasaki, Y., Miyake, H., and Taniguchi, M. (2016). Salinity induces membrane structure and lipid changes in maize mesophyll and bundle sheath chloroplasts. *Physiol. Plant.* 157, 13–23. doi: 10.1111/ppl.12404

Pierrugues, O., Brutesco, C., Oshiro, J., Gouy, M., and Kazmaier, M. (2001). Lipid phosphate phosphatases in *Arabidopsis*: regulation of the atlpp1 gene in response to stress. *J. Biol. Chem.* 276, 20300–20308. doi: 10.1074/jbc.M009726200

Shen, W., Li, J. Q., Dauk, M., Huang, Y., Periappuram, C., Wei, Y., et al. (2010). Metabolic and transcriptional responses of glycerolipid pathways to a perturbation of glycerol 3-phosphate metabolism in *Arabidopsis*. *J. Biol. Chem.* 285, 22957–22965. doi: 10.1074/jbc.M109.097758

Sulian, L., Fang, T., Jie, G., Ping, J., Kangqi, L., Duoliya, W., et al. (2020). Phosphatidylserine synthase from *Salicornia europaea* is involved in plant salt tolerance by regulating plasma membrane stability. *Plant Cell Physiol.* 2020:pcaa141. doi: 10.1093/pcp/pcaa141

Szymanski, J., Brotman, Y., and Willmitzer, L. (2014). Linking gene expression and membrane lipid composition of *Arabidopsis*. *Plant Cell* 26, 915–928. doi: 10.1105/tpc.113.118919

Troncoso-Ponce, M. A., Cao, X., Yang, Z., and Ohlrogge, J. B. (2013). Lipid turnover during senescence. *Plant Sci.* 20, 13–19. doi: 10.1016/j.plantsci.2013.01.004

Welti, R., Li, W., and Li, M. (2002). Profiling membrane lipids in plant stress responses. Role of phospholipase D alpha in freezing-induced lipid changes in *Arabidopsis*. *J. Biol. Chem.* 277, 31994–32002. doi: 10.1074/jbc.M205375200

Zheng, G., Li, L., and Li, W. (2016). Glycerolipidome responses to freezing- and chilling-induced injuries: examples in *Arabidopsis* and rice. *BMC Plant Biol.* 16:70. doi: 10.1186/s12870-016-0758-8

Conflict of Interest: XX was employed by company Beijing Hortipolaris Co., Ltd.

The remaining authors declare that the research was conducted in the absence of any commercial or financial relationships that could be construed as a potential conflict of interest.

frontiers in Plant Science

ORIGINAL RESEARCH
published: 15 April 2021
doi: 10.3389/fpls.2021.639132

Membrane Lipids' Metabolism and Transcriptional Regulation in Maize Roots Under Cold Stress

Xunchao Zhao[1,2†], Yulei Wei[1†], Jinjie Zhang[1], Li Yang[1], Xinyu Liu[1], Haiyang Zhang[1], Wenjing Shao[1], Lin He[1], Zuotong Li[1], Yifei Zhang[1] and Jingyu Xu[1]**

[1] Key Lab of Modern Agricultural Cultivation and Crop Germplasm Improvement of Heilongjiang Province, College of Agriculture, Heilongjiang Bayi Agricultural University, Daqing, China, [2] College of Agriculture, Northeast Agricultural University, Harbin, China

OPEN ACCESS

Edited by:
Lina Yin,
Northwest A&F University, China

Reviewed by:
Joaquín J. Salas,
Instituto de la Grasa (IG), Spain
Qiang Li,
Huazhong Agricultural University, China

***Correspondence:**
Jingyu Xu
xujingyu2003@hotmail.com
Yifei Zhang
byndzyf@163.com

[†] These authors have contributed equally to this work

Specialty section:
This article was submitted to Plant Metabolism and Chemodiversity, a section of the journal Frontiers in Plant Science

Received: 08 December 2020
Accepted: 18 March 2021
Published: 15 April 2021

Citation:
Zhao X, Wei Y, Zhang J, Yang L, Liu X, Zhang H, Shao W, He L, Li Z, Zhang Y and Xu J (2021) Membrane Lipids' Metabolism and Transcriptional Regulation in Maize Roots Under Cold Stress. Front. Plant Sci. 12:639132. doi: 10.3389/fpls.2021.639132

Low temperature is one of the major abiotic stresses that restrict the growth and development of maize seedlings. Membrane lipid metabolism and remodeling are key strategies for plants to cope with temperature stresses. In this study, an integrated lipidomic and transcriptomic analysis was performed to explore the metabolic changes of membrane lipids in the roots of maize seedlings under cold stress (5°C). The results revealed that major extraplastidic phospholipids [phosphatidylcholine (PC), phosphatidylethanolamine (PE), phosphatidic acid (PA), and phosphatidylinositol (PI)] were dominant membrane lipids in maize root tissues, accounting for more than 70% of the total lipids. In the transcriptome data of maize roots under cold stress, a total of 189 lipid-related differentially expressed genes (DEGs) were annotated and classified into various lipid metabolism pathways, and most of the DEGs were enriched in the "Eukaryotic phospholipid synthesis" (12%), "Fatty acid elongation" (12%), and "Phospholipid signaling" (13%) pathways. Under low temperature stress, the molar percentage of the most abundant phospholipid PC decreased around 10%. The significantly up-regulated expression of genes encoding phospholipase [phospholipase D (PLD)] and phosphatase PAP/LPP genes implied that PC turnover was triggered by cold stress mainly *via* the PLD pathway. Consequently, as the central product of PC turnover, the level of PA increased drastically (63.2%) compared with the control. The gene-metabolite network and co-expression network were constructed with the prominent lipid-related DEGs to illustrate the modular regulation of metabolic changes of membrane lipids. This study will help to explicate membrane lipid remodeling and the molecular regulation mechanism in field crops encountering low temperature stress.

Keywords: maize (*Zea mays* L.), lipid metabolism, lipidome, transcriptome, cold stress

Abbreviations: PC, phosphatidylcholine; PE, phosphatidylethanolamine; MGDG, monogalactosyldiacylglycerol; DGDG, digalactosyldiacylglycerol; SQDG, sulfoquinovosyldiacylglycerol; PI, phosphatidylinositol; PE, phosphatidylethanolamine; PS, phosphatidylserine; PA, phosphatidic acid; DAG, diacylglycerol; PLD, phospholipase D; PLC, phospholipase C.

INTRODUCTION

Maize (*Zea mays* L.), originated from subtropical zones, is a typical thermophilic crop that requires a relatively high growth temperature, especially in the seedling and vegetative growth stage (Rodríguez et al., 2014). In northeastern China (around 44° north latitude), low temperatures in early spring and sudden temperature drops in late spring seriously affects the growth and development of maize seedlings.

Understanding the response of plants to low temperature stress at the molecular level is of great importance in developing cold-resistance crops. The plant membrane is the first barrier to cope with external environmental stimuli, which could be attributed to its typical fluidity and certain protective properties (Chinnusamy et al., 2007). When plants are exposed to low temperatures, the fluidity of the plant cell membrane will be improved, which will increase the tolerance of the plant to low temperatures (Chinnusamy et al., 2007; Gao et al., 2015). The alteration of membrane glycerolipids composition and saturation has been considered as a major strategy for plants to respond to temperature stress (Zheng et al., 2011; Barrero-Sicilia et al., 2017). Low temperature stress increased the unsaturation of fatty acids, which increased the fluidity of the plant membrane, reduced the tendency of non-bilayer phase formation, and enhanced the integrity and function of the plant membrane (Uemura and Steponkus, 1997; Hou et al., 2016).

Glycerolipids are essential components of the plant membrane that include extraplastidic phospholipids such as phosphatidylcholine (PC), phosphatidylethanolamine (PE), phosphatidic acid (PA), phosphatidylinositol (PI), and phosphatidylserine (PS), and plastidic lipids such as monogalactosyldiacylglycerol (MGDG), digalactosylmonoacylglycerol (DGMG), phosphatidylglycerol (PG), and sulfoquinovosyldiacylglycerol (SQDG). Among the extraplastidic phospholipids, PC is the most abundant lipid in eukaryotic cells, which accounts for 25–60% of non-plastidic membrane lipids in plants (Ohlrogge and Browse, 1995; Li-Beisson et al., 2010). In *Arabidopsis*, PC was initially established by transferring P-choline from CDP choline to *sn-1*,*2*-diacylglycerol (DAG) (Tasseva et al., 2004). PA is the simplest glycerophospholipids in structure, yet it is a very important phospholipid class. Although the proportion of PA is not large, it is an important signaling lipid, and is also known as the key precursor for the synthesis of major glycerophospholipids and glyceroglycolipids (Dubots et al., 2012). Glycerolipids contain various molecular species, in which the length of acyl chains and the number of acyl double bonds at *sn-1* and *sn-2* position are different, and lipid remodeling occurs at different developmental stages or under non-optimal growth conditions (Testerink and Munnik, 2011).

An increasing number of studies have shown that membrane lipids' metabolism plays important roles in the temperature stress response of plants (Li et al., 2016; Narayanan et al., 2016; Gu et al., 2017). Lipids' remodeling and the enzymes involved in related processes are particularly critical for plants to adapt to cold environments (Li et al., 2016; Gu et al., 2017). The phospholipase PLD (phospholipase D) was activated under low temperature, which led to an increased accumulation of lipid signaling molecules PA (Ruelland et al., 2002). The content of PA can increase rapidly and maintain a high level only for a few minutes after low temperature exposure (Peppino Margutti et al., 2017). The resistance of *Arabidopsis* PLD mutant to cold was decreased, which might be attributed to the reduced PA content (Li et al., 2004). In *Brassica napus*, the unsaturation of PC and MGDG increased gradually under a low temperature (Tasseva et al., 2004). In *Arabidopsis*, the percentage of PA (34:6) was elevated under a low temperature (Zheng et al., 2016).

The expression of lipid-metabolism-related genes has been suggested to be associated with low temperature response in plants. In rice, over-expression of *AtGPAT* enhanced the unsaturated fatty acid content of PG and increased cold tolerance (Li et al., 2018). In *Arabidopsis*, the *Atdgat1* mutants were found to be more sensitive to chilling and freezing stresses compared with wild-type plants (Tan et al., 2018). The expression of *AtDGK2* is induced in various tissues under low temperature stress, which plays an important role in the cold signaling process (Gómez-Merino et al., 2004). The knock-out of *OsFAD8* further reduced membrane fluidity in rice under cold stress (Tovuu et al., 2016).

In a previous report, the lipid metabolism in leaves of maize seedlings under low temperature stress was elaborated by our group, which showed that maize was an 18:3 plant and cold stress exerted significant impacts on membrane lipids' metabolism (Gu et al., 2017). Since the knowledge of lipids' metabolism in root tissues is limited, the lipidomic and transcriptomic analysis of maize roots under low temperature stress was conducted in this study. This study will provide an overall understanding of the lipid metabolism in maize seedlings in adaptation to low temperature stress.

MATERIALS AND METHODS

Plant Growth, Treatments, and Sampling

The inbred line He344, a major maize variety planted in Northeast China, was used as experimental material. Maize seeds of the same size were selected and disinfected with 10% NaClO for 30 min. After repeated washing with distilled water, the seeds were put into a 25°C incubator for dark germination. After germination, maize seedlings were cultured with 1/2 Hoagland nutrient solution (pH = 5.5) in a growth chamber. Hoagland nutrient solution was used for precise temperature control and sampling of root tissues. The temperature of the chamber was set at 22°C, with 16/8 h (light/dark) photoperiodic cycle. About half of the 2-week-old maize seedlings were moved into a 5°C chamber, and the rest of the seedlings were kept in the 22°C growth chamber as control. Maize root samples were collected 3 days after cold treatment, and each sample had at least three replicates. The collected samples were wrapped in silver paper quickly, rapidly put into liquid nitrogen for freezing, and then stored at −80°C.

RNA-seq Analysis and qRT-PCR Validation

Total RNA was extracted from root tissues of 2-week-old maize seedlings after 3 days under 5°C treatment (samples from 22°C growth chamber were used as control) using TRIzol reagent (Invitrogen). The purity and concentration of RNA samples were examined, and then the library was constructed. After the database was qualified, it was sequenced by Illumina platform. The RNA-seq data were mapped to the maize reference genome B73 RefGen_v3.

Fragments Per Kilobase of exon model per Million mapped reads (FPKM) of each gene were measured from the length of the gene and reads count mapped to the genes. The counting of the read numbers mapped to each gene was performed by HTSeq v0.6.1. The screening of DEGs (differentially expressed genes) was performed using the Bioconductor package "edgeR" in R among the treatment samples. DEG parameters were set at false discovery rate (FDR) < 0.01 and $|$ Log2 fold-change$| \geq 1$. The KOBAS (v2.0.12) software was used to test the statistical enrichment of the DEGs in the Kyoto Encyclopedia of Genes and Genomes (KEGG) pathways, and a modified *P*-value (*q*-value) ≤ 0.05 was the criteria for significantly enriched KEGG pathways.

In order to further validate the reliability of the RNA-seq results, qRT-PCR analysis was implemented. The cDNA was compounded using the ReverTra Ace qPCR RT Master Mix (TOYOBO, Osaka, Japan). Real-time quantitative RT-PCR was accomplished in 96-well plates with a SYBR Select Master Mix RT-PCR system. *ZmACTIN* and *ZmGAPDH* were used as internal control, and the qRT-PCR primers are listed in **Supplementary Table 1**. The results of qRT-PCR were reckoned by $2^{-\Delta\Delta ct}$ method, and the data from the maize samples grown in 22°C were used as the calibrators (Czechowski et al., 2005; Zhang et al., 2014).

Membrane Lipid Extraction and Analysis

The method was modified according to a previous report (Narayanan et al., 2016). A total of 3 ml isopropanol (0.01%BHT) was added to a 50 ml glass tube and the glass tube was placed in the nitrogen blowing instrument and preheated to 75°C. About 200 mg maize root samples were rapidly added to the preheated glass tube and kept at 75°C for 15 min. Distilled water (0.6 ml) and chloroform (1.5 ml) were added to the tube, vortexed, and shaken for 1 h in a shaking table, and then the extract was transferred to a new glass tube. Next, 4 ml chloroform: methanol (2:1) mixture was added to the glass tube, vortexed, and shaken for 30 min on a shaking table. The extraction procedure was repeated 3–4 times, and then the mixed liquids were compounded and washed with KCl (1 ml). The upper liquid was discarded, and the remaining liquid was blown to full evaporation with a nitrogen blowing instrument, and then stored at −20°C. Lipids were analyzed by Electrospray Ionization-Mass Spectrometry (ESI-MS/MS), which was accomplished at Kansas Lipidomics Research Center (KLRC, United States).

The precursor (Prec) and neutral loss (NL) scans were applied to obtain polar lipid profiles. The samples were introduced into the electrospray ionization source for further generation of lipid molecular ions, including PC, lysoPC, PE, and lysoPE positive $[M + H]^+$ ions, MGDG, DGDG, PG, PI, PA, and PS positive $(M+NH4)^+$ ions, and lysoPG negative $(M-H)]^-$ ions. A series of peak values of lipid content were detected by electrospray ionization. The peaks on the spectra were quantified in comparison to a group of internal standards. The data for each lipid molecular species were normalized and displayed as mol% of the total lipids analyzed.

Co-expression Analysis of Lipid Related DEGs

Pearson correlation coefficient was calculated according to the expression data of DEGs (differentially expressed genes, $|$ Log2FC$| \geq 1$). After removing the self-pairing and duplication, the relevant cut-off value of 0.9 was applied, and the co-expression network was constructed with the reserved gene pairs. The constructing and visualizing of the co-expression network was carried out with the Cytoscape software.

Statistical Analysis

All statistical analyses were conducted with SPSS statistics 19.0 (SPSS Inc.), and significance levels of the data were calculated by Student's *t*-test method. $^*P < 0.05$ and $^{**}P < 0.01$ represent different significance levels.

RESULTS

Changes of Membrane Lipids in Maize Roots Under Cold Stress

To explore the changes of membrane lipid species in the roots of maize seedlings under low temperature conditions, polar lipids extracted from maize roots samples under 5°C (and 22°C control) were analyzed by lipidomic approach. A total of 12 different types of lipids were detected, including six phospholipid classes (PC, PE, PA, PI, PS, and PG), three classes of *lyso*-phospholipids (LPC, LPE, and LPG), two galactolipids (MDGD and DGDG), and one sulfolipid (SQDG).

As shown in **Figure 1**, phospholipids are the main membrane lipids in maize root tissues, accounting for more than 70% of the total lipids. Among all phospholipids, PC is the most abundant lipid, accounting for around 40% of the total lipids, while the remaining phospholipids account for about 30%. Under low temperature (5°C) stress, the molar percentage of PC decreased around 10% (9.5%) compared with the control (22°C). A significantly enhanced accumulation of PA was observed under cold treatment, with a 63.3% increase compared with the control. The molar percentage of PE was found increased by 14.5%, whereas the proportion of PI and PS were not altered significantly. The level of the exclusive plastidic phospholipid PG was also increased, which was 17.1% higher than the control. The galactolipids MGDG and DGDG each accounted for about 6% of the total polar lipids, while the sulfolipid SQDG content was extremely low. Under low temperature stress, the content of MGDG decreased significantly, while DGDG and

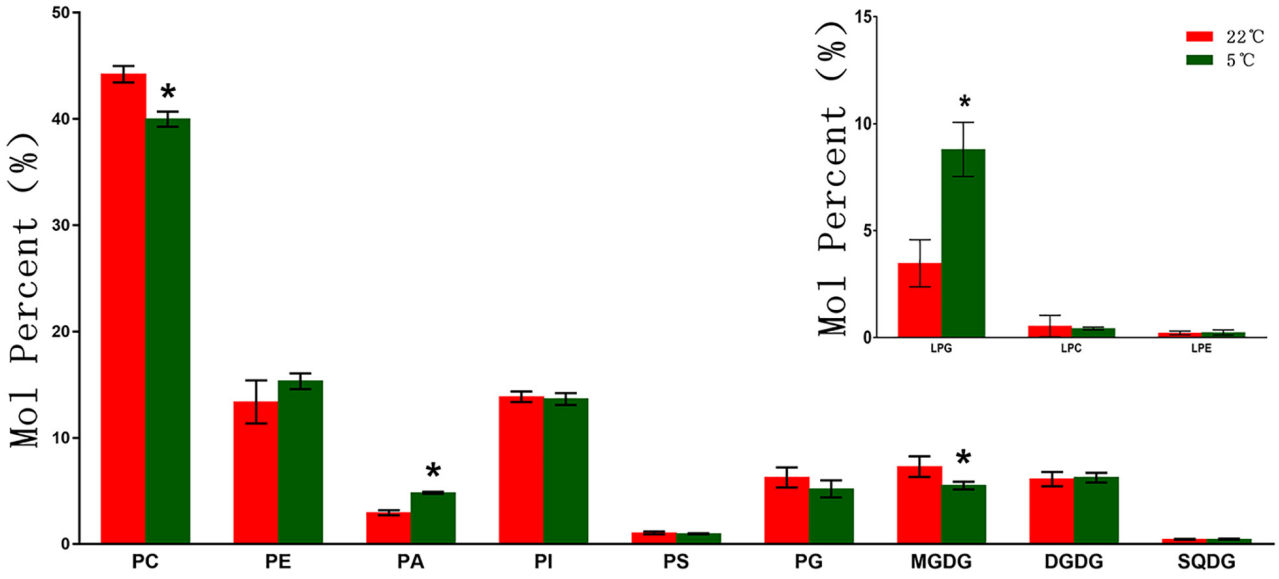

FIGURE 1 | Changes of glycerolipids species in maize roots under cold stress (5°C). PC, phosphatidylcholine; PE, phosphatidylethanolamine; PA, phosphatidic acid; PI, phosphatidylinositol; PS, phosphatidylserine; PG, phosphatidylglycerol; MGDG, monogalactosyldiacylglycerol; DGDG, digalactosyldiacylglycerol; SQDG, sulfoquinovosyldiacylglycerol; LPC, *Lyso*-PC; LPA, *Lyso*-PA; LPG, *Lyso*-PG. Values (mol%) are means 5 ± standard deviation (SD) (n = 5). "*" indicated that the value was significantly different from the control ($P < 0.05$).

SQDG increased slightly. Under low temperature stress, the level of *lyso*-phospholipids altered to varying degrees, and the content of LPG increased more than 1.5 times in comparison with the control.

Alterations in Molecular Species of Membrane Lipids in Maize Roots Under Cold Stress

The molecular species of lipids samples from maize roots were analyzed by ESI-MS/MS and were presented as the numbers of carbon atoms and double bonds (total number of carbon atoms: total number of double bonds) of two fatty acid chains on each lipid class. The molecular species in phospholipids are dominated by C34 and C36 species, of which C34:2 and C36:4 account for a relatively high proportion in phospholipids (**Figure 2**). Compared with the control, C34:2 had no significant changes, while the content of C36:4 significantly decreased 11.9% in PC. In the plastidic phospholipid PG, the molar percentage of C34:2 decreased by 18.7%, while that of C36:4 increased 19.9% compared with the control. In PA, the molar percentage of C34:2 and C36:4 both increased significantly. The levels of C34:2 and C36:4 altered with an opposite trend in PI under cold treatment. In PS, the molar percentages of C34:1, C36:4, and C36:6 were all raised under cold stress, while the molar percentage of C36:2 decreased compared with the control (**Figure 2**).

As shown in the lower panel of **Figure 2**, C36 molecular species are dominant in galactolipids MGDG, which is consistent with the previous finding that maize is an 18:3 plant (Gu et al., 2017). Under low temperature stress, the molar percentage of C36:6 MGDG was significantly lowered than that of the control. In DGDG, the percentage of C36:6 and C36:5 molecules decreased under cold stress.

Transcriptomic Analysis of Maize Roots Under Cold Stress

To investigate the transcriptional regulation of the membrane lipids' metabolism in maize roots under cold stress, the transcriptomic analysis was conducted. A total of 55.14 GB clean data were produced by six runs; the clean data of each run reached 8.14 GB at least. The percentage of Q30 base was 94.52%, and it was mapped to the maize reference genome (B73 RefGen_v3). The principal components analysis (PCA) showed that the three replicates of each sample were clustered together, which indicates that the three repeats of the same sample are consistent (**Supplementary Figure 2**).

As shown in **Figure 3**, in the comparison group (5 vs 22°C), a total of 2769 DEGs were annotated in KEGG pathway, and were classified into five categories. The results showed that most of the DEGs were enriched in the metabolic processes (**Figure 3A**), which implied the metabolic processes were greatly affected under cold stress.

In the metabolic pathway, a total of 208 DEGs were annotated in lipid metabolic pathways, and most of them were involved in fatty acid metabolism, suggesting that those pathways were significantly influenced under cold stress (**Figure 3B**). The lipid-related DEGs were categorized into 13 pathways as shown in **Figure 3C**, and the most enriched pathway was the "Glycerophospholipid metabolism" pathway. There were 45 DEGs in the "Glycerophospholipid metabolism pathway," including 28 up-regulated and 17 down-regulated DEGs, respectively. In the "Fatty acid elongation" and "Biosynthesis

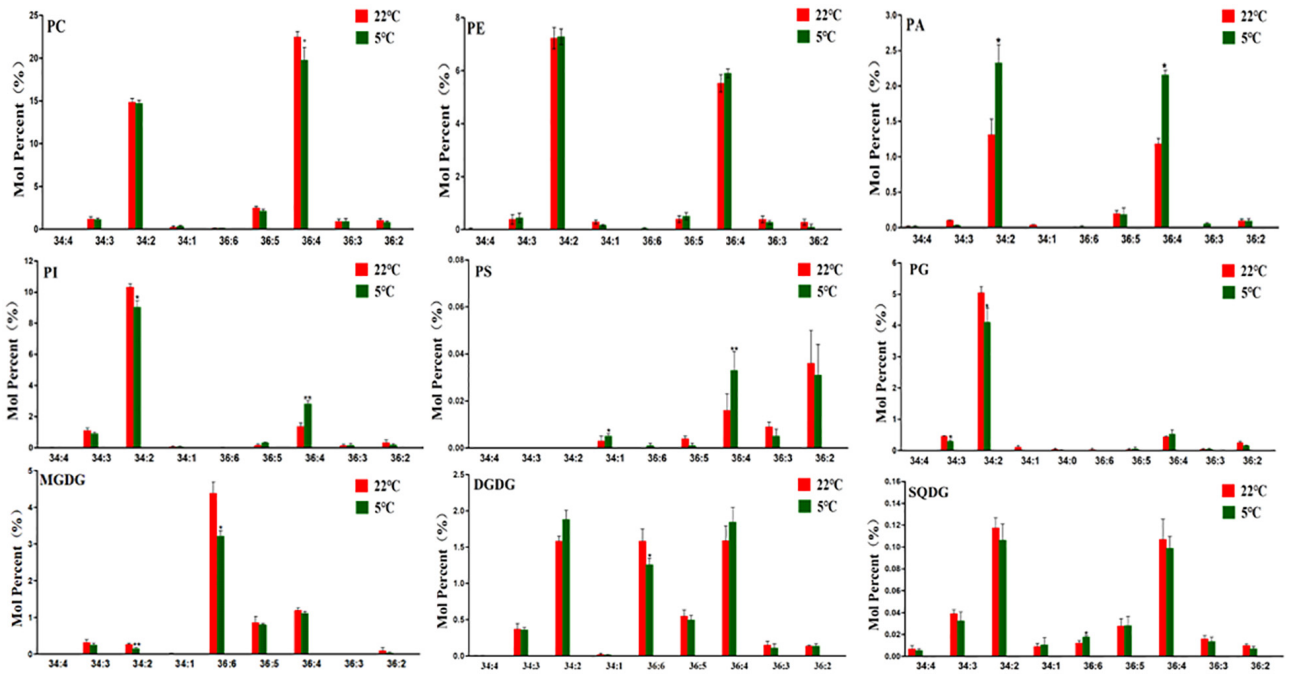

FIGURE 2 | Changes in molecular species of major membrane lipids in maize roots under cold stress (5°C). PC, phosphatidylcholine; PE, phosphatidylethanolamine; PA, phosphatidic acid; PI, phosphatidylinositol; PS, phosphatidylserine; PG, phosphatidylglycerol; MGDG, monogalactosyldiacylglycerol; DGDG, digalactosyldiacylglycerol; SQDG, sulfoquinovosyldiacylglycerol. Values (mol%) are means 5 ± standard deviation (SD) (n = 5). "*" indicated that the value was significantly different from the control ($P < 0.05$). "**" Indicated that the value was extremely different from the control.

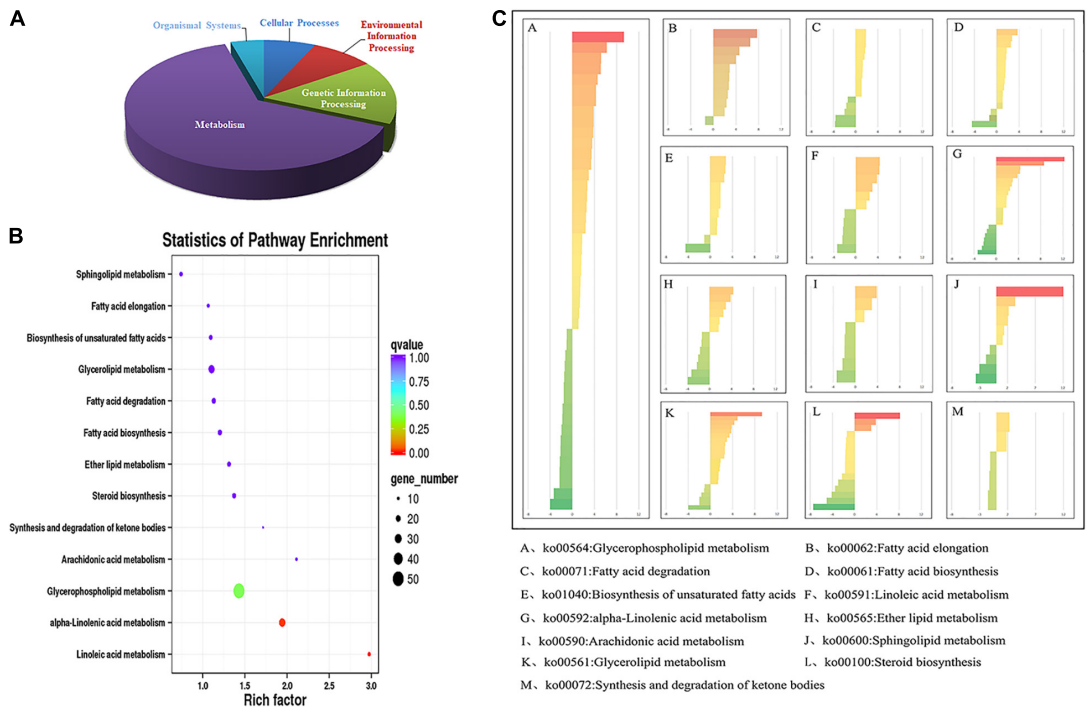

FIGURE 3 | Lipid-related DEGs annotated in KEGG pathways under cold stress (5°C). DEGs, differentially expressed genes; KEGG, Kyoto Encyclopedia of Genes and Genomes. **(A)** The distribution of metabolism-related DEGs identified in the maize roots transcriptome; **(B)** the statistics of KEGG pathway enrichment of DEGs related to lipid metabolism; **(C)** the DEGs involved in different lipid metabolic pathways. The number of the genes in each category were displayed on the x-axis.

of unsaturated fatty acids" pathway, most genes were up-regulated (**Figure 3C**).

Differential Responses of Lipids Related DEGs in Maize Roots Under Cold Stress

Maize lipid-related genes were further screened from maize root transcriptome data according to the previously published *Arabidopsis* lipids-related gene databases (Beisson et al., 2003; Troncoso-Ponce et al., 2013). A total of 189 lipid-related DEGs were annotated and recruited, most of which were involved in the "Eukaryotic phospholipid synthesis" (12%), "Fatty acid elongation" (12%), and "Phospholipid signaling" (13%) pathways (**Supplementary Figure 2**).

In order to demonstrate the differential regulation of lipid-related DEGs in each metabolic pathway, the bar chart representing the up/down regulated DEGs is shown in **Figure 4**. The left panel represents up-regulated genes, and the right panel represents down-regulated genes. In each category, the green columns represent the total DEGs, and the red columns represent the significant DEGs (Log2FC $\geq$ 1 or ≤ -1). As shown in **Figure 4**, most of the DEGs involved in "Phospholipid signaling," "Fatty acid elongation," "Eukaryotic phospholipid signaling," and "Triacylglycerol & Fatty acid degradation" pathways were significantly up-regulated, and the number of the significantly up-regulated DEGs (Log2FC $\geq$ 1) was among 10–14. A number of DEGs involved in "Eukaryotic galactolipid & Sulfolipids synthesis," "Phospholipid signaling," and "Oxylipin metabolism" were found significantly down-regulated (Log2FC ≤ -1), which demonstrated differential regulation of major lipids' metabolism pathways under cold stress.

Analysis of Significant DEGs Involved in Lipid Metabolism Under Cold Stress

Among the lipid related DEGs, some significantly up-regulated DEGs were involved in the major lipid metabolism pathway. As shown in **Figure 5**, in the endoplasmic reticulum (ER) TAG (triacylglycerol) *de novo* synthesis pathway (the Kennedy pathway), genes encoding glycerol-3-phosphate acyltransferase (GPAT) and lysophosphatidic acyltransferase (LPAAT) were significantly up-regulated under low temperature, including four GPATs (the most up-regulated isoform GRMZM2G070304, Log2FC = 9.28), two LPAAT (GRMZM2G079109, Log2FC = 3.43), and one DGAT1 (GRMZM2G130749, Log2FC = 2.09). In the PC and PE *de novo* biosynthesis pathway, the related genes were also significantly up-regulated, including CCT (choline phosphate cytidylyltransferase, Log2FC = 2.69) and CEK (choline kinase, Log2FC = 1.11). One DEG encoding PAH (PA phosphatase) was significantly up-regulated (GRMZM2G099481, Log2FC = 4.27).

Phosphatidylcholine and PE could be hydrolyzed by PLD and non-specific phospholipase C (NPC) to generate PA and DAG. In the "PC turnover and DAG formation" process, two PLD (GRMZM2G054559 and GRMZM2G179792) were found significantly up-regulated (Log2FC > 4) under low temperature stress, while two NPC were found significantly down-regulated (**Figure 6** and **Supplementary Table 2**). Another major pathway for PC degradation is mediated by phospholipase A (PLA) to form phospholipase C (PLC). Two PLA1 genes were drastically up-regulated (Log2FC is 4.66 and 5.65), which suggested enhanced degradation of PC under cold stress. Monogalactosyldiacylglycerol synthase (MGD) and digalactosyldiacylglycerol synthase (DGD) are key enzymes responsible for the biosynthesis of plastidic galactolipids MGDG and DGDG. Under low temperature stress, two DGDs were up-regulated, and the most significant one had a Log2FC of 2.56.

The synthesis of fatty acids is accomplished in plastids. A number of genes involved in the *de novo* synthesis and desaturation of fatty acids were up-regulated under cold stress, including FAB2, FAT, and LACS. A set of fatty acid desaturase (FADs) were also involved in the fatty acid desaturation in both phospholipids and galactolipids metabolism pathways. Under low temperature stress, two genes encoding FAD8 were significantly up-regulated, and the Log2FC was 4.66 and 5.65, respectively. A group of lipases that catalyze the hydrolysis of phospholipids and galactolipids to release free fatty acids were also up-regulated, including three diacylglycerol lipase (DGLs) (Log2FC is 4.3 and 6.05).

To verify the gene expression in transcriptome data, ten lipid-related genes were selected for quantitative RT-PCR analysis. The results showed that under low temperature stress, the expression of genes such as ZmLPP, FATB, and ZmFAD8 increased significantly, which is consistent with the trends in transcriptome data (**Supplementary Figure 3**).

The Co-expression Analysis of Lipid-Related Genes

Pearson correlation coefficient was calculated according to the expression data of DEGs, and the constructing and visualizing of the co-expression network was carried out with the Cytoscape software. A total of 62 lipid-related genes involved in different lipids' metabolic processes were screened in the transcriptome data, and the co-expression analysis was performed. The results indicated that the expression of 19 genes was closely correlated (**Figure 7**). Most of the genes were co-expressed with multiple genes. The expression of *ZmGPAT10* (GRMZM2G020320) was found to be correlated with 22 genes, including *ZmPAP1* (GRMZM2G024144, r = 0.96), *ZmFAD8* (GRMZM2G074401, r = 0.99), *ZmDGD* (GRMZM2G092588, r = 0.99), and *ZmPETC* (GRMZM2G155357, r = 0.99).

The transcriptome data was screened using the online transcription factor database[1]. A total of 42 transcription factor families were identified, comprising of 553 transcription factors, among which the most abundant transcription factor families were SLD, WRKY, and NAC (**Supplementary Figure 4**).

A co-expression analysis among transcription factors and lipid-related genes was conducted and revealed that there were 201 TFs related to the TAG/PC *de novo* synthesis pathway. Among them, important regulatory genes related to lipid biosynthesis and seed development were discovered, including AP2/ERF(25), bHLH(14), B3(5), and MYB(12). At the same time, there are 110 TFs related to PC turnover and DAG formation, and

[1]http://planttfdb.cbi.pku.edu.cn/

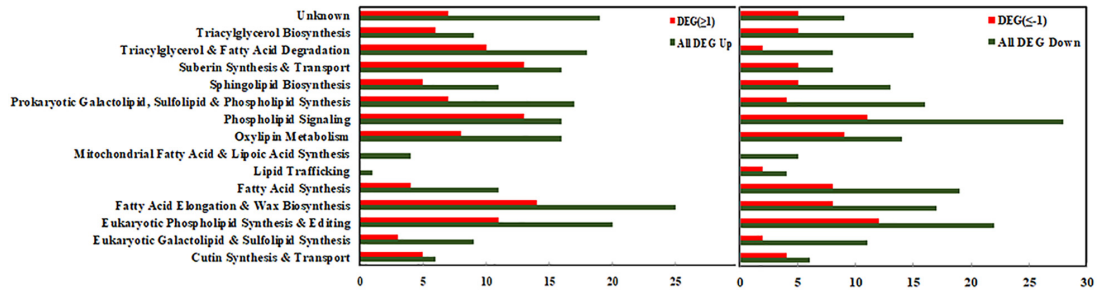

FIGURE 4 | Functional categorization of lipid-related genes from maize roots transcriptome under cold stress (5°C). **Left** columns represent up-regulated genes, and **right** columns represent down-regulated genes. In each category, the green colored column represents the total differentially expressed genes (DEGs), and the red colored column represents the significantly differentially expressed genes (DEGs with Log2FC ≥1 or ≤−1). The number of the genes in each category were displayed on the *x*-axis (the ones on the upper *x*-axis indicate the DEGs with Log2FC ≥1 or ≤−1).

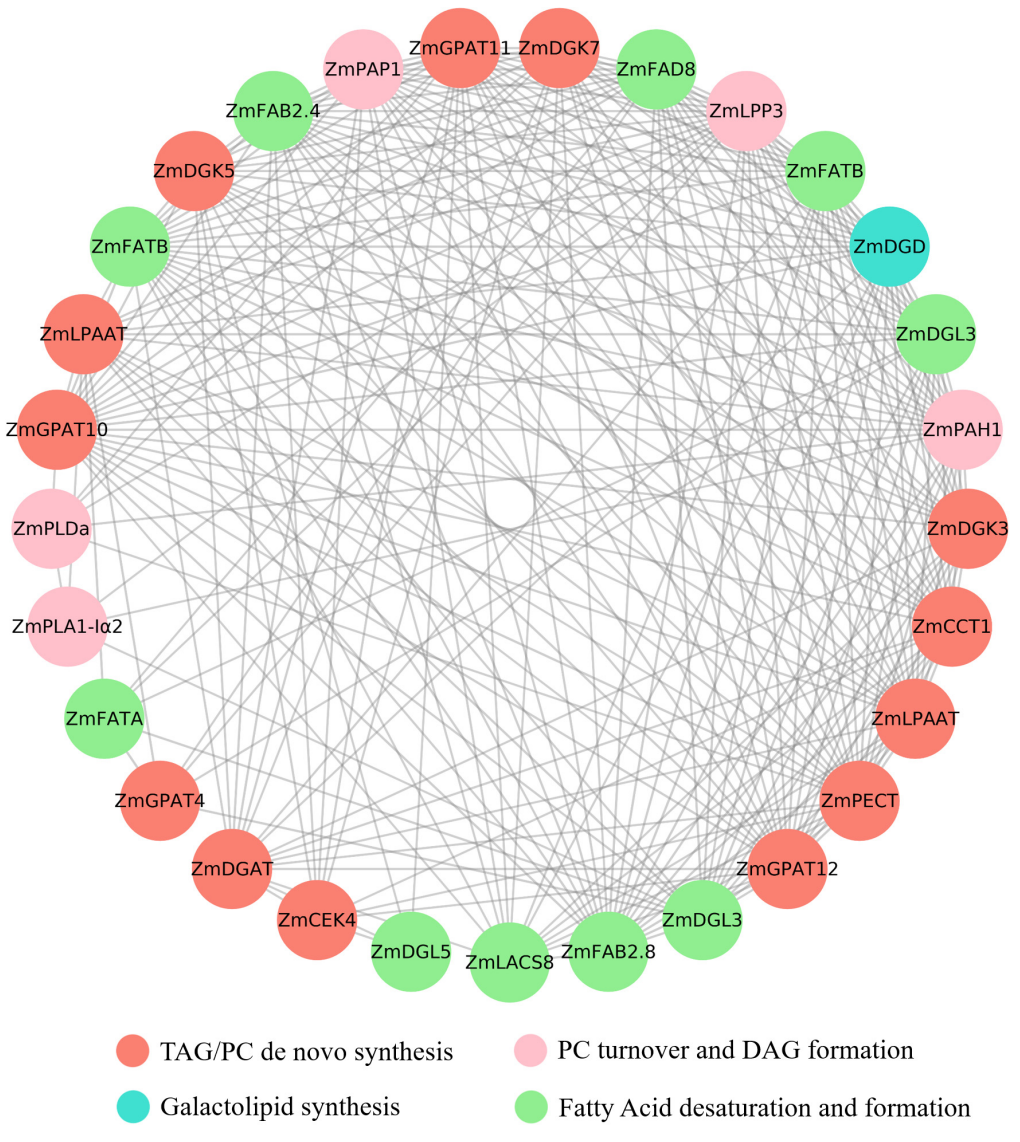

FIGURE 5 | Co-expression of lipid related genes. Different colors represent different genes. The co-expression network was constructed with the reserved gene pairs. The constructing and visualizing of the co-expression network was carried out with the Cytoscape software.

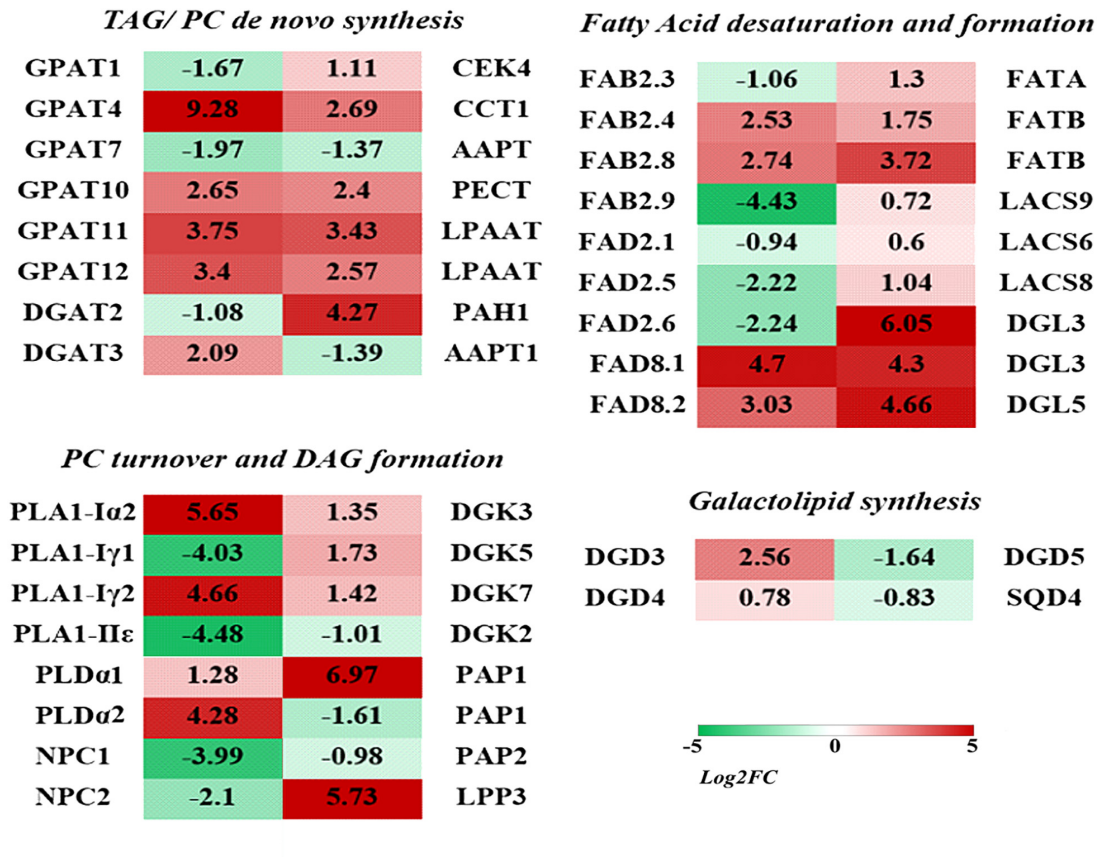

FIGURE 6 | Differentially expressed genes (DEGs) involved in major lipid metabolism pathways in maize roots under cold stress (5°C). The heatmaps were constructed to illustrate the differential expression profiles of significant lipid related DEGs. The number in each color block represents the Log2(fold-change) of the corresponding genes, and the negative number represents down-regulated DEGs. The color scale was provided. Red color indicates higher expression level, and green color indicates lower expression level.

174 TFs related to fatty acid desaturation and formation, which all contain different numbers of TFs, such as AP2/ERF, bHLH, B3, and MYB. This result indicated that these genes might play important roles in lipid metabolism in coping with cold stress (**Supplementary Figure 5**).

The Gene-Metabolite Network of Lipids Metabolism in Maize Roots Under Cold Stress

Based on the combined analysis of the transcriptomic and lipidomic data, a scenario diagram was constructed to illustrate the gene-metabolite network. As shown in **Figure 7**, the metabolic pathways of glycerolipids were described, and the differential gene expression profiles and lipid changes were marked with colored heatmap icons.

Phosphatidylcholine is the most abundant phospholipids in maize root tissues, which is initially synthesized by transferring P-choline from CDP-choline to DAG in ER. The *de novo* production of DAG is through the Kennedy Pathway catalyzed by GPAT, LPAT, and PAH, which were all up-regulated at the transcriptional level under low temperature stress as observed in the cold transcriptome. The ER generated PC is also an essential precursor to generate PA and DAG. Both PLD and NPC were involved in hydrolyzing PC (and/or PE) to produce PA and DAG. Under low temperature treatment, two PLD genes were found significantly up-regulated, whereas two NPCs were found down-regulated (**Figure 6** and **Supplementary Table 2**), which might suggest that the PLD pathway was responsible for PC turnover in maize roots under cold stress. Furthermore, two genes encoding PLA1, which mediates PC degradation to form PLC, were drastically up-regulated. These findings suggested enhanced PC turnover under cold stress, which might explain the decreased PC content as revealed by lipidomic analysis. The enhanced accumulation of PA could be attributed to the activated PC hydrolyzation *via* PLD pathway.

The membrane lipids in plastid/chloroplasts have a distinct composition, which are dominated by galactolipids MGDG and DGDG. Under low temperature conditions, one DGD1 and FAD8 (**Figure 7**), which were involved in DGDG synthesis and desaturation, respectively, were obviously up-regulated. However, the molar percentage and unsaturation of DGDG did not change a lot in metabolic aspects. The plastidic lipids MGDG decreased significantly under cold stress, which might be due to

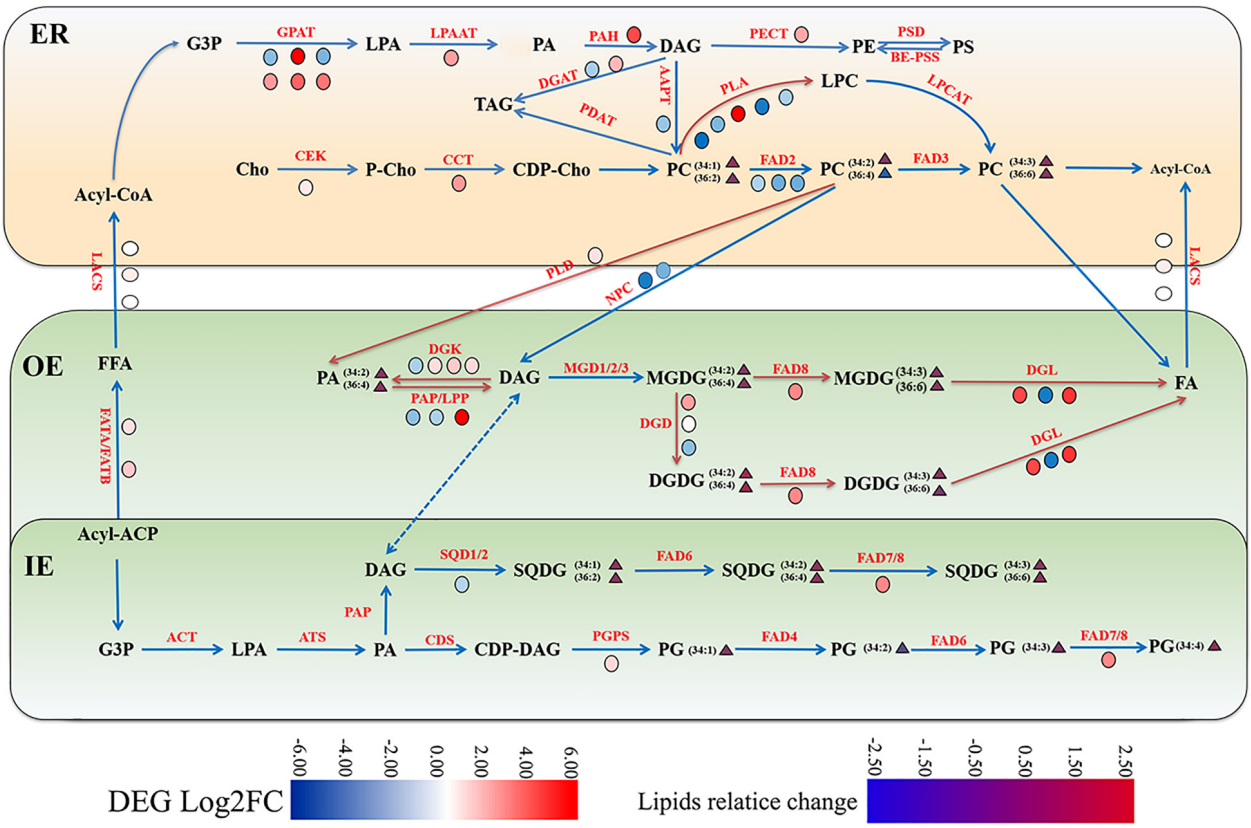

FIGURE 7 | Gene-metabolite network illustrating membrane lipid metabolism in maize under cold stress. The glycerolipids synthesis pathways were depicted and the involved genes and lipid metabolites were symbolized. The relative change of lipid molecular species and the relative expression levels of selected genes were marked as heatmap icons. The color scale is provided. Red color indicates higher expression level, and green color indicates lower expression level. The red arrows represent activated steps by cold. ER, endoplasmic reticulum; OE, outer envelope. IE, inner envelope.

the enhanced conversion to DGDG by the action of DGD, and both DGDG and MGDG could undergo degradation through the cold triggered DGLs.

DISCUSSION

Membrane lipid metabolism and remodeling are key strategies for plants to cope with temperature stresses (Moellering et al., 2010; Li et al., 2016). In a previous study, we provided evidence that maize is an 18:3 plant with dominating C36:6 (two 18: 3 acyl chains) molecular species in their galactolipids DGDG and MDGD (Gu et al., 2017). In this study, a combined lipidomic and transcriptomic strategy was used to explore the lipidomic changes and the transcriptional regulation in root tissues of maize seedling under cold stress. As shown in **Figure 8**, the changes of glycerolipids profiles, the differential expression of lipid-related genes, and co-expression network of transcription factors and lipid genes were interactively investigated.

A number of lipidomic studies have shown that membrane glycolipid profiles are largely influenced by cold stress, however, most of the research was conducted in the above-ground tissues of the plants (Degenkolbe et al., 2012; Zheng et al., 2016). The extraplastidic phospholipids classes (PC, PE, PA, and PI) are the most abundant lipid species. Under low temperatures, a significant decrease of PC was observed. In the parallel transcriptomic analysis, the eukaryotic PC *de novo* biosynthesis pathway and PC degradation and signaling pathway were activated by cold stress as manifested by the up-regulation of genes involved in those pathways. Nevertheless, the dropped PC level suggested that PC degradation mediated by PLD and PLA was dominant under low temperature stress. PC is known as the major "bilayer lipid," which is crucial in maintaining the membrane integrity under stress conditions (Li et al., 2015; Lin et al., 2016; Zheng et al., 2016). The reduction of PC under cold stress might result in a certain degree of membrane damage in plant cells.

Phosphatidic acid is the major central lipids' intermediate and signaling molecule. In addition to the PA generated through the phosphorylation of DAG by PAH in the ER, a large proportion of PA could be produced by hydrolysis of phospholipids, including PC and PE, through the PLD and PLC/DGK pathways (Laxalt and Munnik, 2002; Ruelland et al., 2002; Arisz et al., 2009; Benning, 2009). PA plays important roles in a variety of cellular processes involving plant growth, reproduction, and signal transduction under abiotic stresses (Ruelland et al., 2015;

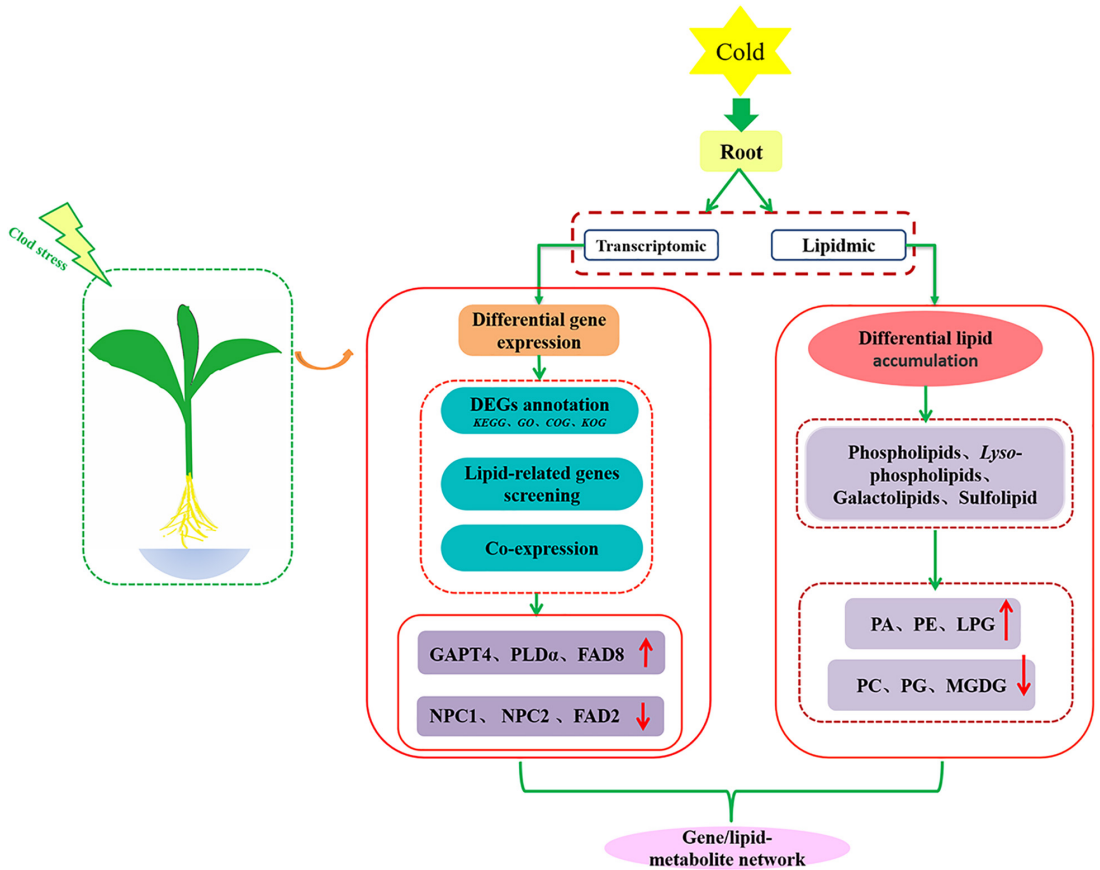

FIGURE 8 | Schematic diagram of transcriptomic and lipidomic analysis strategies.

Meringer et al., 2016; Tan et al., 2018). Previous research had shown that the increase of PA content was beneficial in reducing the damage of reactive oxygen species to *Arabidopsis* under cold stress (Moellering et al., 2010; Li et al., 2016). In this study, we found that the accumulation of PA significantly improved in maize roots under cold stress, which suggested that the increase of PA content may help to alleviate the damage of maize seedlings under cold stress. As illustrated in the gene-metabolite network (**Figure 7**), the up-regulated PLD genes and down-regulated NPCs suggested that the PLD pathway was responsible for PC turnover in maize root under cold stress. In a previous study, we found that PA produced by the action of PLD was significantly enhanced and contributed to the plastidic lipids' synthesis in maize leaves under cold stress (Gu et al., 2017). These findings implied that generation of PA *via* the PLD pathway was triggered by cold in both above-ground and under-ground tissues of maize seedlings.

In plants, the unsaturation PG was considered to be closely related to low temperature response (Mikami and Murata, 2003). In tobacco, the increase of saturated fatty acid level of PG makes plants sensitive to cold stress (Mikami and Murata, 2003). Fatty acid desaturases FAD8 and catalyzes the desaturation of FAs that are esterified to PG and result in high linolenate (18:3) lipid species (Zhao et al., 2019). The knocked-out *FAD8* led to reduced membrane fluidity in rice under low temperature stress (Tovuu et al., 2016). In this study, two genes encoding FAD8 annotated in the transcriptomic data (*ZmFAD8.1* and *ZmFAD8.2*) were significantly up-regulated under low temperature stress. Moreover, in the parallel lipidomic analysis, an obvious increase in 36:4 species was observed. This result indicates that the increased unsaturation of PG may be beneficial to the adaptation of cold stress for the root tissue of maize seedlings.

Membrane lipid remodeling occurs when plants encounter cold stress (Chen and Thelen, 2016). Previous studies have shown that, as the growing temperature deceased, the content of DGDG increased and the ratio of MGDG/DGDG decreased, which could help to enhance the cell membrane stability under stress (Campos et al., 2003; Moellering et al., 2010). In this study, a significant decrease of MGDG and a slight increase of DGDG was observed, resulting in a large reduction in the MGDG/DGDG ratio in maize seedlings under cold stress. MGD catalyzes the galactose transfer from UDP-galactose to DAG framework to form MGDG, and then the second galactose is diverted from UDP-galactose to MGDG by DGD for the final formation of DGDG (Wang et al., 2020). In our transcriptomic data, the expression of two maize *DGDs* were up-regulated, and the most apparent one had a Log2FC of 2.56.

A number of reports have indicated that the over-expression of DGAT and DGK could regulate the dynamic balance of DAG, PA, and TAG in *Arabidopsis* under cold stress (Moellering et al., 2010; Li et al., 2016). Over-expression of AtDGAT1 enhances cold tolerance of *Arabidopsis* (Arisz et al., 2018). AtDGAT1, AtDGK2, AtDGK3, and AtDGK5 were shown to be responsible to cold stress tolerance in *Arabidopsis* (Tan et al., 2018). In this study, the up-regulation of a member of DGAT and DGK isoforms suggested DAG-TAG and DAG-PA pathways were activated under cold stress, which may contribute to cold adaptation of maize seedlings. The accumulation of TAG is influenced by a series of transcription factors, including WRI1, MYB, and bZIP (Song et al., 2013; Liu et al., 2014; Chen et al., 2020). Researchers have shown that the over-expression of *AtWRI1* gene in maize and rapeseed enhanced TAG production (Cernac and Benning, 2004; Shen et al., 2010). In this study, two *ZmWRI1* genes (GRMZM2G124524, Log2FC = 1.88 and GRMZM2G174834, Log2FC = 2.62) were up-regulated under cold stress. The activation of TAG biosynthesis in maize roots under low temperature stress might be attributed to increased fatty acids derived from hydrolytic enzymes, and these excess FAs may be temporarily stored in TAG.

CONCLUSION

In summary, we observed active changes of membrane lipids in maize roots under cold stress, including decreased PC and increased PA contents, and the enhanced transcription of a set of lipid-related genes. The results revealed the activation and interaction of phospholipid and galactolipid synthesis pathways in response to cold, and the modular regulation of metabolite accumulation and gene expression in the respective processes. It should be noted that this model is based on combined analysis of transcriptomic and lipidomic changes, and the possibility of posttranscriptional regulation on proteins/enzymes could not be excluded. Since information on the regulation of lipid metabolism in 18:3 plants is still lacking, there are still a great deal of unanswered questions that need further investigation.

DATA AVAILABILITY STATEMENT

The original contributions presented in the study are publicly available. This data can be found here: NCBI repository, accession numbers SRR13312968, SRR13312969, SRR13312971, and SRR13312972.

AUTHOR CONTRIBUTIONS

XZ and YW performed the experiments and prepared the manuscript. JZ, LY, XL, and WS prepared the samples. HZ, LH, and ZL analyzed the data. JX and YZ conceived the experiments and revised the manuscript. All authors contributed to the article and approved the submitted version.

FUNDING

This work was supported by grants from the National Key Research and Development Program of China (2016YFD0101002 and 2017YFD0300302), National Transgenic Science and Technology Program (2019ZX08010003), National Natural Science Foundation of China (31701328), Natural Science Foundation of Heilongjiang Province (ZD2020C007), and the Heilongjiang Bayi Agricultural University graduate student innovation fund projects (YJSCX2019- Y05).

ACKNOWLEDGMENTS

We kindly acknowledge Ruth Welti and Mary Roth (Kansas Lipidomics Research Center) for their help with lipidomic analysis, and Liying Song (Harbin Botai Bio-tech Co., Ltd.) for her assistance in bioinformatics analysis.

SUPPLEMENTARY MATERIAL

The Supplementary Material for this article can be found online at: https://www.frontiersin.org/articles/10.3389/fpls.2021.639132/full#supplementary-material

Supplementary Figure 1 | Quality inspection of maize seedling root transcriptome data under low temperature stress.

Supplementary Figure 2 | Functional annotation of genes related to lipid metabolism in maize roots under low temperature stress.

Supplementary Figure 3 | Verification of differentially expressed genes in maize seedling roots under low temperature stress by qRT-PCR.

Supplementary Figure 4 | Enrichment of transcription factors of genes related to lipid metabolism in maize roots under low temperature stress.

Supplementary Figure 5 | Co-expression analysis of transcription factors and lipid-related genes.

Supplementary Table 1 | Related genes qRT-PCR verification primers.

Supplementary Table 2 | Expression of lipid-related genes under cold stress.

REFERENCES

Arisz, S. A., Heo, J., Koevoets, I. T., Zhao, T., Van Egmond, P., Meyer, J., et al. (2018). DIACYLGLYCEROL ACYLTRANSFERASE1 contributes to freezing tolerance. *Plant Physiol.* 177, 1410–1424. doi: 10.1104/pp.18.00503

Arisz, S. A., Testerink, C., and Munnik, T. (2009). Plant PA signaling via diacylglycerol kinase. *Biochim. Biophys. Acta* 1791, 869–875. doi: 10.1016/j.bbalip.2009.04.006

Barrero-Sicilia, C., Silvestre, S., Haslam, R. P., and Michaelson, L. V. (2017). Lipid remodelling: unravelling the response to cold stress in *Arabidopsis* and its extremophile relative Eutrema salsugineum. *Plant Sci.* 263, 194–200. doi: 10.1016/j.plantsci.2017.07.017

Beisson, F., Koo, A. J., Ruuska, S., Schwender, J., Pollard, M., and Thelen, J. J. (2003). *Arabidopsis* genes involved in acyl lipid metabolism. A 2003 census of the candidates, a study of the distribution of expressed sequence tags in organs, and a web-based database. *Plant Physiol.* 132, 681–697. doi: 10.1104/pp.103.022988

Benning, C. (2009). Mechanisms of lipid transport involved in organelle biogenesis in plant cells. *Annu. Rev. Cell Dev. Biol.* 25, 71–91. doi: 10.1146/annurev.cellbio.042308.113414

Campos, P. S., Quartin, V., Ramalho, J. C., and Nunes, M. A. (2003). Electrolyte leakage and lipid degradation account for cold sensitivity in leaves of *Coffea* sp. plants. *J. Plant Physiol.* 160, 283–292. doi: 10.1078/0176-1617-00833

Cernac, A., and Benning, C. (2004). WRINKLED1 encodes an AP2/EREB domain protein involved in the control of storage compound biosynthesis in *Arabidopsis*. *Plant J.* 40, 575–585. doi: 10.1111/j.1365-313X.2004.02235.x

Chen, B., Zhang, G., Li, P., Yang, J., Guo, L., Benning, C., et al. (2020). Multiple GmWRI1s are redundantly involved in seed filling and nodulation by regulating plastidic glycolysis, lipid biosynthesis, and hormone signaling in soybean (*Glycine max*). *Plant Biotechnol. J.* 18, 155–171. doi: 10.1111/pbi.13183

Chen, M., and Thelen, J. J. (2016). Acyl-lipid desaturase 1 primes cold acclimation response in *Arabidopsis*. *Physiol. Plant* 158, 11–22. doi: 10.1111/ppl.12448

Chinnusamy, V., Zhu, J., and Zhu, J. (2007). Cold stress regulation of gene expression in plants. *Trends Plant Sci.* 12, 444–451. doi: 10.1016/j.tplants.2007.07.002

Czechowski, T., Stitt, M., Altmann, T., Udvardi, M. K., and Scheible, W. R. (2005). Genome-wide identification and testing of superior reference genes for transcript normalization in *Arabidopsis*. *Plant Physiol.* 139, 5–17. doi: 10.1104/pp.105.063743

Degenkolbe, T., Giavalisco, P., Zuther, E., Seiwert, B., Hincha, D. K., and Willmitzer, L. (2012). Differential remodeling of the lipidome during cold acclimation in natural accessions of *Arabidopsis thaliana*. *Plant J.* 72, 972–982. doi: 10.1111/tpj.12007

Dubots, E., Botté, C., Boudière, L., Yamaryo-Botté, Y., Jouhet, J., Maréchal, E., et al. (2012). Role of phosphatidic acid in plant galactolipid synthesis. *Biochimie* 94, 86–93. doi: 10.1016/j.biochi.2011.03.012

Gao, J., Wallis, J. G., and Browse, J. (2015). Mutations in the prokaryotic pathway rescue the fatty acid biosynthesis1 mutant in the cold. *Plant Physiol.* 169, 442–452. doi: 10.1104/pp.15.00931

Gómez-Merino, F. C., Brearley, C. A., Ornatowska, M., Abdel-Haliem, M. E., Zanor, M. I., and Mueller-Roeber, B. (2004). AtDGK2, a novel diacylglycerol kinase from *Arabidopsis thaliana*, phosphorylates 1-stearoyl-2-arachidonoyl-sn-glycerol and 1,2-dioleoyl-sn-glycerol and exhibits cold-inducible gene expression. *J. Biol. Chem.* 279, 8230–8241. doi: 10.1074/jbc.M312187200

Gu, Y., He, L., Zhao, C., Wang, F., Yan, B., Gao, Y., et al. (2017). Biochemical and transcriptional regulation of membrane lipid metabolism in maize leaves under low temperature. *Front. Plant Sci.* 8:2053. doi: 10.3389/fpls.2017.02053

Hou, Q., Ufer, G., and Bartels, D. (2016). Lipid signalling in plant responses to abiotic stress. *Plant Cell Environ.* 39, 1029–1048. doi: 10.1111/pce.12666

Laxalt, A. M., and Munnik, T. (2002). Phospholipid signalling in plant defence. *Curr. Opin. Plant Biol.* 5, 332–338. doi: 10.1016/s1369-5266(02)00268-6

Li, Q., Shen, W., Zheng, Q., Fowler, D. B., and Zou, J. (2016). Adjustments of lipid pathways in plant adaptation to temperature stress. *Plant Signal. Behav.* 11:e1058461.

Li, Q., Zheng, Q., Shen, W., Cram, D., Fowler, D. B., Wei, Y., et al. (2015). Understanding the biochemical basis of temperature-induced lipid pathway adjustments in plants. *Plant Cell* 27, 86–103. doi: 10.1105/tpc.114.134338

Li, W., Li, M., Zhang, W., Welti, R., and Wang, X. (2004). The plasma membrane–bound phospholipase Dδ enhances freezing tolerance in *Arabidopsis thaliana*. *Nat. Biotechnol.* 22, 427–433. doi: 10.1038/nbt949

Li, X., Liu, P., Yang, P., Fan, C., and Sun, X. (2018). Characterization of the glycerol-3-phosphate acyltransferase gene and its real-time expression under cold stress in paeonia lactiflora pall. *PLoS One* 13:e0202168. doi: 10.1371/journal.pone.0202168

Li-Beisson, Y., Shorrosh, B., Beisson, F., Andersson, M. X., Arondel, V., Bates, P. D., et al. (2010). Acyl-lipid metabolism. *Arabidopsis Book* 11:e0161. doi: 10.1199/tab.0161

Lin, Y., Chen, L., Herrfurth, C., Feussner, I., and Li, H. (2016). Reduced biosynthesis of digalactosyldiacylglycerol, a major chloroplast membrane lipid, leads to oxylipin overproduction and phloem cap lignification in *Arabidopsis*. *Plant Cell* 28, 219–232. doi: 10.1105/tpc.15.01002

Liu, Y., Li, Q., Lu, X., Song, Q., Lam, S., Zhang, W., et al. (2014). Soybean GmMYB73 promotes lipid accumulation in transgenic plants. *BMC Plant Biol.* 14:73. doi: 10.1186/1471-2229-14-73

Meringer, M. V., Villasuso, A. L., Margutti, M. P., Usorach, J., Pasquaré, S. J., Giusto, N. M., et al. (2016). Saline and osmotic stresses stimulate PLD/diacylglycerol kinase activities and increase the level of phosphatidic acid and proline in barley roots. *Environ. Exp. Bot.* 128, 69–78. doi: 10.1016/j.envexpbot

Mikami, K., and Murata, N. (2003). Membrane fluidity and the perception of environmental signals in cyanobacteria and plants. *Prog. Lipid Res.* 42, 527–543. doi: 10.1016/s0163-7827(03)00036-5

Moellering, E. R., Muthan, B., and Benning, C. (2010). Freezing tolerance in plants requires lipid remodeling at the outer chloroplast membrane. *Science* 330, 226–228. doi: 10.1126/science.1191803

Narayanan, S., Prasad, P. V., and Welti, R. (2016). Wheat leaf lipids during heat stress: II. Lipids experiencing coordinated metabolism are detected by analysis of lipid co-occurrence. *Plant Cell Environ.* 39, 608–617. doi: 10.1111/pce.12648

Ohlrogge, J., and Browse, J. (1995). Lipid biosynthesis. *Plant Cell* 7, 957–970. doi: 10.1105/tpc.7.7.957

Peppino Margutti, M., Reyna, M., Meringer, M. V., Racagni, G. E., and Villasuso, A. L. (2017). Lipid signalling mediated by PLD/PA modulates proline and H_2O_2 levels in barley seedlings exposed to short- and long-term chilling stress. *Plant Physiol. Biochem.* 113, 149–160. doi: 10.1016/j.plaphy.2017.02.008

Rodríguez, V. M., Butrón, A., Rady, M., Soengas, P., and Revilla, P. (2014). Identification of quantitative trait loci involved in the response to cold stress in maize (*Zea mays* L.). *Mol. Breeding.* 33, 363–371. doi: 10.1007/s11032-013-9955-4

Ruelland, E., Cantrel, C., Gawer, M., Kader, J. C., and Zachowski, A. (2002). Activation of phospholipases C and D is an early response to a cold exposure in *Arabidopsis* suspension cells. *Plant Physiol.* 130, 999–1007. doi: 10.1104/pp.006080

Ruelland, E., Kravets, V., Derevyanchuk, M., Martinec, J., Zachowski, A., and Pokotylo, I. (2015). Role of phospholipid signalling in plant environmental responses. *Environ. Exp. Bot.* 114, 129–143. doi: 10.1016/j.envexpbot.2014.08.009

Shen, B., Allen, W. B., Zheng, P., Li, C., Glassman, K., Ranch, J., et al. (2010). Expression of ZmLEC1 and ZmWRI1 increases seed oil production in maize. *Plant Physiol.* 153, 980–987. doi: 10.1104/pp.110.157537

Song, Q., Li, Q., Liu, Y., Zhang, F., Ma, B., and Zhang, W. (2013). Soybean GmbZIP123 gene enhances lipid content in the seeds of transgenic *Arabidopsis* plants. *J. Exp. Bot.* 64, 4329–4341. doi: 10.1093/jxb/ert238

Tan, W., Yang, Y., Zhou, Y., Huang, L., Xu, L., Chen, Q., et al. (2018). DIACYLGLYCEROL ACYLTRANSFERASE and DIACYLGLYCEROL KINASE modulate triacylglycerol and phosphatidic acid production in the plant response to freezing stress. *Plant Physiol.* 177, 1303–1318. doi: 10.1104/pp.18.00402

Tasseva, G., de Virville, J. D., Cantrel, C., Moreau, F., and Zachowski, A. (2004). Changes in the endoplasmic reticulum lipid properties in response to low temperature in *Brassica napus*. *Plant Physiol. Biochem.* 42, 811–822. doi: 10.1016/j.plaphy.2004.10.001

Testerink, C., and Munnik, T. (2011). Molecular, cellular, and physiological responses to phosphatidic acid formation in plants. *J. Exp. Bot.* 62, 2349–2361. doi: 10.1093/jxb/err079

Tovuu, A., Zulfugarov, I. S., Wu, G., Kang, I. S., Kim, C., Moon, B. Y., et al. (2016). Rice mutants deficient in ω -3 fatty acid desaturase (FAD8) fail to acclimate to cold temperatures. *Plant Physiol. Bioch.* 109, 525–535. doi: 10.1016/j.plaphy.2016.11.001

Troncoso-Ponce, M. A., Cao, X., Yang, Z., and Ohlrogge, J. B. (2013). Lipid turnover during senescence. *Plant Sci.* 205-206, 13–19. doi: 10.1016/j.plantsci.2013.01.004

Uemura, M., and Steponkus, P. L. (1997). Effect of cold acclimation on the lipid composition of the inner and outer membrane of the chloroplast envelope isolated from rye leaves. *Plant Physiol.* 114, 1493–1500. doi: 10.1104/pp.114.4.1493

Wang, F., Ding, D., Li, J., He, L., Xu, X., Zhao, Y., et al. (2020). Characterisation of genes involved in galactolipids and sulfolipids metabolism in maize and *Arabidopsis* and their differential responses to phosphate deficiency. *Funct. Plant Biol.* 47, 279–292. doi: 10.1071/FP19082

Zhang, Z., Zhang, J., Chen, Y., Li, R., Wang, H., Ding, L., et al. (2014). Isolation, structural analysis, and expression characteristics of the maize (*Zea mays* L.) hexokinase gene family. *Mol. Biol. Rep.* 41, 6157–6166. doi: 10.1007/s11033-014-3495-9

Zhao, X., Wei, J., He, L., Zhang, Y., Zhao, Y., Xu, X., et al. (2019). Identification of fatty acid desaturases in maize and their differential responses to low and high temperature. *Genes* 10:445. doi: 10.3390/genes10060445

Zheng, G., Li, L., and Li, W. (2016). Glycerolipidome responses to freezing- and chilling-induced injuries: examples in *Arabidopsis* and rice. *BMC Plant Biol.* 16:70. doi: 10.1186/s12870-016-0758-8

Zheng, G., Tian, B., Zhang, F., Tao, F., and Li, W. (2011). Plant adaptation to frequent alterations between high and low temperatures: remodelling of membrane lipids and maintenance of unsaturation levels. *Plant Cell Environ.* 34, 1431–1442. doi: 10.1111/j.1365-3040.2011.02341.x

Conflict of Interest: The authors declare that the research was conducted in the absence of any commercial or financial relationships that could be construed as a potential conflict of interest.

Advantages of publishing in Frontiers

OPEN ACCESS
Articles are free to read for greatest visibility and readership

FAST PUBLICATION
Around 90 days from submission to decision

HIGH QUALITY PEER-REVIEW
Rigorous, collaborative, and constructive peer-review

TRANSPARENT PEER-REVIEW
Editors and reviewers acknowledged by name on published articles

Frontiers
Avenue du Tribunal-Fédéral 34
1005 Lausanne | Switzerland

Visit us: www.frontiersin.org
Contact us: frontiersin.org/about/contact

REPRODUCIBILITY OF RESEARCH
Support open data and methods to enhance research reproducibility

DIGITAL PUBLISHING
Articles designed for optimal readership across devices

FOLLOW US
@frontiersin

IMPACT METRICS
Advanced article metrics track visibility across digital media

EXTENSIVE PROMOTION
Marketing and promotion of impactful research

LOOP RESEARCH NETWORK
Our network increases your article's readership